Author:
Lo Jacomo, Anna

Title:
Multi-hazard exposure of cities and implications for urban infrastructure

Multi-hazard exposure of cities and implications for urban infrastructure

Anna Lo Jacomo

Department of Civil Engineering

University of Bristol

A dissertation submitted to the University of Bristol in accordance with the requirements of the degree of Doctor of Philosophy in the Faculty of Engineering.

November 2020

Abstract

Urban populations rely on infrastructure for basic services like water supply, energy, and transport, whose disruption can have important implications for health, society, and the economy. While there are now strategies to reduce disruption from single hazards, few strategies take into account the exposure of systems to multiple different hazards. Failing to account for multiple hazards can lead to maladaptation of infrastructure in two important ways: first, mitigation measures for one hazard could increase the risk of another hazard; and second, infrastructure systems could be under-prepared for combined (i.e. coinciding, compound, or cascading) hazard events. This research explores how integrating existing methods for single hazard resilience can help address maladaptation in the face of multiple hazards, focusing on urban water and road networks.

In the first part, global hazard datasets are assembled and used to assess urban exposure to combinations of five damaging hazards (river and coastal flood, tropical cyclone wind, earthquake, and landslide). Results show that overall, there is high variability in hazard conditions across urban areas. Significant hazard combinations are found to include flooding and tropical cyclone wind (particularly in Asia and North America); river and coastal flooding (particularly in Europe and Asia); and low levels of seismic and wind hazards. The diversity of hazard conditions across cities may be a barrier to transferring solutions aimed at a specific combination of hazards. Therefore, a similarity-based approach is proposed for finding cities with comparable hazard conditions. The hazard data is also evaluated at the city scale by using qualitative information from the Rockefeller Foundation network of 100 resilient cities.

The second part looks at understanding the impacts of consecutive hazard events. Specifically, it investigates whether consecutive impacts may be greater than the sum of impacts of the single

events. This is done by simulating the disruption (in person-hours of service loss) due to a consecutive earthquake and cyclone event on a water supply system (for the hypothetical city of C-Town). The simulation uses the open source hydraulic model WNTR (Water Network Tool for Resilience). Earthquake damage is modelled using fragility curves from HAZUS-MH. Monte Carlo simulation is used to account for uncertainties in damage and to stochastically vary the timing of the two events over a five day period. Results show that on average (across multiple equally likely instances of damage), the increase in disruption is not significant, however, in individual instances, disruption can increase by more than 50% when the events happen consecutively, relative to the sum of the single hazards. The amount of increase is found to depend on the interval between hazards (a decrease is seen for intervals of less than 5 hours, a significant increase is seen for intervals between 5 and 25 hours, and for intervals of more than 25 hours, consecutive event disruption is equivalent the sum).

The third part explores the feasibility, and possible benefits, of analysing multi-hazard consequences in practice. a case study is carried out in the flood-prone city of Jingdezhen in China. The functionality of the road network is assessed under single and combined hazard scenarios of river flooding and debris flows. Hazard information is generated using two openly available hazard models: river flooding is modelled using LISFLOOD-FP, a two-dimensional hydrodynamic model; and debris flow is modelled using Flow-R, an empirical susceptibility model. Road network functionality is represented using efficiency and betweenness metrics from graph theory. Results show potential value from combined hazard assessments even with limited data availability.

The thesis demonstrates some of the limitations of a single hazard approach to infrastructure resilience, and shows how an integrated approach across hazards might help reduce future disruptions to service. As data and methods for single hazards continue to steadily improve, there is significant potential for multi-hazard approach to help increase the resilience of cities.

Plain language summary

In a disaster, people living in urban areas can face interruptions to water supply, electricity supply, transport, and other services, sometimes with severe consequences (e.g. closure of hospitals, impacts on vulnerable populations, social unrest). The difficulty is that in many cities, interruptions can be caused by various hazards (e.g. river floods, storm surges, earthquakes, storms, landslides). Therefore, infrastructure services need to be made resilient not just to one type of hazard, but to the multiple hazards that could affect them. If the infrastructure is designed specifically for one type of hazard, it may become more vulnerable to another hazard (e.g. placing a facility on a hill to avoid flooding might expose it to landslides). Focusing on a single type of hazard could also means the services are not sufficiently prepared if multiple hazards happen at the same.

To address this, the research starts by addressing the lack of awareness of exposure of cities to multiple hazards. Indeed, hazards like floods or earthquakes are often dealt with by different people or institutions, with data often held separately, which limits understanding of exposure to multiple hazards. Therefore, this study collects, processes, and analyses data across five different hazards (river and coastal flood, earthquakes, storms, and landslides). The analysis reveals that cities in North America and Asia are more likely than cities on other continents to face two or more of the hazards. Also, it shows that globally, many of the same cities face both flood and storm events, as well as both storm and earthquake events.

A crucial concern is that if hazards happen at the same time, they could have disproportionately larger consequences than if they had happened separately. Yet there is a lack of methods for measuring and mitigating the consequences of hazards happening together. The next part of the work addresses this issue, by proposing a way of measuring the consequences on service

of two hazards occurring together. The method is applied to a hypothetical scenario where an earthquake and storm happen in a city within the same week. The event is assumed to cause limited overall damage, but to affect the supply of water by damaging underground pipes and pumping stations. The consequences of the events are measured in terms of the number of people affected and duration of interruption to water supply. The scenario is modelled for a hypothetical city using real information on the damage that the hazards cause to the water supply infrastructure. The results show that there could be up to 50% more disruption when the earthquake and storm happen within a day of each other, compared to if the same two events had happening separately, simply because of the timing of the events. The results demonstrate the importance of better understanding the effects of combined events. The method used also helps to identify some of the causes of increased disruption.

The third part explores how we can analyse disruption from combined hazards in an actual city given limited data availability. A case study is carried out in the flood-prone city of Jingdezhen in China. The analysis looks at the disruption to the road network of the city, as road data is generally less prone to security concerns than other infrastructure data and more likely to be available. Disruption to travel is analysed under river flooding, and under combined river flooding and debris flows. The analysis helps to identify roads that are important for the city to operate under different hazard scenarios, showing the value of analysing combined hazard events even with limited data availability.

Overall, the work reveals limitations in a single hazard approach to infrastructure resilience, and shows that bringing together existing data and methods for single hazards can provide valuable understanding of multi-hazard impacts to infrastructure services.

Acknowledgements

Looking back at the highs and lows of the last few years, I have learnt some unforgettable lessons and feel grateful to have had this opportunity into research. Clearly, this thesis could not have happened without the many people who inspired, supported, and guided me throughout the years, and I would like express my gratitude to them.

Thanks first of all to my supervisors, Dawei Han and Alan Champneys. I am grateful for your input, availability, patience, and kindness throughout the years. You gave me an incredible opportunity to follow my curiosity across a broad field of knowledge, while guiding me and giving me the confidence to continue. I would have been lost without our frequent meetings, and without your enthusiasm and encouragements. I am very grateful for your open-mindedness and for the support you gave me.

Thanks to Thorsten Wagener for creating the WISE-CDT, forming a great research environment and holding the group together, and to the University of Bristol, and the EPSRC, for funding the project. Thanks also to the NERC funded RESIST project for financial support.

Thanks to Francesca Pianosi and to Katsu Goda for your input, and to Lorenzo Campo, Weihua Fang, Gabriel Bernal, Omar Cardona, Mattia Amadio, and Jeffrey Neal for kindly replying to my e-mails and sharing data.

Thanks to Jing Huang, Qiang Dai, Qiqi and Zheqiang for hosting me in Nanjing. Jing, thanks for introducing me to the work you were doing in Jingdezhen, without you Chapter 5 would not have been possible. Qiqi and Zheqiang, thanks for taking me under your wing and helping me uncover a bit of the amazing Chinese culture.

Thanks to the other early career researchers working on multi-hazards, for connecting me to a wider research community, and for making conferences such a fun and fulfilling experience, including Faith Taylor, Stefano Terzi, Silvia De Angeli, Anais Couasnon, Alois Tilloy, and Joel Gill.

Thanks to everyone at Woodland Road, especially Wouter, Barney, Moonhuyk, Yiheng, Lu, for answering my questions while I was still taking my first steps in research and making me feel cool in the process; Vale and Will, for reminding us that changing the world starts locally; Sebastian, Charlie, Lina, Giulia, Melike, Elisa, Giorgios, and others for the good vibes while also questioning my (sometimes unfounded) ideas for changing the world. Thanks also to the wise friends, especially Olivia, Cain, Arthur, Paul, for the memories created and others still to come. Thanks to everyone else who has kept me sane and cheered me up when things got tough.

A huge thanks to my housemates Elisa and Ludo, for keeping me grounded, listening to my ideas, and sharing the good and bad times throughout the years (to name just a few). It would definitely not have been the same without you.

Thanks most of all to my eclectic and wonderful family, Mama, Papa, Steph, Martha, Mak, Baka, Deda, Mamie, for shaping who I am, for your insight, and for your support. Among other things, Mama (for your wisdom), Steph (pour ta discipline qui inspire); Papa (pour nos discussions mathématiques); Mak, (for proofreading the work); and everyone else (including Ruby) for being a joy in my life. A special thought goes out to Deda and Mamie, both of whom gave me stability and taught me a lot about rigour, hard work, and perseverance, and will remain role models for me going forward.

Author’s declaration

I declare that the work in this dissertation was carried out in accordance with the requirements of the University’s *Regulations and Code of Practice for Research Degree Programmes* and that it has not been submitted for any other academic award. Except where indicated by specific reference in the text, the work is the candidate’s own work. Work done in collaboration with, or with the assistance of, others, is indicated as such. Any views expressed in the dissertation are those of the author.

SIGNED:

Date:

06/11/2020

Table of contents

This page was intentionally left blank

Chapter 1. Introduction

1.1 Context

Disasters happen when a hazard (natural or man-made) affects a community or society that is not adequately prepared for the event (Smith, 2013). Disasters can be defined as events that overwhelm the local capacity to cope, resulting in the community or society requiring external assistance (e.g. people, resources, or funds) to recover from an undesirable state (CRED, 2020). A hazard (e.g. an earthquake or flood) only causes a disaster if it overwhelms the systems that the society depends on; a given hazard event could, but may not, result in a disaster. For example societies throughout history have benefitted from river floods; in Egypt and China, floods were valued as they deposited sediment on agricultural land (De Bruijn, 2005). Similarly, earthquake engineers use the phrase "earthquakes don't kill people, buildings do" to reflect the role of people in the devastation caused by earthquakes (Pokharel & Goldsworthy, 2017). Also, natives from Pacific Islands affected by the tsunami of 2004 survived thanks to a tradition of moving to high ground when the ocean recedes, while many tourists who did not understand these natural patterns were killed (Munasinghe, 2007). These examples highlight that the built environment and human behaviours of a place need to adequately account for the natural extremes of that location. Of course, not all disasters are caused by nature; some disasters, such as terrorist attacks, traffic accidents, or chemical explosions, are man-made (Smith, 2013). Nevertheless, disaster records suggest that natural events (particularly earthquakes, floods, and storms) have been by far responsible for the largest disaster impacts over the last three decades (Figure 1.1).

The Hyogo Framework for Action was the first coordinated international agreement that set out to tackle and address disasters caused by natural hazards (UNISDR, 2005), but despite significant progress since its implementation, natural hazards continue to be a burden for communities and the economy (UNISDR, 2015b). In 2017 alone, natural hazards caused an estimated 340 billion US$ in losses, and more than 10,000 deaths (MunichRE, 2018). Also, data from the EM-DAT database, the largest freely available database of disasters, shows that over 4.2 billion people have been affected since 1990 by earthquakes, floods, storms, and landslides (CRED, 2020). Globally, storms have been the most costly hazard, floods have affect the greatest number of people, and earthquakes have been responsible for the highest number of deaths (Figure 1.1). The EM-DAT database is known to underestimate the importance of small and frequent events (UNISDR, 2015b); for example Petley et al. (2005) has recorded nearly twice as many deaths from landslides as the number reported by the database. The database also only reports the number of people directly affected, and does not reflect the population affected through indirect impacts, such as loss of livelihoods, poverty, anxiety, discomfort, or inconveniences as a result of hazards (CRED, 2020; UNISDR, 2015b).

While significant progress has been made towards reducing the number of lives lost in disasters, trends show that disruptions to society and the economy have been increasing over time (MunichRE, 2018). Activities such as enforcing building codes, providing early warning, building storm shelters and flood defences has contributed to lower death rates; for example, almost 10,000 people were killed in Odisha, India, in 1999 due to a cyclone, but an equivalent cyclone in 2013 caused fewer than 50 deaths (UNISDR, 2015b). However, disruption to communities and livelihoods, and the cost of destruction, continues to increase (MunichRE, 2018; UNISDR, 2015b). An important driver of increasing impacts is the growth of population, particularly in cities in Asia and Africa, resulting in more people living in hazard prone areas

(UNDRR, 2019). The population in seismic areas has nearly doubled in less than 50 years, and today, 1 in 3 people live in an area prone to earthquakes (Pesaresi et al., 2017). Also, many of the largest and fastest growing cities are located in coastal areas and face hazards like tropical cyclones, river flooding and coastal flooding (Jongman et al., 2012). Furthermore, the storms and floods affecting these cities are projected to become more severe in the future, as human activities affect mean surface temperatures, leading to sea level rise and changes in rainfall patterns (Field et al., 2012). Another driver of a rise in impacts is the increasing interdependency between economic, social, and physical systems (Godschalk, 2003). Interdependencies can take many forms and amplify impacts both locally and over larger areas (Rinaldi et al., 2001). For example, a loss of electricity can also affect access to water, as seen during recent power outages in various places, with consequences for healthcare, businesses, and vulnerable urban populations (Chang et al., 2007). Global supply chains are also responsible for increasing impacts; for example Hurricane Maria in the Caribbean affected the supply of medical equipment in hospitals throughout the US (UNDRR, 2019).

Increasingly, disasters are being amplified by disruptions to critical infrastructure services such as water, energy, and transport. The 2007 summer floods in the UK left 350,000 people without water for almost three weeks, and caused widespread disruptions to transport and power, with the majority of those affected living outside of the immediately flooded area (Pitt, 2008). Hurricane Sandy made landfall in New York in 2012 and caused loss of power to millions of people while flooding the subway system, bringing the entire city to a standstill for days (Haraguchi & Kim, 2016). This resulted in one of the most expensive disasters to date (Kaufman et al., 2012). In Japan, the Hanshin earthquake that struck the city of Kobe in 1995 caused over a million people to lose access to water, gas, electricity, drainage and transport (Edgington, 2016). An insufficient water supply exacerbated the spread of fires that ignited

through the city as a result of damage to the gas network (Edgington, 2016). Recent earthquake events around the world have also caused widespread damage to infrastructure hampering recovery efforts, in Chile, New Zealand, and China (Cimellaro et al., 2010; Cimellaro et al., 2014; Curinovski et al., 2014; Dueñas-Osorio & Kwasinski, 2012; Lekkas et al., 2011; Mostafavi et al., 2018; Zhao & Taucer, 2010). In New Orleans, violent, armed robberies, both of essential and non-essential items, were seen following Hurricane Katrina in 2005 (Munasinghe, 2007). The event was an example of how the loss of essential infrastructure services, and the subsequent undermining of law enforcement, government, or banks, can result in social unrest. Those most affected by the loss of water supply during the 2007 UK floods were the elderly and vulnerable, who struggled to collect water from alternative sources (Pitt, 2008). Indeed, the consequences of disasters are often disproportionately felt by the most vulnerable (UNDRR, 2019).

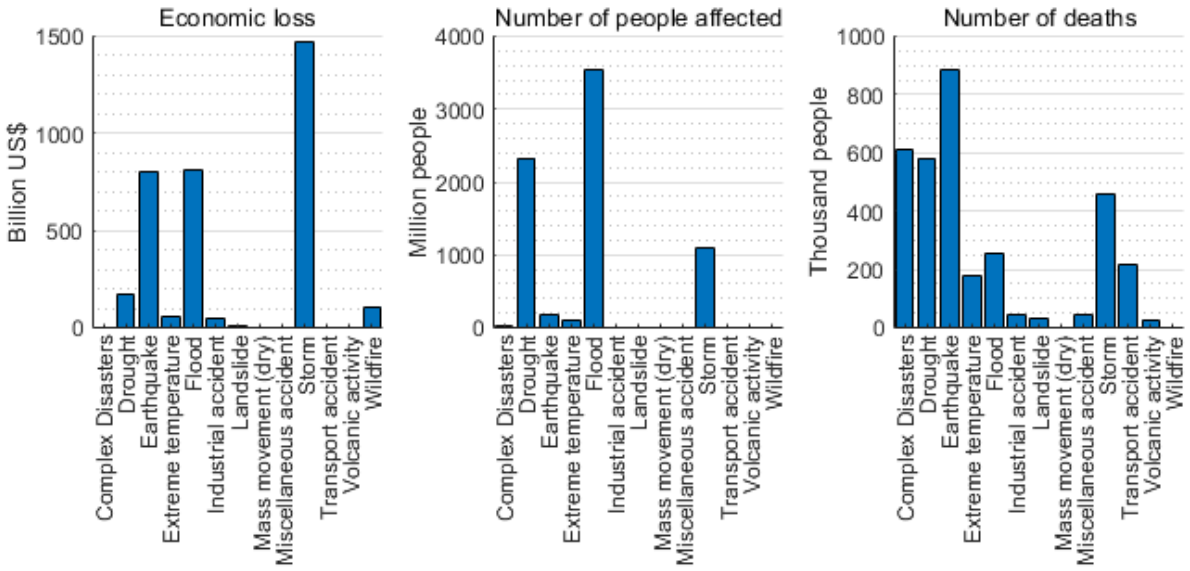

Figure 1.1 The total economic loss, number of people affected, and deaths from hazards between 1980 and 2019. Includes all events that caused at least one of the following: 10 or more people dead; 100 or more people affected; the declaration of a state of emergency; a call for international assistance. Data from the EM-DAT database (CRED, 2020).

In response to the challenges faced, policies are emphasising the need for infrastructure to be made resilient to various hazards. The Sendai Framework for Disaster Risk Reduction has set a target to "substantially reduce disaster damage to critical infrastructure and disruption of basic services, (…), including through developing their resilience by 2030" (UNISDR, 2015a). The Coalition for Disaster Resilient Infrastructure was set up at the 2019 Climate Action Summit of the United Nations, with the aim of promoting "the resilience of new and existing infrastructure systems to climate and disaster risks, thereby ensuring sustainable development". Resilience is used in the context of the European Union Global Strategy (European Union, 2016) to reflect the need for a holistic approach to risk: "the concept of resilience brings under the same umbrella different short- and long-term approaches to risk management, which deal not only with imminent disasters (i.e. flooding, fires) but also with (…) risk trends (i.e. climate change, environmental degradation, demographic changes)" (Pawlak, 2016). In their report "Disaster resilience: a national imperative", the US National Research Council emphasise "the importance of an "all-hazards" approach to resilience" and state that upgrades are needed to "nationwide infrastructure (…) to encompass disaster-resilient designs" (National Research Council, 2012).

Currently, efforts to address disruptions to critical services mostly focus on preventing damage through various forms of protection (De Bruijn, 2004; Gardoni & LaFave, 2016; Golz, 2015; Rogers & Grigg, 2008; Serre, 2018). Protective measures include placing infrastructure out of reach of the hazards (e.g. moving facilities away from the floodplain, raising structures above the flood line, burying pipes or cables underground to prevent wind damage), constructing protective walls or barriers (e.g. sea walls, flood embankments, dams, landslide barriers), or designing infrastructure components that can withstand hazard forces. Protective measures make an important contribution to mitigating hazard impacts, and there has been impressive

engineering progress in protecting from, and resisting, hazards. It is now possible to design buildings or road bridges to withstand some of the strongest earthquakes ever recorded (Monfared, 2020; Kitagawa, 2004), and protect cities from a 1-in-10,000 year flood (Kwadijk et al., 2010). Often, the design of protective measures will take into account the relevant combinations of hazard forces (e.g. combined earthquakes and flooding on bridges, winds and storm surge for coastal infrastructure; Gehl & D'Ayala, 2018; Kameshwar & Padgett, 2014; McCullough et al., 2013).

However, protection alone is considered to be insufficient to offset the increase in impacts (Aven, 2015; Rogers et al., 2012). There are many ways infrastructure components could be damaged by hazards (Figure 1.2). Protecting from each of the effects incurs additional costs in design, construction and maintenance, and the money is not always available or justifiable (Hudson et al., 2012). Also, regardless of the protection level provided, there will be an event sooner or later that will exceed it, with potentially dramatic consequences (Aven, 2015). For example, the Wenchuan earthquake in China in 2008 exceeded the ground motion stipulated by the Chinese design codes, and resulted in extensive damage to dams, roads, and bridges (Zhao & Taucer, 2010). Protection can also create a false sense of security that leads to counterproductive behaviours and further increases the consequences when protection levels are exceeded, for example construction on a floodplain protected by embankments (Di Baldassarre et al., 2013). In addition, decisions on the appropriate level of protection are sensitive to uncertainties about the hazards (Di Baldassarre & Montanari, 2009). Another concern is that protection cannot effectively address all the possible combinations of events, many having a very low probability but potentially high consequences, and may not have occurred before (Aven, 2015).

Figure 1.2 Hazards and their effects on physical infrastructure components. Figure from Zaghi et al. (2016).

Therefore, researchers have been looking for new ways of understanding and reducing the impacts of hazards on infrastructure services. Infrastructure can be seen as mediating between the environment and society (Figure 1.3). From that perspective, there are different stages through which a hazard affects society, starting with physical damage to infrastructure components, followed by a loss of service, through to consequences on the population. There are therefore also multiple opportunities for intervention. Protecting the system from damage addresses the first stage in the impact chain. Other opportunities exist that instead address the second and third stages of impact (i.e. reducing loss of service once damage occurs, and making the population less vulnerable to a loss of service). The second stage in particular, reducing the loss of service once damage occurs, has been a focus area of infrastructure research. One way of preventing damage from spreading across large areas is by ensuring that services are sourced and provided locally, and that communities, or even households, are self-sufficient. Technologies that support local self-sufficiency include for example rainwater harvesting (for water supply), and rooftop solar panels (for electricity). However, local self-sufficiency is not always possible (i.e. resources may be not be present locally in sufficient quantity to meet the needs of a dense population), making networks that can distribute resources over larger areas necessary, and in some cases beneficial to the resilience of a community. Therefore, understanding the best way to become resilient in a given setting is not straight forward. Research has been taking inspiration from other systems with characteristics comparable to those of infrastructure systems, looking for generalisable properties that make these systems resilient. The study of ecosystems, that inspired the modern notion of resilience (Holling, 1973), provides interesting lessons for resilience, showing the value of system properties such as redundancy, modularity, or diversity. Inspiration for resilience is also seen to come from fields such as physics or mathematics, including research areas such as graph theory or percolation theory.

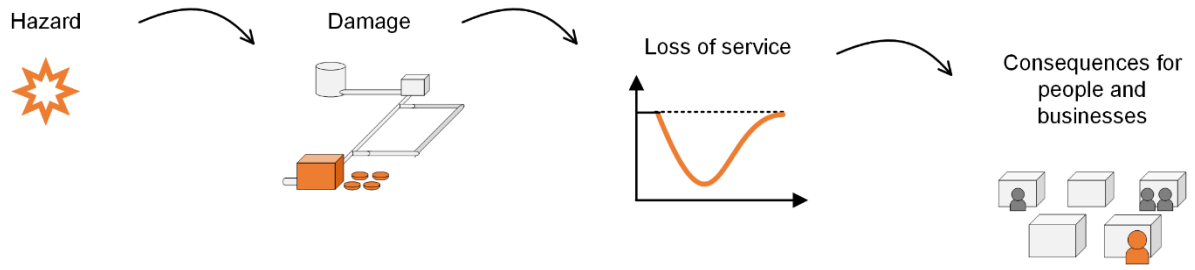

Figure 1.3 A framework for infrastructure resilience, showing how hazards events propagate through infrastructure systems to affect society, based on Butler et al. (2014) and Zaghi et al. (2016).

There is a rapidly growing array of methods and tools (see for example https://www.resilienceshift.org/tools) to help infrastructure professionals and other stakeholders adapt infrastructure systems based on principles of resilience (Hickford et al., 2018). Broadly speaking, methods and tools for resilience aim to integrate elements not previously considered together (e.g. infrastructure, society, politics, environment), and to understand the connections between these elements. These methods and tools can take many forms, such as frameworks or models. Optimisation, while powerful in finding the best or most adapted solution among a multitude of solutions, does not feature strongly within methods and tools for resilience. Optimisation is a powerful way of making a system highly adapted to a set of predefined constraints and objectives. However, it is limited to constraints and objectives that are knowable or foreseen. As discussed by Meerow et al. (2016), high adaptedness can limit adaptability. Indeed, optimising a system for a specific threat or set of threats can undermine the redundancy, flexibility, diversity, and 'alertness' (i.e. readiness to respond) of the system (Meerow et al., 2016). Given that infrastructure in many countries is reaching the end of its design life and needing replacement (Dunn et al., 2017), and that the infrastructure that will support the future population in growing cities still needs to be built (Godfrey & Savage, 2012), methods and tools for making infrastructure system more resilient play a crucial role in reducing future hazard impacts.

1.2 Problem analysis

While resilience principles have been shown to be useful for analysing and reducing consequences from single hazards (e.g. Chang et al., 2002; Klise et al., 2017; Pregnolato et al., 2016), there is still a lack of studies accounting for multiple hazards (Zaghi et al., 2016). Events like Hurricane Sandy in New York suggest that urban systems like transport, energy, and healthcare may be under-prepared for combined hazard events (Haraguchi & Kim, 2016). The consequences of combined hazard events on infrastructure are still poorly understood and often not addressed because of their low probability of occurrence (Aven, 2015). Yet disasters are not necessarily the result of extreme events, but could occur because a number of small, localised, independent hazards combine to produce consequences that are more than the sum of the parts (Perrow, 2011). For example, a flash flood and a landslide could damage different sections of a road network and leave people trapped on the road. Studies of combined failures on infrastructure systems seem to mostly consider generic failures (e.g. assigning an equal probability of failure to all parts of the system), without accounting for the spatial and temporal characteristics of real hazards (Diao et al., 2016; Mugume et al., 2015).

Several reasons may explain the lack of modelling of real hazard combinations on infrastructure systems. Some reasons are common to both single and multi-hazard studies, such as the difficulty in modelling how a system performs when damaged. Models that are used in the design and operation of infrastructure (e.g. traffic models, water distribution system models) are generally not intended to represent the system during a disaster (e.g. Rossman, 2000), and the post-disaster period involves unique processes such as population movements and repairs that are often not included within those models. Other reasons are specific to modelling of multi-hazard events. One possible reason is a lack of awareness of exposure to multiple hazards by infrastructure operators and designers, due to hazard information often still

being held by different agencies or organisations (Kappes et al., 2012). While stakeholders often have a reasonably good understanding of possible scenarios within their own sector (Ciurean et al., 2018), there is a lack of oversight of challenges affecting different sectors, that could combine to cause disruption at the city scale. Another reason is insufficient understanding of the extent to which impacts could be amplified as a result of two hazards occurring together (De Ruiter et al., 2019). Risk assessments sometimes assume a simple sum of impacts, yet many highlight that the combined impacts could differ from the sum of impacts of single hazards (Ciurean et al., 2018; Gallina et al., 2016; Kappes et al., 2012; Terzi et al., 2019; Zaghi et al., 2016). Yet there is still a lack of evidence of the extent to which impacts might increase (or decrease) when hazards interact, and a lack of methods for comparing single and multi-hazard impacts on infrastructure performance. Finally, insufficient studies apply multi-hazard methods in actual geographic contexts rather than in simulated environments (Ciurean et al., 2018).

Recently, improvements have been made in understanding infrastructure performance for single hazards. Approaches based on simplified representations of the system, for example using graph theory, provide an efficient an rapid way of estimating performance, as well as to model different infrastructure types and their interactions (Buldyrev et al., 2010). The use of pressure-driven demand models for water supply makes it possible to represent their performance when damaged (Dawson et al., 2011; Dueñas-Osorio et al., 2007; Klise et al., 2017; Miles & Chang, 2011). Significant work has also been done on modelling and improving the recovery process after a disaster (Tabucchi et al., 2010). Furthermore, data on hazards is becoming increasingly available (Ward et al., 2020). Also, emphasis at the policy level of the importance of an all-hazards approach is helping to overcome silos (UNISDR, 2015a). Meanwhile, significant improvements are being made in understanding how natural hazards

interact (Couasnon et al., 2020; Gill & Malamud, 2014; Matthews et al., 2019; Wahl et al., 2015; Zscheischler et al., 2018). Given the context and opportunities discussed, it is both timely and necessary to begin to better understand multi-hazard events and their effects on infrastructure performance.

1.3 Aim and research questions

The overall aim of this thesis is to contribute to increasing city resilience, through improving our understanding of infrastructure response to multi-hazard events. The thesis is centred on urban water challenges, and is primarily addressed at water engineers. However, the problem of loss of service during a disaster concerns, and involves, other disciplines as well, making parts of the work also relevant to policy makers, disaster risk reduction experts and hazard scientists. Specifically, the thesis aims to make progress in the consideration of multiple hazards by addressing three identified gaps: (1) the lack of awareness of exposure to multiple hazards, (2) insufficient understanding of combined impacts, and (3) the lack of case studies on real systems. The work is structured around the following research questions:

1. *What combinations of hazards are urban infrastructure systems exposed to?*
2. *Can the response of a system to single hazards be used to predict the response to a combined hazard event?*
3. *Can the consequences of multi-hazard events be assessed at the city scale given limited data availability, and what are some of the challenges?*

Regarding (1), the aim is to use existing global hazard maps, along a recent dataset of urban areas, to analyse the exposure of urban areas across five damaging hazards. The analysis will look for trends across combinations of hazards and aim to identify common combinations of

hazards. The data used will also be evaluated to determine its accuracy. Possible further uses of the data will then be considered and discussed, taking into account data quality.

To address question (2), the aim is to simulate the performance of a water supply system during a consecutive event, and to compare it to the performance during single events. It will be done by modelling a (realistic but low-probability) scenario of an earthquake and tropical cyclone occurring consecutively within the same week. The simulations will be carried out within a Monte Carlo framework to account for hazard uncertainty, using the Water Network Tool for Resilience (WNTR) (Klise et al., 2017).

Regarding (3), the aim is to look at multi-hazard challenges in the rapidly growing and flood-prone city of Jingdezhen in China. Specifically, the plan is to analyse the loss of functionality under different hazard scenarios, for the current and future network. To incorporate realistic hazard information into the assessment, the intention is to use two open source models, LISFLOOD-FP (Bates et al., 2013) and Flow-R (Horton et al., 2013), to model scenarios of river flooding and debris flows, respectively. Metrics from graph theory will be used to represent the network functionality.

1.4 Thesis outline

The structure of the thesis is shown in Figure 1.4.

Chapter 2 provides a review of the literature on infrastructure resilience. It starts by looking at how resilience is interpreted across different disciplines, and at the types of events that infrastructure systems need to be resilient against. Practical methods that apply resilience to infrastructure systems, in particular water and transport networks, are identified. Insights from previous studies that address impacts to infrastructure from multiple hazards are also discussed.

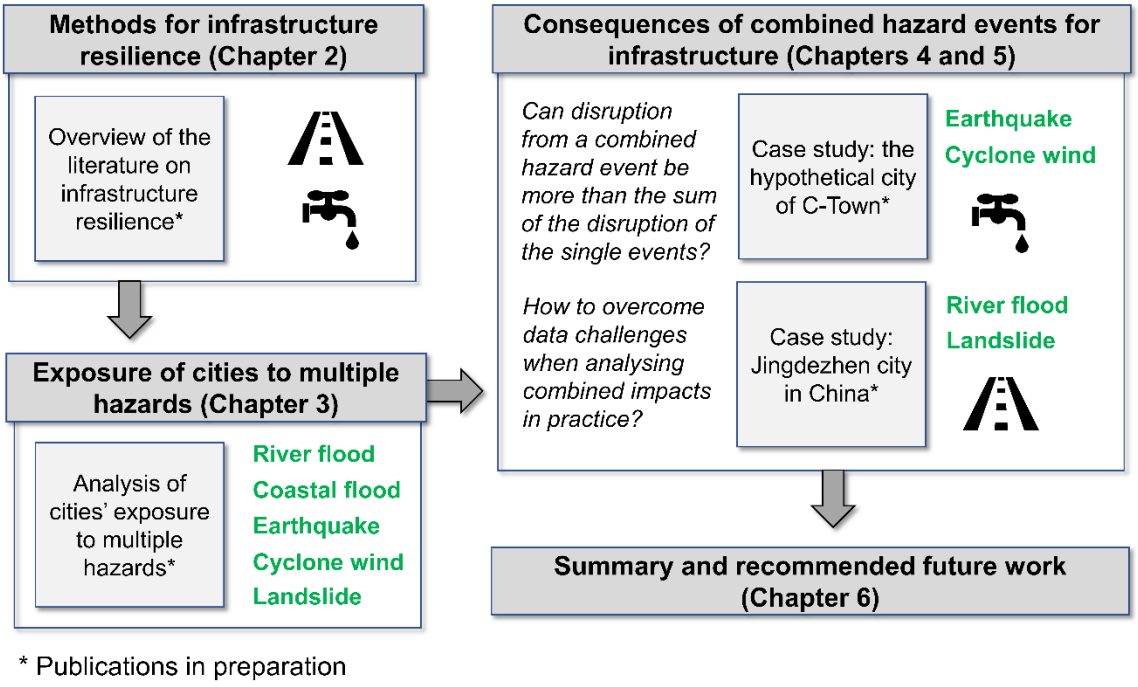

Figure 1.4 The structure of the work presented in this thesis. The text in italics shows the questions addressed in each case study. The green text shows the hazards included in each part.

Chapter 3 combines global hazard datasets to understand patterns of exposure to multiple hazards in cities.

Chapter 4 investigates how disruption due to consecutive hazards compares to disruption from single hazards, by modelling a consecutive event (an earthquake and cyclone occurring within the same week) and its impact on the water supply in a hypothetical city (C-Town).

Chapter 5 uses open source models and data to analyse the impact of river flooding and debris flows on the road network in the city of Jingdezhen in China. The functionality of the road network is quantified using graph theory.

Chapter 6 summarises the findings and contributions of the thesis and proposes some directions for future research.

Chapter 2. Reviewing methods for infrastructure resilience

2.1 Background and definitions of resilience

Resilience as a concept has a long and diverse history. Alexander (2013) traced back uses of the word and suggested that it originally comes from ‘resilire’ in Latin, which means “to bounce”. The concept of resilience re-emerged from ecology where it refers to the ability of ecosystems to absorb change and disturbance and still persist (Holling, 1973). In mechanical engineering, resilience has been used to mean the amount of strain energy which can be stored in a structure without causing permanent damage to it (Gordon, 1978). Resilience has also been used in environmental sciences, for example Timmerman (1981) used it to describe the capacity of societies to absorb and recover from the occurrence of a hazardous event. Hashimoto (1982) proposed resilience as a property of reservoir systems, referring to the average time needed to recover from a water deficit. A sample of definitions of resilience can be found in Table 2.1.

Recently, resilience has re-emerged as a strategy for addressing the effects of hazards in cities (Godschalk, 2003). The concept has been discussed in different disciplines that play a role in addressing hazards in cities, such as urban planning, engineering, and disaster risk reduction (Bruneau et al., 2003; Manyena, 2006; Meerow et al., 2016). The concept has also developed both in the context of earthquake engineering (Chang & Shinuzoka, 2004) and flood risk management (De Bruijn, 2004). Some consider that its value might be as a bridging concept for increased collaboration between disciplines (Davidson, 2015). Table 2.1 lists some of the influential definitions of resilience from different disciplines.

Table 2.1 Definitions of resilience.

Source	Definition
Ecology (Holling, 1973)	A measure of the persistence of systems and of their ability to absorb change and disturbance and still maintain the same relationships between populations or state variables
Ecology (Folke, 2006)	The capacity of a system to absorb disturbance and reorganize while undergoing change so as to retain essentially the same function, structure, identity, and feedbacks
Psychology (Tugade & Fredrickson, 2004)	The ability to bounce back from negative emotional experiences and flexible adaptation to the changing demands of stressful experiences
Water resources (Hashimoto, 1982)	How quickly a system is likely to recover or bounce back from failure once failure has occurred
Earthquake engineering (Bruneau et al., 2003)	The ability of the system to reduce the chances of a shock, absorb a shock if it occurs, and recover quickly after a shock
Urban hazard mitigation (Godschalk, 2003)	Local resiliency with regard to disasters means that a locale is able to withstand an extreme natural event without suffering devastating losses, damage, diminished productivity, or quality of life and without a large amount of assistance from outside the community
Water engineering (Butler et al., 2014)	The degree to which the system minimises level of service failure magnitude and duration over its design life when subject to exceptional conditions
Transport engineering (Mattsson & Jenelius, 2015)	The property of a material of springing back into shape, position, etc. after being stretched, bent or compressed
Management (Vogus & Sutcliffe, 2007)	The maintenance of positive adjustment under challenging conditions such that the organization emerges from those conditions strengthened and more resourceful
Geography (Cutter et al., 2010)	A system's ability to absorb disturbance and re-organize into a fully functioning system
Disaster risk reduction (Manyena, 2006)	The intrinsic capacity of a system, community or society predisposed to a shock or stress to adapt and survive by changing its non-essential attributes and rebuilding itself.
Computer science (Sterbenz et al., 2010)	The ability of the network to provide and maintain an acceptable level of service in the face of various faults and challenges to normal operation
Urban planning (Meerow et al., 2016)	The ability of an urban system-and all its constituent socio-ecological and socio-technical networks across temporal and spatial scales-to maintain or rapidly return to desired functions in the face of a disturbance, to adapt to change, and to quickly transform systems that limit current or future adaptive capacity
Sustainability (Elmqvist et al., 2019)	The capacity of an urban system to absorb disturbance, reorganize, maintain essentially the same functions and feedbacks over time and continue to develop along a particular trajectory
Intergovernmental Panel on Climate Change (Field et al., 2012)	The ability of a system and its component parts to anticipate, absorb, accommodate, or recover from the effects of a hazardous event in a timely and efficient manner, including through ensuring the preservation, restoration, or improvement of its essential basic structures and functions
The Rockefeller Foundation (Spaans & Waterhout, 2017)	The capacity of cities to function, so that the people living and working in cities – particularly the poor and vulnerable – survive and thrive no matter what stress or shocks they encounter
United Nations (UNDRR, 2015)	The capacity of a system, community or society potentially exposed to hazards to adapt, by resisting or changing in order to reach and maintain an acceptable level of functioning and structure. This is determined by the degree to which the social system is capable of organizing itself to increase this capacity for learning from past disasters for better future protection and to improve risk reduction measures.
National Research Council (2012)	The ability to prepare and plan for, absorb, recover from, or more successfully adapt to actual or potential adverse events

Table 2.1 shows that resilience generally refers to the ability of a systems absorb disturbances, recover from failure, and adapt, however its meaning varies with the context in which it is being used. Figure 2.1 shows word clouds produced from the titles of the most cited publications on resilience from eight different disciplines. Some words emerge as common themes, for example the word 'community' is strongly featured in the resilience literature from ecology, water resources, psychology, environmental sciences, and geosciences. Climate change can be seen most in environmental sciences, ecology, and geosciences, and to a lesser extent in water resources, but is not closely associated with resilience in civil engineering or telecommunications. The word 'urban' can be seen in environmental sciences, water resources, and geosciences, while 'infrastructure' is most prominent in civil engineering.

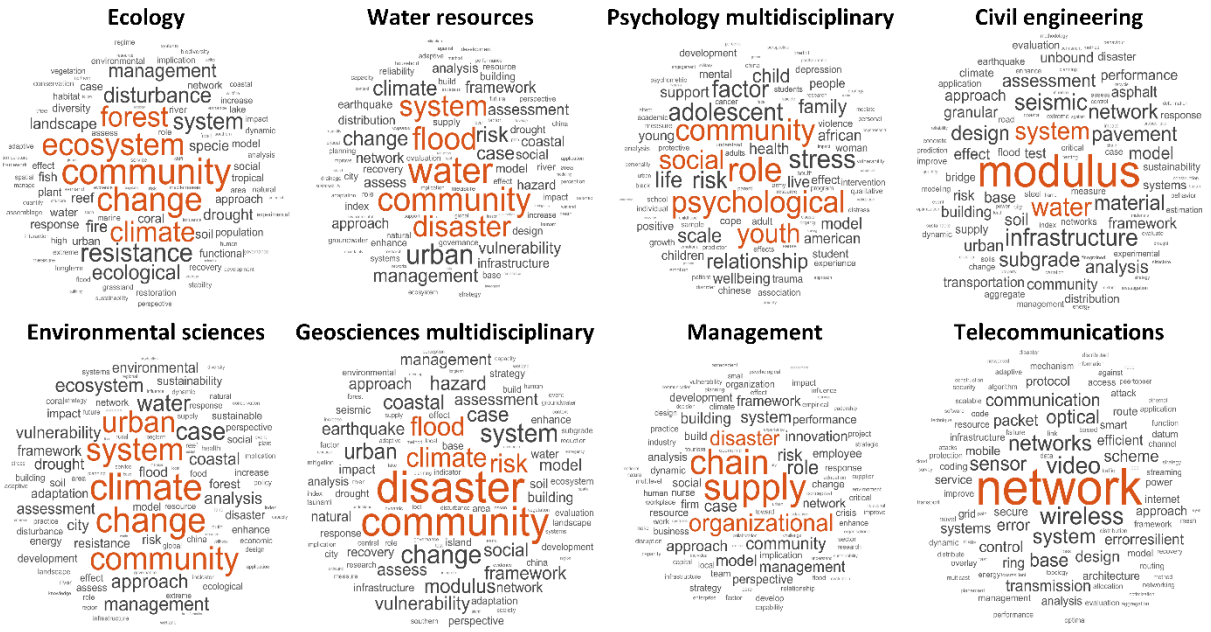

Figure 2.1 World cloud of the titles of the 500 most cited articles from Web of Science under the search term "resilience" for each discipline.

2.2 Resilience of what to what

Given that resilience has a broad meaning and can be interpreted in multiple ways, it is important to specify the context in which it is being used, both in terms of the system being considered and of the threats to the system (Carpenter et al., 2001; MacAskill & Guthrie, 2014). Carpenter summarises this as "resilience of what and to what" (Carpenter et al., 2001).

2.2.1 The city and its infrastructure

The town of Dunwich in the UK used to be a major port, and has been gradually eroded away by the sea, yet the UK as a country has successfully absorbed the change, by gradually adapting and shifting capacity to other ports (Hudson et al., 2012). The example shows that resilience can exist at different scales; what may look like failure at the city scale may be a necessity for resilience at larger scales. A look at history shows that cities have tend to recover sooner or later from a disaster, though perhaps to a different form than before the event (Vale & Campanella, 2005). Furthermore, some states are highly resilient, for example poverty, a dictatorship, or dependence on fossil fuels, and are difficult to change, and yet are not desirable (Martin-Breen & Anderies, 2011; Meerow et al., 2016). Therefore, assessments need to specify what is being resilient.

This thesis focuses on the resilience of urban infrastructure services. Ensuring provision of basic services in cities has been identified as a priority nationally and internationally (Cabinet Office, 2011; UNISDR, 2015a), and people living in cities are highly dependent on infrastructure services such as water, transport, power, and communications (Godschalk, 2003). Those infrastructure services are generally provided in cities through infrastructure systems. The focus is primarily on civil infrastructure networks including water and transport

systems, but a holistic approach is taken to account for interdependencies between infrastructure systems.

An infrastructure system is defined as an "integrated socio-technical system that delivers a service to society" (Di Mauro et al., 2010). The boundaries of infrastructure systems are challenging to define, as infrastructure extends over large areas, and involve not just physical assets, but also operators, maintenance and repair processes, supply chains, and the customers themselves (Di Mauro et al., 2010). A useful framework for representing infrastructure was proposed by Butler et al. (2014), and a similar framework was also proposed by Zaghi et al. (2016). Both frameworks distinguish:

1. **The hazard**, or forces caused by an event (e.g. ground shaking, flood waves, wind)
2. **The damage**, or physical impairment of a component (e.g. a broken pipe, damaged tank)
3. **The loss of service**, or decrease in performance of the system (e.g. lack of water supply)
4. **The consequences for people and businesses** (e.g. closure of a hospital)

Given that infrastructure systems are interdependent (i.e. failure in one system can cause failure in another), there has been a lot of research on cascading failures among infrastructure sectors (Ouyang, 2014; Rinaldi et al., 2001). Electricity networks are most likely to cause cascading failures in other systems (Pescaroli & Alexander, 2016), but civil infrastructure including water supply, drainage, and roads also need to consider their interdependence with other systems. Reiner and McElvaney (2017) suggest that all systems are dependent on roads for their operation (e.g. operators travelling to site, carrying out maintenance), as well as when recovering from a hazard. Dong et al. (2020) for example model how disruption to roads affects can affect drainage systems. Other studies have modelled the dependence of water supply on electricity, showing that the consequences of a hazard (e.g. an earthquake or flood) are greater

when this interdependency is taken into account (Adachi & Ellingwood, 2008; Guidotti et al., 2016; McDaniels et al., 2007; Rinaldi et al., 2001).

2.2.2 Multi-hazard events

Infrastructure systems need to manage a variety of hazards, from both natural and human sources (Butler et al., 2014; Flax et al., 2016; Spaans & Waterhout, 2017). It is useful to distinguish shock and stress type hazards (Butler et al., 2014; Spaans & Waterhout, 2017). Shocks refer to acute, infrequent and severe events (e.g. earthquakes, storms, terrorist attack), while stresses represent chronic, frequent and low impact events, that can take a toll on the system over time (e.g. asset deterioration). Specifically, stresses are used here to mean damage that does not lead to a loss of service (e.g. a small pipe leak in a water supply network, or a single traffic accident in a road network), while shocks refer to damaging events that lead to a loss of service Butler et al. (2014) distinguishes acute shocks and chronic stresses.

Reliability standards in infrastructure systems generally account for stresses (Butler et al., 2014; Mattsson & Jenelius, 2015), but other strategies (e.g. resilience) are needed for addressing shocks (Butler et al., 2014). In particular, there is an interest in the possibility of using resilience strategies to address surprise events (Aven, 2015). Surprises may occur because a shock exceeds the magnitude of previously experienced shocks, but are more often the result of interactions between events. For example, the Fukushima disaster was the result of an unprecedented magnitude earthquake that triggered a tsunami, and also damaged a nuclear power plant (Lekkas et al., 2011).

Disasters are increasingly seen to result from complex interactions between events (Pescaroli & Alexander, 2016). Studies have discussed different types of interactions. The idea of ‘normal accidents’ was introduced by Perrow (2011) to refer to an alignment of multiple low

consequence events, that together create a disaster. Perrow (2011) mainly discussed normal accidents in the context of industrial risk, and suggested that such events are a feature of tightly-coupled complex systems, such as nuclear power plants. Similar to normal accidents is the Swiss Cheese model (Ayyub, 2014), which views disasters as events that occur when multiple layers of defence are breached at the same time by random chance. While normal accidents and the Swiss Cheese model refer to an alignment of events that are not individually damaging, a 'perfect storm' is often thought of as a combination of multiple extreme or damage events occurring at the same time (Aven, 2015). Similarly, De Ruiter et al. (2019) describes 'consecutive disasters', as two damaging events that affect a system in sequence, before the system has had time to recover. Studies are also increasingly referring to 'compound hazards', to mean combinations of hazards that have a common root cause. Compound events are especially studied in relation to climatic hazards (Couasnon et al., 2020; Leonard et al., 2014; Matthews et al., 2019; Wahl et al., 2015; Zscheischler et al., 2018), such as compound river and coastal flooding. Compound events generally involve some level of statistical dependence between hazards (Leonard et al., 2014). Distinct from compound events are hazard cascades, where one hazard triggers another, for example and earthquake triggering a landslide or a tsunami, which are more commonly studied through physically based modelling (Tilloy et al., 2019). Pescaroli and Alexander (2018) distinguish compound, interacting, interconnected, and cascading hazard types, by stating that "while interconnected risk can be seen as one of the preconditions for the manifestation of cascades, compound and interacting dynamics can influence its magnitude". These examples from the literature show the range of events that could affect the resilience of a system.

For clarity, the hazards described in the literature are summarised here as different combinations of shocks and stresses. Normal accidents are considered to be a combination of

multiple stresses (i.e. high-probability low-magnitude events) occurring at the same time; perfect storms are considered to be two or more shocks (i.e. low-probability high-magnitude events) occurring at the same time; and consecutive disasters are considered to be two or more shocks occurring one after the other. Other combinations are also possible, for example a shock occurring at the same time as a stress and leading to amplified consequences.

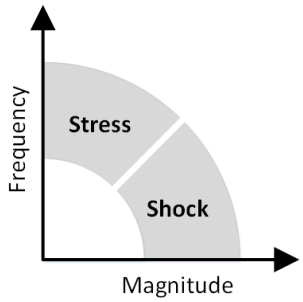

Figure 2.3 The difference between shocks and stresses. Stresses generally refer to frequent, low magnitude events, while shocks refer to low frequency high magnitude events.

The events described so far do not address the relation between hazards in space. Yet for infrastructure systems that extend over large areas, distinguishing where the damage occurs is also important. Kappes et al. (2012) identify four cases, each with different implications, based on whether the hazards occur in the same place or in different places, and at the same or at a different time (Table 2.2).

Table 2.2 Implications of different combinations of events for infrastructure systems, adapted from (Kappes et al., 2012).

	Same time	**Different time**
Same place	Implications for damage to components, for example a combination of wind and storm surge could damage a tank that would resist the events happening individually (Bernier & Padgett, 2019).	Implications for design, for example a building with a lightweight roof structure is a better choice for earthquakes, but the building would be more vulnerable to wind (Li et al., 2012).
Different place	Implications for performance, through interactions at the system or network level (Zaghi et al., 2016).	Possible implications for long term decisions, relating to adaptation, supply chains.

For infrastructure networks, same place is taken to mean that the two affect the same component or set of components (e.g. same node or link in a network), while same time is taken to mean that there is an overlap between the impacts of the two events (i.e. the second event occurs before the system has recovered from the first event).

There are a few examples where hazards have combined to affect infrastructure systems in complex ways. In 2010, the Pacaya volcanic eruption in Guatemala was closely followed by storm Agatha. The ash from the volcano blocked drains, and exacerbated flooding caused by the subsequent storm (Gill & Malamud, 2014). In another example, the Christchurch earthquake in New Zealand in 2011, was followed by widespread damage to drainage systems resulted in increased severity of rainfall flooding, years after the event (Cavalieri et al., 2016).

2.3 Measuring resilience capacities in infrastructure systems

Section 2.1 showed that resilient infrastructure services means having the capacity to absorb, recover, and adapt to various events. This section discusses examples of studies that measure and address these resilience capacities in urban water and transport systems. The aim is to provide an overview of how resilience concepts can be implemented in practice. Where possible, studies are identified that consider multiple hazards.

2.3.1 Absorbing

Absorptive capacity can be considered to be the ability of an infrastructure system to undergo damage and still provide adequate levels of performance. There are many studies on the absorptive capacity of systems, although studies may refer to it with different names (e.g. vulnerability analysis, global resilience assessment, stress testing) (Diao et al., 2016; Galvan & Agarwal, 2020; Hu et al., 2016; Mugume et al., 2015; Murdock et al., 2018; Shiraki et al.,

2007; Wang et al., 2019). Generally speaking, systems with high absorptive capacity can provide good performance even after being severely damaged, while systems with low absorptive capacity show large losses in performance under limited damage.

Often, absorptive capacity is represented using a system response curve, obtained through modelling the system response to incremental numbers of failures (Diao et al., 2016; Mugume et al., 2015; Murdock et al., 2018; Shiraki et al., 2007; Wang et al., 2019). The system response curve relates the number of failures (or hazard magnitude) to the level of performance of the damaged system. Figure 2.4 shows some example response curves for water supply and wastewater networks (Diao et al., 2016; Mugume et al., 2015). Diao et al. (2016) for example assessed the absorptive capacity of water distribution networks to four different failure modes, including pipe break, pump failure, changes in demand, and substance intrusion. For each failure mode, failures were applied stochastically to the system. The curves in Figure 2.4 show the minimum and maximum performance recorded across multiple stochastic failure scenarios. By analysing the absorptive capacity of water supply systems to different hazards (or failure modes), Diao et al. (2016) identified a design trade-off at the system level between two types of hazards. Specifically, they found that increasing storage capacity in a water distribution system makes the system perform better in the event of pipe breaks, but perform worse in the event of substance intrusion (i.e. contaminants entering the water supply).

Some studies have tried to identify general system properties that correlate with absorptive capacity. For example, diversity of function makes ecosystems better able to absorb shocks (Elmqvist et al., 2003), and can also be beneficial in water supply services subject to shocks (Mostafavi et al., 2018). Specifically, Mostafavi et al. (2018) shows that following the Ghorka earthquake in Nepal, there was no severe water shortage in Kathmandu despite damage to the centralised water supply network. The reason was that a diversity of water sources were readily

available at the time of the earthquake, including water trucks ready to be dispatched, and water storage tanks in houses -the result of an unreliable centralised water supply pre-earthquake, that made alternatives necessary-. Assessing the level of diversity in a system is therefore one possible indication of its ability to absorb a shock. Todini (2000) looks for properties of absorptive capacity specifically in water distribution networks, and proposes the total amount of extra pressure at nodes as a good indication of the ability of the network to maintain performance under pipe breaks. According to Dunn (2014), identifying properties that tend to correlate with better performance in response to shocks in networks, and increasing those properties in existing networks, is an effective strategy for managing risks from surprise events.

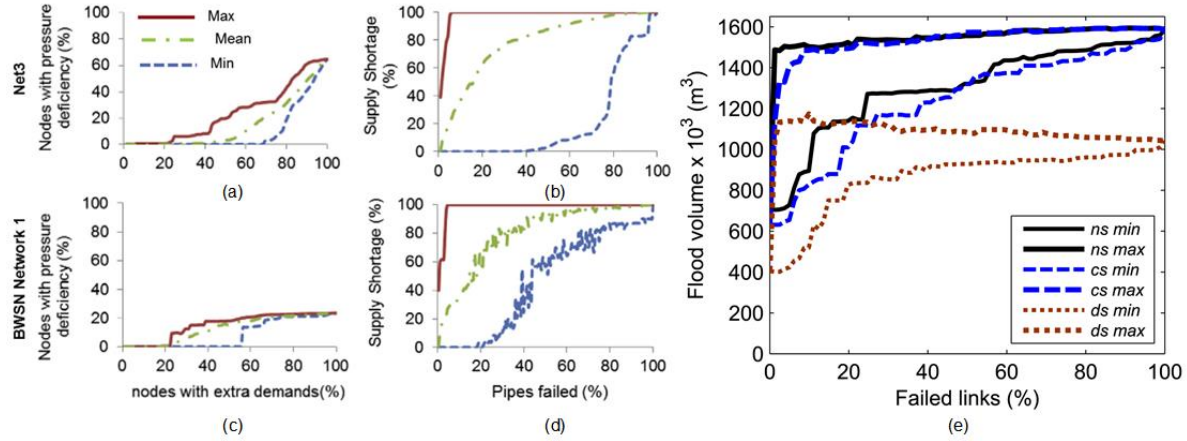

Figure 2.4 Examples of system response curves for (a) – (d) water supply and (e) wastewater. Figures (a) to (d) from Diao et al. (2016) and Figure (e) from Mugume et al. (2015).

In graphs, a relation exists between the node degree distribution, and the ability to absorb shocks (Dunn et al., 2013). Generally, nodes with broader degree distributions (i.e. a few highly connected nodes) perform better under random failures (Dunn et al., 2013). However, Buldyrev et al. (2010) demonstrates that the same properties that improve the ability of single networks to absorb random failures (i.e. a broad degree distribution), instead lead to a less absorptive

capacity in interdependent networks. Networks can also show different levels of performance depending on where in the network damage occurs. For example, Bozza et al. (2017) model the road network performance of a small city in Italy to two hazards (a landslide and earthquake). The earthquake caused damage throughout the city, while the landslide damage is focused in one part of the city. Although a similar number of roads are damaged by each of the hazards, the pattern of damage caused by the earthquake is more severe for the performance of the network. Others also try to identify parts of networks (i.e. nodes or links) that are most critical for the performance Lhomme et al., 2013).

2.3.2 Recovering

In some systems, recovery happens naturally after a shock or stress. For example drainage networks recover naturally from excess rainfall, as water eventually drains away; similarly, road networks recover naturally from a snow event when the snow melts (Hu et al., 2016; Mugume et al., 2015). In those cases, the process of recovery is relatively simple to model. However in other cases, recovery is an intentional process which requires strategic planning and involves decisions on prioritisation and allocation of resources.

Kammouh et al. (2018) collects restoration times for water, gas, energy, and communications from multiple earthquakes events, and uses the information to estimate average time needed to restore systems after an earthquake. The time to recovery is shown to be very variable between events, and not necessarily related to the magnitude of the earthquake. On average, energy systems are often the fastest to recover.

Others develop models of the recovery process which can be used to compare different recovery strategies (Cavallaro et al., 2014; Miles & Chang, 2011; Tabucchi et al., 2010). For example, Cavallaro et al. (2014) compares post-earthquake reconstruction strategies for the

city of Acerra in Italy. Kong et al. (2019) models a consecutive hurricane and flood scenario on the energy system (electricity, oil, and gas) for the city of Toronto in Canada. The scenario is based on a historical event, Hurricane Hazel, that affected the city in 1954. The study compares two restoration strategies, one where restoration begins immediately after the hurricane damage, and another where it begins after both hazards have occurred. Interestingly, the consequences are lower if restoration begins immediately after the first event (Kong et al., 2019). The study also demonstrates that the consecutive event affects disproportionately more people than the individual events. Some studies try to identify general strategies for networks that result in the most effective recovery process. For example, Hu et al. (2016) compare strategies for recovering from localised failures, including reconnecting the largest population to the network, or reconnecting edges.

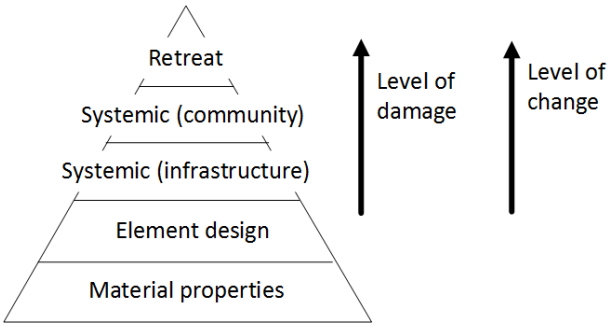

Figure 2.5 framework for relating incremental damage to opportunities for change. Figure reproduced from MacAskill and Guthrie (2014).

Some consider the ability to recover to a better state than before the failure (Fang & Sansavini, 2017; MacAskill & Guthrie, 2014; Taleb, 2012). The property of being strengthened after a failure sometimes referred to as 'antifragility' (Taleb, 2012). Some industries, such as the space and airline industry, are considered antifragile because any failure generally leads to improving processes and procedures so that the same failure cannot be repeated (Taleb, 2012). Fang and Sansavini (2017) show that energy networks can be antifragile by incorporating changes to the

network after a failure. In the context of water infrastructure, MacAskill and Guthrie (2014) propose a framework that shows that incremental levels of damage also unlock increasing opportunities for change and improvement.

Others show the importance of accounting for population behaviour in post-disaster recovery. Bagheri et al. (2010) show that the influx of reconstruction workers to the city after the Bam earthquake in Iran significantly increased water demand, and was the main reason for a water shortage. Guidotti et al. (2019) on the other hand shows that evacuation of the population following an earthquake in Seaside, Oregon, reduces water demand and means that performance was higher than what would be assumed if water demand stays constant. Didier et al. (2018) provide a comprehensive mathematical framework for measuring performance based on the relation between service supply and demand.

2.3.3 Adapting

Adaptability is the ability to change and evolve in order to maintain or improve the ability to absorb and recover from hazards under changing conditions (Meerow et al., 2016). According to Sage et al. (2015), adaptability is the ability of a system to adapt its structure, but not necessarily its function, in response to long term changes. Although adaptability is included within many definitions of resilience, few studies discuss how the adaptability of infrastructure can be measured and increased in practice (Sage et al., 2015). Some consider adaptability to mean the ability to find substitutes in the short term (Mostafavi et al., 2018; Rose, 2004). However, this ability is part of system properties that enable absorption. Instead, adaptability here refers to implementing long term and usually irreversible changes.

Improvements to adaptive capacity can come from techniques for making decisions under uncertainty. Haasnoot et al. (2013) introduced the technique of adaptation pathways to support

policy making on flood risk management in the Netherlands. The technique of adaptation pathways provides a road map in time, showing when adaptation measures will need to be implemented in order to be effective in the context of long term change. The technique has been used mostly for flood risk management, but has also be trialled in planning transport infrastructure.

Some studies model systems under long term changes (Makropoulos et al., 2018; Ning et al., 2013), while others prefer to use narratives for describing the evolution of systems (Markolf et al., 2018; Tellman et al., 2018). Markolf et al. (2018) for example use a narrative approach to look at the issue of rising sea-levels in Miami. The government in the city of Miami recently invested in pumping systems that can pump out excess water from the city. However, pumping stations represent a significant cost for the city, which is recovered by collecting tax money. Yet to recover the high cost of implementing pumping stations, municipal authorities may be tempted to allow more commercial development in coastal areas, where economic benefit are high and could raise tax revenues. However, construction in coastal areas will in turn require higher levels of protection, which will increase costs, encourage more development to recover the cost, thus locking the city into a pathway where it is reliant on increasing investment into infrastructure to fight off rising sea levels, and where alternative options such as relocation become increasingly unviable (Markolf et al., 2018). Tellman et al. (2018) describes the evolution of the water system of the city of Mexico over multiple centuries, driven by an interplay between society, the natural environment, and technical developments.

Sage et al. (2015) integrates absorption and recovery with adaptability, by exploring response to shocks under future scenarios. For example, in a future scenario where transport has largely shifted from cars to bicycle transport, flooding could lead to lower disruption to transport than under present conditions, but snowy days could lead to greater disruption to transport.

Although adaptability may appear to be a property of social systems, physical assets can also have adaptability. De Neufville & Scholtes (2011) show that making systems adaptable when designing for uncertain conditions is cost effective. They discuss five characteristics that can make physical systems adaptable:

1. Phased design (building in small units as more information becomes available)
2. Modular design (a plug-and-play approach),
3. Design for expansion (designing the built in capacity to expand in size)
4. Platform design (designing a common core that can accommodate multiple added parts)
5. Shell design (including extra capacity without attributing it a function, for example extra rooms within a hospital building)

Djalante et al. (2011) argues for the value of multi-stakeholder platforms as a method for adaptability. Multi-stakeholders platforms are essentially decision making bodies, either voluntary or statutory, that bring together stakeholders that perceive the same management problem, are aware of their interdependence in solving it, and come together to agree on strategies for solving the problem. Integrating knowledge from across disciplines is also considered valuable for resilience within engineering (Davidson, 2015; Pearson et al., 2018), and engineering education (Pearson et al., 2018).

2.4 Overview and research needs

The review aimed to show methods that are commonly used for addressing resilience in infrastructure systems. Methods are seen to range from conducting stress tests on infrastructure models, to understanding and modelling the infrastructure recovery process, all the way to exploring long term interactions between infrastructure, the natural environment and society. MacAskill and Guthrie (2014) highlighted that the meaning of resilience depends on the

context in which it is used. Arguably, the methods that are most appropriate for measuring and increasing resilience will also vary with context. Figure 2.6 shows an example of how resilience priorities may vary when considering the system at different levels (e.g. single physical component, physical network, complex system, complex adaptive system) and external conditions (e.g. stability, uncertainty, or rapid change).

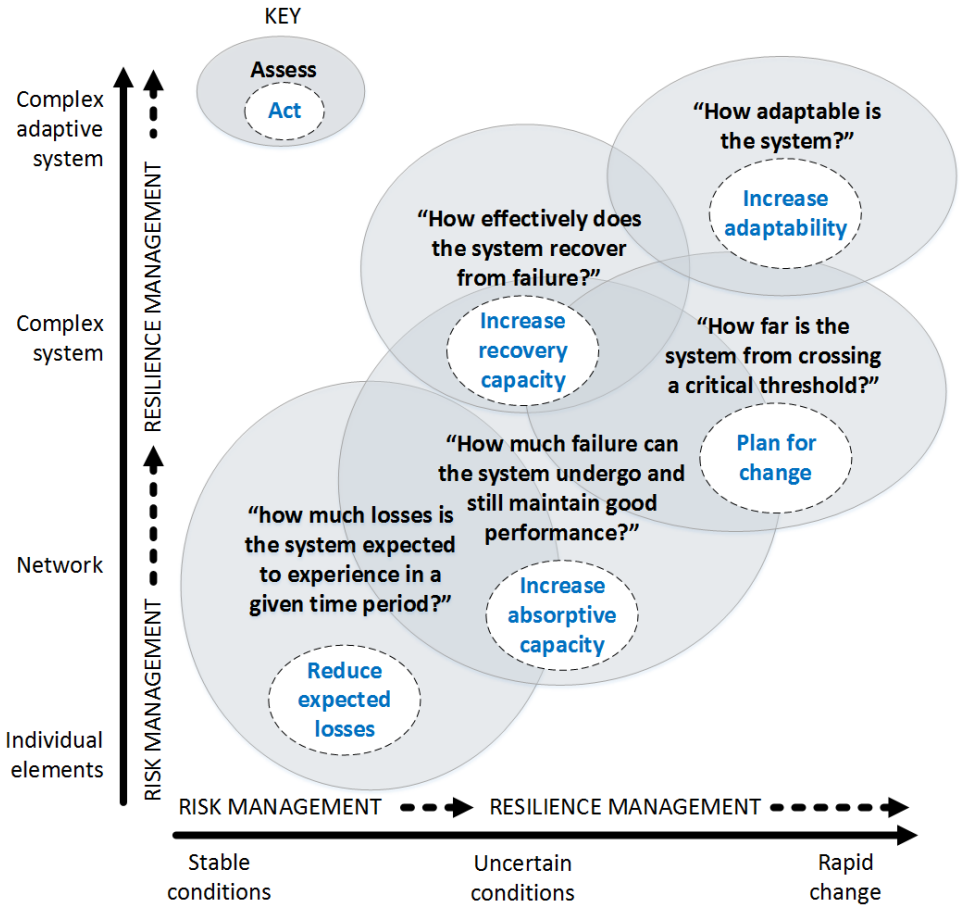

Figure 2.6 Resilience activities considered most relevant for different external conditions (e.g. stability, uncertainty, change) and system characteristics (e.g. single physical component, network, complex system, complex adaptive system).

Risk management is generally considered to be most suitable at the level of single elements, and for addressing hazards that are well understood (Ayyub, 2014; De Bruijn, 2004). The objective of risk management is generally to accurately assess the probable losses, and reduce

those losses to a level that is at the same time tolerable and affordable (Ayyub, 2014; Hudson et al., 2012). However, for hazards that are more uncertain, such as extreme or combined events, probable losses can usually not be accurately determined and a risk approach is often not viable.

To address uncertain events, an alternative to risk management is to focus on ways of maintaining the performance of the system even once parts of the system become damaged. Here, system response curves (i.e. relationships between the damage and performance of the system as a whole) are a useful tool. System response curves can quantify the amount of damage that the system can absorb. However, several limitations are also identified. First, modelling all possible failure combinations to produce comprehensive response curves, for example as in Diao et al. (2016), is computationally expensive, and the number of scenarios required for a comprehensive analysis increases rapidly with larger systems. According to Galvan and Agarwal (2020) "the number of disruption scenarios is necessarily smaller than the complete set of scenarios by orders of magnitude". Second, the results can show a very large spread of possible outcomes (e.g. Figure 2.4 (b)), making it of limited value to support decision making. Third, Diao et al. (2016) shows that the same characteristics that allow a system to absorb one type of hazard can also decreases its ability to absorb another type of hazard.

The limitations identified can be overcome when hazard information is included to narrow down the range of scenarios. By using information such as flood maps or landslide susceptibility maps, it might be possible to delimit the spatial extents, and therefore define a subset of components of the system likely to become damaged. This approach could still consider the hazards as uncertain and model a full range of plausible events. But by including characteristics of the hazard into the model, current limitations of response curve modelling, and the difficulty of extending the approach to multiple hazards, could be overcome.

To further reduce losses, absorption should be complemented with recovery measures, to minimise the downtime of the system when it fails. The recovery process may be influenced by factors like population movements (Guidotti et al., 2019) or interdependencies between infrastructure, population, and businesses (Miles & Chang, 2011), possibly requiring wider system boundaries and models that can represent complex systems, or complex adaptive systems (Bagheri et al., 2010; Dawson et al., 2011).

Modelling recovery may pose a bigger challenge than modelling damage, as it requires defining a restoration strategy (Hu et al., 2016), and few studies to date have modelled disaster recovery in the context of multiple hazards (Kong et al., 2019; Wisetjindawat et al., 2017). Nevertheless, the examples available reveal that the combined effects of two hazards on system performance (including recovery) can be bigger than that of the single hazard (Kong et al., 2019; Wisetjindawat et al., 2017), and that the optimal recovery strategy may be to start repairs immediate on the system after the first hazard, rather than to wait until after the system has been damaged by both hazards (Kong et al., 2019).

Where rapid change is necessary, planning for recovery to 'normal' may become a lower priority than enhancing the adaptability of the system. Adaptability can be enhanced in those cases through techniques for thinking about the future (e.g. Kwadijk et al., 2010; Rogers et al., 2012).

Based on the reviewed literature, the following directions for future research are identified: analyse the hazard environment of cities and distinguish places that may require different resilience approaches; supplement a response curve analysis with information on real hazards to narrow down the range of relevant scenarios; model and better understand the consequences of consecutive events on networked infrastructure.

This page was intentionally left blank

Chapter 3. Assessing the exposure of urban systems to earthquakes, floods, wind, and landslides

3.1 Introduction

Natural hazards that occur in urban areas pose a considerable challenge, due to the complexity and interdependence of systems on which the urban population depends (UNDRR, 2019). Cities are in constant flux and characterised by daily cycles of people commuting to and from work, schools, shopping, and entertainment. The flows of people, resources, and services in cities are highly dependent on interconnected infrastructure networks (Chang et al., 2007). Hazard impacts to these networks (e.g. flooding of a major road) can cause disruptions that propagate to other parts of the city (e.g. traffic congestion and delays), causing cascading consequences on other systems (Rinaldi et al., 2001). Therefore, urban areas have become a focus of efforts to address hazards (Godschalk, 2003).

While individual infrastructure sectors may be equipped to deal with damage from localised accidents (e.g. a pipe burst in a water supply network), they are mostly not equipped to withstand a low-frequency, high-consequence event (Butler et al., 2014). Yet the proximity and connectedness between systems means that a failure in one system is likely to generate cascading failures in other systems (e.g. roads could be blocked by debris from buildings after an earthquake, which could interfere with repairs to the water supply system). While stakeholders often have a relatively clear understanding of the challenges faced within their own sector (Ciurean et al., 2018), the extent to which urban systems as a whole are exposed to multiple types of hazards is still unclear.

Meanwhile, the availability, quality, and coverage of open hazard data has improved steadily (Simpson et al., 2014). Global hazard maps are now available for various hazards, free of charge, from online platforms such as the Data Portal of the EU Joint Research Centre (JRC) (https://data.jrc.ec.europa.eu/), the GFDRR GeoNode (https://www.geonode-gfdrrlab.org/), and the PREVIEW platform by the United Nations Environment Programme (Giuliani & Peduzzi, 2011) (https://preview.grid.unep.ch/). These platforms make hazard information increasingly easy for anyone to access. Specifically, The Global Facility for Disaster Risk Reduction (GFDRR) and the World Bank recently developed a tool aimed at raising awareness of possible hazard exposure, intended to provide information for development projects in data scarce regions (http://www.thinkhazard.org/).

Overall, global hazard data is now available for various hazards (e.g. river floods, cyclones, earthquakes, or landslides) at high resolution. These global datasets have been used in a number of previous studies to look at exposure of people, wealth, or infrastructure to single hazards (Pesaresi et al., 2017; Ward et al., 2020), and to combinations of multiple hazards (De Ruiter et al., 2019; Dilley et al., 2005; Gill & Malamud, 2014; Gu, 2019; Jongman et al., 2012; Koks et al., 2019; Shen et al., 2018).

For example, Dilley et al. (2005) estimated that approximately 790 million people are directly exposed to at least two hazards, and that 105 million people are exposed to three or more hazards. The study considered exposure to earthquakes, floods, cyclones, landslides, volcanic eruptions, and droughts, and included both urban and rural populations. More recently, Gu (2019) assessed exposure to the same six hazards but focusing on urban areas, and found that 14% of cities are highly exposed to at least two hazards. The study also mapped cities based on the number of different hazards faced (Figure 3.1). Their objective was to inform urban planners and policy makers on the need to “strengthen resilience, improve preparedness, and

adapt strategies of cities to address the effects of natural disasters" (Gu, 2019). However, the study does not distinguish between the types of hazard combinations faced in each city. Yet a city facing for example earthquakes and landslides will require very different types of adaptation measures for resilience than a city exposed to river and coastal flooding.

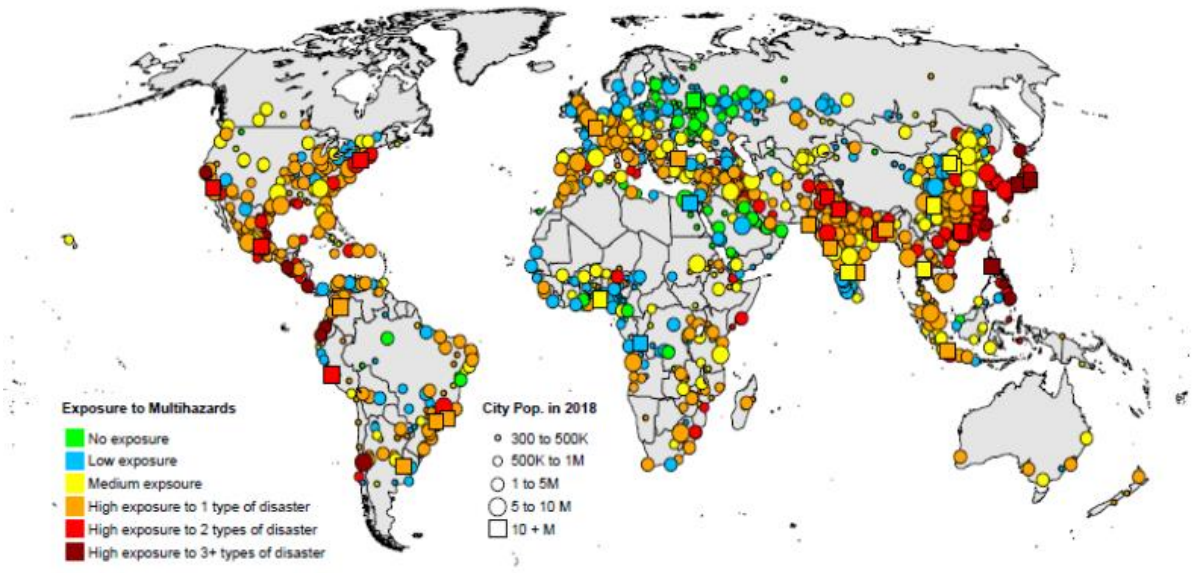

Figure 3.1 The location of cities by population size and level of exposure to natural hazards. Figure from Gu et al. (2019).

The aim of this chapter is therefore to analyse the exposure of cities to combinations of hazards, while specifically distinguishing the types of hazards that co-occur spatially. The remainder of this chapter is structured as follows. Section 3.2 introduces the hazard and urban area datasets used, and explains how the data is processed to enable comparison across different hazard types. Section 3.3 shows the number of cities and the population exposed to combinations of hazards, and describes how the information is evaluated. Section 3.4 then highlights three combinations of hazards that are found to be relatively common, discusses potential uses of the data, and presents the limitations of the study. Section 3.5 provides conclusions.

3.2 Data and methods

The datasets used in this study include the spatial distribution of earthquakes (Cardona et al., 2014), river floods (Dottori et al., 2016), coastal floods (Muis et al., 2016), cyclone wind (Cardona et al., 2014) and landslides (Nadim et al., 2006), and the extent of urban areas (Moreno-Monroy et al., 2020). All of the data used has previously been made openly available by the authors of the datasets, which allows the results of the present study to be reproduced.

3.2.1 Urban areas data

After reviewing different options (e.g. Balk et al., 2006; Florczyk et al., 2019), the boundaries of urban areas are represented by the Functional Urban Areas (FUA) dataset by Moreno-Monroy et al. (2020). The FUA dataset has been developed to map city centres and their surrounding area of influence (or commuter area) globally using a consistent methodology (Figure 3.2). Specifically, urban areas in the FUA are defined based on observed population densities, built up area, and roads. Moreno-Monroy et al. (2020) trained a classification model with existing functional urban area boundaries from OECD countries, before applying it worldwide. The urban areas therefore have a physical meaning. Specifically, each FUA is considered to be a node of densely interconnected infrastructure systems. FUAs correspond to city centres and their surrounding area of influence from where people travel into the centre for work and leisure. The data can be obtained at https://ghsl.jrc.ec.europa.eu/download.php.

In total, the dataset identifies more than 9,000 urban areas across five continents. It includes all urban areas with populations of 50,000 or more. Collectively, this represents a total urban population of 3.9 billion people. Figure 3.2 shows examples of some of the functional urban areas. Urban centres with more than one densely populated cluster of 500,000 inhabitants or more are divided into separate FUAs (Moreno-Monroy et al., 2020). Also, urban centres are

divided up if they have more than 20 million inhabitants and a surface area of at least 2,500 km^2, around identified densely populated city centres within the area of influence. Figure 3.2 shows for example that Hong Kong is divided into several functional urban areas, while London is represented as a single large functional urban area.

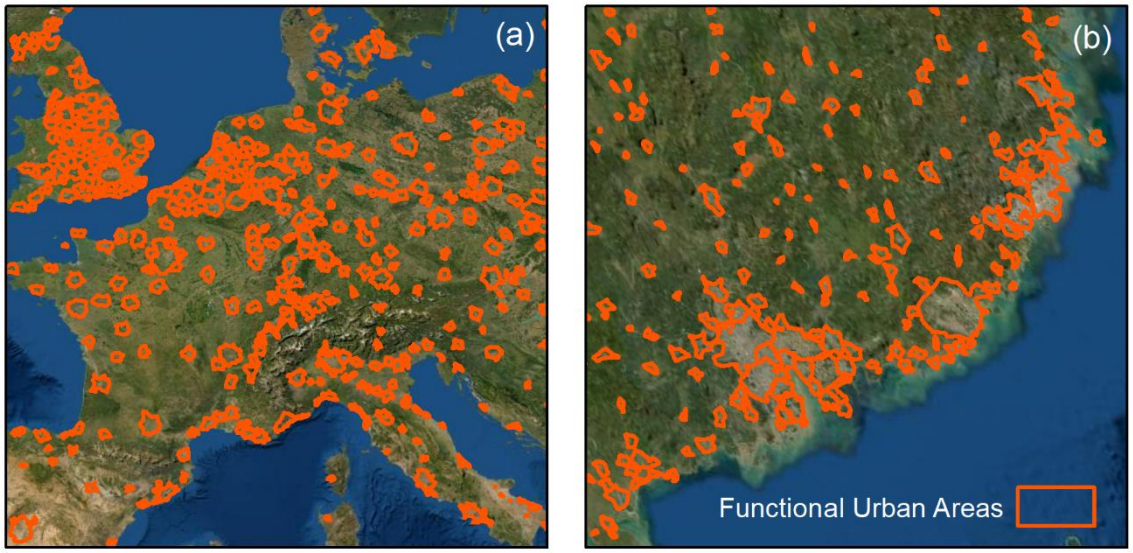

Figure 3.2 Urban areas used in this study. Sample from (a) Western Europe (b) Southern China. The data comes from the Functional Urban Areas dataset (Moreno-Monroy et al., 2020).

3.2.2 Hazard data

The difference in hazard severity between cities is determined by using hazard maps from probabilistic hazard models. The advantage of using outputs from hazard models is that the models are informed by hazard events that occurred in the past, but complement this information to also represent the hazard in areas where they have not previously been recorded, but could occur. The probabilistic maps show the distribution of hazard intensity for various return periods. A short summary of the datasets used for each hazard are provided in the following paragraphs. Full information on how the hazards maps were produced can be found in the original publications.

Earthquake hazard is represented by maps of earthquake acceleration produced for the UNISDR Global Assessment Report 2015 (Cardona et al., 2014), available from https://risk.preventionweb.net. The earthquake hazard map represents the expected peak ground acceleration (in cm/s^2) in each grid cell due to all possible earthquake sources, modelled using Probabilistic Seismic Hazard Analysis, for return periods between 250 and 2475 years (Cardona et al., 2014). The data has a resolution of 0.5 degree (approximately 50 km).

River flooding is represented by flood maps from the Joint Research Centre of the European Commission (Dottori et al., 2016), available at https://data.jrc.ec.europa.eu/collection/floods. The maps provide flood depth globally at 30 arc-second resolution (approximately 1 km) for return periods between 10 and 500 years. The flood maps use streamflow data from the Global Flood Awareness System (GloFAS) and a two-dimensional hydrodynamic model (AC2D). As the streamflow is based on coarse resolution climate data, the data excludes flooding for catchments smaller than 5000 km^2, and flood defences are not represented in the dataset (Dottori et al., 2016).

Coastal flooding is represented using flood maps by Muis et al. (2016), available from https://www.geonode-gfdrrlab.org/. The maps represent coastal flooding due to storm surges and tidal effects. The data comes from a coastal hydrodynamic model forced by climatic reanalysis data from ERA-Interim. Data is provided at 30 arc-second (approximately 1 km) resolution. As with river flooding, the coastal flood maps do not include the presence of flood defences. The maps also exclude the effects of land subsidence (Muis et al., 2016).

Tropical cyclone wind is represented by hazard maps for the UNISDR Global Assessment Report 2015 (Cardona et al., 2014), available from https://risk.preventionweb.net. The cyclone hazard maps show the probable 3-second gust wind speed (in km/h) for return periods between 25 and 250 years, at 1 degree (approximately 100 km) resolution. The data is based on

probabilistic modelling of historical tropical cyclone tracks. The model takes into account the effects of higher surface roughness in urban areas. The data does not include other causes of extreme wind such as extra-tropical cyclones and convective storms.

Landslides are represented using the landslide hazard map developed for the Natural Disaster Hotspots study (Nadim et al., 2006), available from https://sedac.ciesin.columbia.edu/. Landslide occurrences are usually triggered by other hazards such as earthquakes and extreme rain, and are difficult to represent probabilistically in the same way as earthquakes, floods, and cyclones. The data by Nadim et al. (2006) provides the gridded landslide hazard by combining both susceptibility and triggering factors. The result is a hazard map with grid cells classified into five classes (6-10). Each class is associated with an estimated number of occurrences per million years (see Table 3.1). The data is provided at 2.5 arc-minute (approximately 5 km) resolution.

3.2.3 Hazard severity levels

Comparing across hazards is a common difficulty in multi-hazard studies, as hazards have different characteristics and are measured through different parameters (e.g. ground acceleration, water depth) (Kappes et al., 2012). Often, hazards are compared based on their consequences (e.g. the number of people affected, the total cost of the damage). By measuring the consequences, an assumption is made about the vulnerability of the exposed elements (e.g. buildings, people), or how fragile or susceptible to damage they are.

To classify hazard values into severity levels, the same approach as the one implemented in the ThinkHazard! tool is selected for this study (Fraser et al., 2016). The ThinkHazard! tool classifies hazards into four hazard severity levels. The four levels correspond to:

1. **High**: Potentially severe damage from this hazard. Without taking measures to mitigate the hazard and risk, high levels of damage can be expected to occur within the project or human lifetime.
2. **Medium**: Potentially damaging effects of this hazard. Potentially damaging events can be expected to occur within the project or human lifetime and measures to mitigate the hazard and risk should be considered.
3. **Low**: Potentially damaging events are less likely to occur within the project or human lifetime but are still possible. Measures to mitigate the hazard and risk would be considered at critical locations. There is still potential that damaging events could occur during the project or human lifetime.
4. **Very low**: Available data suggest that potentially damaging effects are unlikely to occur, on average, in the project or human lifetime. There is still potential for damaging events.

Note that the levels correspond to hazard levels and do not indicate vulnerability; two cities with the same hazard severity can have different levels of vulnerability to the hazard, and experience different losses from the same hazard event. The levels represent the damage expected if no mitigation measures are provided. It provides an estimate of the amount of mitigation that a location requires to make sure that people, structures, and critical activities are safe. Table 3.1 shows the return period and intensity values used for each hazard and hazard level.

Earthquake severity is based on the frequency and peak ground acceleration (PGA) of earthquakes. *High* severity means that the a PGA exceeding 196 cm/s^2 (one fifth of the acceleration of gravity) is experienced on average once every 250 years. According to Worden et al. (2012), a PGA of 196 cm/s^2, or 0.2 g, corresponds to a Mean Mercalli Intensity (MMI)

level of VII. The MMI scale describes incremental damage levels from earthquakes. A level of VII corresponds to "limited damage in buildings with good design; slight to moderate in well-built ordinary structure; and considerable damage in poorly built or badly designed structures; some chimneys broken" (Wood & Neumann, 1931). *Medium* severity means that a PGA of 98 cm/s^2 (0.1 g) is experienced on average once every 475 years. A 1-in-475 year event has a 10% probability of occurring at least once in 50 years. A peak ground acceleration of 0.1 g corresponds to an MMI level VI, which is "felt by all, many frightened. Some heavy furniture moved; a few instances of fallen plaster. Damage slight" (Wood & Neumann, 1931). *Low* severity means that a PGA of 98 cm/s^2 (0.1 g) is experienced on average once every 2475 years. Earthquake return periods of 475-years and 2475-years are commonly used return periods in seismic design codes for buildings, bridges, and dams (Fraser et al., 2016).

Table 3.1 Values represent the lower bound of the high, medium, and low hazard levels, from Fraser et al. (2016). If the hazard is below the low hazard threshold in a given city, it is classified as very low.

	High	**Medium**	**Low**
Earthquake	196 cm/s^2 in 250 years	98 cm/s^2 in 475 years	98 cm/s^2 in 2475 years
River flood	0.5 m in 10 years	0.5 m in 50 years	0.5 m in 500 years
Coastal flood	2.0 m in 10 years	0.5 m in 50 years	0.5 m in 100 years
Cyclone	80 km/h in 50 years	80 km/h in 100 years	80 km/h in 1000 years
Landslide	250 per 1 x 10^6 years	125 per 1 x 10^6 years	63 per 1 x 10^6 years

Flood severity is based on the frequency and maximum depth of flooding. A flood depth of 0.5 metres is used as the damaging threshold for flooding. At 0.5 metres, sandbags can no longer be used to control the flooding, and water reaches the level of light switches and tables surfaces (Fraser et al., 2016). *High, medium,* and *low* river flood severity corresponds to a flood depth of 0.5 metres being exceeded on average every 10-, 50-, and 500-years. *High, medium,* and

low river flood severity corresponds to a flood depth of 0.5 metres being exceeded on average every 10-, 50-, and 100-years.

Tropical cyclone severity is based frequency and maximum wind speed. A wind speed of 80 km/h is used as the damaging wind threshold. A speed of 80 km/h falls within the 50-60 miles per hour hurricane warning threshold used by the U.S. National Oceanic and Atmospheric Administration (NOAA). On the Beaufort wind force scale, a mean wind speed of 80 km/h corresponds to a strong gale, causing "slight structural damage (chimney pots and slates removed)" (Fraser et al., 2016). The *high, medium,* and *low* hazard thresholds are defined for the threshold wind speed being reached on average once every 50-, 100-, and 1000- years, respectively. Dunn et al. (2018) showed that damage to overhead electricity lines becomes significant above 100 km/h, based on data from the UK, but the vulnerability of electricity systems may be higher (or lower) in other countries.

Landslide severity is assigned somewhat differently to the other hazards. Landslides do not have an inherent frequency of occurrence but are generally triggered by other events like rainstorms or earthquakes. Therefore, landslides maps often express the susceptibility of a location to landslides, based on factors such as slope, soil type, and vegetation, without specifying frequency (e.g. Stanley & Kirschbaum, 2017). Nevertheless, Nadim et al. (2006) produced a landslide hazard map at the global scale that combines susceptibility information and landslide triggers (rainfall and earthquakes). The resulting map expresses the average frequency with which a landslide is expected to occur within the grid cell. Landslide levels are classified based on the following conversion from the four classes of landslide hazard. The first two classes are set to *high*, the third class is set to *medium*, the fourth class is set to *low*, and the fifth class is set to *very low*. The frequency of occurrence of landslides for each class, estimated by Nadim et al. (2006), are shown in Table 3.1.

3.2.4 Data processing

To calculate exposure, hazard datasets are projected from their original geographic (latitude and longitude) coordinate reference system, WGS 1984 (EPSG:4326), to a projected (metres) coordinate reference system, World Mollweide (ESRI: 54009), or the coordinate reference system in which the urban areas dataset is provided. The projected maps are then resampled from their original resolutions to a 1 km grid, and aligned with the urban boundaries. Bilinear resampling is used for earthquake and wind data, as the distribution of intensities is relatively continuous over space, and nearest neighbour resampling is used for flooding and landslides, as they have higher spatial variability over short distances. The resampled grids are then overlaid with the urban area boundaries, and the maximum value within each urban boundary is recorded. This is repeated for each return period in Table 3.1. The hazard level (*very low*, *low*, *medium*, *high*) for each urban area is then calculated using the maximum values and the threshold values in Table 3.1. This is repeated for each hazard.

The processed data is stored in a table, with cities as rows and hazards as columns, and each cell assigned a value representing the hazard level (1 = very low, 4 = high). The table also includes the name, country, continent, total population, and total area of each city, as provided in the urban boundary information by Moreno-Monroy et al. (2020).

Matlab is used to analyse the data systematically for each combination of hazards. The analysis for two hazards, for example, shows the number of cities exposed to specific levels of the two hazards (e.g. high flood and high earthquake), irrespective of their exposure to other hazards. The analysis for three hazards shows the number of cities exposed to specific levels of three hazards (e.g. high flood, high earthquake and medium landslide), irrespective of exposure to the other two hazards.

3.3 Results

Figure 3.3 shows total exposure per hazard, where colours represent different levels of exposure (yellow = *low*, red = *medium*, dark red = *high*). Overall, most exposure to *high* intensity and frequent hazards is seen for river flooding (31% of cities), followed by cyclones (23% of cities), coastal flooding (5%), earthquakes (2%), and landslides (1%). Note that the figures show exposure in absolute number of cities, while percentages are given in the text.

In comparison, the study by Gu (2019) previously found that 37% of cities are highly exposed to flooding, 20% to cyclones, 5% to earthquakes, and 3% to landslides. The values found are therefore comparable to those previously found by Gu (2019). Differences between the two are likely because of the different methods used for defining *high* hazard levels (i.e. Gu (2019) classifies all cities within the top three deciles as highly exposed, while a specified intensity and return period is used here). Given the difference in classification method, the results obtained are surprisingly consistent with those in Gu (2019).

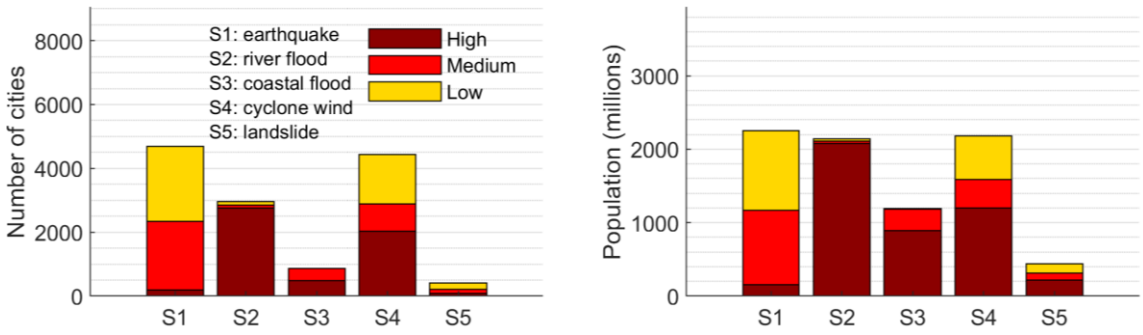

Figure 3.3 Exposure of urban areas to five hazards. Shows the number of cities exposed to each hazard, and the total population living in the exposed cities. Colours correspond to high, medium and low hazard levels (see Table 3.1).

When looking at exposure to both *medium* and *high* levels for each hazard, a third of cities (32%) are exposed to river flooding and a third (32%) to cyclone wind, 26% to earthquakes,

9% to coastal flooding, and 2% to landslides. While only a small proportion of cities (2%) are exposed to *high* earthquake hazard levels, many (26%) face at least *medium* earthquake hazard levels. In total 52% of cities are exposed to *low* or above earthquakes levels, 49% to cyclone wind, 32% to river flooding, 10% to coastal flooding, and 5% to landslides. Differences between exposure by number of cities and exposure by population is seen for river and coastal flooding suggest that river and coastal flooding are more likely to affect larger cities.

The next sections will present: the exposure to combinations of hazards (section 3.3.1), the exposure by continent (Section 3.3.2), the exposure by area exposed to specific hazards (Section 3.3.3), the evaluation of the data (Section 3.3.4), and the sensitivity of the data to changes in the classification values (Section 3.3.5).

3.3.1 Exposure to combinations of hazards

Results suggest that approximately 1 in every 10 cities (11%) faces a *high* level of at least two hazards, and that 1 in 4 cities (26%) face at least *medium* levels of two or more hazards. Previously, Gu (2019) found that 14% of cities were highly exposed to at least two hazards. The comparison is given for illustrative purposes, but it should be noted that the two studies include different hazards; Gu includes volcanic eruption and droughts, and excludes coastal flooding. Exposure to each combination of two hazards can be seen Figure 3.4. The combinations of hazards are labelled C1 to C10, and the maps show cities with low or above levels of two hazards. A full overview of all exposure values is provided in Appendix A.1.

Looking at differences in exposure by type of hazard, the most common hazard combination is river flooding and cyclone winds (C6), with 8% of cities highly exposed to both hazards. The combination is mostly seen for cities on the east coast of China, and on the east coast of the United States. After river flooding and wind, most cities (3%) are exposed to combined coastal

flooding and cyclone wind (C8). Note that the combinations are not mutually exclusive, and some cities could belong to both groups. The combination of river and coastal flooding (C5) is found to be the third most common hazard combination and concerns 2% of cities.

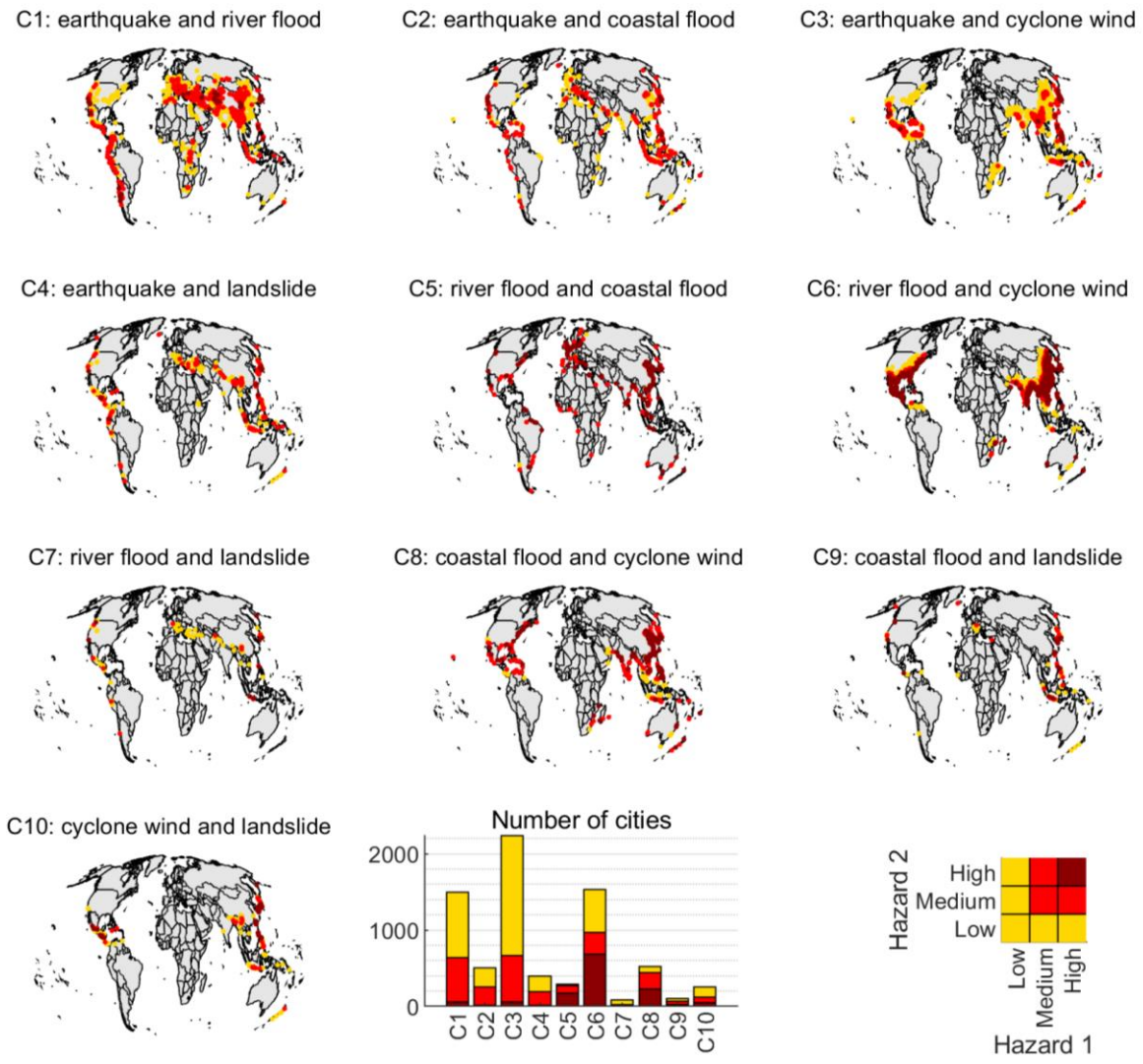

Figure 3.4 Maps of exposure to the ten combinations of two hazards (C1 – C10). Colours correspond to combinations of hazard levels as shown in the legend (bottom right). The bar plot shows the total number of cities exposed to each combination.

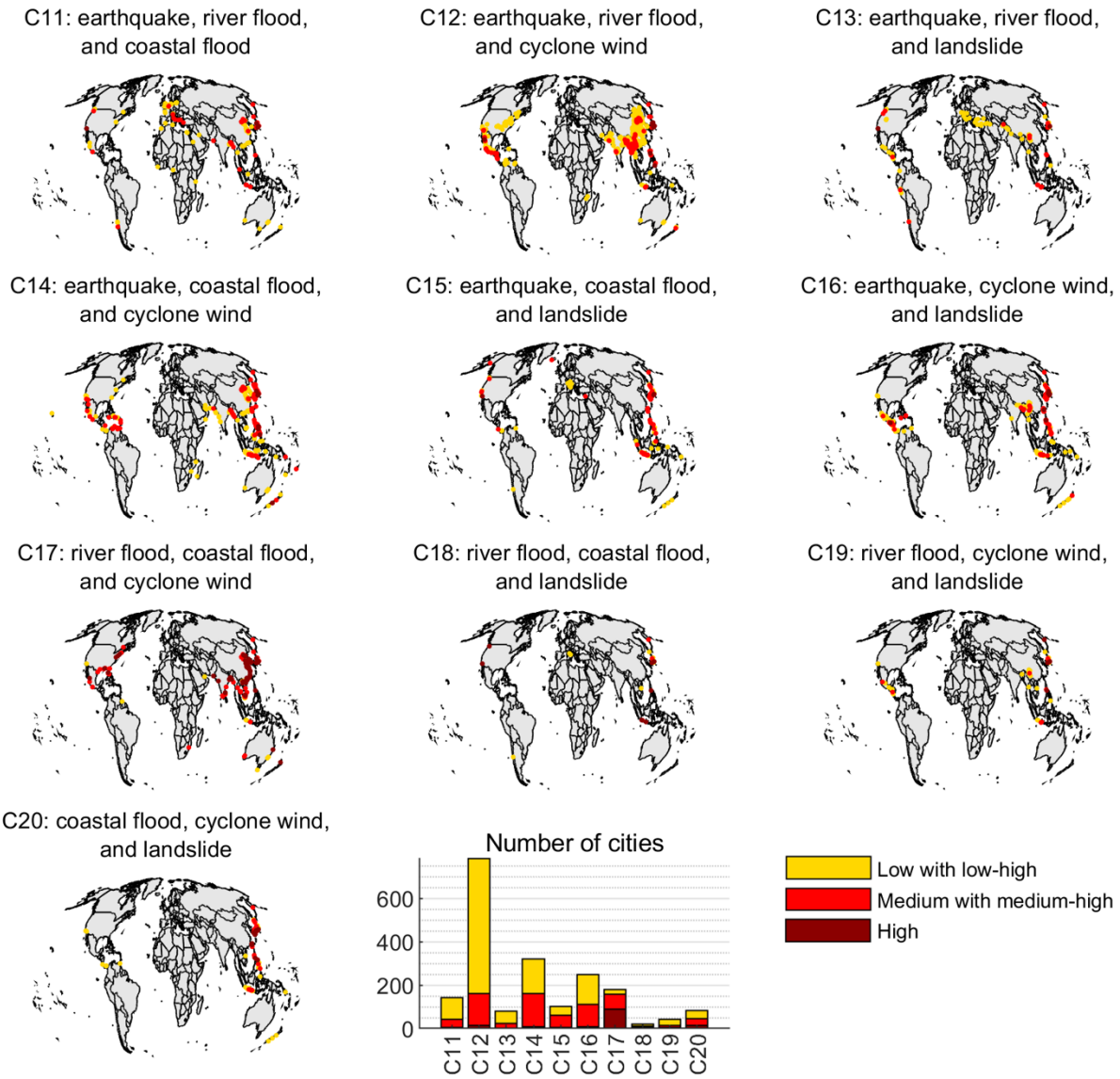

Figure 3.5 Maps of exposure to the ten combinations of three hazards (C11 – C20). Colours correspond to combinations of hazard levels as shown in the legend (bottom right). The bar plot show the total number of cities exposed to combinations of three hazards.

River flooding and cyclones is also the most common combination of *medium* and *high* hazard, seen for 11% of cities. However combinations of *medium* to *high* earthquakes and river flooding (C1) and *medium* to *high* earthquakes and cyclone wind (C3), are found to also be common, with 7% of cities exposed. In total, more cities have *medium* or *high* exposure to

earthquakes with river floods/wind, than have *medium* or *high* exposure to coastal flooding and river floods/wind. When also considering *low* hazard levels, exposure to earthquakes and cyclone wind (C3) is found to be the most common hazard combination in cities. In total, 1% of cities (511 cities) have *high* exposure to three or more hazards, and 6% have *medium* to *high* exposure to three or more hazards. Cities exposed to combinations of three hazards are shown in Figure 3.5. By far the largest exposure to *high* levels of three hazards is exposure to river, coastal, and cyclone hazards (C17). Many of the exposed cities are on the east coast of China and the east coast of the United States. However exposure to earthquakes, river flooding and cyclone wind (C12) is the combinations of three hazards that occurs by far in the largest number of cities when including exposure to *low* hazard levels and above. The combination of earthquakes, river flooding and cyclone wind is found in many cities in China and across Asia, in Australia and New Zealand, in Central America, and in the United States.

Eight cities are found to have *high* exposure to four different hazards (see Appendix A.1) including Kyoto, Niigata, Hamamatsu, Tokyo, Shizuoka, Mishima, Manila, and Los Angeles, and one city has *high* exposure to all five hazards, the city of Tokyo. A recent study by the reinsurance company Swiss Re (2013) ranked Tokyo as the top most hazard exposed city, which supports this finding. Six of the eight cities with *high* exposure to at least four hazards are found in Japan. Also, all of the cities exposed to four or more hazards are relatively large cities, with populations of at least 800,000 inhabitants.

3.3.2 Multi-hazard exposure by continent

The dataset contains approximately 5,000 cities in Asia, 1,800 cities in Africa, 900 cities in Europe, 600 cities in North America, 600 cities in South America, and 40 in Oceania. Given the small number of cities in Oceania, these are grouped with cities Asia, to make the results easier to present.

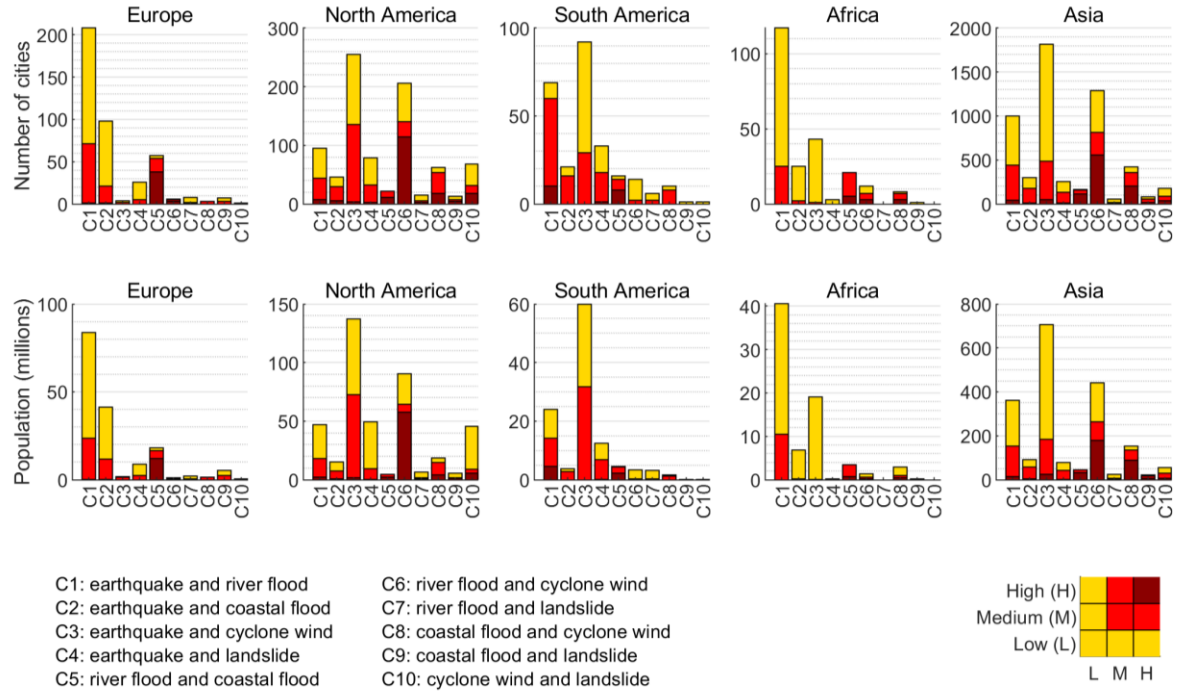

Figure 3.6 Exposure to combinations of two hazards (C1 – C10) by continent. Colours correspond to combinations of hazard levels as shown in the legend (bottom right). The total number of cities and the corresponding population is shown for each continent.

Figure 3.6 shows the exposure to combinations of two hazards per continent. Cities in North America and Asia are found to be most exposed to combined *high* river flooding and cyclones (C6). Cities in Europe, on the other hand, are most exposed to combined coastal and river flooding (C5) for *high* hazard levels, and to earthquakes and river flooding (C1) when including both *medium* and *high* hazard levels. According to the data, more cities are exposed to combined river and coastal flooding (C5) in Europe than in North America. While in North America, combined exposure to river and coastal flooding (C5) is found to be less common, combined exposure to river flooding and cyclones wind (C6), or flooding and hurricanes, is a more widely shared challenge for cities. Cities in South America are most exposed to combined earthquakes and river flooding (C1). A comparison between exposure by number of cities and by population suggests that combined earthquakes and river flooding (C1) in South America

mostly affects small cities, as exposed population is relatively lower for this hazard combination than the exposed number of cities. Cities in Africa are found to have relatively low exposure to all combinations of the five hazards in this study. Most significant is exposure to river and coastal flooding (C5), and to river and earthquakes (C1). However, the hazards do not include droughts, heat waves, and other events that also have severe societal and economic consequences.

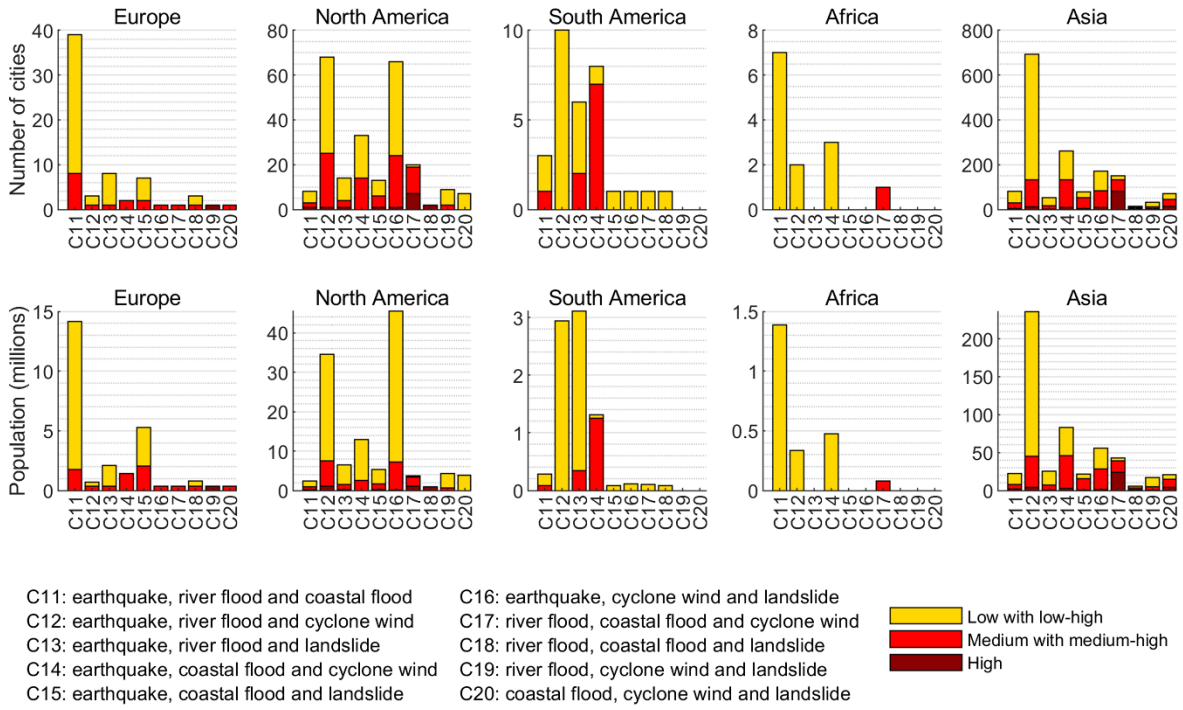

Figure 3.7 Exposure to combinations of three hazards (C11 – C20) by continent. Colours correspond to combinations of hazard levels as shown in the legend (bottom right). The total number of cities and the corresponding population is shown for each continent.

Figure 3.7 shows the exposure to combinations of three hazards per continent. Far more cities are exposed to three hazards in Asia than on any other continent. The figure confirms that combined river, coastal, and cyclone hazard (C17) occurs mostly in Asia and North America. *Medium* to *high* exposure to earthquake, cyclones and landslides (C16) is almost as common

as *medium* to *high* exposure to river floods, coastal floods, and cyclones (C17) in North America. Most exposure to three hazards in Europe can be seen for earthquakes, river and coastal flooding (C11), although only a few cities are concerned. Only 10 cities in South America and only one city in Africa are shown to have *medium* to *high* levels of three types of hazards.

3.3.3 Multi-hazard exposure by area exposed to specific hazards

Exposure is also analysed across specific hazard regions. This means understanding, for example, how many among the cities exposed to flooding are also exposed to earthquakes. For that, cities exposed to both flood and earthquake are counted, and the number is divided by the total number of cities exposed to flooding. In general, the proportion P_L of cities exposed to a level L or above for hazard *h1* that are also exposed to a level L or above for hazard *h2* is calculated as:

$$P_L(h1, h2) = \frac{N_{h1,h2}}{N_{h1}} \quad (3.1)$$

where $N_{h1,h2}$ is the number of cities exposed to a level L or above of hazards *h1* and *h2*, and N_{h1} is the number of cities exposed to a level L or above of hazard *h1*. Hazard matrices as in Gill and Malamud (2014) are used to present the results.

Table 3.3 The number of cities exposed to medium and high hazard levels globally and per continent. The values are used to calculate the percentage probabilities in Figure 3.8.

	Global	Europe	N. America	S. America	Africa	Asia
Earthquake	2347	188	187	229	209	1509
River flood	2852	409	263	363	363	1603
Coastal flood	857	163	75	63	63	480
Cyclone wind	2884	8	398	59	59	2347
Landslide	205	8	40	1	1	135

Table 3.3 shows the total number of cities exposed to *medium* or *high* levels per hazard and per continent. These values correspond to N_{h1} in Equation 3.1 and are used as the denominators in calculating the proportion of overlap between two hazards, shown in Figure 3.8. Note that some values are based on very small samples of cities (e.g. for landslides in Europe, South America and Africa, and for cyclone wind in Europe) while others come from much larger samples (e.g. for Asia).

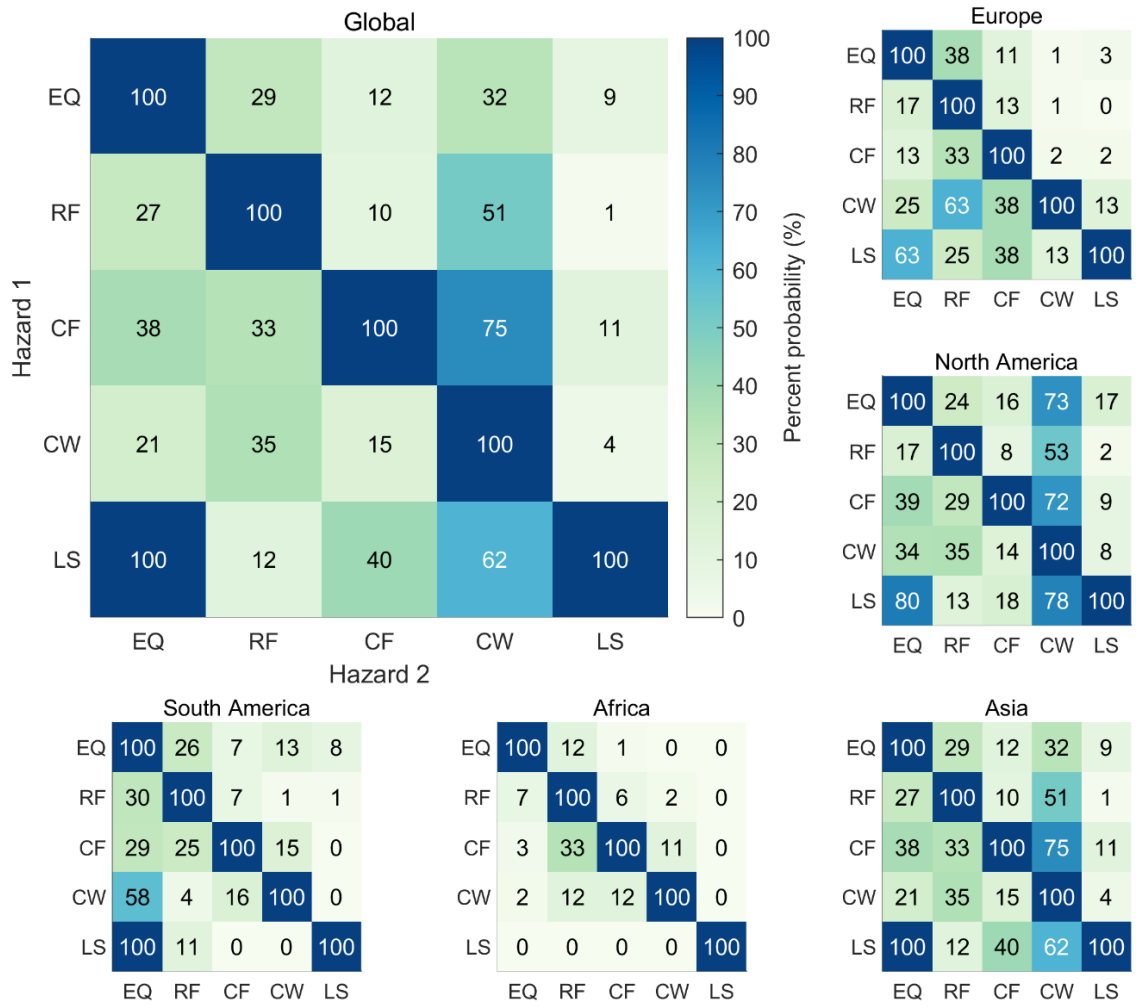

Figure 3.8 Percentage probability that a city exposed to hazard 1 is also exposed to hazard 2, globally and for different continents. EQ = Earthquake; RF = River flood; CF = Coastal flood; CW = Cyclone wind; LS = Landslide. Note that some values are based on a very small sample of cities (Table 3.3). Note also that the proportions are given to the nearest whole number, so 100% does not necessarily mean complete overlap between hazards.

The values in Figure 3.8 represent the proportion of joint exposure to hazards. Looking at the values for the global case, the highest proportion, not including the values along the diagonal, can be seen for landslide areas that are also exposed to earthquake exposure. As percentage probability is rounded to the nearest whole number, 100% does not necessarily mean complete overlap between hazards. However it indicates that the large majority (>99%) of cities exposed to *medium* to *high* landslides in the dataset are also exposed to earthquakes. The values for Asia, given the large number of Asian cities, can be seen to also determine the global average. Elsewhere, probabilities differ from the global average. North America tends to have higher than average probabilities of joint exposure across pairs of hazards, although not for coastal areas that are also exposed to river flooding, while Africa tends to have lower than average probabilities of joint exposure.

3.3.4 Evaluating the hazard data

Evaluating probabilistic global hazard datasets is challenging (Dottori et al., 2013). In this study, the specific interest is to evaluate the hazard severity obtained for each city, and to understand whether it is representative of actual hazard conditions in those cities. Evaluation data is needed that can provide consistent and comparable information across multiple cities and across the five hazards in this analysis. An interesting and unique dataset is identified that provides such information in qualitative form: the resilience strategies from the one hundred resilient cities (100RC) network of cities.

The 100RC network is an initiative of the Rockefeller Foundation that aims to help cities become more resilient to natural, social, and economic challenges (Spaans & Waterhout, 2017). Cities in the 100RC network are guided to develop a resilience strategy using a consistent participatory process, where information from experts, the public and private sector, non-governmental organisations, and the local population is collected (Berkowitz & Kramer, 2018).

The 100RC network includes cities from all continents and from a range of hazard contexts (Figure 3.9). The UK cities of Bristol and Glasgow were part of the 100RC network. During the development of the resilience strategy for Bristol for example, over 1,600 people were engaged through meetings, focus groups, workshops, and events (Bristol City Council, 2016). This participatory process helps to comprehensively identify the important challenges faced in the city.

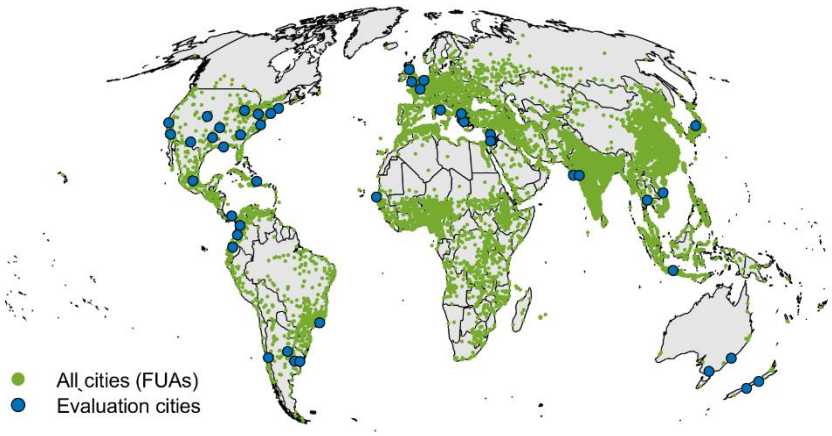

Figure 3.9 Locations of the 100RC evaluation cities. Green dots show all cities from the Functional Urban Areas dataset (Moreno-Monroy et al., 2020), and blue dots show cities for which evaluation data is collected from 100RC Resilience Strategies.

The information in the reports of the 100RC provides an interesting comparison to the severity levels calculated in this study. The benefits of using information from the reports is that it reflects the local knowledge, captures information from local experts, and should in theory include all the hazards that the city faces. A downside is that the resilience strategies are recognised to be influenced by political priorities (Pitidis et al., 2018; Spaans & Waterhout, 2017). This is taken into account when analysing the evaluation results. The next part explains how the qualitative information in the reports is retrieved and processed in order to compare it to the severity levels.

The resilience strategy documents are downloaded from the 100RC online portal. Of the 100 cities, 51 cities have published a resilience strategy at the time of download (November 2019). Three of the cities are excluded, one because it does not appear in the urban areas dataset, one because it does not have a resilience strategy in English, and one because the document format does not enable word search. In two cases, two cities with independent resilience strategies are part of a single urban commuter area. In those cases, only the evaluation city with the largest population is included. In total, 46 cities are therefore included in the evaluation (Table 3.4).

Each strategy is reviewed to collect evidence (or lack thereof) for each of the five hazards (earthquakes, river floods, coastal floods, cyclone wind, and landslides). The following information is considered as evidence of the hazard: a) the hazard is listed under key challenges for the city, b) a past occurrence of the hazard is described, c) there are ongoing or planned activities that address the hazard. Cities where evidence of the hazard being a challenge for the city is found in the resilience strategy are recorded in black font in Table 3.4, and cities where no evidence of the hazard is found are recorded in grey font in Table 3.4.

The strategies are all organised according to the following sections: a description of the city context (e.g. important historical events, geographic features); an overview of the consultation process; *key challenges*; and proposed or ongoing activities for increasing resilience. First, the key challenges section is checked and any hazards listed are recorded (see page numbers in Table 3.4). Then, a search through the document is carried out to identify additional evidence of hazards not included in the key challenges, using the following keywords:

- Earthquake: “earthquake”, “seism”
- River flood: “flood” (“river”, “basin”, “catchment”)
- Coastal flood: “flood”, “storm surge” (“coast”, “shore”, “tidal”, “erosion”, “wave”)

- Cyclone wind: “cyclone”, “typhoon”, “hurricane”, “strong wind”, “extreme wind”, “wind storm”, “superstorm”
- Landslide: “landslide”, “landslip”, “debris flow”, “mudslide”, “slope failure” (“slope”, “hill”)

A keyword count is also used to estimate the relative severity of hazards across cities. Words in brackets are used for additional contextual information but are not considered keywords as such. Occurrences of each keyword (so excluding the words in brackets) are counted by utilising Python word count capabilities. The total keyword count per hazard, so the sum of the count for each keyword of that hazard, is normalised by dividing by the number of pages. The normalised values are shown in Table 3.4. Note that the procedure used also counts keywords that appear as part of a word; for example “earthquake” is counted in “earthquakes”, “earthquake-proof”, and so on.

The data shows that of the 46 evaluation cities, the largest number are exposed to river flooding (31), followed by earthquakes and coastal flooding (22), landslides (14) and cyclone wind (12). Two cities are exposed to all five hazards (Panama and Christchurch), 4 cities are exposed to four hazards (Los Angeles, Rio de Janeiro, Mexico City, and Wellington), 15 cities are exposed to three hazards, 10 are exposed to two hazards, 10 are exposed to one hazard, and only 5 cities are not exposed to any of the hazards (Atlanta, Chicago, Dallas, El Paso, Glasgow). Overall, the set of cities show a wide range of hazard profiles, providing insight into a range of different urban multi-hazard contexts.

Table 3.4 Evaluation data collected from the 100RC Resilience Strategies. The numbers in the table show how many times hazard keywords appear on average per page (black = evidence of hazard, grey = no evidence of hazard). Page numbers refer to the electronic page number.

	City	Country	Page with city challenges	Earth-quake	River flood	Coastal flood	Cyclone wind	Landslides
1	Amman	Jordan	30	**0.01**	0.09	0.09	0.00	0.00
2	Athens	Greece	14	**0.14**	0.05	0.05	0.00	0.00
3	Atlanta	United States	14	0.00	0.26	0.26	0.00	0.00
4	Bangkok	Thailand	23 (26, 88)	**0.23**	**1.23**	**1.23**	0.01	0.00
5	Boston	United States	20	0.00	0.27	**0.27**	**0.01**	0.00
6	Boulder	United States	10 (14)	0.00	**0.92**	0.92	0.00	0.00
7	Bristol	UK	38	0.01	0.28	**0.28**	0.00	0.00
8	Buenos Aires	Argentina	29 (121)	0.01	**0.22**	0.22	0.00	0.00
9	Byblos	Lebanon	13	0.07	0.07	**0.07**	0.02	0.00
10	Cali	Colombia	28	**0.24**	**0.33**	0.33	0.00	**0.04**
11	Chicago	United States	29	0.00	0.37	0.37	0.01	0.00
12	Dakar	Senegal	14	0.03	0.23	**0.23**	0.00	0.00
13	Dallas	United States	15	0.03	0.18	0.18	0.00	0.00
14	Da Nang	Vietnam	11	0.00	**2.77**	**2.77**	**0.68**	0.00
15	El Paso	United States	32	0.02	0.14	0.14	0.01	0.00
16	Glasgow	UK	20	0.00	0.17	0.17	0.00	0.00
17	Christchurch	New Zealand	32 (20, 90, 92)	**1.01**	**0.15**	**0.17**	**0.02**	**0.01**
18	Los Angeles	United States	13 (42)	**2.21**	**0.66**	**0.66**	0.02	**0.21**
19	Medellin	Colombia	8 (30)	**0.15**	**0.18**	0.18	0.00	**0.24**
20	Melbourne	Australia	38 (54, 56, 95)	**0.01**	**0.29**	**0.30**	0.00	0.00
21	Mexico City	Mexico	16 (20)	**0.50**	**0.45**	0.45	**0.03**	**0.06**
22	Montevideo	Uruguay	14 (17)	0.00	**0.63**	**0.63**	0.03	0.00
23	Montreal	Canada	16 (27, 36)	**0.07**	**0.45**	0.45	**0.02**	0.00
24	New Orleans	United States	12	0.00	**0.48**	**0.49**	**0.24**	0.00
25	New York City	United States	35	0.01	**0.84**	**0.88**	**0.09**	0.00
26	Norfolk	United States	18	0.02	**0.75**	**0.80**	**0.13**	0.00
27	Oakland	United States	10	**0.69**	0.53	**0.53**	0.00	0.00
28	Panama	Panama	25 (58)	**0.25**	**0.67**	**0.67**	**0.05**	**0.14**
29	Paris	Oakland	20	0.00	**0.51**	0.51	0.02	0.00
30	Pittsburgh	United States	14 (17, 20)	0.00	**0.25**	0.25	0.00	**0.16**
31	Quito	Ecuador	18 (60, 65)	**0.42**	**0.17**	0.18	0.03	**0.27**
32	Ramallah	Palestine	18 (44)	**0.22**	0.03	0.03	0.00	0.01
33	Rio de Janeiro	Brazil	12 (25)	0.00	**0.37**	**0.47**	**0.10**	**0.22**
34	Rome	Italy	40	**0.06**	**0.13**	0.13	0.00	**0.01**
35	Rotterdam	Netherlands	12 (43)	0.02	**0.28**	**0.28**	0.06	0.00
36	San Francisco	United States	7	**2.32**	0.13	**0.13**	0.03	0.00
37	Santa Fe	United States	31	0.01	**0.36**	0.36	0.01	0.00
38	Santiago	Chile	28	**0.20**	**0.11**	0.11	0.00	**0.04**
39	Santiago	Dom. rep.	31	**0.47**	**0.53**	0.53	**0.14**	0.02
40	Semarang	Indonesia	45	0.01	**0.32**	**0.32**	0.00	**0.09**
41	Surat	India	20	0.01	**0.34**	**0.35**	0.01	0.00
42	Sydney	Australia	36 (39)	0.01	**0.15**	**0.15**	0.00	0.00
43	Thessaloniki	Greece	20	**0.08**	**0.16**	0.16	0.00	0.00
44	Toyama	Japan	15	**0.24**	**0.85**	0.85	0.00	**0.11**
45	Tulsa	United States	21	**0.06**	**0.07**	0.07	0.01	0.00
46	Wellington	New Zealand	8 (19, 37)	**1.34**	0.20	**0.22**	**0.07**	**0.02**

The word count in the case of earthquakes, cyclones, and landslides, confirms the collected evidence of the hazard (i.e. high keyword count for cities where there is evidence of the hazard, and low keyword count for cities where there is no evidence of the hazard). For flooding, the situation is a bit more complicated. References to flooding include all types of flooding (fluvial, coastal, and pluvial). Therefore when recording evidence of fluvial and coastal flooding, contextual information is used to determine the type of flooding. For example for the city of Chicago, flooding is discussed in the context of stormwater and combined sewer overflows, which suggests pluvial (rainfall) flooding. As no evidence of flooding is found other than the evidence indicating pluvial flooding, no river flooding is recorded for the city of Chicago, despite many uses of the word 'flood' in the document. As word count for flooding corresponds to any mention of flooding across different types of flooding, it is a poor indication of specific flood types.

The hazard levels for the 49 evaluation cities are compared to the evaluation data in Figure 3.10. The y-axis shows the four hazard levels. Each dot corresponds to a city, and numbers show the corresponding city in Table 3.4. Overall, both 'false positives' (cities with high hazard level but no evidence of the hazard in the resilience strategy, i.e. grey dots) and 'false negatives' (cities with very low hazard levels but with evidence of the hazard in the resilience strategy, i.e. coloured circles) can be seen. The low and medium hazard levels are not discussed in the evaluation. The best match (fewest false positives or false negatives) can be seen for earthquakes and coastal flooding, and a relatively good match can be seen for cyclone wind. However, more false negatives can be seen for landslides, and many false negatives can be seen for river flooding.

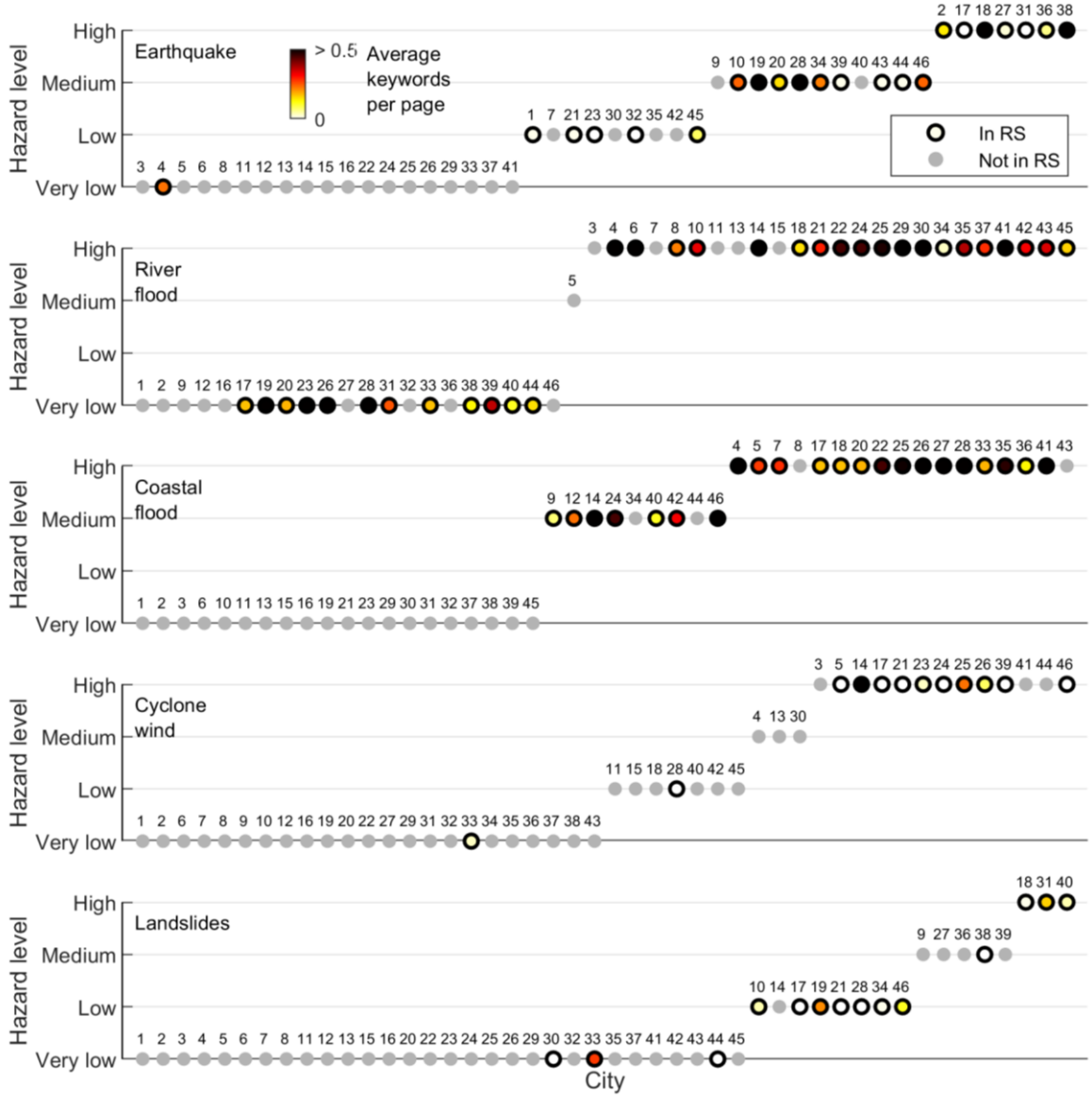

Figure 3.10 Hazard levels compared with evaluation data from the 100RC resilience strategies (RS). Each point represents a city. Numbers refer to the city numbers in Table 3.4. The hazard level is shown on the y-axis. Grey dots mean that there is no evidence of the hazard in the resilience strategy, while open circles mean that evidence of the hazard is found in the resilience strategy. For city/hazard combinations where evidence is found, the colour shows the average number of occurrences of hazard keywords per page.

Next, the five hazards are each discussed in turn, drawing on evidence from the resilience strategies to identify likely reasons for mismatch between the two.

Earthquake

Bangkok reports earthquakes as a challenge to the city despite low hazard levels according to the global data. A search through literature shows that earthquake ground motion can be amplified by soil conditions in Bangkok by up to a factor of 5 (Ashford et al., 2000). However, the global earthquake data used in calculating the hazard level approximates ground conditions over large regions and does not capture local variability in soil type. In this case, the mismatch is therefore likely to be due to the coarse representation of soil conditions in the global hazard model.

River flooding

In total, 12 out of the 46 cities (Christchurch, Medellin, Melbourne, Montreal, Norfolk, Panama, Quito, Rio de Janeiro, Santiago de Chile, Santiago de los Caballeros, Semarang, and Toyama) show evidence of river flooding in the resilience strategy, yet are classified as having 'very low' river flood hazard based on the global hazard maps. The resilience strategy for the city of Christchurch (New Zealand) states that: "much of Greater Christchurch sits on a floodplain. Major defences protect communities from catastrophic flooding by the Waimakariri River". Yet the city is classified as having 'very low' river flood hazard according to the hazard data. Some of the difference can be explained by cities being in small catchment areas which are excluded in the global flood maps. Differences could also be due to the evidence in the resilience strategy not indicating a significant flood hazard. For example the evidence of river flood hazard in Quito consists of planned improvements to flood defences as part of a river restoration project, which may, but does not necessarily, indicate that the city is exposed to river flooding.

River flooding also shows some false positives. For example, Atlanta (United States) is classified as having *very high* river flood hazard according to the global data, but does not give any evidence of river flooding in their resilience strategy, although it discusses concerns with rainfall flooding. High standards of river flood protection in cities in the United States may explain the difference (Scussolini et al., 2016). The same reason could apply to the other false positives (Atlanta, Bristol, Chicago, Dallas, and El Paso). All cities with false positives are in the United States or United Kingdom, where flood protection standards are high (Scussolini et al., 2016).

In summary, differences in river flood hazard may be the result of global flood maps not including flooding in small catchments, the maps not accounting for high levels of flood protection present in certain cities, and insufficient evidence in some resilience strategies to determine whether river flooding is severe (in doubt, it is considered severe).

Coastal flooding

The cities of Buenos Aires (Argentina) and Thessaloniki (Greece) are classified as having *high* coastal flood hazard levels according to the global data, but do not identify coastal flooding as a challenge in their resilience strategy. The two cities both have plans to regenerate the coastal area with housing, shops and offices. Lack of mention of coastal flood hazards in this case may be an indication of political bias. Slightly worrying in the context of the resilience strategy is that sections discussing coastal redevelopment plans do not include any mention of assessment or mitigation of coastal flood risks.

Extreme wind

Rio de Janeiro lists strong wind as a challenge, while it has a *very low* cyclone wind hazard level according to the global data. The reason is that the city is not on the path of tropical

cyclones, and strong wind is storms other than tropical cyclones, which are not included in the global hazard dataset. On the other hand, Atlanta (United States), Surat (India), and Toyama (Japan) do not include evidence of wind hazard in their resilience strategy despite having a *very high* cyclone wind hazard level according to the global data. The mismatch could be due to the cities being highly adapted/prepared to the hazard (particularly Japan). Also, as cyclone events often combine strong wind with extreme rainfall and storm surges, another reason for the data seemingly overpredicting the hazard may be that wind hazard is ignored next to the more significant impacts of flooding.

Landslides

Three cities discuss landslides in their resilience strategy, but have a *very low* landslide hazard level according to the global data, including Pittsburgh (United States), Rio de Janeiro (Brazil), and Rome (Italy). The major source of uncertainty for the landslide dataset is attributed to quality and resolution of the input datasets for representing the spatial distribution of landslide factors (Nadim et al., 2006). In Rio de Janeiro, informal housing (favelas) constructed on slopes could be a factor generating landslide hazard. This informal housing is not represented in the global or regional hazard datasets, and yet are known to be a critical factor in landslide occurrence (Bozzolan et al., 2020). While slope conditions in Rio de Janeiro may not point to significant landslides occurrences, when coupled with informal housing and the associated deforestation, slope cutting, loading, and poor drainage, occurrences of landslides become significantly exacerbated.

Overall, mismatch comes from both limitations of the global hazard data (e.g. not accounting for the effect of local geology on earthquake acceleration, not including flooding over small catchment areas), and limitations of the evaluation data (e.g. biased information due to political priorities, ambiguities between type of flooding, cities not providing evidence for hazards that

they are highly adapted/prepared for). Causes of mismatch lead to both underestimation and overestimation of the hazard. In other words, the modelled data appears to both under- and over-predicts hazard severity in approximately equal measure relative to the local data. Certain factors will systematically weaken the hazard across cities (e.g. including flood defences). Other factors would systematically strengthen the hazard across cities (e.g. land subsidence). Considering all factors together may not make a big difference at the global scale. On the other hand, it may lead to significant differences in individual cities. It is possible, also, that some factors are common to all cities in a given part of the world, which would create regional bias. In general the hazard levels calculated from the global hazard data seem to provide a relatively good representation of earthquake, cyclone wind, and coastal flood hazard levels in cities, while levels of river flooding and landslides are found to be more uncertain.

3.3.5 Sensitivity of the classification

This section assesses the influence that the choice of values in Table 3.1, used for classifying hazard levels, has on the results. The influence is checked for earthquakes, river flooding, and cyclone wind, which are expected to have the greatest influence on multi-hazard exposure overall. Results are shown here for three cases, each varying the return period and hazard intensity values for one of the three hazards. Some additional cases are included in Appendix A.2.

Figure 3.11 shows the sensitivity of river flood hazard levels to the classification values. Here, depths are changed from 0.5 metres to 2.0 metres for all hazard levels, and the return period for the low hazard level is changed from 500 to 100 years (both of these changes correspond to fewer cities being exposed). The dotted lines in Figure 3.11 show all cities exposed to low, medium or high hazard levels using the baseline values in Table 3.1, and the coloured bars

show exposure using the alternative values. The results suggest that exposure to river flooding does not change significantly when threshold values are varied.

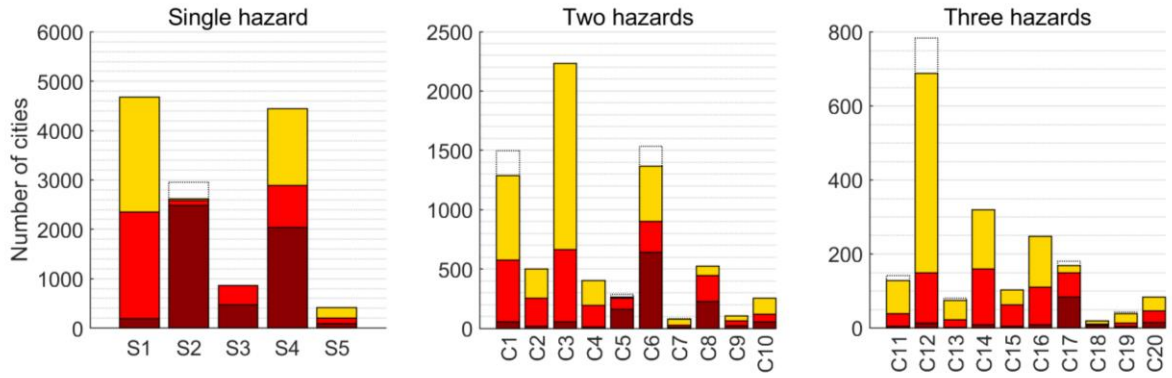

Figure 3.11 Exposure to combinations of one, two or three hazards when river flood threshold values are changed from those Table 3.1. Colours represent hazard levels, and x-labels correspond to hazard combinations (see Figures 3.6 and 3.7).

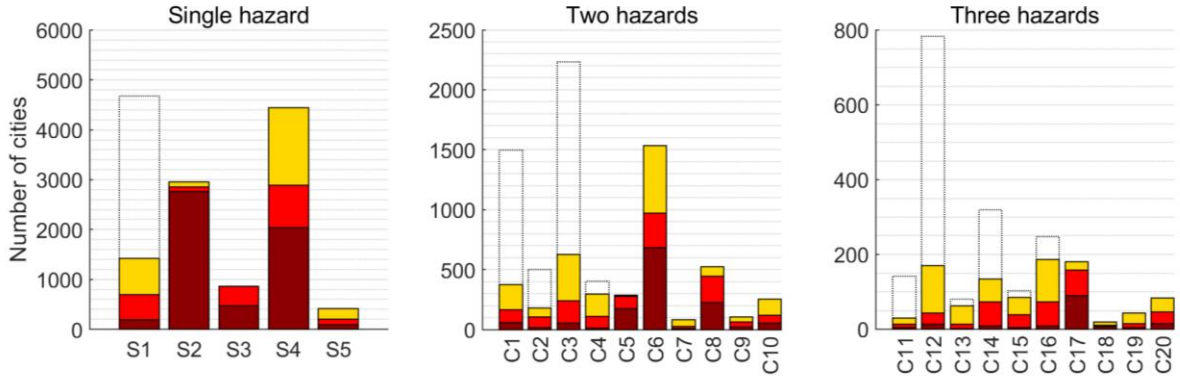

Figure 3.12 Exposure to combinations of one, two or three hazards when earthquake threshold values are changed from those Table 3.1. Colours represent hazard levels, and x-labels correspond to hazard combinations (see Figures 3.6 and 3.7).

Exposure to earthquakes is found to change significantly when changing the classification values (Figure 3.12). Figure 3.12 shows the exposure when a return period of 975 years, instead of 2475 years, is used to define low earthquake hazard levels, and when the intensity for medium and low hazard is changed from 0.1 g to 0.2 g (196 cm/s^2). Exposure to earthquakes,

and to combinations of earthquakes with other hazards becomes far less significant in this case, both in absolute number of cities exposed, and relative to other hazard combinations.

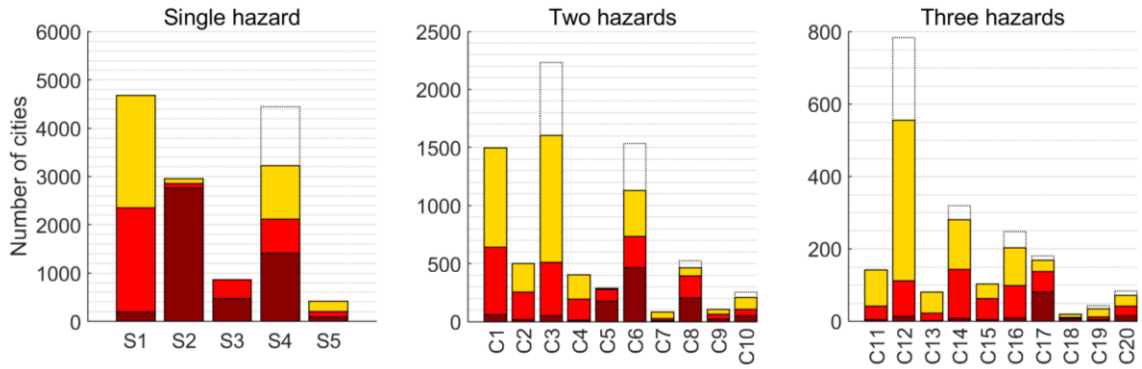

Figure 3.13 Exposure to combinations of one, two or three hazards when cyclone wind threshold values are changed from those Table 3.1. Colours represent hazard levels, and x-labels correspond to hazard combinations (see Figures 3.6 and 3.7).

Figure 3.13 shows the results when classification values are varied for cyclone wind hazard. Here, return period is changed from 1000 years to 250 years for the low hazard level, and hazard intensity is changed from 80 km/h to 100 km/h for all hazard levels. While exposure values are lower in this case, the changes do not significantly affect the relative exposure across hazard types.

3.4 Discussion

Looking across the information collected in this analysis, both on hazard severity and number of cities exposed, three multi-hazard contexts are identified for further research. The first is the combined exposure to river flooding and cyclones, seen in many cities, both coastal and inland, particularly across Asia and North America. The second is the combined exposure to river and coastal flooding, particularly in coastal cities in Asia and north of Europe. And the third is the combined exposure to (*low*) earthquake and cyclone wind, and (*low*) earthquake and river flood

hazards. The first two contexts are the subject of a lot of research, including by meteorologists, climate change adaptation scholars, hydrologists, and others (Couasnon et al., 2020; Gallina et al., 2016), but understanding the challenges associated with earthquakes and floods; and with earthquakes and cyclones, is still in its infancy and requires further work (Hart et al., 2015; De Ruiter et al., 2019). The analysis and results presented are primarily intended to inform researchers and others working to develop tools or methods for increasing resilience in cities, particularly in relation to physical damage and impacts to infrastructure. The next section provides a short summary of the information for the three contexts, including considerations on data accuracy.

3.4.1 Common multi-hazard environments

The analysis found that approximately 8% of cities are exposed to both *high* cyclone and *high* river flood hazards. *High* flood levels in this analysis means that without mitigation measures, (a part of) the city would have a 10% chance of flooding each year, while *high* levels of cyclone wind refer to wind speeds reaching 80 km/h at least once every 50 years. Figure 3.13 shows a more detailed view of the exposed cities. Note that the analysis does not distinguish the area of flooding in each city. Therefore, *high* exposure can apply to cities with a small area and cities with a large area exposed. Large cities are more likely to be identified as highly exposed simply due to a larger surface area.

In terms of accuracy of the global data on which the results are based, Dottori et al. (2016) previously evaluated the river flood model in various parts of the world. Evaluation was carried out in Europe, South America, Africa, and India. They compared the flooded extent to official national flood maps, and to flooded extents from satellite imagery. Overall, Dottori et al. (2016) shows that the model is able to reproduce the overall flood extent well over large regions and in different parts of the world, but the ability to correctly predict flood location at the grid cell

level is fairly low. This suggests that the flood levels might not be representative for specific cities, particularly for smaller cities. However, overall exposure to flooding might be representative when the results are aggregated. Given that wind hazard varies relatively constantly over space, the total overlap between the two hazards might therefore be representative even if results for individual cities are not. It is worth noting that although the accuracy of the flood depths in the model are not evaluated (Dottori et al., 2016), the hazard levels are relatively insensitive to a variations in flood depth (Figure 3.11).

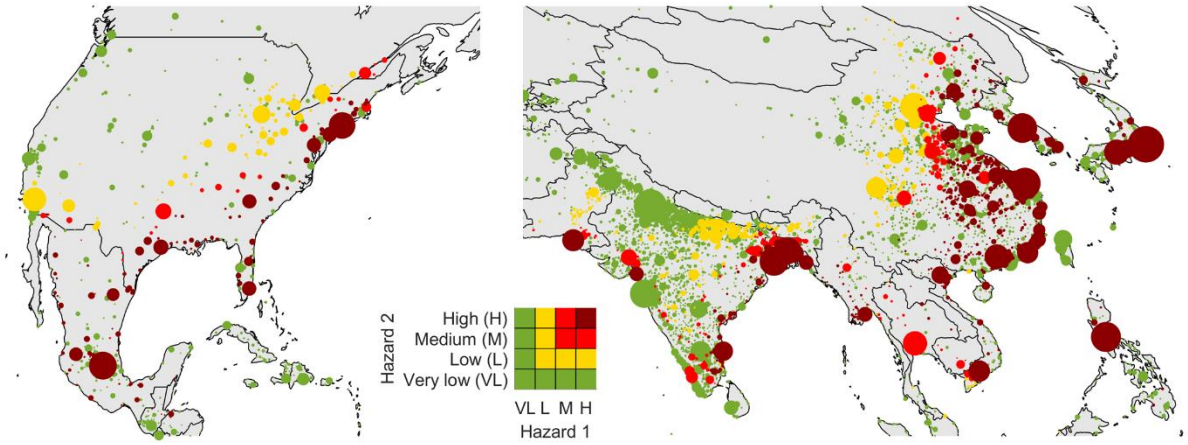

Figure 3.13 Distribution of combined cyclone wind and river flood hazard in North America (left) and Asia (right). Each point represents a city. The area is proportional the population of that city.

Results show that 2% of cities are exposed to high river and coastal flooding. The majority of these cities are in Asia and Europe, including multiple cities in The Netherlands (Figure 3.14). In this study, *high* flood hazard for both river flooding and coastal flooding represents flooding from a 1-in-10 year event, under present climate, if flood defences were not included. Figure 3.14 shows that multiple large coastal cities are exposed to combined river and coastal flood hazards.

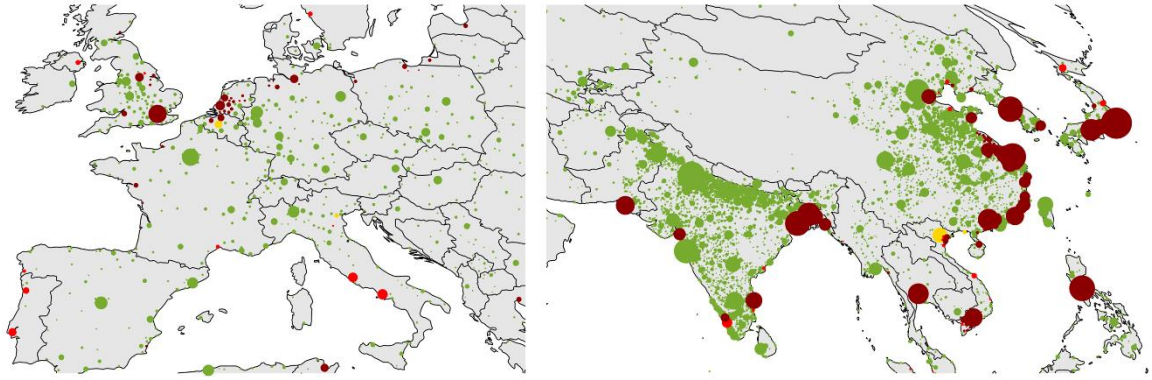

Figure 3.14 Distribution of combined river and coastal flood hazard for Europe (left) and Asia (right). For colour scheme see Figure 3.12.

River and coastal flooding could occur at the same time as compound flooding (Couasnon et al., 2020), which could have implications for the overall extent of flooding. The probability of the two hazards occurring at the same time depends on the main drivers of each type of flooding, and varies along the global coastline, as shown by Couasnon et al. (2020).

Finally, results also found that 25% of cities are exposed to combined *low+* earthquake and cyclone hazard, that 17% of cities are exposed to combined *low+* earthquake and river flooding, and that 8% of cities are exposed to *low+* levels of all three hazards. Exposure decreases significantly when only *medium* and *high* hazard levels are considered (Figure 3.15). Figure 3.15 (a) shows the distribution of exposure to *high*, *medium*, and *low* levels of combined earthquake and river flooding. The combination occurs across parts of China and extends through the middle East, Turkey, and into parts of Europe in particular Italy. Figure 3.15 (b) shows the distribution of exposure to *high*, *medium*, and *low* levels of combined earthquake and cyclone wind. The combination is most common in Asia, including Japan, Taiwan, the Philippines, and mainland China, as well as central America, the west coast of the United States, and along the west coast of South America.

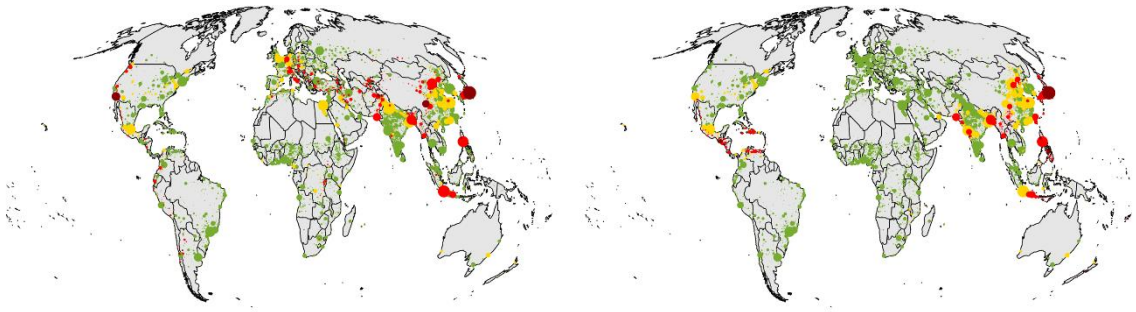

Figure 3.15 Distribution of combined earthquake and river flooding (left) and earthquake and cyclone wind (right) (for colour scheme see Figure 3.13).

Earthquakes and flooding, and earthquakes and cyclones, are independent of each other, but could have joint implications if the city is still recovering from one event when the other occurs (De Ruiter et al., 2019). It can sometimes take several years to rebuild and recover after a damaging hazard event, and the consequences of a second hazard in that period could be more than the sum of the consequences of the individual events (Gallina et al., 2016; Gill & Malamud, 2014). Places exposed to earthquakes and floods may consider whether measures to mitigate one hazard increases the risk of another (for example a dam to prevent flooding may create a possible risk of dam-break flooding due to an earthquake), and whether there are opportunities for jointly addressing the hazards (for example, avoiding construction on floodplains, that face both flood risk and possible liquefaction risk during an earthquake).

3.4.2 A dataset of combined hazard levels

To analyse the exposure of cities to combinations of hazards, this chapter assembled a dataset of combined hazard levels, or 'COHAZLE' dataset. The COHAZLE dataset has the following potentially beneficial characteristics:

1. It combines information for five hazards -earthquakes, river flooding, coastal flooding, tropical cyclone wind, and landslides- all of which can cause physical damage to infrastructure and are responsible for significant losses each year.
2. For each hazard, it provides a severity level (*very low*, *low*, *medium*, *high*) that broadly describes the expected amount of damage from the hazard if no mitigation measures were provided, based on both the return period and intensity of the hazard.
3. It provides hazard information for more than 9,000 cities, in theory all cities with 50,000 inhabitants or more (Moreno-Monroy et al., 2020).
4. A city is defined according to observed population densities and extent of infrastructure (e.g. buildings and roads), and therefore has a consistent physical meaning across countries.
5. The city includes the suburban commuter area, whose infrastructure (e.g. water supply, drainage, roads) is likely to be functionally integrated with the rest of the city.
6. The hazard levels (*very low*, *low*, *medium*, *high*) are calculated in the same way as in the online ThinkHazard! tool (https://thinkhazard.org/) provided by the Global Facility for Disaster Risk Reduction (Fraser et al., 2016).
7. The data is in spreadsheet format and is therefore easily accessible to non-experts.

These characteristics of the data make it potentially valuable for addressing multi-hazard risks in cities, however, there are also some notable limitations that need to be accounted for when using the data:

1. The hazard data and models on which the information is based are uncertain
2. The severity levels are intended to be representative of a developing context, and may therefore report the hazard as more severe than it would be in practice even without targeted mitigation measures.

3. The severity of a hazard (likelihood of being damaged without mitigation measures) will be different for different infrastructure sectors.
4. The level of damage from the hazards also depends strongly on the characteristics of the city, for example how long ago the water supply and drainage networks were built, the age of buildings, or the construction materials used.

In summary, the dataset supplements existing data by making exposure information for multiple hazards easily accessible and comparable. The advantage is that it enables users to identify cities that may be exposed to combinations of hazards. However, given that severity is only expressed in relative terms, that no spatial information about the hazards is included, and that the information is uncertain and sometimes inaccurate, the dataset cannot replace more detailed hazard assessments. The dataset provides insights about the hazards that could be significant in a city of interest, but does not provide the information needed to address the hazards. Addressing the hazards requires more detailed assessments, where the hazards are expressed in physical units (e.g. flood depth, peak ground acceleration), and where local factors are accounted for (e.g. variability in ground conditions, vegetation, flood defences) (Gill & Malamud, 2017).

3.4.3 Towards collaboration networks based on city similarity

The dataset could potentially contribute to developing 'learning networks' between stakeholders (e.g. local authorities, infrastructure service providers, researchers) across cities that have similar (multi-)hazard environments. Inter-city partnerships are common in local government, with examples like the C40 cities, the Asian Cities Climate Change Resilience Network (ACCCRN), of the 100 Resilient Cities. Similar partnerships could also be beneficial between infrastructure professionals, as they allow data, tools and examples of best practice to be shared (Hickford et al., 2018). Infrastructure resilience is already associated with

partnerships, although so far the focus has mainly been on partnerships between sectors within the same city (Hickford et al., 2018). Meanwhile, collaboration in relation to hazards and the built environment is also taking place between cities, for example Japan and Turkey are visited by engineers to learn about earthquake mitigation, while The Netherlands is considered a role model in flood engineering. Cities in different countries may have similar (multi-)hazard challenges, and one benefit of the COHAZLE data could be helping to connect stakeholders in these cities.

Similar cities could be identified relatively easily by searching through the dataset. However, if the dataset was to grow by including additional hazards, or by differentiating more than four severity levels, finding similar cities may become challenging. In that case, a useful approach would be to use a similar coefficient.

Chang et al. (2015) proposed such an approach using the Gower coefficient (Gower, 1971) to calculate similarity between coastal communities. In the approach by Chang et al. (2015), the coefficient is used to identify communities using vulnerability indicators as input data.

The Gower coefficient is one of various possible methods for calculating the similarity of a set of objects (in this case cities) based on a set of attributes (in this case the hazard levels). The Gower coefficient defines the similarity between two objects based on the sum of differences between their attribute values. Missing data is accounted for through a coefficient *b*. The similarity between two objects *i* and *j* is:

$$S_{ij} = \frac{\sum_{h=1}^{H} s_{ijh}\, b_{ijh}}{\sum_{h=1}^{H} b_{ijh}}, \tag{3.2}$$

where s_{ijh} is a similarity score that is calculated according to the data type for attribute *h*, and b_{ijh} defines whether the comparison is possible between the values of attribute *h* for objects *i* and *j*, and *H* is the total number of attributes. The variable *b* takes a value of 1 if attribute data

is available for both *i* and *j*, and 0 if data is missing for one of the two objects. For continuous data, the score s_{ijh} is:

$$s_{ijh} = 1 - \frac{|x_{ih} - x_{jh}|}{R_h} \tag{3.3}$$

where x_{ih} is the value of attribute *h* for object *i*, x_{jh} is the value of attribute *h* for object *j*, and R_h is the maximum range of the attribute *h*. For binary and nominal data the score s_{ijh} is simply:

$$s_{ijh} = \begin{cases} 1 & \text{if } x_{ih} = x_{jh} \\ 0 & \text{otherwise} \end{cases}. \tag{3.4}$$

Therefore, for all data types, if two objects have the same values for all attributes, S_{ij} is 1. If the attribute values of two objects, for all attributes, are on two opposite ends of the attributes' range, the similarity will be 0. If values are the same for some attributes but different for others, or if all attribute values differ a bit, the similarity will be some fraction between 0 and 1.

When $\sum_{h=1}^{H} b_{ijh} = 0$, i.e. when none of the attributes can be compared because some of the data is missing for all attributes, S_{ij} is undefined. As S_{ij} can be obtained even if data is only available for one attribute, Chang et al. (2015) proposes calculating the quality *C* of the comparison using:

$$C_{ij} = \frac{\sum_{h=1}^{H} b_{ijh}}{H}. \tag{3.5}$$

The quality of the comparison C_{ij} ranges between 0 and 1, where 0 means that no data is available for comparison, and 1 means that all the data is available (i.e. that objects *i* and *j* can be compared on all the attributes).

The coefficient also provides the option of weighting variables (Gower, 1971). Weights can be applied by simply multiplying the similarity term by a constant value, using:

$$S_{ij} = \frac{\sum_{h=1}^{H} s_{ijh}\, b_{ijh}\, w_h}{\sum_{h=1}^{H} b_{ijh}\, w_h} \quad (3.6)$$

where w_h represents a weight defined for a specific attribute. The Gower coefficient therefore provides an simple method for measuring similarity that can be applied to nominal, binary, and interval data for calculating hazard similarity.

The COHAZLE data is of ordinal type, and in order to apply the Gower coefficient to the data, the following mapping is used to transform the data from ordinal to interval data: 4 = high, 3 = medium, 2 = low, and 1 = very low. The values can then be used to calculate the similarity score using Equation 3.2. This method assumes equal intervals between consecutive levels. An alternative method could also assign bigger intervals for specific cases (e.g. 5 = high, 4 = medium, 2 = low, and 1 = very low), or use alternative methods such as Goodall (1966) or Podani (1999). However, the simple mapping approach considered suitable for our case, as it allows the similarity scores to be easily interpreted.

With the unweighted Gower coefficient, all differences between levels have an equal effect on the similarity. However, defining some weights w_h and using the weighted similarity in Equation 3.6 can give more importance to specific hazards in the similarity. This is shown with the example of three cities, A, B, and C (Table 3.5).

Table 3.5 Three example cities to demonstrate the proposed similarity index.

	Earthquake	**River flood**	**Extreme wind**
City A	2 (low)	4 (high)	3 (medium)
City B	4 (high)	4 (high)	3 (medium)
City C	3 (medium)	4 (high)	2 (low)

Cities A and B in Table 3.5 have the same exposure to river flooding and wind, but a different exposure to earthquakes. Cities B and C have the same exposure to floods, but vary slightly in

exposure to earthquakes and storms. Using Equation 3.6 to calculate the similarity between cities A and B, and A and C, the two pairs both have a similarity of 0.78. Supposing there is specific interest in earthquake exposure, a weight of $w_h = 2$ is applied to the earthquake levels. The similarity between A and B is now 0.67, whereas the similarity between A and C is 0.75. In both cases the similarity decreases because the dissimilarity in earthquake levels is given more importance, but it decreases more between cities A and B, where the difference in earthquake levels is greatest. Weights can therefore be used to change the relative influence of hazards on the similarity, or to ignore certain hazards altogether, by setting w_h for selected hazards to zero. The data can therefore easily and intuitively be weighted to include user preferences.

An of the use of the coefficient is provided here for the city of Bristol. First, the hazard context of the city is briefly described, and then similar cities are identified and compared. According to a flood risk assessment conducted for the city of Bristol in 2013, tidal flooding from the river Avon represents one of the main drivers of flood risk in central Bristol (Hyder Consulting, 2013). The worst case scenario for flooding in the city is expected to be a combination of a 1-in-200 year tidal flood combined with a 1-in-2 year river flow. Their coincidence is expected to occur once every 200 years. Overall, most of the city centre has protection standards for up to a 1-in-200 year flood. However, the standards will be driven down by climate change. In 100 years, 1,400 properties are expected to be at risk of flooding (Figure 3.16). A new plan is currently under consultation for addressing the anticipated increase in flooding in the centre of Bristol. Previously, the city experienced severe flooding in 1968, when nearly all streams and river in the city broke their banks. Flooding is usually caused by long duration storms and there is tendency for flooding to occur in winter. However there are recorded instances of flooding being driven by summer rainstorms. Localised flooding often occurs during seasonal high tides.

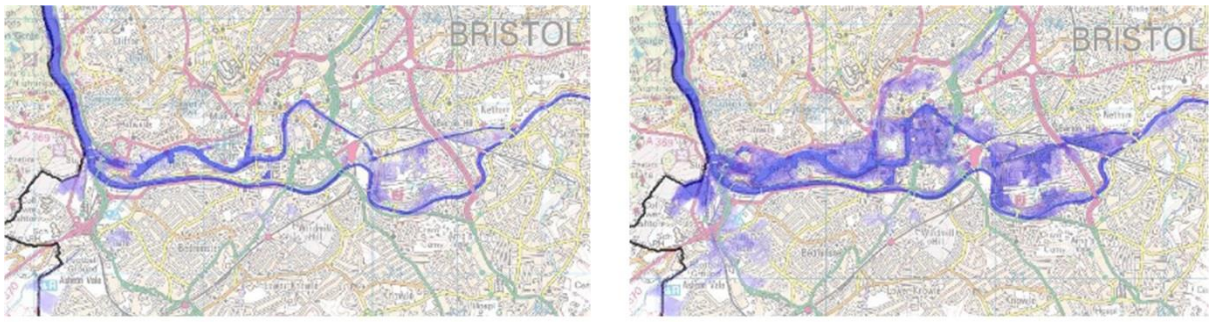

Figure 3.16 The modelled combined 0.5% AEP tidal the 50% AEP river flooding in Bristol under (a) present, (b) 2110 scenario (CAFRA, 2013).

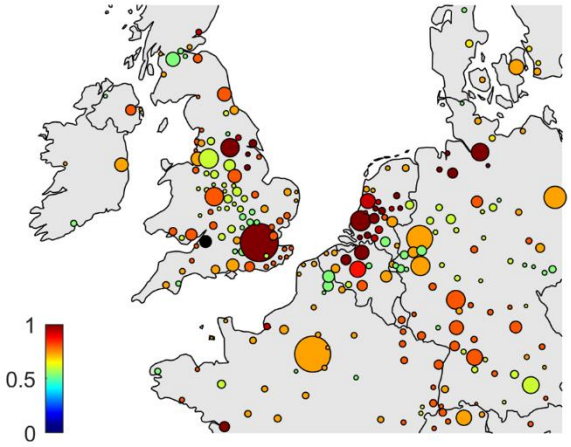

Figure 3.17 City similarity for the city of Bristol based on COHAZLE.

In the COHAZLE dataset, Bristol is classified as having high exposure to coastal flooding, and very low exposure to other hazards. More than 10 cities are found to have a value of S_{ij} = 1, in other words to have identical hazard levels as Bristol. Therefore, geographic distance is included as an additional criterion to help select 10 similar cities. The closest cities to Bristol identified with the same hazard profile include London, Lincoln, Leeds, Scunthorpe, Hull, Nantes, Gent, Roosendaal, Rotterdam, and Antwerp.

An internet search reveals that many of these cities are part of the STAR FLOOD EU funded project for increasing city resilience to river flooding (https://www.starflood.eu/). The project

includes multiple case study cities, for which it describes the flood context including the main types of flooding faced, the mitigation measures in place, and any damaging flooding that occurred in recent memory. Among case studies are London, Hull, Leeds, Rotterdam, Le Havre, and Antwerp. Looking for example at Hull, it is said that "flood risk management for tidal and fluvial flooding has a long legacy in Hull". Hull also uses an interesting and relatively unique system of protection, combining a 'high level system' that raises the level of the river upstream of the city above that of the surrounding land and in that way prevents rainwater from draining from the land into the river. Several flood storage lagoons are also being delivered to address flood risk.

This brief example shows us two things: one is that partnerships and exchange of best practice between cities is indeed valued and being used to advance hazard management, and that when applied to Bristol, the tool acts as a simple and successful filter for rapidly identifying a set of cities with similar hazard characteristics.

An organisation could develop and champion a working version of the proposed tool, for example through a dedicated web platform. The tool could be used to help engineers, planners, hazard risk managers or local authorities in a city to rapidly find other similar cities facing the same challenges. The tool may be particularly beneficial for small and mid-size cities, that often receive less attention than megacities (Birkmann et al., 2016). Yet the majority of urban growth is expected to happen in small and mid-sized cities (Birkmann et al., 2016). The tool is also likely to be most useful to cities that face high levels of multiple hazards.

The evaluation showed that the global hazard data does not always provide a good estimate of the hazard for individual cities, particularly in the case of river flooding. Therefore, there is a concern that implementing the data into a tool may lead to cities either overestimating or underestimating their level of exposure to certain hazards. However, the tool could easily work

by only including the data internally. In other words, rather than providing the data itself to users, the data would be used to output the names of other cities, provided to users as starting points for further data collection. At best, the guidance would help users find useful and relevant information that is applicable to their hazard context. At worst, users would lose time searching through information about cities that is not perceived as relevant to their context. As data continues to improve, the datasets used within the system could be updated. Other parameters could also be included for example total population, building characteristics, or extent of green space.

3.4.4 Study limitations

The main limitation of this study is the uncertainty of the input datasets. To address this, evaluation of the data is carried out for a 46 cities by collecting qualitative information from city strategy reports. The results of the evaluation show that the available global data deviates from reality in a number of cities. It deviates least for earthquakes, cyclone wind, and coastal flood datasets than for river flooding and landslides. This would be expected as flooding and landslides are more dependent on local factors, and therefore more difficult to represent at the global scale. The main factor that is currently hindering improvements to large scale probabilistic flood and landslide datasets is the quality and resolution of input datasets for parameters such as elevation, soil type, and climate (Nadim eta l., 2006; Hawker et al., 2018). The quality of modelled data will likely improve as better resolution satellite data becomes available, making the use of global datasets for assessment at the city scale more viable in the future.

Interactions between hazards, both spatially and temporally, are not explicitly accounted for in the analysis. Hazards can interact in different ways (e.g. coinciding, compound, cascading) (Tilloy et al., 2019), and interactions make some hazards more likely to happen together than

others. For example, storm surges are often coupled with strong winds during storms. On the other hand, storm surges and earthquakes result from separate processes and are less likely to happen at the same time. The distinction between hazards affecting a city together or separately is important because the consequences of the hazards happening together could, in some cases, be more than the sum of the separate hazards. However, determining the probability of hazards happening together is still a challenge. Difficulties exist both conceptually (within what interval of time can hazards be considered to happen together), and methodologically (e.g. how might climate change influence the interaction between hazards). The likelihood of hazards having combined consequences on a community depends on interactions between the hazards (Tilloy et al., 2018), but also on the time that the affected community needs to recover the hazards (De Ruiter et al., 2019). More research is therefore needed, both in terms of natural interactions between the hazards, but also in understanding combined impacts. Exploring how research on hazard interactions could be incorporated into the analysis, and how it might influence the findings, would be an interesting direction for further research.

The results presented are relatively sensitive to the choice of values used to define hazard levels. The hazard levels from Fraser et al. (2016) selected for this study show the intensity at which a hazard would become damaging in an area if no protective measures were taken against it. As damaging intensities in practice vary in different parts of the world due many factors, such as building types, materials, age, maintenance, and so on, Fraser et al. (2016) selects a low damage threshold, that reflects conditions in vulnerable areas. However choosing different damage thresholds has a strong influence on exposure, and results need to be interpreted in light of the relatively conservative (low) threshold values used in this study.

The study does not include certain hazards that are of high concern to cities, including rainfall flooding and heat waves, wildfires, volcanic eruptions, and tsunamis. Rainfall or pluvial

flooding is challenging to model over large scales as is highly dependent on characteristics of the drainage infrastructure. However there have been some studies that model pluvial flooding over large areas (e.g. Guerreiro et al., 2017). The additional hazards could introduce new types of interactions. For example, wildfires can deforest slopes and amplify landslide hazards (Gill & Malamud, 2017), and a loss of tree cover caused by wildfires may amplify exposure to strong wind. Future increase in occurrence of wildfires as a result of climate change may make it an important consideration for urban hazard. In the future, new datasets and improvements in data quality could be used to extend the analysis to other hazards.

The population values show the total population of the urban area. For population numbers to correspond to the number of people affected by the hazard, the impacts of the hazards in one part of a city would have to extent throughout the rest of the city. This simplifying assumption is unlikely to be correct particularly in large cities, and does not take into account any existing features, such as modularity, or redundancy, that is preventing networks from undergoing total failure. Recent work on applying graph theory to represent the connections between elements of the city could contribute to a better understanding of how shocks spread through complex networks (e.g. Arosio et al., 2020), and could provide more accurate estimates of the true affected urban population. It should be noted that population affected through cascading impacts that initiate outside of the urban area, either at the outskirts (e.g. impacts to a reservoir) in neighbouring cities, is also not included in this study (e.g. Koks et al., 2019).

3.5 Conclusions

In this chapter, hazard severity levels for five hazard types (earthquakes, river flooding, coastal flooding, cyclone wind and landslides) were calculated for urban areas globally using openly available datasets. Patterns in exposure to various hazard combinations were analysed.

Three hazard combinations were found to be important for cases for further study: combined exposure to river flooding and cyclone wind; combined exposure to river and coastal flooding; and combined exposure to (*low*) earthquake and cyclone wind, and (*low*) earthquake and river flood hazards. Hydrometeorological hazard combinations including cyclones and flooding, and compound river and coastal flooding, currently appear to be more widely studied than earthquakes and flood/wind combinations, and the implications of the latter for urban infrastructure still need to be better understood.

This page was intentionally left blank

Chapter 4. Modelling disruption to water supply from a consecutive earthquake and cyclone

4.1 Introduction

Providing reliable access to water when and where it is needed is essential to the proper functioning of any town or city. Water supply in most cities depends on extensive networks of buried pipelines, pumps, storage tanks, and treatment works, designed to efficiently deliver water in appropriate volume, pressure, and quality (Trifunovic, 2006). Water supply systems face various types of threats, such as random failures, attack, and natural hazards (Butler et al., 2014). Natural hazards like earthquakes and cyclones can cause failure in multiple system components, with severe consequences for functionality (e.g. Arrighi et al., 2017; Chang et al., 2002). De Ruiter et al. (2019) suggested that 10% of the global population are potentially exposed to an earthquake and tropical cyclone occurring within 30 days of each other.

Disruption to water supply during hazard events severe affect the ability of communities to cope and recover from the event. For example, the 1995 Kobe earthquake in Japan damaged the water supply system and affected firefighting capabilities. As a result, the fires that ignited after the earthquake (due to damage to gas pipelines) caused almost as much overall damage to the city as the earthquake itself (Kitagawa & Hiraishi, 2004). In the UK, the summer floods of 2007 left 350,000 people without mains water supply for over two weeks. The lack of mains water supply particularly affect those who struggled to collect water from temporary sources, (e.g. bottled water, tanker trucks), including vulnerable people and those without means of transport (Pitt, 2008). The Tohoku earthquake and subsequent tsunami in Japan in 2011 affected water supply to more than 2.2 million households for several weeks (Nojima, 2012).

The lack of water access meant that much of the international relief was focused on providing drinking water alternatives to the affected communities (Bross et al., 2019).

While there have been a number of studies that model impacts to water supply from single hazards (Chapter 2), there is a lack of studies looking at the impacts of consecutive hazards, including on water supply. Consecutive events could have consequences that cannot be predicted from simply aggregating the effects of single hazards (Kong et al., 2019; Sitzenfrei et al., 2011; Wisetjindawat et al., 2017). Importantly, the consecutive event could lead to a loss of service that is greater than that of the two hazard events occurring separately, if the second event happens while the system is still affected by the first event. A consecutive hazard event is defined in this study as "two or more hazard events affecting a specific system in succession, before recovery from a previous event is considered to be completed" (De Ruiter et al., 2019). Selva et al. (2013) proposed the term "persistence time window" to refer to the time interval during which the effects of a given hazard type are still present on the exposed element.

Assessing the effects of consecutive hazard events on water supply can provide vital information to help communities become better prepared. It is important to understand whether, why, and for how long disruption could increase due to a hazard occurring while the system is still damaged. A better understanding of consecutive hazards can help water service providers identify suitable mitigation measures, and can help emergency managers and local authorities develop appropriate plans to reduce potential consequences on the community. Both earthquakes and cyclones can disrupt water supply, and multiple cities, particularly across China and in the US, are exposed to both hazards (as shown in Chapter 3). The aim of this chapter is to demonstrate a modelling approach that can be used to assess the effect that a consecutive occurrence of the hazards would have on water supply. The modelling approach is demonstrated for an example water supply network representative of a mid-sized city, to

understand whether assessing disruption from the hazards separately might underestimate the consequences of the consecutive event. The mechanisms that might increase disruption are investigated, and the benefits of different mitigation measures are compared.

The remainder of this chapter is organised as follows: Section 4.2 presents the metrics used to quantify the impacts of the single and consecutive events, and defines the concept of 'interacting impacts'. Section 4.3 presents the hydraulic model of the water supply system, Section 4.4 describes how earthquake damage and restoration are modelled, and Section 4.5 describes how the storm effects are modelled (including interactions with the earthquake). Section 4.6 introduces the case study network and the hazard scenario used to demonstrate the proposed approach. Then, Section 4.7 presents the results and Section 4.8 provides a discussion and conclusions.

4.2 Measuring disruption to water supply

Disruption to water supply is assessed in terms of the ability of the system to meet the demand for water over time (Didier et al., 2018). A service deficit is considered to occur when the water supply is less than the demand. A common perspective in infrastructure resilience studies is to consider both the magnitude and the duration of service deficit (Bruneau et al., 2003). Indeed, even moderate impacts to supply could become significant if they extend for a long period of time. Assessing the disruption therefore involves assessing both the amount of loss of service due to the hazard, and the duration for the system to recover from the event.

Let us assume that water is consumed at a set of nodes i across the network. The variable $C_i(t)$ represents water consumption at a node i over time t. Assuming that the system is able to fully meet the demand for water under normal conditions, consumption $C_i(t)$ under normal conditions is equal to demand $D_i(t)$ for water at point i. Following the hazard event(s), the

system to be unable to meet demand at certain locations, causing some loss of service at those locations. Service is considered to be affected whenever consumption $C_i(t)$ falls below demand $D_i(t)$ at a given location and point in time (Didier et al., 2018). The level of service $S_i(t)$ here is represented by a binary variable. The variable takes a value of 1 if the ratio of consumption to demand is above some critical threshold α, and 0 otherwise (Klise et al., 2017).

$$S_i(t) = \begin{cases} 1 & \text{if } C_i(t) / D_i(t) \geq \alpha \\ 0 & \text{otherwise} \end{cases} \quad (4.1)$$

The combined service across all nodes in the network $S(t)$ can then be calculated by aggregating the values of $S_i(t)$. Note that the number of people relying on the network could vary at different points i, meaning that loss of service at different nodes will not impact the same number of people. The difference in population at different nodes can be reflected by weighting the $S_i(t)$ at each node by the node population, and dividing by the total population supplied by the network. The service $S(t)$ across N would then be:

$$S(t) = \frac{\sum_{i=1}^{N}(S_i(t) \times pop_i)}{\sum_{i=1}^{N} pop_i} \quad (4.2)$$

where $S(t)$ represents the proportion of the population receiving a satisfactory level of service at a given time, and pop_i is the population at node i. Values of $S(t)$ range between 0 and 1. A value of 0 corresponds to all of the population receiving less than a threshold α of the usual demand, and a value of 1 corresponds to all of the population receiving more than a threshold α of the usual demand. The threshold α is set to 1% in this study. By using a threshold of 1%, it is possible to clearly identify the population that is without water. A value of $SD(t)$ equal to 0 means that all of the nodes are receiving less than 1% of the demand, and value of $SD(t)$ equal to 1 means that all nodes are receiving at least 1% of the demand. For the modelled case study, service was found to rapidly drop between 1 and 0, and to recover rapidly from 0 to 1, resulting

in only small differences in service levels for different values of α. However, where this is not the case, a threshold of 1% could underestimate service recovery, and previous studies have used higher threshold, for example a threshold of 80% was used in Klise et al. (2017). Multiple thresholds could also be used where the service levels are more sensitive to the chosen threshold value.

To compare the overall effect of different events, the total service deficit (TSD) is calculated by integrating the service deficit (i.e. the proportion of the population not receiving adequate service) over time:

$$TSD = \int_{t_0}^{t_r} 1 - S(t)\ dt \tag{4.3}$$

where t_0 and t_r correspond to the start and end time of the event of interest. The start and end time would be chosen according to the scope of the assessment. The start time t_0 will often be the time of occurrence of the hazard, while t_r will often be set to the time when service is considered to have recovered, i.e. when $S(t)$ is equal to 1 (Didier et al., 2018). The value of *TSD* can therefore be applied for any hazard or sequence of hazard events, by selecting appropriate values of t_0 and t_r. The total service deficit from hazard *A* would be calculated by integrating the loss of service between time $t_{0,A}$ corresponding to the occurrence time of the hazard, and time $t_{r,A}$ at which service recovers (Figure 4.1). Similarly, the total service deficit from the consecutive event *AB* (i.e. sequence of hazard events *A* and *B*) would be calculated by integrating between time $t_{0,A}$ when the first hazard occurs, and time $t_{r,AB}$ when service has recovered from the consecutive event. For simplicity when comparing different events and combinations of events, *TSD* can also be calculated between some simulation start time $t_{s,0}$ and some simulation end time $t_{s,f}$, as long as $t_{s,0} < t_{0,A}$ and $t_{s,f} > t_{r,AB}$.

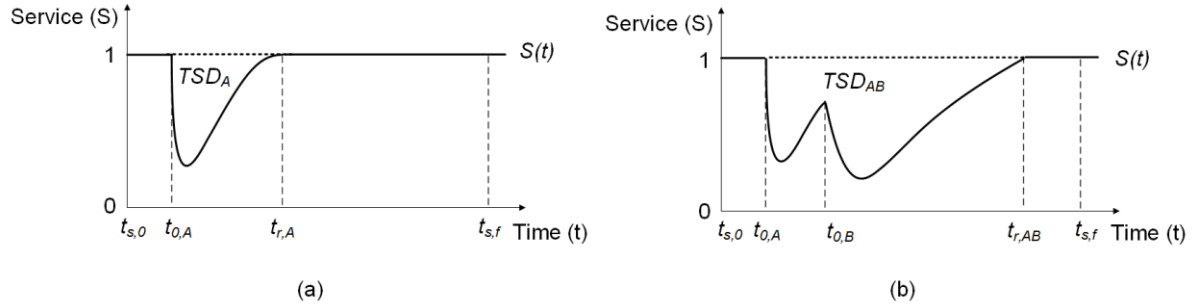

Figure 4.1 Service levels *S(t)* over time for (a) just event *A* and (b) events *A* and *B* occurring consecutively. Times t_0 and t_r represent the start and end times of the events, and times $t_{s,0}$ and $t_{s,f}$ represent the start and end time of a simulation. The area *TSD* is the total service deficit from each event. The dashed line is the level of service under damage.

Figure 4.1 shows the variation in service over time *S(t)*, and the total service *TSD*, in the case of a single and a consecutive hazard event. In Figure 4.1 (a), a single event *A* causes a temporary loss of service, before the supply is restored by repairing or replacing of affected elements. In Figure 4.1 (b), the same event *A* occurs, but a second event *B* occurs before repairs are completed for event *A.* The second event causes a further drop in service, which lasts until repairs are completed. In both cases, the total service deficit corresponds to the total area between the normal level of service and the level of service under damage.

To assess the effect that the events coinciding in time has on the system, a new quantity is defined here, the 'change in total service deficit' *ΔTSD.* The value of *ΔTSD* corresponds to the difference between the total loss of service from the consecutive event, and total loss of service from the two hazards occurring independently. Figure 4.2 shows an example of the service deficit from two events *A* and *B* occurring independently, and the same events overlapping. As shown in Figure 6.2, *ΔTSD* is the difference between the loss of service attributed to the independent hazards, and the actual loss of service during the consecutive event, represented by the grey area in Figure 4.2 (b).

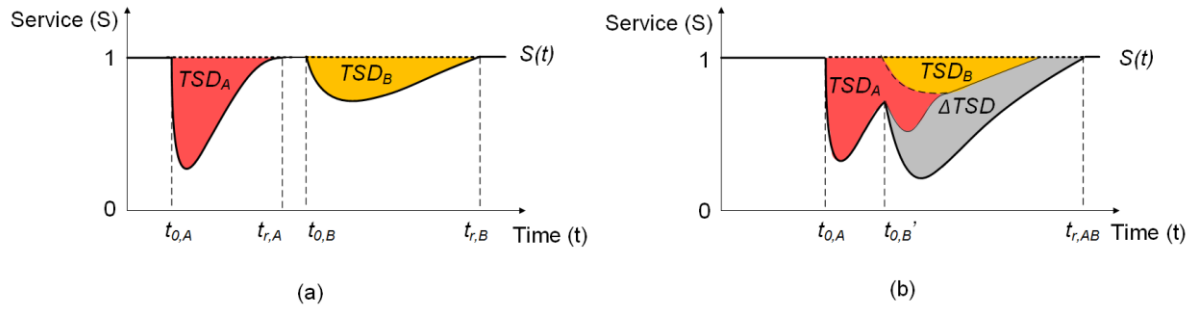

Figure 4.2 The service levels for (a) events *A* and *B* occurring separately, and (b) a consecutive occurrence of events *A* and *B*. *ΔTSD* is the service deficit due to the interacting effects of the two hazards on the system.

The value of ΔTSD is calculated as:

$$\Delta TSD = TSD_{AB} - (TSD_A + TSD_B), \quad (4.4)$$

Where TSD_A and TSD_B is the total service deficit from two single events, and TSD_{AB} is the total service deficit for a consecutive occurrence of the two events. Calculating ΔTSD isolates the effect of the consecutive events relative to individual events, and can be used to identify the mechanisms by which disruption increases during a consecutive event. This will be shown for an example water supply network, but first, the next section introduces the hydraulic model used in this study.

4.3 Model of a water distribution system

The water supply system consists of junctions, tanks, reservoirs, pipes, pumps, and valves, that are used to distribute water from a source to the point of demand (Figure 4.3). The system is modelled as a pressurised pipe network using a hydraulic model (Trifunovic, 2006). This section provides a brief overview of the model used and introduces the key variables for

understanding the level of service. Further information can be found in Rossman (2000) and Klise et al. (2017).

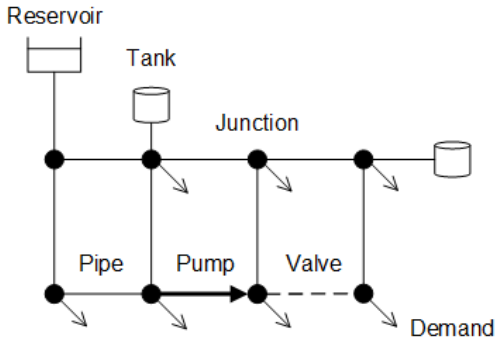

Figure 4.3 The components and layout of a water distribution network. Water leaves the network at junctions based on the demand at that junction.

The elements of the water supply system are represents simply as a network of nodes and links (e.g. Klise et al., 2017; Morley & Tricarico, 2008; Muranho et al., 2012; Pathirana, 2010; Rossman, 2000). Each link caries some flow q_j each node has some pressure p_i at a given point in time. Other node and link variables vary between elements. A reservoir element represents an 'infinite' source of water (e.g. a river, groundwater aquifer, or treatment plant). Reservoirs have constant water pressure and represent a boundary condition of the model. Junctions are nodes that connect pipes. Each junction has some time-varying demand $D_i(t)$. Water leaves the network through junctions, representing water consumption $C_i(t)$ over time. Tanks are nodes that store water. Each tank has a minimum and maximum water level. If water in a tank falls below the minimum level, outflow from the tank stops. Similarly, if the tank reaches a maximum level, inflow stops. Pipes are links that connect two junctions. As water travels through pipes it loses energy due to friction. In contrast, pumps are links that add energy to the water. The amount of energy that a pump can add to the water is described by a pump curve. The pump curve represents the relation between pressure and flow (the higher the flow rate,

the less energy the pump can add to the water). Valves are links that can be used to regulate flow or pressure.

Flow in the network is governed by the conservation of mass (i.e. all water that enters the system must either leave or accumulate within the system), and conservation of energy (i.e. all changes in energy of the water are accounted for through friction loss or pumping). The energy of the water, or total head *H,* consists of three components, its potential energy (due to height), its pressure energy, and its kinetic energy*:*

$$H_i = z_i + \frac{p_i}{\rho g} + \frac{v^2}{2g} \tag{4.5}$$

where H_i is the total head at a given node, z_i is the elevation of the water at the node (m), p_i is the gauge water pressure at the node (Pa), ρ is the water density (kg/m^3), g is the acceleration of gravity (m/s^2), and v is the flow velocity (m/s^2). The sum of the potential and pressure energy, the first two terms in Equation (6.3), is referred to as the hydraulic (or piezometric) head (Trifunovic, 2006). The hydraulic head is expressed in units of metres equivalent water height. Hydraulic head determines the direction of flow. Water flows through the network from nodes with the greatest hydraulic head, to node with lower hydraulic head.

Inputs to the model include the network topology, node elevations, and component characteristics (e.g. tank diameter, pipe diameter, pipe roughness). The model computes the flows and nodal pressures at each timestep. Simulation over time consists in solving the pressure and flows that meet the conservation of mass and conservation of energy requirement at consecutive timesteps. Controls can be used to define the behaviour of pumps and valves based on tank levels. For example, a pump could be switched on when levels in a corresponding tank reach some level, or pressure, p_i (as water in the tanks is assumed to be static, the pressure p_i at tank nodes is equivalent to the water level).

4.3.1 Demand-driven and pressure-driven modelling

There are several freely available hydraulic models of water supply systems (e.g. Rossman, 2000; Klise et al., 2017). Models can be grouping into demand-driven, and pressure-driven models. Demand-driven models treat the outflow at junctions as constant (i.e. a boundary condition) (e.g. Rossman, 2000). In other words, the consumption $C_i(t)$ at nodes is assumed to always be equal to the time-varying demand $D_i(t)$ at the node. This approach is suitable when modelling a network that operates under normal conditions where demand is always met (Klise et al., 2017). However, demand-driven models cannot represent changes in outflow (i.e. supply) due to hazard damage (e.g. leaking pipes, damage to pumping stations). Yet when a hazard occurs, the network is often unable to supply the necessary volume of water. In such cases, an alternative approach has been proposed, referred to as 'pressure-driven' modelling. In a pressure-driven model, the extent to which outflow $C_i(t)$ meets demand $D_i(t)$ at each junction depends on the available pressure at the junction.

There are several different pressure driven hydraulic models including EPANETpdd (Morley et al., 2008), WaterNetGen (Muranho et al., 2012), and the Water Network Tool for Resilience (WNTR) (Klise et al., 2017). The Water Network Tool for Resilience (WNTR, pronounced 'winter') is a hydraulic model provided by the US Environment Protection Agency (US EPA) for analysing how water supply systems respond to various hazards (Klise et al., 2017). WNTR is selected for this study, as it provides easy to use methods for adding damage to the network (leaks and pump outage), and is implemented in Python which makes it highly flexible for carrying out a probabilistic analysis (Klise et al., 2017). The WNTR simulation engine is based on the conservation of mass and head-loss equations from Rossman (2000). The conservation of mass at each node *i* is represented through:

$$\sum_{j \in M_i} q_{ij} - C_i = 0 \tag{4.6}$$

where M_i is the set of pipes connected to node i, $q_{j,i}$ is the flow rate of water to node i from pipe j, and C_i is the water being consumed (i.e. leaving the network) at node i. The head-loss (or friction loss) h_L through a pipe between two nodes is calculated using the Hazen-Williams formula:

$$h_{L,j} = 10.667\, {c_j}^{-1.852} {d_j}^{-4.871} L_j {q_j}^{1.852} \tag{4.7}$$

where c_j is the Hazen-Williams roughness coefficient of the pipe, L_j is the pipe length (in m), d_j is the diameter of the pipe (in m), and q_j is the flow through the pipe (in m^3/s). WNTR uses a reformulation of Equation (6.2) to allow the calculation of negative flow rates (Klise et al., 2017). The roughness coefficient depends on pipe material and age. Pressure driven demand in WNTR is solved using (Wagner et al., 1988):

$$C_i = \begin{cases} 0 & p_i \leq 0 \\ D_i \sqrt{\dfrac{p_i}{P_f}} & 0 < p_i < P_f \\ D_i & p_i \geq P_f \end{cases} \tag{4.8}$$

where C_i is the actual flow of water being consumed at a node (m^3/s), D_i is the water demand at node i (m^3/s), p_i is the pressure at node i (Pa), and P_f is a threshold pressure at which full demand is considered to be met (Pa). Node demand decreases when pressure at the node falls below P_f and reaches zero when pressure falls to zero. P is set to 15 metres in this study. WNTR solves the system of simultaneous equations (4.6) to (4.8) at each timestep using a Newton-

Raphson algorithm (Klise et al., 2017). Note that the model assumes steady uniform flow at each timestep.

In this study, the model is run in pressure-driven mode using a timestep Δt of 5 mins. The model recalculates flow, nodal pressure, and nodal demand at each timestep. A value of Δt of 5 mins is found to provide a good balance between accuracy and computational time. Reducing the timestep makes a negligible difference to the calculated values of flow and pressure, but increasing the timestep introduces some deviation in the results. If a tank empties between two timesteps, or if a time based control changes pump operations between two timesteps, the model automatically reduces the timestep.

4.3.2 Modelling damage to components

WNTR includes methods for adding pipe leaks and pump outage to a network. WNTR models pipe leaks by splitting a pipe into two separate pipe sections at the midpoint and adding a new junction (see Figure 4.5). The rate of leakage D_{leak} (in m^3/s) at the new junction is a function of the pressure at the junction, calculated using (Crowl & Louvar, 2001):

$$D_{leak,i} = C_d \times A_i \times {p_i}^{\alpha} \times \sqrt{\frac{2}{\rho}} \tag{4.9}$$

where C_d is the discharge coefficient (unitless), A_i is the area of the hole (m^2), p_i is the pressure inside the pipe (Pa), α is another discharge coefficient, and ρ is the density of the fluid. The coefficients C_d and α are influenced by the flow regime, pipe material, and orifice shape (Klise et al., 2017). The default values of C_d and α included in WNTR are used in this study (0.75 and 0.5 respectively, corresponding to large leaks out of steel pipes). Note that pressure-dependent leak demand D_{leak} is different to pressure-dependent consumption C_i. An important difference

is that D_{leak} is unbounded, and continues to increase with pressure. On the other hand, C_i does not increase beyond D_i (see Figure 4.2). Leak repairs are modelled by removing the demand node and replacing the two pipe sections with the original unbroken pipe.

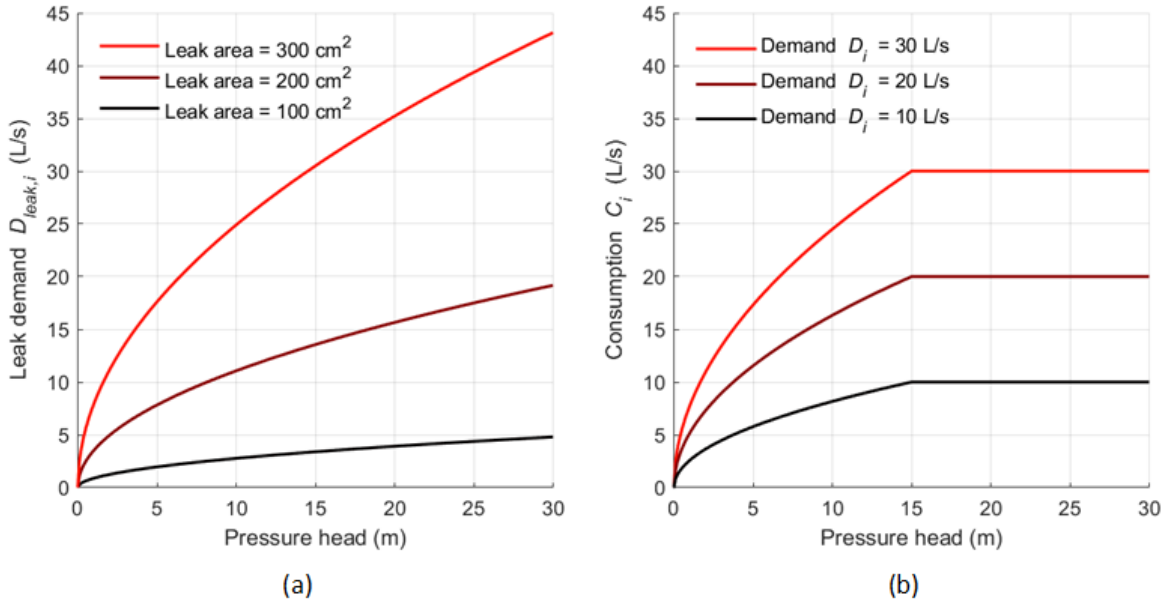

Figure 4.2 A comparison between leak demand D_{leak} and pressure-driven water consumption C_i at a node. (a) shows the variation in leak demand D_{leak} with node pressure for different leak areas A_i. (b) shows the variation in pressure-driven consumption C_i with node pressure p_i for different levels of demand D_i. Leak demand is unbounded and continues to increase with pressure, while consumption C_i has a maximum value equivalent to the nodal demand D_i at a given timestep. Pressure head corresponds to p_i / (ρg).

The method for applying pipe leaks is also applied to model leakage from tanks. For tanks, slight changes are made to the network layout before applying the tank leaks. As shown in Figure 4.5 (b), before running the simulation, a junction (with demand equal to zero and elevation equal to that of the tank) is added next to the tank. The original pipe connecting the tank to the network is replaced with two pipes, one connecting the new node to the tank, and the other leading from the new node to the rest of the network. The same is done for all tanks in the network prior to modelling the hazard scenario (WNTR makes it possible to automate

the process of adding and changing network elements). If the tank is damaged in a simulation, a pipe leak is applied to the new pipe.

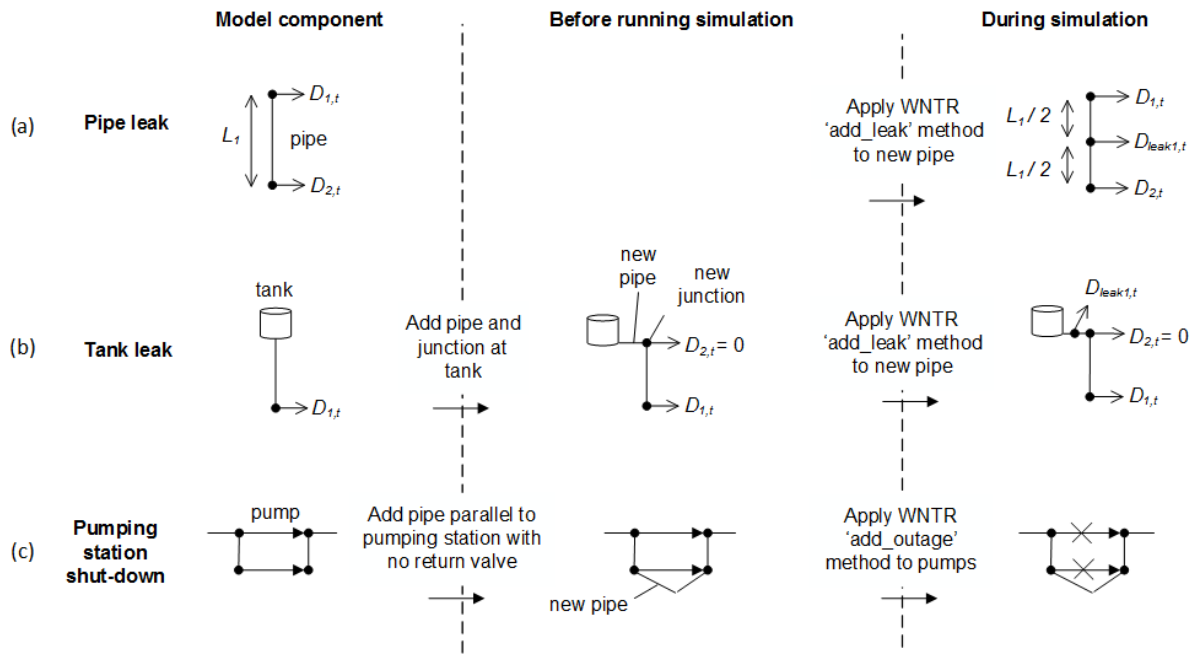

Figure 4.5 Adding leakage to (a) pipes and (b) tanks, and (c) adding bypass pumps to model pump outage.

Pumps can be switched on or off automatically throughout the simulation using controls. Controls are rules included in the model that change the pump status at a specified time, or depending on a specified value (e.g. a control could switch on a pump if tank levels fall below a specified level). WNTR models pump outage using these controls. Given the start and end time of the outage for a selected pump, WNTR adds two new time based controls to the pump (the added controls have priority over any previous controls at the pump). The first control shuts down the pump at the specified start time of the outage, and the second control restarts the pump at the end of the outage. The pump then resumes operating as normal, including responding to any pre-existing controls.

When a pump is shut down, no flow passes through the pump. Therefore, if the pump is the only connection between two parts of the network, pump shut down was found to cause problems with model convergence. To overcome this, a 'bypass pipe' was added alongside each pumping station as shown in Figure 4.5 (c). Note that a 'pumping stations' is used to refer to two or more pumps in parallel at the same location. The bypass pipe includes a no-return valve to ensure flow only occurs in the direction of pumping. The diameter of the bypass pipe is set to the largest of the diameters of the pipes that it connects to (on either side of the pumping station), and the roughness value of the pipe is set to the average of the connecting pipes. The bypass pipe enables flow of water, without adding any energy to the water. For the modelled case study scenario, the addition of the bypass pipe was found to significantly improve model convergence (convergence increased from approximately 50% of simulations to more than 95%).

4.4 Modelling earthquake damage and restoration

Multiple studies of earthquake damage and restoration to water supply networks can be found in the literature (e.g. Chang et al., 2002; Guidotti et al., 2016; Isoyama et al., 2000; Klise et al., 2017; Tabucchi et al., 2010). The damage caused by a specific earthquake event (i.e. an earthquake of specific type, magnitude, and location) to a water supply system depends on many uncertain factors. There are uncertainties in earthquake attenuation, geological conditions, pipe age and material and other factors that influence damage. Damage from an event is therefore generally represented probabilistically, as a probability of an element exceeding a given damage state (FEMA, 2003). Determining the probability of damage of components is done by calculating earthquake ground motion at the component, identifying different component damage states, and using component fragility functions for each damage state. Each step is described in more detail in sub-sections 4.4.1 to 4.4.3. Each component will

have one value of probability for each damage state. Typically, components will have a lower probability of reaching a higher damage state.

To model the effect of the damage on service, the probabilities need to be coupled with the physically-based model presented in Section 4.3. This can be done by generating multiple equally likely *instances* of damage. To generate an instance of damage, random numbers a_k between 0 and 1 are generated for all components k (nodes and links) in the network. Each random number is compared to the component probability values $P_{DSx,k}$ of exceeding each damage state of that component. If $P_{DSx,k}$ is greater than a_k, the component is considered to be in the corresponding damage state. Each component is assigned the greatest damage state whose probability is exceeded. Each instance of damage will therefore consist of one damage state value (this includes DS0, no damage) for each component. Components with higher probabilities of failure will tend to be damaged more often and more severely across multiple 'instances' of damage.

A specific instance of damage (consisting of a set of damage state values DS_k for all components) can then be represented in the model as described in Section 4.3.2. Running a simulation on the damaged system provides service levels over time for the specific instance of damage. Repeating this process across multiple instances of damage provides insights into the probable time-varying service levels.

The restoration time for a given scenario will depend on the amount of damage, as well as on the number of repair teams available (Tabucchi et al., 2010). Restoration time is calculated in this study based on the component damage and number of repair teams, using a resource-constraint approach (Section 4.4.4). Damage states and probabilities of damage, as well as pipe repair times are based on values from the Federal Emergency Management Agency (FEMA,

2003). The model representation of damage states and the repair times for tanks and pumping stations is based on Klise et al. (2017).

4.4.1 Earthquake attenuation

Earthquake effects include ground shaking as well as permanent ground displacement such as lateral spread, liquefaction, or landslides. Depending on soil type, liquefaction can occur over large areas and is a significant concern for water supply pipes (Eidinger, 2012). Therefore, both ground shaking and liquefaction effects are represented in the model. The probability of tank and pumping station damage is calculated from peak ground acceleration (PGA), while the probability of pipe damage is calculated from both peak ground velocity (PGV) and peak ground displacement (PGD) (FEMA, 2003). Therefore, estimates of all three ground motion parameters are needed.

The ground motion prediction equation by Campbell and Bozorgnia (2008) is selected for this study, as it provides consistent and widely applicable equations (based on data collected worldwide) to calculate the values of all three parameters, *PGA*, *PGV* and *PGD* (Douglas, 2014). The variation in ground motion *Y* with distance from the epicentre is calculated using:

$$ln(Y) = c_0 + c_1 M + (c_4 + 0.17\,M) \times \ln\sqrt{{R_{RUP}}^2 + {c_6}^2} + f_{site} \tag{4.10}$$

$$f_{site} = c_{10} \times \ln\left(\frac{Vs30}{k_1}\right) + k_2\left(\ln\left(A_{1100} + 1.88\left(\frac{Vs30}{k_1}\right)^{1.18}\right) - \ln(A_{1100} + 1.88)\right), \tag{4.11}$$

where *Y* corresponds to *PGA*, *PGV*, or *PGD* depending on the coefficient values selected from Table 4.1. R_{RUP} is the closest distance to the co-seismic fault rupture (km), *Vs30* is the average

shear wave velocity in the top 30 metres of the site (m/s), and A_{1100} is the peak ground acceleration (m/s^2) on reference rock conditions (i.e. *Vs30* = 1100 m/s). The form of the equation shown applies to a magnitude 5.5, strike-slip (rake angle of 0 and dip angle of 90 degrees), shallow crustal earthquake. Other parameter values implicit in Equation 4.10 include a depth to the co-seismic rupture of 10 km and a sediment depth of 2 km. Equation 4.10 only applies for values of *Vs30* up to 400 m/s. To calculate the reference PGA value A_{1100} corresponding to a *Vs30* value of 1100 m/s, the following simplification of Equation (4.11) is used:

$$f_{site} = (c_{10} + 1.18\,k_2)\,\ln\left(\frac{Vs30}{k_1}\right) \tag{4.12}$$

where *Vs30* is set to 1100 m/s. The various parameter values are selected based on average or recommended values in Campbell and Bozorgnia (2008). The aleatory uncertainty in ground motion is not included in the model.

Table 4.1 Parameter values for Equations 4.10 – 4.12 from Campbell and Bozorgnia (2008).

	c0	C1	C4	C6	C10	K1	K2
PGA	-1.715	0.500	-2.118	5.60	1.058	864	-1.186
PGV	0.954	0.696	-2.016	4.00	1.694	400	-1.955
PGD	-5270	1.600	-2.000	4.00	-0.820	400	0.000

4.4.2 Damage states

Earthquake damage to components is represented through several damage states (FEMA, 2003). The focus in this study is on estimating the functionality of the system after the hazard event, rather than calculating the damage itself and the associated cost of repairs. Therefore, only damage states that correspond to a loss of system functionality are included in the model.

In total, two damage states for pumping stations, three damage states for pipes, and four damage states for tanks are considered in the study (Table 4.2).

Table 4.2 The earthquake damage states included in this study, based on FEMA (2003). The model representation of earthquake damage states is based on Klise et al. (2017).

Component	Damage state	Description	Model representation in this study
Pumping station	DS0	None	No damage
	DS1	Malfunction for a short time (less than three days) due to loss of electric power and backup power if any, or slight damage to buildings	Shut-down (no flow through pump)
Pipe	DS0	None	No damage
	DS1	Small leak due to ground shaking	Leak diameter between 1 and 5 cm*
	DS2	Large leak due to liquefaction	Leak diameter between 5 and 15 cm (only in liquefaction-prone areas)*
Tank	DS0	None	No damage
	DS1	Considerable damage with only minor loss of content	Leak diameter of 10 cm
	DS2	Severe damage, tank going out of service	Leak diameter of 30 cm
	DS3	Tank collapsing and losing all of its content	Leak diameter of 100 cm

* The model representation of pipe damage is a simplification of the damage observed during actual events. In practice, leaks can vary widely in shape and size, depending on factors such as pipe diameter, pipe material, type of joint, or soil conditions. Both ground shaking and liquefaction could result in catastrophic leakage beyond what is represented here.

Table 4.2 gives the description of each of the selected damage states provided by FEMA, and the corresponding representation in the model. Where a range of leak diameters is provided (i.e. for pipes), the leak is sampled from a uniform distribution. Note that damage states are provided for pumping stations rather than individual pipes. A single damage state is therefore used to represent the functionality of all pumps at the same pumping station in the model (i.e.

all pumps that work in parallel at the same location). Note also that DS2 for pipes only occurs in liquefaction prone areas.

4.4.3 Probability of reaching a damage state

The probability of components reaching a given damage state is determined using fragility functions provided by FEMA. The fragility functions are based on damage inventories of past earthquake events and on expert elicitation (FEMA, 2003).

The probability of pipe damage is represented by an expected number of pipe failures per unit length of pipe. The expected number of small leaks per unit length of pipe is calculated based on *PGV*, using:

$$R_{DS1} = 0.0001 \times PGV^{2.25}, \quad (4.13)$$

where *PGV* is the peak ground velocity in cm/s at the midpoint of the pipe. The number of large leaks (DS2) per unit length of pipe is calculated based on *PGD*, using:

$$R_{DS2} = P_{liqu} \times PGD^{0.56}, \quad (4.14)$$

where *PGD* is the peak ground displacement at the mid-point of the pipe (in inches), and P_L is the probability (between 0 and 1) of liquefaction occurring. The value P_L depends on peak ground acceleration, earthquake magnitude, liquefaction susceptibility, and the depth to groundwater, and is calculated using the corresponding functions in FEMA. No correction factor is applied for depth to groundwater, equivalent to assuming a default depth of 1.5 metres. The probability of a given pipe being damaged can then be determined using:

$$P_{DS} = 1 - e^{-R_{DS} \times L}, \quad (4.15)$$

where P_{DS} is the probability of the pipe reaching a given damage state, L is the length of the pipe in kilometres, and R_{DS} is the expected number of repairs per kilometre for the corresponding damage state. Note that the equation corresponds to modelling failures as a Poisson process with mean failure rate $R_{DS} \times L$.

FEMA provides fragility curves for different types of tanks and pumping stations (buried, on-ground or elevated tanks, different tank materials, and pumping stations of different sizes). The parameters of fragility curves for on-ground steel tanks, and for small pumping stations are shown in Table 4.3 (these are used in the modelled case study). Different fragility curves are used to distinguish between unanchored tanks or pumping station sub-components, representing the baseline case with no mitigation, and anchored tanks and pumping station sub-components.

Table 4.3 Median and beta parameters for the lognormal probability curves FEMA (2003).

Component	**Damage state**	**Probability**	
		Median	Beta
Unanchored (without mitigation)			
Pumping station	DS1	0.15	0.70
Tank	DS1	0.35	0.75
	DS2	0.68	0.75
	DS3	0.95	0.70
Anchored (with mitigation)			
Pumping station	DS1	0.15	0.70
Tank	DS1	0.35	0.75
	DS2	0.68	0.75
	DS3	0.95	0.70

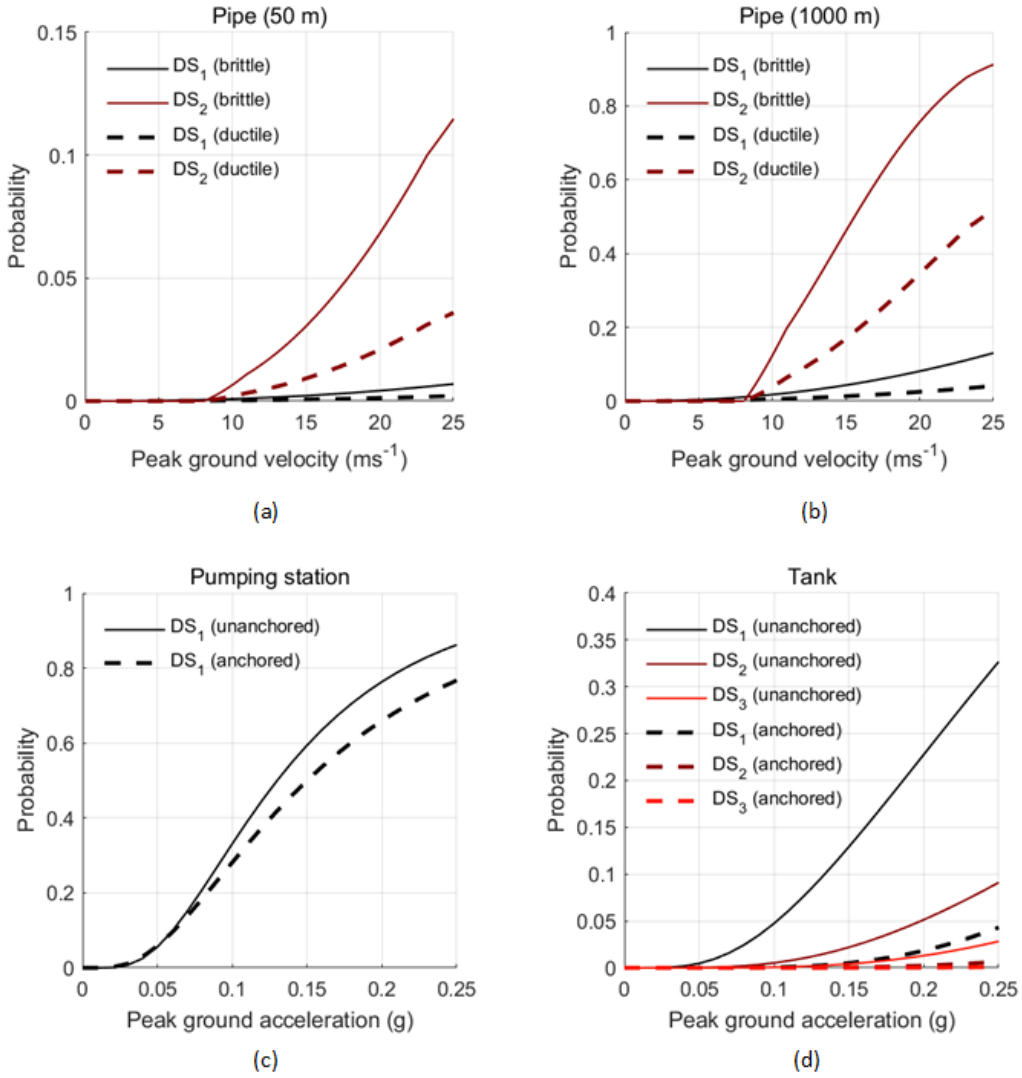

Figure 4.6 Fragility curves plotted from equations FEMA (2003), for (a) 50 metre pipe (brittle and ductile material) (b) a 1000 m pipe (brittle and ductile material) (c) pumping stations (with and without anchoring) (d) tanks (with and without anchoring). Note the different scales on the y-axis.

The lognormal fragility curves corresponding to the parameter values from Table 4.3 can be seen in Figure 4.4. Figures 4.4 (a) and (b) shows that the variation in the probabilities of failure with peak ground velocity for a 50 metre and a 1000 metre pipe. It can be seen for example that the probability of a 50 metre brittle pipe reaching DS2 (i.e. large leak due to ground displacement) is 0.1 for a peak ground velocity of 25 m/s, while for a 1000 metre brittle pipe it

is 0.9, significantly higher. A value of 0.9 suggests that long pipes in liquefaction zones are almost certain to fail at the corresponding peak ground velocity. Also, in Figures 4.4 (c) and 4.4 (d), the effect of anchoring tanks can be seen to have a far higher effect of functionality than the effect of anchoring pumping station sub-components, which is significant when interpreting the results.

4.4.4 Earthquake restoration time

Restoration times from the earthquake are modelled by running a simple restoration routine. The restoration routine takes as inputs the number of workers available, the priority of repairs and the time needed for each repair, and returns the end time of each repair. It assigns teams of workers to repairs in order of priority until all the repairs are completed. Separate crews are assumed to repair pipes, tanks, and pumps, and the time is calculated separately in each case. Pipe repairs are prioritised by diameter, starting with larger diameter pipes (Chang et al., 2002; FEMA, 2003), and tank and pump station repairs are prioritised by tank capacity and maximum flow capacity respectively, with largest capacity components repaired first.

Table 4.4 Repair time for individual components included in this study.

Component	Type	Restoration time (hours)*
Pumping station	Any	8
Pipe	pipe diameter ≤ 300 mm, DS1	4
	pipe diameter ≤ 300 mm, DS2	6
	pipe diameter > 300 mm, DS1	8
	pipe diameter > 300 mm, DS2	12
Tank	Any	12

* pipe restoration times are based on values used in HAZUS-MH in the US while pump and tank restoration times have been suggested for demonstration purposes in Klise et al. (2017). They may not be representative of actual restoration times and may not be representative for different parts of the world.

A random component is added to the calculated restoration times for each hazard, to represent uncertainty in repair times. The random number is sampled from a normal distribution with mean zero and standard deviation of one hour. The minimum possible repair time for any component is set to two hours.

4.5 Modelling cyclone damage and restoration

Cyclones affect urban areas through strong winds, rain, and possible flooding. Many forms of damage to water supply systems from the effects of cyclones have been observed. Pipes can be damaged when wind uproots trees, or crushed in severely flooded area (Copeland, 2005). Elevated water storage tanks can be affected by wind, and on-ground storage tanks can be damaged or overturned by flooding (Karamouz et al., 2017). In particular, a major problem for water supply during Hurricane Katrina was the loss of power and the lack of backup generators (Patterson et al., 2007). Other events have also shown that power outages can be a major cause of disruption to water supply during a tropical cyclone, windstorm, or flood event (Klinger & Owen Landeg, 2014; Pant et al., 2018). The storm is therefore represented in this study by a loss of functionality of the pumping stations due to a power loss. Two cyclone damage states are included in the model, as shown in Table 4.5.

Table 4.5 The cyclone damage states included in this study.

Component	Damage state	Description	Model representation in this study
Pumping station	DS0	None	No damage
	DS1	Malfunction for a short time due to loss of electric power and lack of backup power	Shut-down (no flow through pump)

To account for uncertainty in the storm damage to the system, storm impacts are represented using the same probabilistic approach as for the earthquake. The probability of pumping station

failure is considered to be a function of the wind speed, with greater probability of failure as storm intensity increases. The probability could be determined, for a given case study, given information about the power network (location of critical components, layout, connection to the water system). For example, Dunn et al. (2018) provides functions for the expected number of failures per kilometre of overhead electricity cables, and Guidotti et al. (2016) models the cascading effects of power on water. These approaches could be used to calculate probability of failure values of pumping stations for a given storm intensity. In this study, the storm is directly represented by a probability value at each pumping station for the selected hazard scenario (Section 4.5.2).

The time needed to restore power will depend on the amount of damage and the number of repair teams available. An expected time needed to restore power could be determined, given information about the power network, by using the same resource-constraint model as for the earthquake. However, only the expected restoration time *E(s)* is assumed to be available to represent the probable time needed to restore power for the selected hazard scenario. A random value sampled from a normal distribution with mean 0 and standard deviation of 1 hour is added to *E(s)* to account for the uncertainty in restoration times within each model run. Note that in each model run, the same recovery time is used for all pumping stations (i.e. all pumping stations recover at the same time, representing the time when the power is restored).

4.6 Application to a case study

The modelling approach is now applied to an example water supply system representative of a water supply system for a mid-sized city. The case study is used to demonstrate the potential of this approach for assessing the service deficit from consecutive hazards.

4.6.1 C-Town

In this study, the approach is demonstrated on the water supply system of C-Town. The C-Town water supply system has been used in previous studies for testing expansion strategies (Marchi et al., 2014) and assessing resilience (Diao et al., 2016), and is openly available for download in EPANET format (Ostfeld et al., 2012). Under normal conditions, the C-Town network supplies approximately 15 megalitres per day of water. The population of C-Town is estimated at each node based on consumption, using Equation 6.10 (Klise et al., 2017):

$$pop_i = \frac{\int_{t=0}^{t=7\ days} D_i(t)\,dt}{D_{ppd} \times 7} \tag{6.10}$$

Where pop_i is the population at node i, $D_i(t)$ is the consumption under normal conditions, or demand, at node i (m^3/day), and D_{ppd} is the total demand per person per day (m^3/day). D_{ppd} is assumed to be 0.15 in this study, (i.e. 150 litres per day, which represents an reasonable estimate for a city. Amsterdam for example has a consumption of 130 litres per day according to Trifunovic (2006). As a result, the population of the town is approximately 100,000 inhabitants.

The network consists of 442 pipes, 396 junctions, 7 storage tanks and 11 pumps in total distributed at 5 pumping stations. Figure 4.7 shows the C-Town network layout, including the location of tanks (T1 to T7) and of pumping stations (S1 to S5). All of the water is supplied from a single source to five different pressure zones (Zones 1 to 5). In each zone, the pressure is regulated by a specific pumping station and tank(s). The pumps are regulated by controls based on water levels in the tanks, switching on when level are low, and switching off when the tanks fill up. The demand varies on a daily cycle, with a peak in the morning and evening, and low levels overnight. The demand pattern provided in the original file has a resolution of

1 hour. As the model is run at a 5 minute timestep, the demand pattern is interpolated (using cubic interpolation) to a 5 minute timestep to match the modelling resolution. Detailed information on pump operations, daily demand variability, pump and tank capacity and pipe characteristics is provided in the original EPANET file available from Ostfeld et al. (2012).

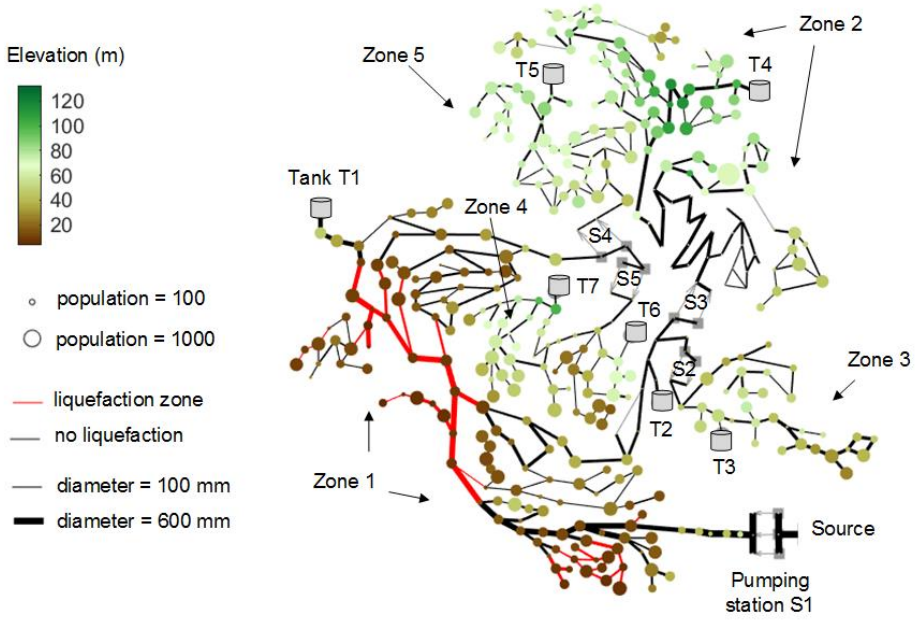

Figure 4.7 The case study water supply network of C-Town.

To model the response of the network to the hazard scenario, assumptions are made regarding the susceptibility of pipes to liquefaction, and regarding the number of repair teams. The area is assumed to have a moderate susceptibility to liquefaction, which corresponds to 10% of the area at risk according to FEMA. In general, liquefaction often occurs in places underlain by alluvial deposits such as floodplains (FEMA, 2003). Therefore, the 10% of pipes at the lowest elevation are selected as being prone to liquefaction. The pipes prone to liquefaction are shown in red in Figure 4.7. Finally, C-Town is assumed to have a total of 6 repair teams available (2 teams of 4 workers each for repairs to pipes, 2 teams for tank repairs and 2 for repairs to pumping stations).

4.6.2 Hazard scenario and mitigation measures

An example consecutive hazard scenario is selected and modelled on the C-Town network. The selected scenario is an moderate magnitude earthquake (M = 5.5) within the same week as a cyclone. Dunn et al. (2018) analysed the rates of failure of electricity cables due to wind, and found that rates of failure increase rapidly as windspeeds exceed 30 m/s. This suggests that a power outage could be expected to occur (dependent on the characteristics of the power supply) at wind speeds somewhat over 30 m/s, or approximately 100 km/h. Both 100 km/h winds and a magnitude 5.5 earthquake can be considered as moderate magnitude events, in terms of the expected overall damage on the city. Such events also occur relatively frequently in parts of the world, making a consecutive event plausible in the most exposed cities, in particular in parts of South East Asia. Activities during the hazards are assumed to resume as normal in the city in the modelled scenario, and the water demand is not considered to be affected (i.e. the scenario assumes no population movement such as evacuation out of the city or to temporary shelters). In this context, loss of water supply and other services could represent the most significant impact of the events on the city, through disruption to businesses, possible disruption to hospitals, and the lack of fire protection.

Multiple combinations of the two events are modelled, by randomly sampling the time of occurrence of each event. As start times for the events are sampled of the same period, there is an equal probability of the earthquake occurring before the cyclone, as of the cyclone occurring before the earthquake. The occurrence time of each hazard, $t_{0,A}$ and $t_{0,B}$ is sampled from a uniform distribution between 0 seconds and 432,000 seconds (i.e. over a time interval of 5 days). After estimating the time to restore the system after the events, the start and end times of the simulation are set to $t_{s,0} = 0$ and $t_{s,f} = 604{,}800$ seconds (i.e. the simulation is run for 7

days in model time). In this scenario, running the simulation for seven days ensures that the recovery process is captured for all event occurrence times.

Several standard mitigation measures aimed at reducing earthquake and cyclone impacts, respectively, are applied, and their benefits during the combined event is analysed. The mitigation measures are applied by modifying the stored failures and rerunning the model. The following earthquake mitigation measures are applied:

- M1-E: Anchoring tanks and anchoring sub-components in pumping stations. *This is done by changing the fragility functions of the tanks and pumping stations to reflect the fragility of anchored components, based on FEMA (2003).*
- M2-E: Changing pipe materials from brittle to ductile. *This is done by multiplying the repair rates of pipes by a factor of 0.3 (FEMA, 2003).*
- M3-E: Increasing the number of repair teams. *This is done by changing the number of repair teams from 2 to 5 for the pipes, tanks, and pumping stations, and recalculating the restoration time of components with the new number of repair teams.*
- M4-E: Both changing pipe material and anchoring components.

The following mitigation measures are considered for the cyclone:

- M5-S: Providing backup power for all pumps at the main pumping station. *This is done by setting the probability of failure of all pumps at the main pumping station to zero.*
- M6-S: Providing backup power sufficient for operating one pump at each pumping station. *This is done by setting the probability of failure of the pump with the greatest capacity to zero (the backup generators are assumed to not provide any mitigation during the earthquake event).*

The next section presents the results for the baseline and mitigation scenarios, as well as results of the analysis aimed to identify the causes of increased disruption.

4.7 Results

In total, 5,000 simulations of the scenario are modelled. From the 5,000 simulations, 231 do not converge. Non-convergence of hydraulic simulations under damage scenarios has been noted before (e.g. Chang et al., 2002; Diao et al., 2016). Results from the non-converged simulations are discarded, and the remaining 4,769 simulations are analysed (95% of the total).

4.7.1 Disruption from single and combined hazards

First, the impact of the individual events on service is shown. Service curves from all the simulations can be seen in Figure 4.8. The figure shows the variation in service from 5 hours before the occurrence of the hazard, to 48 hours after the event. Each simulation represents one equally probable outcome of each event, with varying numbers and locations of components failing. Overall, the results show high variability across simulations, ranging from no disruption to more than 70% of the network being without water. Comparing the two events, the earthquake is seen to cause more disruption to water supply than the cyclone. This reflects the fact that the earthquakes affects all the elements in the system, while the cyclone only affects pumping stations. The recovery behaviour is consistent with the model assumptions, namely that repairs to the network following the earthquake are carried out gradually, while pumping stations all regain power at the same time when the power supply is restored. Also, in 99% of simulations, service recovers within 32 hours of the earthquake, and within 12 hours of the storm.

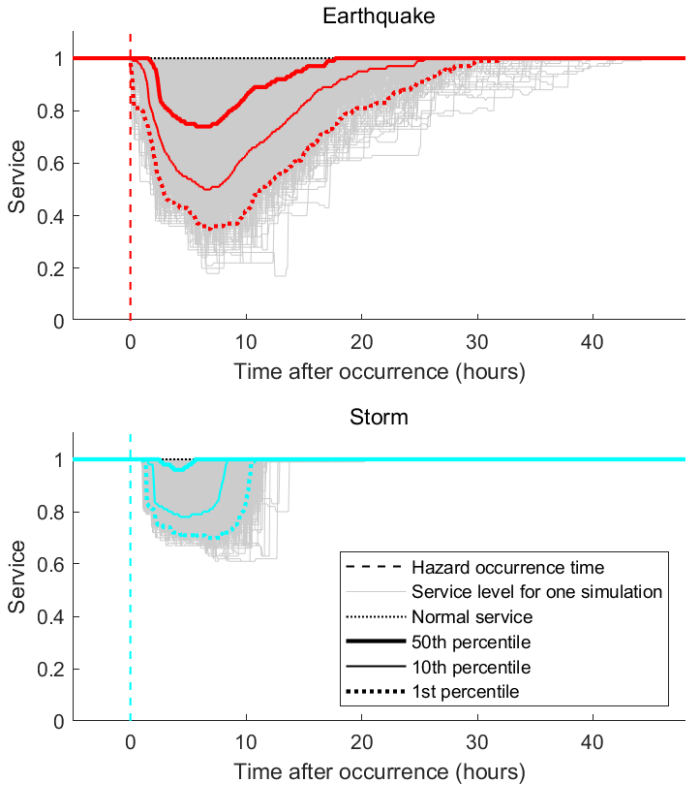

Figure 4.8 – Service curves for the single hazard earthquake and storm simulations. The grey lines represent individual simulations. The xth percentiles are shown (representing the service level at a given timestep exceeded in x% of simulations).

Next, the instances of damage seen in Figure 4.8 are rerun (the damage states and failure times were previously saved), this time with the two events occurring in the same simulation. The two events occur at randomly sampled times within a five day time window. Using this approach allows the change in service deficit ΔTSD to be calculated by comparing service loss from the single events to that of the consecutive events.

The output of the simulation gives a total disruption (exceeded in 1% of simulations) of probable consecutive events to be 853,034 person-hours. In comparison, the cyclone and earthquake caused a disruption of 163,567 and 803,319 person-hours, respectively. The disruption from the consecutive event is therefore more than that of the separate events, as

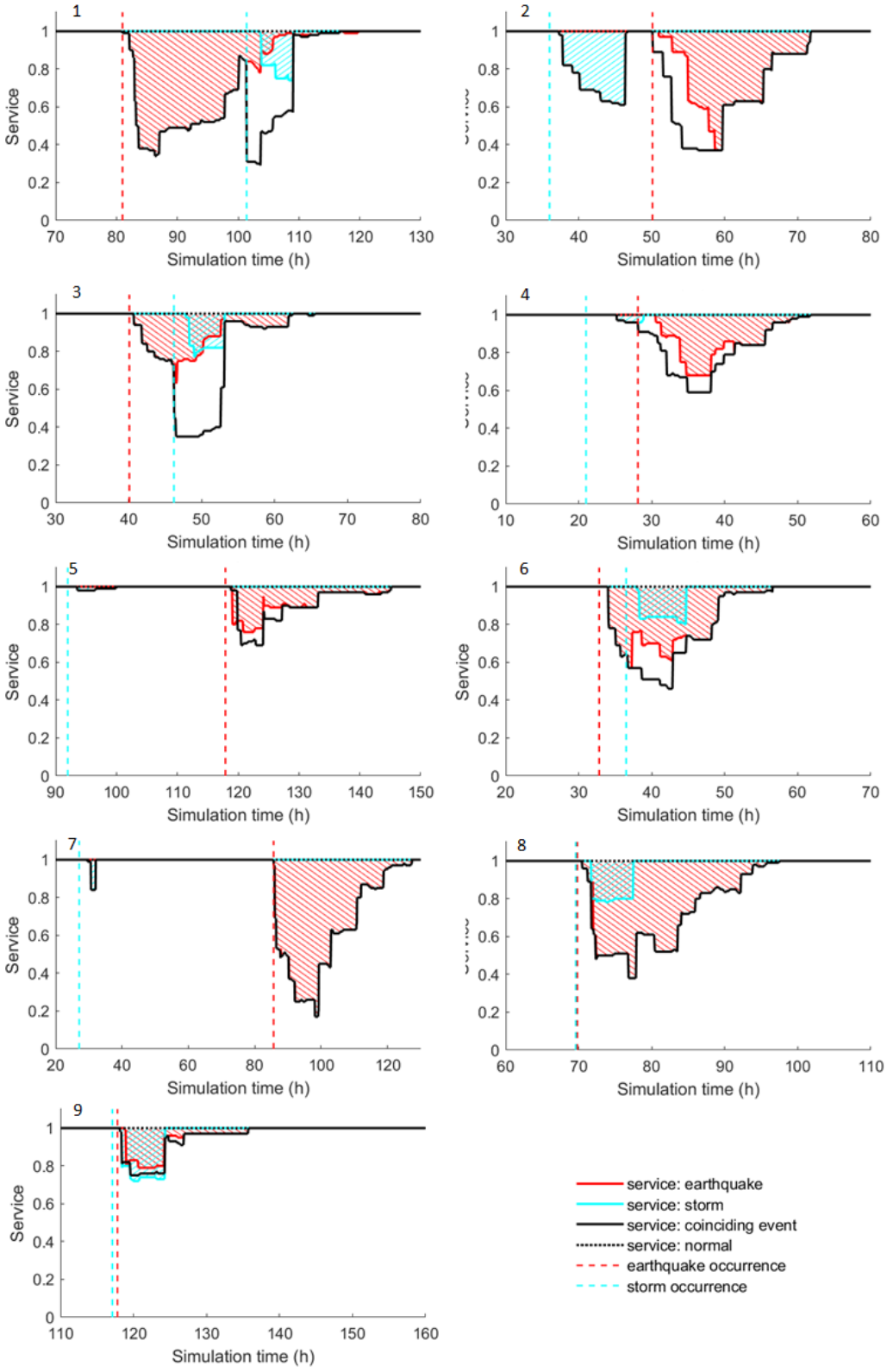

Figure 4.9 Example service curves for selected simulations. The hatched areas represent the disruption from an independent occurrence of the earthquake (red) and storm (blue), and the black line shows the disruption when the events coincide.

expected, but less than the sum of the separate events, when comparing averages across many equally probable scenarios. However, when analysing the results of individual instances, the values of ΔTSD are seen to vary quite significantly across different equally probable instances of the scenario.

Figure 4.9 compares the loss of service for the earthquake, storm, and coinciding event for nine selected instances or cases, numbered 1 to 9. The hatched areas represent the disruption from the single hazards occurring individually, and the area above the black line represents the total disruption from the coinciding event. ΔTSD is the sum of the hatched areas subtracted from the area above the black line. In case 1 for example, the first event occurs 81 hours after the start of the simulation, and causes a loss of service (the red hatched area) over approximately half of the network. Then, 20 hours later at 101 hours, the second event occurs. When the second event occurs on the damaged network, the service level (thick black line) falls below 50%. This means that more than 50% of the population loses water supply. On the other hand, the same failure occurring on the undamaged network (the blue hatched area) affects service to less than 20% of the population. Note that cases 2 and 5 show the first event influencing disruption during the second event, even though service level has recovered (Davis et al., 2014).

4.7.2 Analysing the cause of increase in disruption

Figure 4.10 shows a more detailed look at case 1 in Figure 4.9, and plots the areas of the network where service is disrupted across different time steps of the simulation. It can be seen from the figure that parts of the network (zones 3 and 4 in particular) are unaffected during the single hazard events, but are significantly affected by the coinciding event.

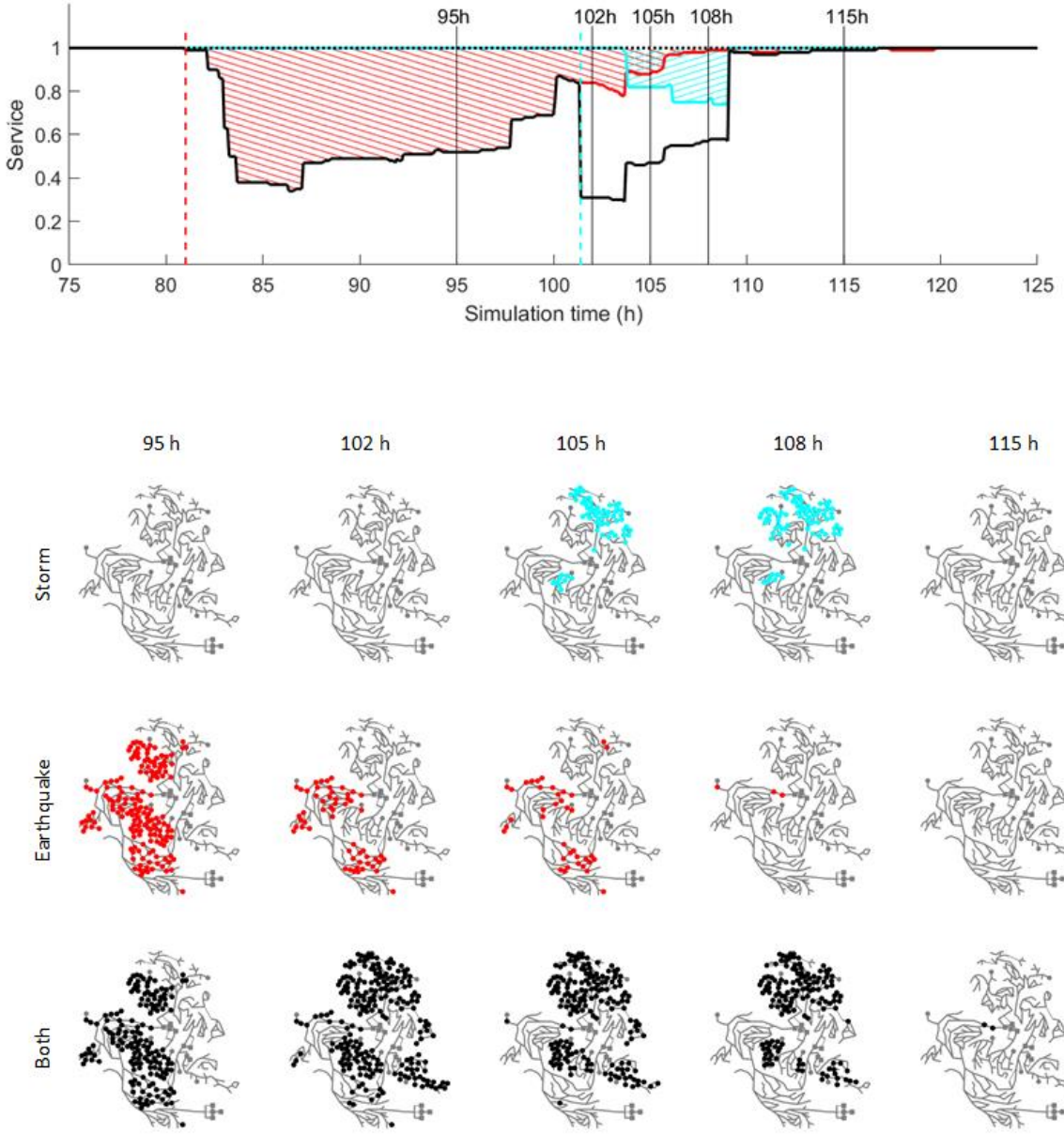

Figure 4.10 Spatial view of service disruption over time for one instance of the events, including (a) the cyclone, (b) the earthquake, and (c) the coinciding event.

The functionality of specific elements (pumps and tanks) in zones 3 and 4 are analysed in Figure 4.11. Different rows show tank and pump levels for each single hazard (rows 1 and 2) and for the consecutive event (row 3). The dashed red and blue lines show the hazard event, the full black line shows tank levels, and dashed black line shows pumping. The grey line show tank levels under normal conditions. The tank in Zone 3 is seen to drain due to damage from

the earthquake (row 2). However, this is compensated by an increase in pumping, which maintains pressures and ensures supply. During the coinciding event however (row 3), the storm affects the pump station and causes both tank levels and pumping to be out of order at the same time, explaining the loss of service seen in the network at that time (Figure 4.10). A similar dynamic explains the loss of service in zone 4.

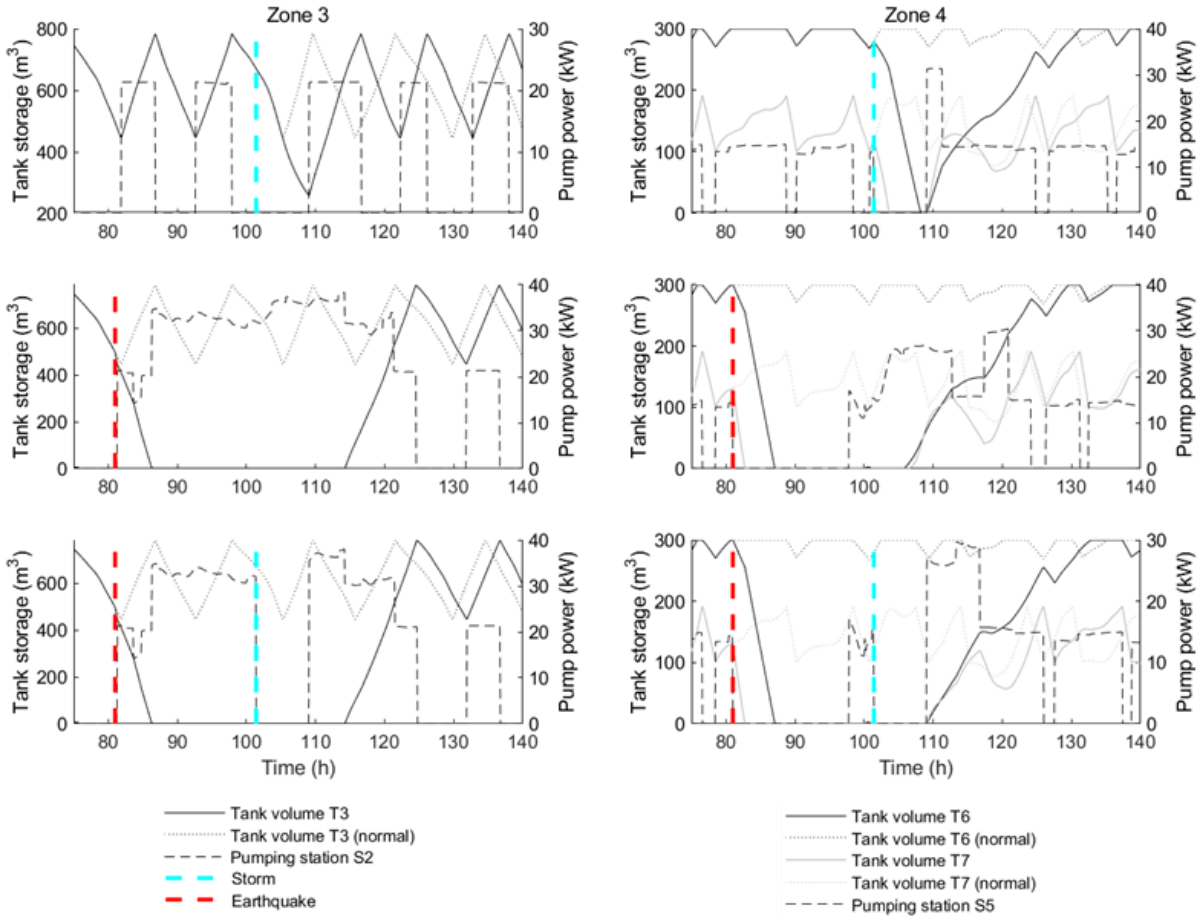

Figure 4.11 Tank and pump levels in zones 3 and 4, for case 1.

4.7.3 Explanatory factors for the increase

Different explanatory factors for the increase are plotted against ΔTSD for all instances of the scenario (Figure 4.12). The figure shows that the total disruption from the single hazards (i.e.

sum of hatched areas) is not a good predictor for *ΔTSD*. On the other hand, the storage deficit at the time of the second event is a relatively good predictor for *ΔTSD*. Indeed, large values of *ΔTSD* (including cases 1, 2, and 3 in Figure 4.9) all occur for a storage deficits of 3000 m^3 or more.

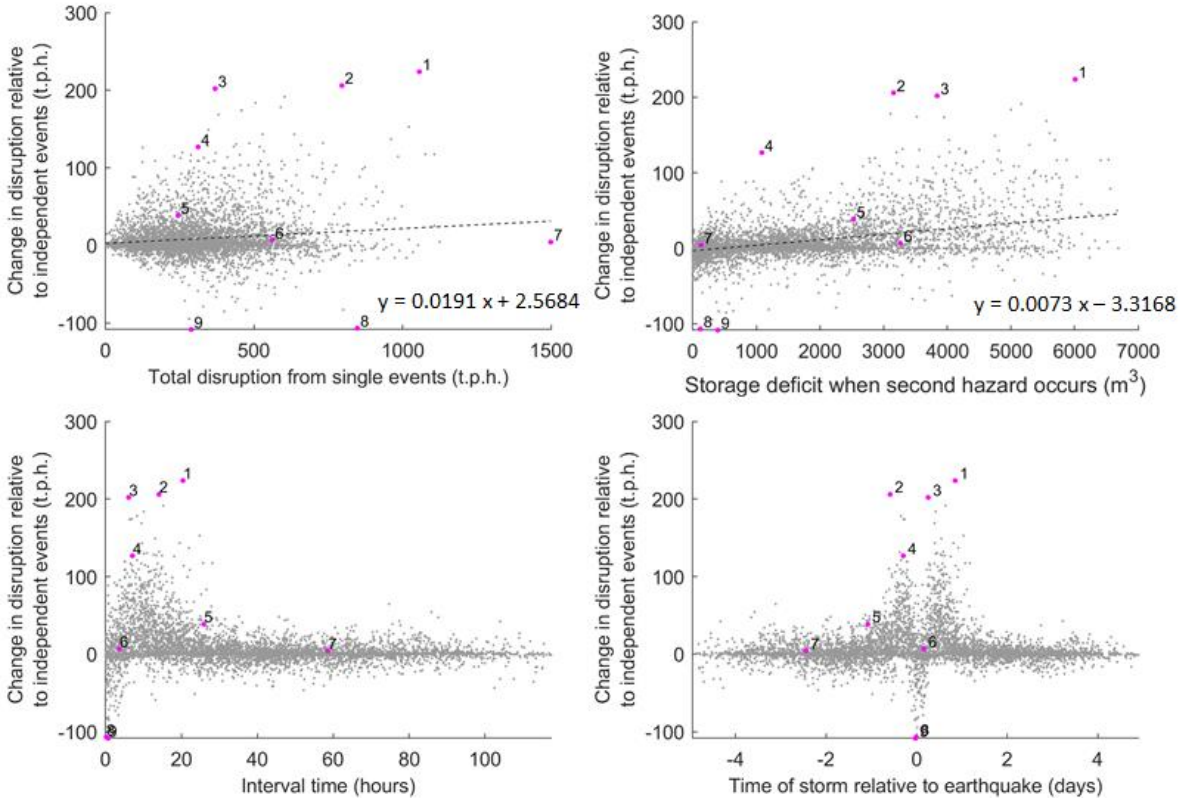

Figure 4.12 Several factors plotted against the change in disruption relative to the sum of the single events (*ΔTSD*), in thousand person-hours (t.p.h.).

A very pronounced pattern can also be seen between *ΔTSD* and the interval time between the two events. *ΔTSD* is mostly negative for interval times < 5 hours, and is randomly scattered about the mean when interval time > 25 hours. However, for interval times between 5 and 25 hours, *ΔTSD* tends to be large (disruption is likely to increase significantly). Between 0 and 5 hours, *ΔTSD* tends to negative, suggesting that when the two events happen at the same time they are likely to affect the same (already affected) elements, and cause less impact overall

than if they happened at different times. A time window can therefore be identified for this system during which consequences of a second event would be amplified. The time window may be associated with a lag between the time at which damaged tanks drain, and the time needed to restore the tanks. However, the results show that large increases in disruption can also occur for low deficits, pointing to other sources of vulnerability to the combined hazards.

4.7.4 Mitigation measures

The analysis is rerun for each of the mitigation measures M1 to M6. In total, 4,519 simulations out of 5,000 converged for all mitigation measures, and for all three of the earthquake, cyclone, and consecutive hazard cases. The effect of mitigation on the single hazard events is shown in Figure 4.13. Only the hazard being targeted by each mitigation measure is shown, since the mitigation measure has no influence on the other hazard (as shown in Table 4.6). In the case of the storm, providing backup pumping for one pump at each station avoids all disruption. This is because the network is designed to operate successfully under normal conditions with a single pump working at each pumping station. The other mitigation strategies all partially help to reduce disruption, but their influence on performance varies. Increasing the number of repair teams (M3-E) reduces restoration time (exceeded in 1% of cases) from 42 to under 32 hours, but does not influence the magnitude of disruption. Changing pipe materials (M2-E), reduces both the magnitude and duration of disruption significantly. However, changing pipe material of all pipes represents and expensive solution, and would likely only be feasible to implement gradually through repair and maintenance cycles. Note that in the case of the earthquake, none of the mitigations measures can eliminate disruption altogether.

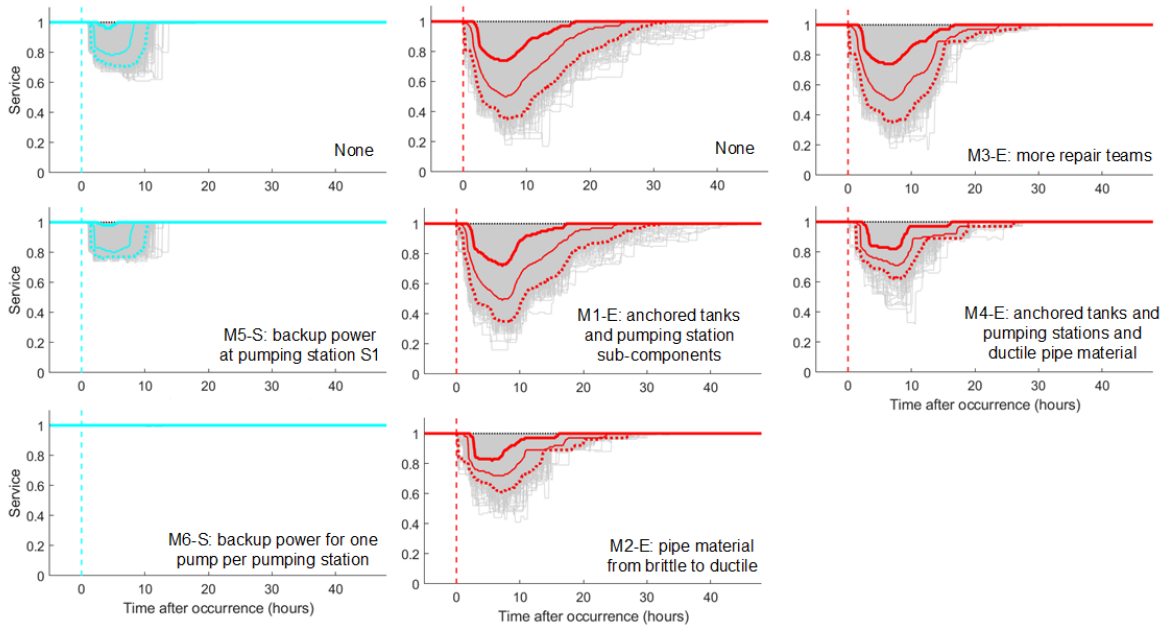

Figure 4.13 Service curves for the single events with different mitigation measures.

Table 4.6 shows the total disruption exceeded in 1% of cases for each mitigation strategy and for the single and coinciding events. The effect of the single hazard mitigation measures varies in the coinciding event. For example, anchoring (M1-E) causes a bigger reduction during the coinciding event than replacing pipes (M2-E), because pump failure is a large contributor to increased disruption as shown in Figure 4.11.

Table 4.6 The total disruption in the case of the storm, earthquake, and coinciding event for different mitigation measures.

Mitigation measure		**Disruption exceeded in 1% of simulations**		
		Storm	Earthquake	Coinciding
-	None	163,567	803,319	853,034
M1-E	Anchored tanks and pumps	163,567	748,731	765,759
M2-E	Ductile pipes	163,567	338,462	429,224
M3-E	Increased number of repair teams	163,567	624,865	697,437
M4-E	Ductile pipes and anchored tanks/pumps	163,567	316,818	373,351
M5-S	Backup power station 1	143,546	803,319	851,473
M6-S	Backup power main pump at all stations	0	803,319	803,319

4.8 Discussion

Results for the C-Town water supply system show that loss of service from individual hazards cannot be used to predict the loss of service during the consecutive event, as consecutive-event loss of service is found to vary from 25% less to over 50% more than the total loss of service of the individual events. In some cases, disruption may also extend to places that are not affected by either of the single events (Figure 4.10).

4.8.1 Measuring the change in total service deficit

The change in total storage deficit is found to be a useful metric for identifying system vulnerabilities to the combined events. No significant relationship is found between ΔTSD and the total disruption from individual events (Figure 4.12). Instead, for the case of C-Town, a relatively good indicator is the total tank storage level at the time of the second event. However, disruption also increases in cases of low storage deficit, suggesting that further analysis is needed to identify remaining vulnerabilities within the system. More work is also needed to understand how these results would translate to other systems, for example systems that are less dependent on tanks and pumps to maintain pressures, but may have other characteristics that make them vulnerable to combinations of events (e.g. Sitzenfrei et al., 2011).

4.8.2 Distinguishing three cases of consecutive events

By stochastically varying the time of occurrence of the two events, a relationship can be seen between interval time and change in disruption (Figure 4.10). The relationship can be explained in terms of three categories of consecutive events:

1. The first category is when **the second event occurs at the same time or very soon after the first event**, while the system is damaged, but still has some buffer capacity.

Here the second event is likely to affect some parts of the system that are already not functioning, therefore adding less disruption. Buffer capacity further helps to maintain the level of service while the damage to both systems is repaired. This category of events means the impact of the second event is less than it would be under normal conditions.

2. The second category is when **the second event occurs some time after the first event**, while the system has only partly recovered and its buffer capacity is depleted. Here the second event might affect the functioning of parts of the system that have just recovered, and depleted buffer capacity cannot cover the demand for the additional time that the system takes to recover. The overall consequences of the combined event in this case are significant.
3. The third category is when **the second event occurs when the system has already recovered**, and therefore no significant interactions are seen.

The behaviour of the system through the three stages seems to follow a 'Mexican hat' type function. Further work is needed to understand the effect of other factors, for example for cases when limited resources need to be distributed between the two events for recovery.

4.8.3 Study limitations

The model used in this study leaves out a number of processes that could influence the results. For example, water demand for firefighting is not modelled, which could increase disruption by reducing pressures in parts of the network (FEMA, 2003). The use of valves for isolating leaking pipes is also not included, which in turn reduce the amount of pipe leakage (Klise et al., 2017). Water demand is also assumed to be the same as under normal conditions. The assumption may in this case be reasonable given that a relatively moderate scenario of the hazards is modelled, but might not apply to a more extreme event. The impact of the earthquake

on smaller service pipes is not included. The model does not consider any obstacles, like debris on roads, that could delay the restoration. The study focuses on the ability of the system to supply water in sufficient quantity, and does not measure other indicators of disruption to water supply, such as pressure or quality requirements (Davis et al., 2014).

4.9 Conclusions

This study demonstrates an approach for looking at impacts of consecutive hazards on water supply systems, demonstrating it with the example of a consecutive earthquake and cyclone event. The two hazards are assumed to occur within a week of each other. Using an example water supply system representative of a real system supplying approximately 100,000 inhabitants (C-Town), the study finds that loss of service from individual hazards cannot be used to predict the loss of service during the consecutive event. The consecutive-event loss of service is found to vary from -25% to +50% relative to the total loss of service of the individual events. By stochastically modelling instances of the two events occurring over a five day time window, the study also identified three different categories of consecutive events, based on interval time between events, that correspond to different categories of system response.

This page was intentionally left blank

Chapter 5. Exposure of roads to flooding and debris flow in a case study city in China

5.1 Introduction

Multi-hazard studies on engineered systems are often demonstrated in simulated environments, and not enough studies apply methods in actual contexts (Ciurean et al., 2018). A likely limitation is the difficulty in accessing the relevant data (Ciurean et al., 2018). As a result, there is insufficient understanding of the advantages and limitations of assessing multi-hazards in practice, and how it could benefit decision making. It is also unclear to what extent proposed methods are compatible with data availability. In particular, cities in China are often exposed to multiple types of hazards (see Chapter 3) and the economy and urban area are growing at a rapid pace, making it essential to integrate multi-hazard information into decision making in order to increase the future resilience of these cities.

The city of Jingdezhen, in Jiangxi province, in the East of China, is used as a case study in this chapter. Jingdezhen is located on the Changjiang river, in a mountainous area downstream of the Huangshang mountain range. It is a mid-sized but rapidly growing city, famous throughout China and beyond for its porcelain (Zhang et al., 2020). The growth of the population and economy mean that the consequences hazards on the city, and on other locations relying on supplies from Jingdezhen, is likely to increase, as the city is home to several important industries and is considered to be an economic hub for the region (Zhang et al., 2020).

Jingdezhen is known to be highly exposed to river flooding (Wang et al., 2018; Zhang et al., 2020). The city is built on the Changjiang river, a tributary of the Yangtze river, and a large

part of the city lies on the floodplain, resulting in frequent and severe flooding (Wang et al., 2018). Particularly large floods occurred in 1998 and 2016 (Wang et al., 2018; Zong & Chen, 2000). Most of the flooding occurs in summer during the rainy season, sometimes driven by typhoon rainfall (Hohai University, 2015). Efforts are ongoing to address the flood risk in the city. Current ongoing projects include the construction of a dam upstream of the city, and flood embankments along the urban portion of the river. Only protection for a 1-in-50 year flood was found to be structurally and economically viable in Jingdezhen (Hohai University, 2015). Therefore, in addition to structural protection, the city is also applying 'soft' and green engineering methods to mitigate flooding. A low lying part of the city has been reclaimed and converted into a lake that can store incoming flow from the tributaries (Figure 5.1 (d)). The city has also worked to increase population awareness of floods (Hohai University, 2015), and research is ongoing to assess the flood resilience of the city. In summary, current flood risk in Jingdezhen remains high, and the protection measures being built will still leave the city vulnerable to flooding, making it necessary to better understand and manage floods when they do occur (Zong & Chen, 2000).

In that context, a multi-hazard approach can contribute to higher preparedness for floods when they do happen, by anticipating interactions between floods and other hazards, with potentially significant consequences. There is evidence that the city is prone to typhoons. However, local information shows limited impacts from wind (Hohai University, 2015), consistent with the fact that the city is located inland where the wind speeds are often lower than on the coast. Nevertheless, typhoons that travel further inland can bring abundant rain, that, in addition to generating river floods, can also cause other hazards, such as surface flooding and slope failures. In particular, debris flows could be an important threat to the city. Debris flows are seen to occur more often near areas where there has been disturbances to the ground, for

example through construction of new buildings and roads, loading and unloading, and deforestation, which are likely consequences of urban expansion activities (Gill & Malamud, 2017).

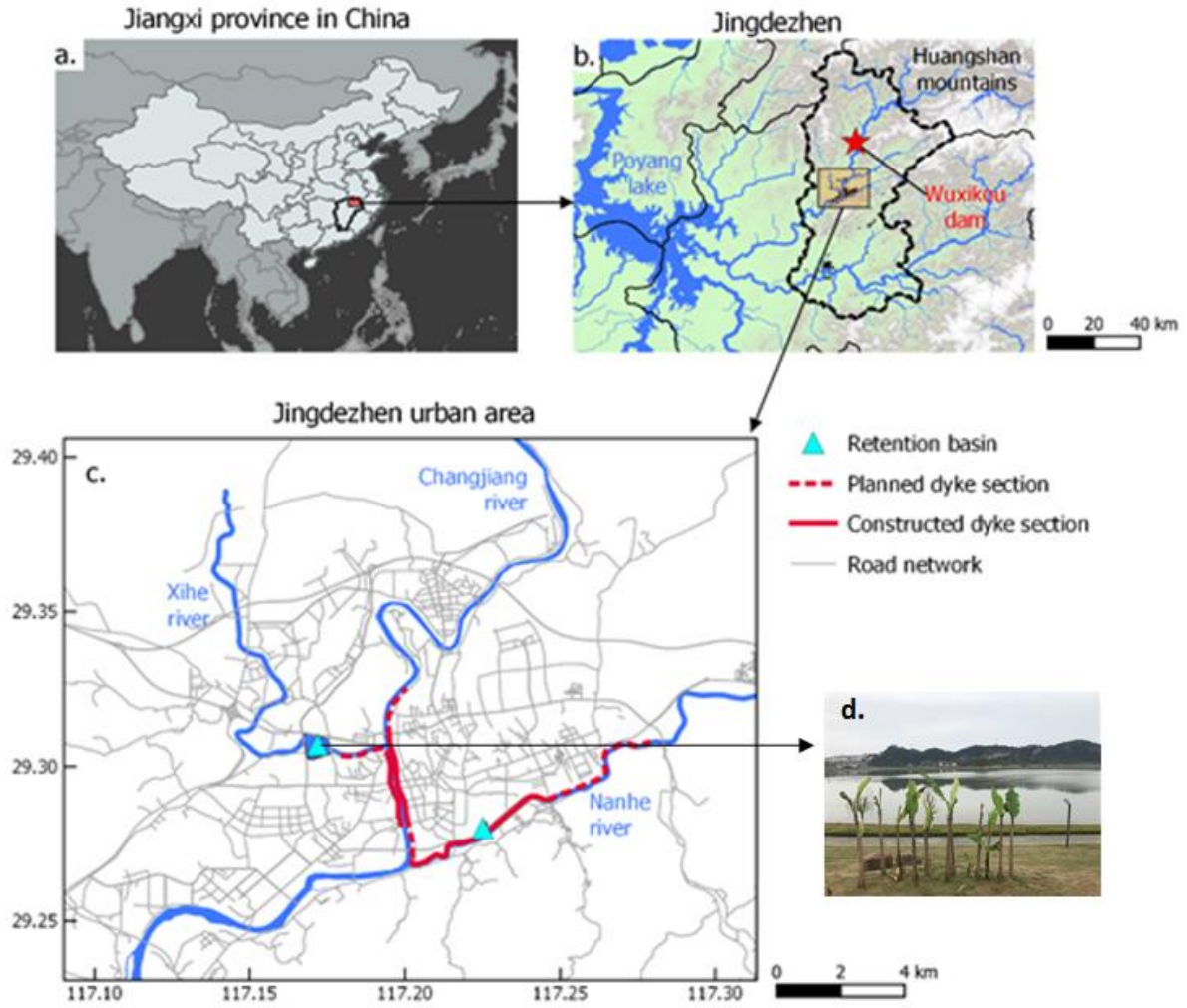

Figure 5.1 Map of the study area, showing (a) Jiangxi province in China, (b) the location of Jingdezhen city between the Huangshan mountains in the North and Poyang Lake in the South, (c) the urban area of Jingdezhen, including the location of flood embankments and flood storage lakes. The road network is obtained from Open Street Map (Haklay & Weber, 2008).

Roads are critical for city function (Reiner & McElvaney, 2017), and can be affected by both flooding and debris flows, making them a suitable focus for this study. Roads enable access between areas of the city, and the performance of the road network under hazards is measured based on the increase in average travel time (assuming constant travel speeds). The performance of the road network can therefore be affected by events such as traffic accidents, congestion, or more severely by the roads being blocked or damaged by hazards. Reduced transport capacity can delay the restoration process, affect the work of emergency and healthcare services, and have consequences on the population.

Therefore, this chapter will analyse the challenges associated with river flooding and debris flows on the road network of Jingdezhen, with the aim of better understanding the limitations to multi-hazard analysis in practice. Section 5.2 introduces the road network data and the method used to measure the functionality of roads at the city scale. Then, Section 5.3 describes how hazard scenarios are modelled. The results of the analysis, showing the effects of river flood, debris flow, and of their combination, are presented in Section 5.4. Finally, Section 5.5 discusses the challenges of this study, aiming to draw useful insights for other similar studies.

5.2 Measuring the performance of the road network

The study represents the road network as a graph of nodes and links (Section 5.2.1), and uses methods from graph theory to understand how its performance decreases when roads (i.e. links) become damaged (Section 5.2.2).

5.2.1 Modelling the roads as a graph of nodes and links

Data representing the layout of the future road network in Jingdezhen, in spatial georeferenced format, is obtained for this study. Specifically, the data obtained shows the road layout that aims to be delivered by 2030 based on the urban masterplan. The original data obtained

represents the roads and intersections in relative detail using sets of parallel lines as shown in Figure 5.2 (a).

Several processing steps are applied to convert the road data to a graph of nodes and links. Nodes represent road intersections, or the points where roads leading out of the city have been cut (which are not necessarily intersections), while links correspond to road sections that connects two nodes. First, the centreline of each road is obtained using the ArcMap 'collapse double line to centre' tool, setting a 100 metre maximum distance between lines. The result can be seen in Figure 5.1 (b). From this, manual editing is used to simplify intersections into single points or node (Figure 5.2 (c)), as well as to smooth out several other aspects of the data. For example, roundabouts are converted to a single node, and roads are aligned so that they meet at a single point. The network is then checked to ensure that roads are all continuous between intersections, and split at intersections (except where one road passes over another without possibility to pass from one to the other). A section of motorway that passes through the city is also added to the network, as it represents an important link between parts of the city and is necessary for understanding the performance, particularly if some of the local roads become blocked. The motorway centreline is obtained from open street map (Haklay et al., 2018) and merged with the network. As the motorway is in fact an overpass that passes over other roads, care is taken to only introduce nodes where there is indeed an intersection between the motorway and a local road. Motorway intersections are shown as triangles in Figure 5.2 (e).

The graph makes several simplifying assumptions about the roads. First, the small roads, used mainly by pedestrians and motorbikes, with restricted access for cars, are excluded. Then, the road capacity (e.g. number of lanes) and travel speed is assumed to be constant for all of the roads. Finally, the roads are all assumed to provide access in both directions.

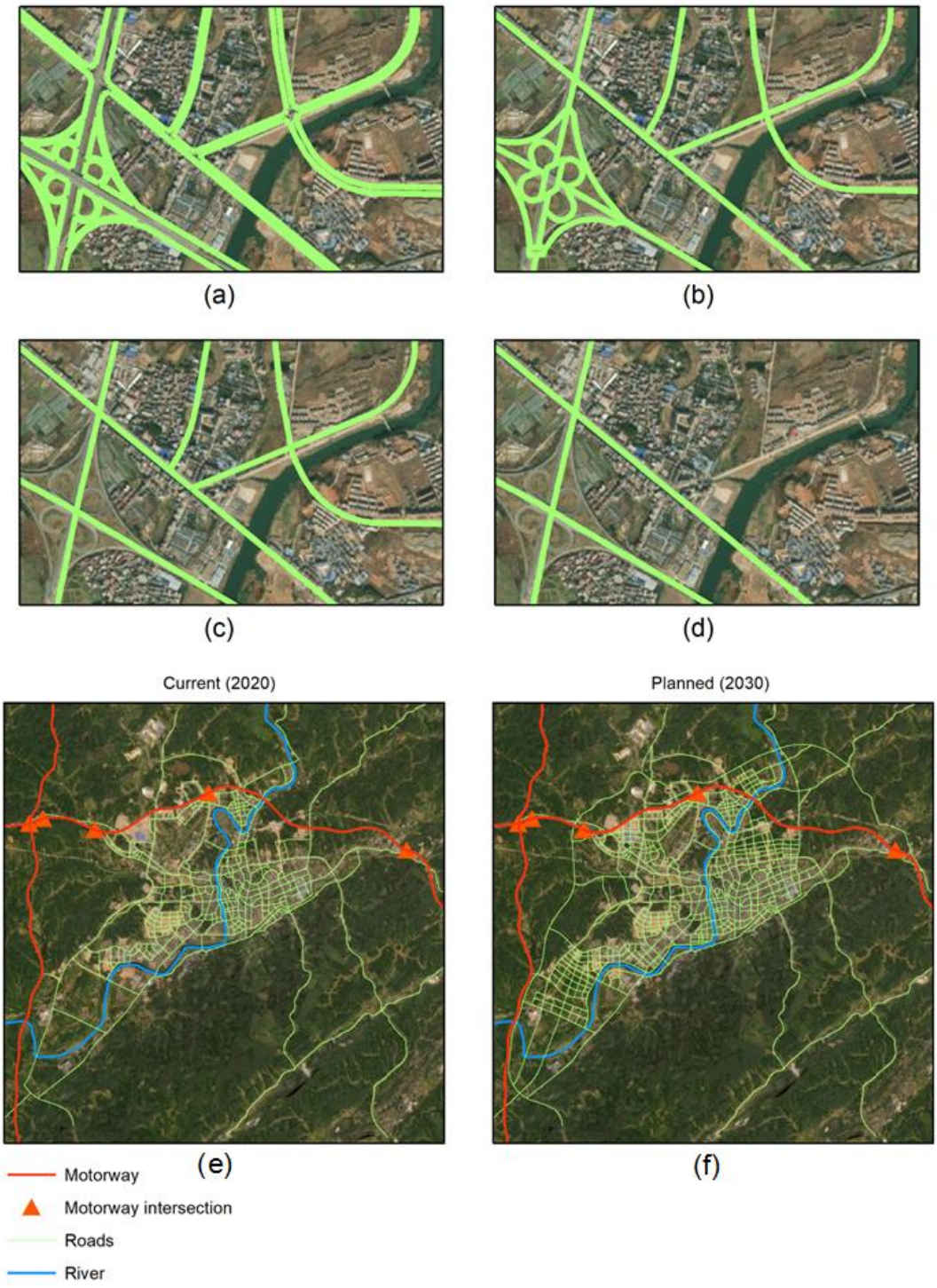

Figure 5.2 Processing the road network. (a) the original data as obtained from Hohai University (b) the network after applying the 'collapse dual lines to centerline' tool in ArcMap (c) intersections to single points, 'future' network (d) removing roads not complete according to satellite imagery, 'current' network. Extent and layout of the (e) current and (f) planned Jingdezhen road network.

From the graph representing the planned network for 2030, a second graph is generated to represent the current road network, to analyse how performance changes between the two. Specifically, the current road network is generated by manually removing links from the 2030 network, based on a comparison between the 2030 network and recent satellite imagery (from ESRI World Imagery).

The ESRI World Imagery layer combines high resolution satellite imagery from multiple providers, and while the imagery does not provide an exact date, the information is said to not date back more than 5 years. For simplicity, the study assumes that the information corresponds to the network in 2020. The satellite images are used to identify the roads that have not yet been built, and these are removed after having made a copy of the graph. The graph is then edited where necessary to ensure that roads are continuous between intersections, which may not be the case where a connecting link has been removed.

The final processing steps includes projecting the current and future network to a projected coordinate system (the UTM 50 N metric projection is used here, corresponding to the part of the world where Jingdezhen is located), and calculating the length of each.

5.2.2 Using graph theory to describe network performance

Methods from graph theory are frequently used to assess the performance of transport networks (e.g. Hu et al., 2016; Pregnolato et al., 2016). Here, two metrics from graph theory are selected to represent performance of the roads in Jingdezhen under alternative hazard scenarios.

The first metric used is the network efficiency (Bozza et al., 2016; Hu et al., 2016). Network efficiency refers to the travel distance between nodes in the network, and is calculated as:

$$\eta = \sum_{i}^{N} \sum_{j}^{N} w_i w_j \frac{1}{d_{ij}}, \quad (5.1)$$

where η is the efficiency of the network, w_i and w_j is the weight applied to nodes *i* and *j*, and d_{ij} is the shortest distance between nodes *i* and *j*. Weights allow nodes to be given more importance in the analysis, for example reflecting differences in population density, or highlighting important locations (e.g. hospitals, schools). However, in this study, all nodes are assumed to have equal importance and are assigned an equal weight ($w = 1$). Fu et al. (2015) previously showed a strong correlation between population density and road intersection density, suggesting that each road intersection, despite their varying catchment area, may serve a similar total population. To compare networks of different sizes (in this case the current and future network), the efficiency is then normalised using:

$$F = \frac{\eta}{\eta_0}, \quad (5.2)$$

where F is the functionality of the network under a given hazard scenario, η is the efficiency of the network given the occurrence of a hazard, and η_0 is the efficiency of the undamaged network. The functionality F takes values between 0 and 1. If $F = 0$, all roads in the network are blocked as a result of the hazard, while if $F = 1$, all roads are accessible. If pairs of nodes are disconnected during a hazard, the distance between them becomes infinite, and the inverse of the distance becomes zero.

The second metric used is road betweenness. Betweenness refers to the likelihood that a road is on the shortest path between two nodes (intersections) in the network. Roads with higher betweenness serve as (part of) the shortest path between many pairs of nodes, while roads with low betweenness are only on the shortest path for a small number of nodes. Unlike efficiency,

betweenness is calculated for each link rather than for the entire graph. The betweenness of a link is calculated as:

$$b(r) = \sum_{s=1}^{N} \sum_{t=1}^{N} \frac{\sigma_{st}(r)}{\sigma_{st}}, \quad (5.3)$$

where $b(r)$ is the betweenness of link *r*, σ_{st} is the number of shortest paths between nodes *s* and *t*, and $\sigma_{st}(r)$ is the number of shortest paths that pass through a link *r*. When calculating the shortest path, the length of each road section is taken into account. Therefore, there is generally a single shortest path between two points, and the fraction inside the summation sign is 1 if the shortest path passes along road *r*, and 0 otherwise. As trips generally prefer taking the shortest possible route, betweenness can be used as an estimate of the traffic flow through roads (Pregnolato et al., 2016). Damage to roads with higher betweenness, and therefore higher traffic flow, is expected to have a higher consequence than damage to roads with low betweenness.

Specifically, the betweenness metric is applied in two different ways, to estimate the flow of traffic a) within the city, and b) during an evacuation from the city. To distinguish the flow in the two cases, Equation (5.3) is applied to a subset of nodes. Specifically, to estimate the flow within the city, nodes *s* and *t* in Equation (5.3) are selected from a subset *k* of all nodes *N*. The set of nodes *k* represents all nodes, except for those at the end of roads that lead out of the city. In contrast, to estimate the flow during an evacuation, values of *s* are sampled from *k*, while values of *t* are sampled only from the end of roads that lead out of the city. For illustrative purposes, the relative betweenness of roads under normal conditions is shown in Figure 5.3.

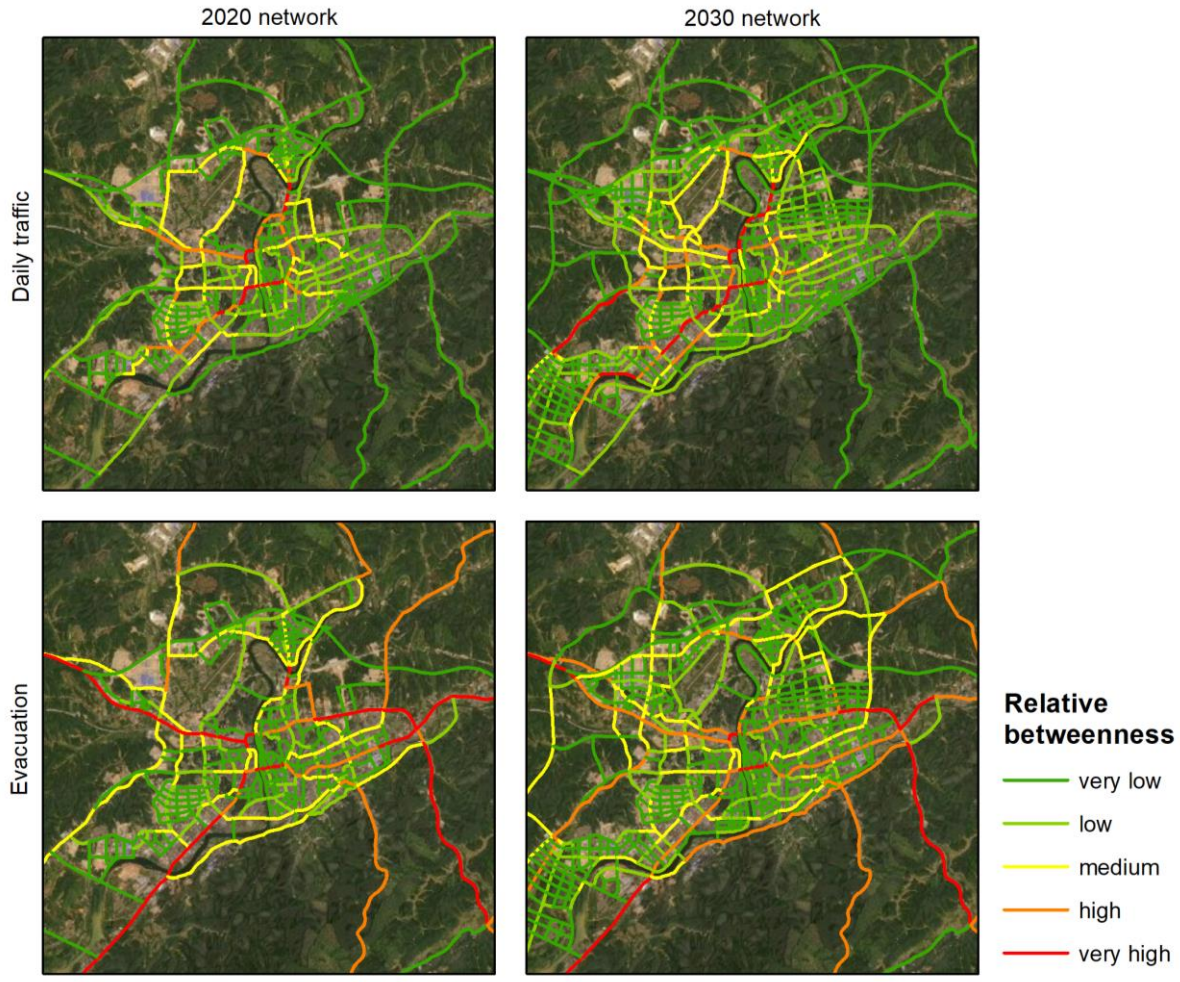

Figure 5.3 The betweenness of roads for the current (2020) and future (2030) networks, for: travel to other parts of the city (daily traffic); leaving the city (evacuation). Betweenness values are classified into five levels (very low, low, medium, high, very high) based on natural breaks in the data, using ArcMap.

Figure 5.3 shows how the flow of traffic would differ depending on whether roads are being used to reach other parts of the city (daily traffic), or to leave the city (evacuation). A daily traffic scenario when modelling the hazards means that the population largely remains within the city, for example people moving from flooded homes to shelters in the same city during a flood. In that case, the roads would be needed for emergency services and healthcare, and may also be important for minimising disruption to business and other activities, to reduce wider socio-economic impacts. On the other hand, the flow of traffic out of the city is most relevant

if the population is required to evacuate, for example if a flood overwhelms the ability of the city to provide shelter for the displaced population, requiring people to travel to neighbouring cities. Although the two cases are distinguished here, it is also possible that part of the population evacuates, and part remains within the city. In general, roads that are more central tend to play a higher role (have a higher relative betweenness) for daily traffic, while arteries leading out of the city become crucial in the event of an evacuation. Roads with few alternatives, particularly bridges that cross the river, have relatively higher betweenness in both cases.

5.3 Modelling hazards

Hazard scenarios in this study include river flooding and debris flows. Rather than focusing on a specific event, the study aims to understand how the performance of the road network is affected under incremental hazard magnitudes. Specifically, the performance will be compared for incremental flood magnitudes, with and without the occurrence of debris flows. River flooding is modelled at the city scale using a two-dimensional hydrodynamic model (Section 5.3.1), while debris flows are modelled using a distributed, empirical model for regional susceptibility assessment (Section 5.3.2).

5.3.1 River flooding

To model river flooding, synthetic flood hydrographs are generated for a 20-, 50-, and 100-year return period flood, based on a time series of peak flows for the period 1952-2010, shown in Figure 5.4 (a). The return period of each flow is calculated using the Weibull formula (Shaw et al., 2010):

$$T = \frac{1}{P} = \frac{N+1}{R}, \tag{5.4}$$

where P is the annual probability of occurrence, R is the rank of the flow (largest value has R = 1 and smallest value has $R = N$), and N is the total number of points in the time series of annual maxima. Given N = 58 years in Jingdezhen, the largest flow to occur in the time series will have a rank of 1, and a return period of (58 + 1) / 1 = 59 years, while the smallest value will have a rank of (58 + 1) / 58 = 1 year. Then, a Gumbel extreme value distribution is fitted to the data (Shaw et al., 2010). From the Gumbel distribution it is possible to read the peak flows at the return periods of interest. Peak flows for a 5-, 10-, 20-, 50-, and 100-year return period in Jingdezhen city are large relative to river flow in the UK, and correspond to 5033, 6045, 7016, 8272 and 9214 m^3/s, respectively. Given lack of information regarding the shape of the flood hydrograph, a symmetric triangular hydrograph is assumed, as shown in Figure 5.4 (c). The duration of the flood is based on information about past floods, that are said to typically last between 3 and 5 days in Jingdezhen (Hohai University, 2015). Here a 4 day duration is assumed.

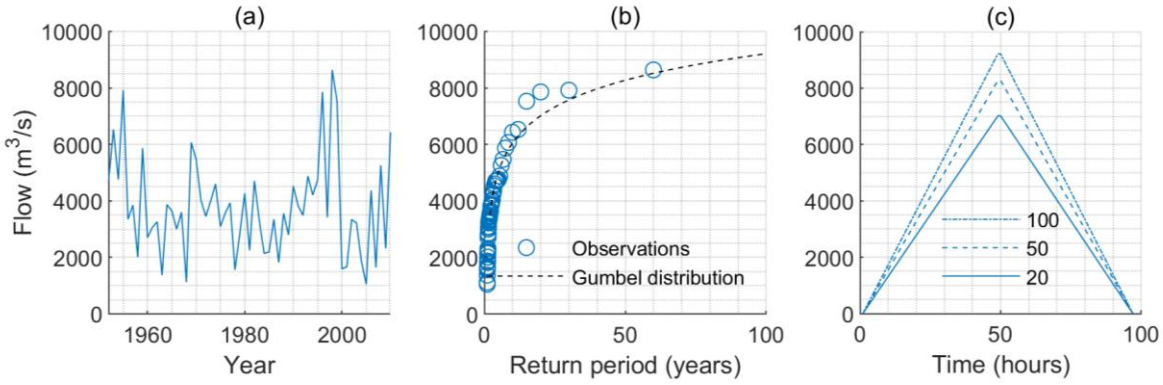

Figure 5.4 (a) maximum annual river flow in Jingdezhen city from the Changjiang river from 1952 to 2010, (b) A Gumbel distribution fitted to the annual maximum flow, (c) synthetic flood hydrographs for the 20, 50, and 100 year return period.

The flood hydrographs are then used as input to a the LISFLOOD-FP hydrodynamic model to obtain inundation extents (Bates et al., 2013). The model uses a simplified implementation of

the shallow water equations to represent the movement of water over a raster grid (Bates et al., 2010). The movement of water is modelled by considering friction slope, water slope, and local acceleration, while convective acceleration is assumed to be negligible. The following shows the conservation of momentum equation:

$$\frac{\partial Q_x}{\partial t} + gA\frac{\partial (h+z)}{\partial x} + \frac{gn^2{Q_x}^2}{R^{\frac{4}{3}}A} = 0, \tag{5.5}$$

where Q_x is volumetric flow rate in the x Cartesian direction, A is the cross sectional area of flow, h is the water depth, z is the bed elevation, g is the acceleration of gravity, n is the Manning friction coefficient, R is the hydraulic radius, t is time and x is the distance in the x Cartesian direction. The first term in the equation is the local acceleration, the second is the water slope, and the third is the friction slope. Conservation of mass is represented in the model as:

$$\frac{\partial A}{\partial x} + \frac{\partial Q}{\partial x} = 0. \tag{5.6}$$

Rivers are represented as sub-grid channels embedded in the two-dimensional domain (Neal et al., 2012). For grid cells that contain a sub-grid channel segment, the flow of water is calculated within the cell, both within the channel and in the adjacent floodplain (Bates et al., 2013).

A 90 metre terrain grid is used in this study for modelling inundation extents, obtained from the MERIT DEM (Yamazaki et al., 2019). Computation time on the 90 metre grid is approximately 1 minute, but increases to approximately 40 minutes if a 30 metre grid is used instead, due to an adaptive time step based on grid size and water depth (Bates et al., 2013). Given the need to assess model sensitivity and compute flood extent for multiple scenarios, using the 30 metre grid cell is found to be infeasible and the 90 metre grid is used instead.

The depth of the channel is calculated by assuming that the maximum channel capacity is equivalent to a 1-in-*T* year flood, and calculating and error term *err* based on the Manning equation:

$$err = \left| \frac{AR^{\frac{2}{3}}\sqrt{S}}{n} - Q_T \right|, \quad (5.7)$$

where *A* is the cross section area of the channel and *R* is the hydraulic radius of the channel. The channel is assumed to be rectangular, so $A = bd$ and $R = bd / (b + 2d)$, where *d* is the channel depth, and *b* is the channel width. The error is calculated for values of *d* between 0 and 30 metres, and the value that minimises the error is selected. The roughness coefficients for the river and floodplain are calibrated through comparison with flood extents from a previous modelling study (Hohai University, 2015). Channel roughness values between 0.03 and 0.15, and floodplain roughness values between 0.1 and 0.5 are tested (Bates et al., 2013). The sensitivity of flood extents to variations in roughness, hydrograph shape, and flood duration, are discussed in Section 5.3.1. This study assumes that the channel capacity is equivalent to a 5-year return period flow. A 5-year return period corresponds to the level of protection before the construction of protective measures (Hohai University, 2015).

Road disruption from flooding is determined by combining information from the raster flood extent and the road network data. If a part of a road section overlaps with a flooded grid cell with a depth of at least 0.5 metres, the road section is considered to be interrupted. This rule is applied for all roads except for the motorway overpass, that passes above other roads and is considered to be unaffected by flooding.

5.3.2 Debris flows

The area susceptible to debris flow is modelled using the Flow-R model (Flow path assessment of gravitational hazards at a Regional scale) (Horton et al., 2013). Flow-R is a spatially distributed empirical model for regional susceptibility assessment of debris flow and freely available from https://www.flow-r.org/. Mapping susceptibility to debris flows involves a) identifying possible sources of debris flow, b) modelling how the flow propagates from the source.

Sources of debris flow are identified according to terrain slope and water input. Terrain data from the 30 metre shuttle radar topography mission is used (Van Zyl, 2001). According to Horton et al. (2013), a resolution in the order of 25 metres provides a good balance between accuracy and computational time in Flow-R. Slope and flow accumulation is calculated from the elevation data using spatial processing tools in ArcMap. A grid cell is identified as a potential source if it has a slope of at least 15 degrees (Horton et al., 2013), and if it has the following critical combination of slope angle and upslope area (surface area that drains through that point):

$$\begin{aligned} tan(\beta_{thres}) &= 0.31\, S_{uca}{}^{-0.15} && if\ S_{uca} < 2.5\ km^2 \\ tan(\beta_{thres}) &= 0.26 && if\ S_{uca} \geq 2.5\ km^2, \end{aligned} \tag{5.8}$$

where β_{thres} is the slope threshold, and S_{uca} is the surface of the upslope contributing area. The hilly areas of Jingdezhen are found to consist of sandy or silty material favourable to the initiation of debris flows (Nachtergaele et al., 2010).

Flow propagation from the source is modelled by Flow-R based on spreading and friction algorithms. The Holmgren algorithm determines the degree of spread of the flow, based on a spread parameter *x*:

$$p_i^{fd} = \frac{(tan\,\beta_i)^x}{\sum_{j=1}^{8}(tan\beta_j)^x} \qquad \forall \begin{cases} tan\,\beta > 0 \\ x \in [1, \infty), \end{cases} \tag{5.9}$$

where *i, j,* are the flow directions, p_i^{fd} is the susceptibility proportion in direction *i*, tan β_i is the slope gradient between the central cell and the cell in direction *i*, and *x* is the variable exponent. When $x = 1$, the spread is equal in all directions, and as *x* increases, the spread decreases. As $x \rightarrow \infty$ the flow reduces to the single flow direction. A persistence functions reproduces the behaviour of inertia, by giving a weight *w* to the flow direction with respect to the previous direction: $w = 1.5$ for flow in the same direction, $w = 1$ for flow at 45, 90, and 135 degrees to the original flow direction, and $w = 0$ for flow at 180 degrees (opposite direction) to the oncoming flow. These weights are combined with Equation 5.9 and used in the propagation of susceptibility from the source. The runout distance is calculated based on frictional laws that control the other cells that can be reached. The energy balance is calculated according to:

$$E_{kin}^i = E_{kin}^0 + \Delta E_{pot}^i - E_f^i, \tag{5.10}$$

where E_{kin}^i is the kinetic energy of the cell in direction *i*, E_{kin}^0 is the kinetic energy of the central cell, ΔE_{pot}^i is the change in potential energy to the cell in direction *i*, and E_f^i is the energy lost in friction to the cell in direction *i.* Horton et al. (2013) use the friction model from Perla (1980), corresponding to the solution of the equation of movement, leading to the velocity V_i of the flow at the end of the segment *i* being:

$$V_i = \sqrt{a_i \omega (1 - e^{b_i}) + V_0^2 e^{b_i}}, \quad (5.11)$$

with

$$a_i = g(sin\,\beta_i - \mu \cos \beta_i),$$

$$b_i = \frac{-2L_i}{\omega},$$

where μ is the friction parameter, ω is the mass-to-drag ratio, β_i is the slope angle of the segment, V_0 is the velocity at the beginning of the segment, L_i is the length of the segment, and g is the acceleration due to gravity. The spreading coefficient in Equation (5.9) is set to 4, the friction parameter is set to 0.02, and the mass-to-drag ratio is set to 200 (Horton et al., 2011). The set of parameter values used is found to maximum debris flow extents and represents a worst case scenario. Sensitivity to different parameter values is shown in Section 5.5.2. A road section is considered to be exposed to debris flows if it overlaps with a grid cell with a susceptibility of at least 0.1.

5.4 Results

5.4.1 Network damage

Figure 5.5 shows the effects of river flooding on the current (2020) and future (2030) road networks in Jingdezhen. Figures 5.5 (a) – (f) show the road sections that become inaccessible due to flooding (in purple), and the road sections that remain useable (in green), for the 20-, 50-, and 100-year floods. In Figures 5.5 (g) and (h), the increase in the number of roads flooded with increasing river flow can be seen. Figure 5.5 (g) shows that the number of roads affected remains approximately constant until a flow rate of 5,000 m^3/s. Above 5,000 m^3/s, the number of flooded roads increases steadily, showing a linear relation with the increase in river flow

rate. The results are consistent with expectations, as a flow rate of 5,000 m^3/s corresponds to a 5-year return period flow, which is the flow rate above which the river is assumed to overflow its banks, and used to calculate the depth of the channel accordingly. As expected, when the 5-year flow is exceeded, impacts on the road network start to increase. Figure 5.5 (g) shows that more than 150 road sections are flooded in the 100-year flood scenario, while more than 280 road sections are flooded in the same flood for the future road network. The number of roads flooded increases proportionally faster with the same increase in flow rate in the future network. However, Figure 5.5 (h) shows that the proportion of road sections flooded, is surprisingly constant across the two networks. This suggests that new roads are built evenly across both flood prone, and non-flood prone areas. Note that the flood damage in Figure 5.5 (g) and (h) includes flow up to extreme flow rates. In practice, floods greater than 13,000 m^3/s have not been recorded at the Changjiang gauging station. Under a hypothetical flood that significantly exceeded the maximum recorded flow and reached a flow rate of 15,000 m^3/s, approximately half of all road sections would be flooded in both the current and future road network.

Looking at the portion of Figures 5.5 (g) and (h) when flow rate is less than the channel capacity (i.e. < 5,000 m^3/s, and should not yet have overflows the channel), a small and constant number of road sections are nevertheless seen to be flooded. The roads flooded before the river overflows onto the floodplain include the bridges that cross the river, and a few roads that closely follow the river banks. By crossing the river, bridges overlap with flood grid cells, and are therefore recorded as flooded, despite flow being contained within the channel. The additional roads flooded along the river banks result from the coarse resolution flood grid cells within the channel to partly overlap with roads along the river. However, this does not affect the part of the graph that is of most interest, when flow exceeds channel capacity.

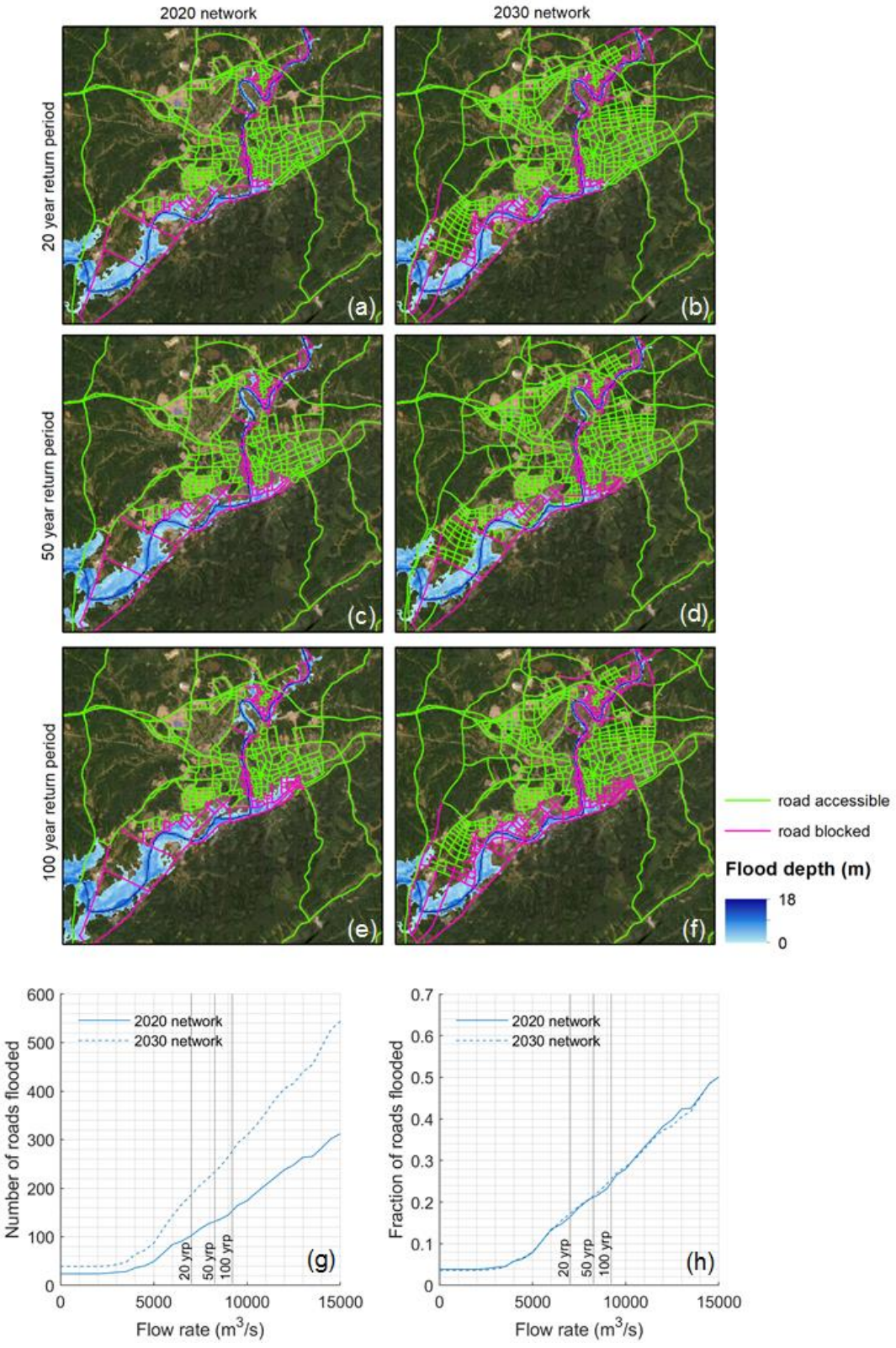

Figure 5.5 Location and number of roads flooded: (a) – (f) show flooding of the current (2020) and future (2030) road networks for the 20-, 50-, and 100-year return period floods. (g) – (h) show roads flooded for incremental flood magnitudes.

Figure 5.6 shows the damage to roads from a maximum plausible debris flow scenario. The damage caused by debris flows is far less than the damage due to flooding in terms of the number of road sections affected (Figure 5.6). However, several critical road sections appear to be susceptible to damage, including one of the main roads leading out of the city towards the north (subplot 1). Figure 5.6 (b) also shows that one of the long newly built roads along the northern half of the network may be susceptible to debris flows (subplot 2). Severe damage could also be caused by debris flow in the south of the city (subplots 3 and 4). There is a possibility, according to the model, that debris flows could be deposited into the channel of the Nanhe tributary (subplot 3). Deposited material in the river could in turn increase the flood risk. However, overall, the debris flow and flood risk are seen to largely occur in different parts of the network, with limited direct interaction between the hazards.

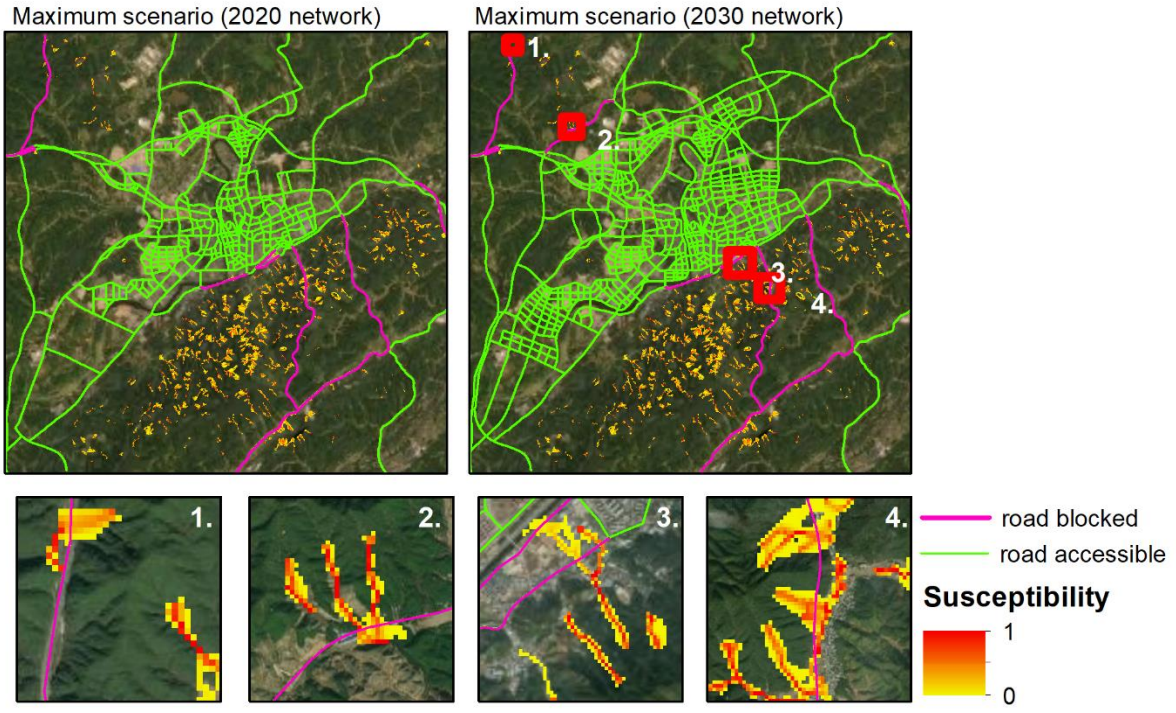

Figure 5.6 Damage to roads from debris flows for the current (2020) and future (2030) road networks under a worst case debris flow. Subplots 1 – 4 show zooms of four critical locations (red squares).

5.4.2 Impacts on network performance

By looking now at the functionality of the road network, this section investigates how the hazards affect the functionality of the network. Figure 5.7 shows the betweenness of roads, with higher betweenness corresponding to greater use of the road, and lower betweenness representing fewer vehicles using the road. The betweenness therefore helps identify the most critical roads. Here, the motorway overpass is assumed to remain accessible during flooding, due to its elevation above the river. On the other hand, bridges and roads along the river are considered to flood when the river overflows its banks. The assumption is based on bridges being level with the surrounding roads, rather than elevated above other roads. The sensitivity of the results to this assumption is discussed in Section 5.5.2. As bridges become inaccessible under all three flood scenarios in the model, the motorway overpass becomes the most critical link for transport within the city (Figures 5.7 (a) – (f)). The betweenness of roads evolves with the magnitude of the flood scenario. For example, comparing Figure 5.7 (a) and (c), traffic is forced to transfer to alternative roads as flood magnitude increases. In particular, the long road section in the north of the city is important in the event of a severe flood scenario, for connecting the area in the northeast of the city to other parts of the city. Comparing the network before and after expansion (Figures 5.7 (a) and (d)), new roads to the west are seen to have high betweenness in the flood scenario, showing that these newly built roads provide additional redundancy during a flood.

Figure 5.8 now shows the betweenness for scenarios where both flooding and debris flows combine. Figures (a) to (f) assume that the city is able to absorb the disruption, meaning that those in the flooded areas are relocated to other parts of the city (e.g. shelters are provided in primary schools), and that the most critical services continue to function. Figures (g) to (l) assume that the population evacuates from the city to shelter in neighbouring cities.

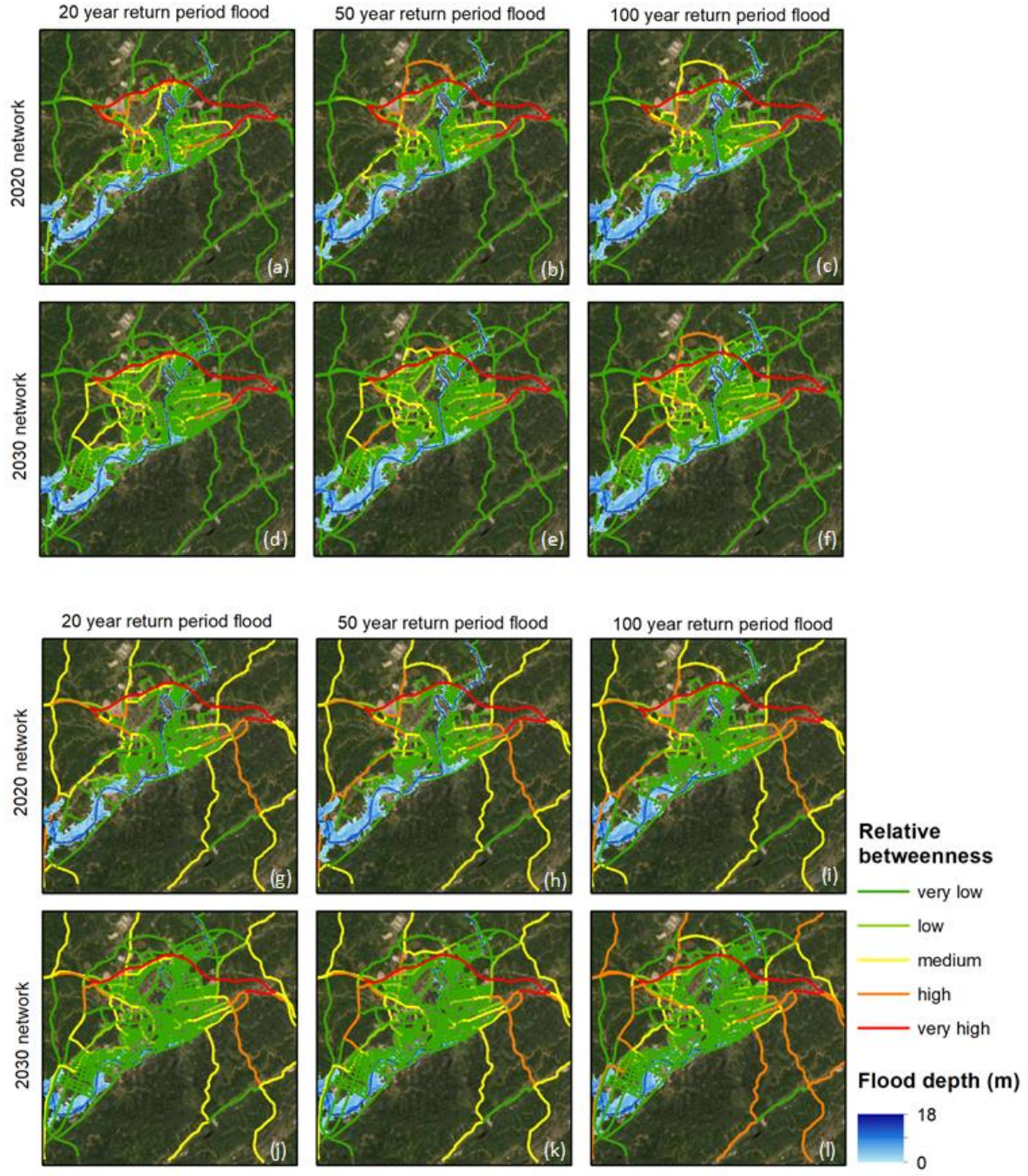

Figure 5.7 The betweenness of road sections in the current (2020) and future (2030) road network, for the 20-, 50-, and 100-year floods. (a) – (f) show the betweenness of roads under a scenario where the population remains in the city, and (g) – (l) show the betweenness for an evacuation scenarios.

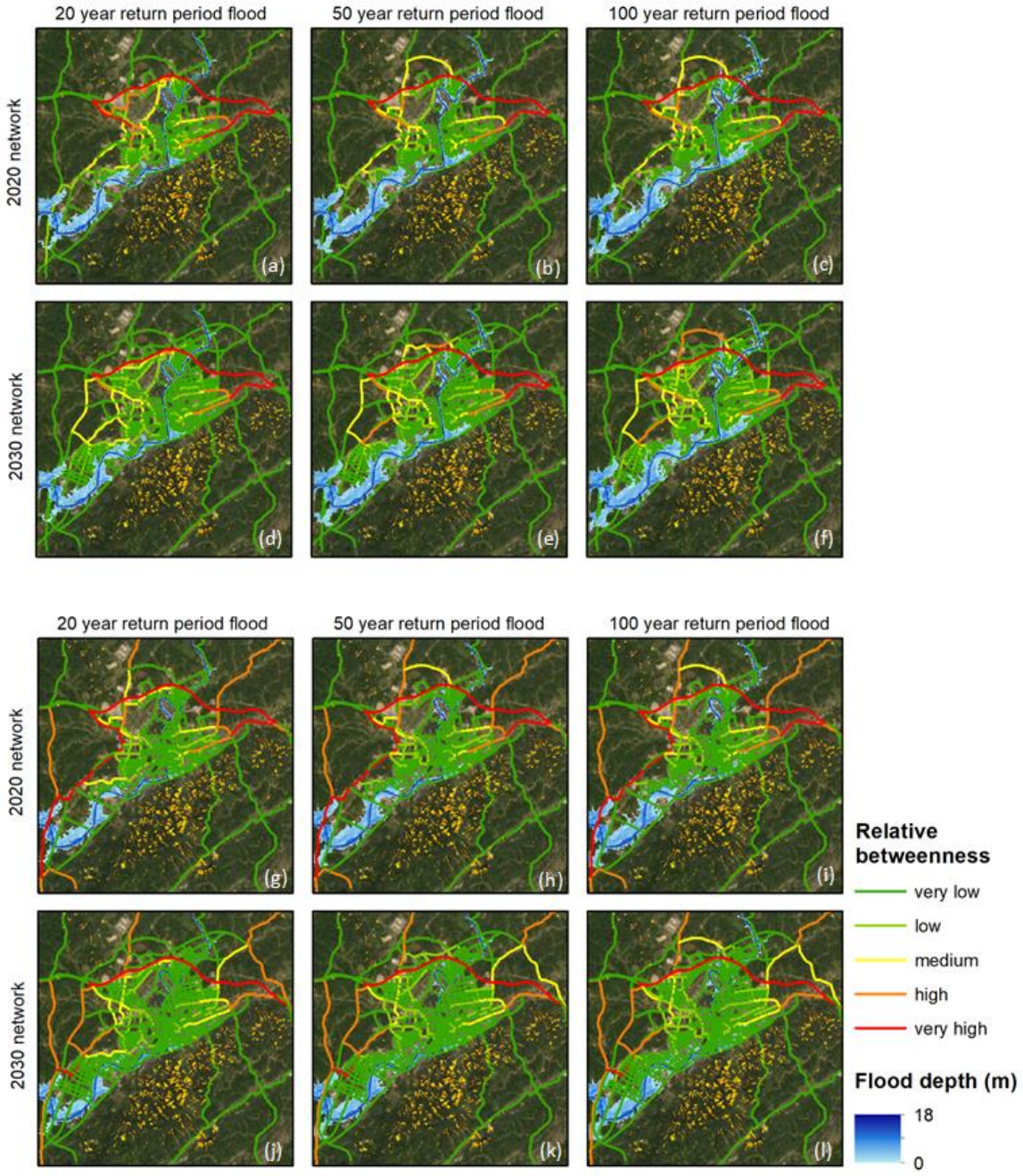

Figure 5.8 The betweenness of road sections in the current (2020) and future (2030) road network, for the 20-, 50-, and 100-year floods, combined with debris flow. (a) – (f) show the betweenness of roads under a scenario where the population remains in the city, and (g) – (l) show the betweenness for an evacuation scenarios.

By comparing Figure 5.7 and Figure 5.8, the influence of debris flows on accessibility can be seen. Overall, the debris flows have a higher influence on accessibility in the case of an evacuation (Figures 5.7 and 5.8 (g) to (l)), than on travel within the city (Figures 5.7 and 5.8 (a) to (f)), as it mostly blocks roads at the edges of the city (including some of the roads leading out of the city).

Under the flood only scenario, exit roads all have comparable betweenness. However when some of those roads become blocked in the debris flow scenario, betweenness is highest on the roads that remain accessible, towards the east, west, and north of the city. Figures 5.7 and 5.8 also show that in all the cases, the motorway remains critical for accessibility, including during evacuation where it provides the shortest path for leaving the city from certain areas. Overall, the betweenness provides a picture of how the flow of traffic varies with road damage, and depending on whether the population evacuates or stays within the city. The next section quantifies the influence of the hazards by calculating the efficiency of the network under incremental flood magnitudes.

Figure 5.9 shows how the efficiency of the network changes for incremental flood magnitudes. The efficiency is approximately constant up to 5000 m^3/s, and then decreases linearly with flow rate, in both the current and future network. Overall, the efficiency of the 2030 network is higher than that of the 2020 network across all floods. Also, efficiency decreases slower in the 2030 network than in the 2020 network. Figure 5.9 (b) compares the efficiency with and without the occurrence of debris flows. The debris flows have almost no influence on efficiency in the 2020 network, while they cause a noticeable loss of efficiency in the 2030 network. Interestingly, the loss of efficiency due to debris flows is greatest when the effects of flooding are limited (i.e. at low flow rates), and becomes smaller under higher flood scenarios.

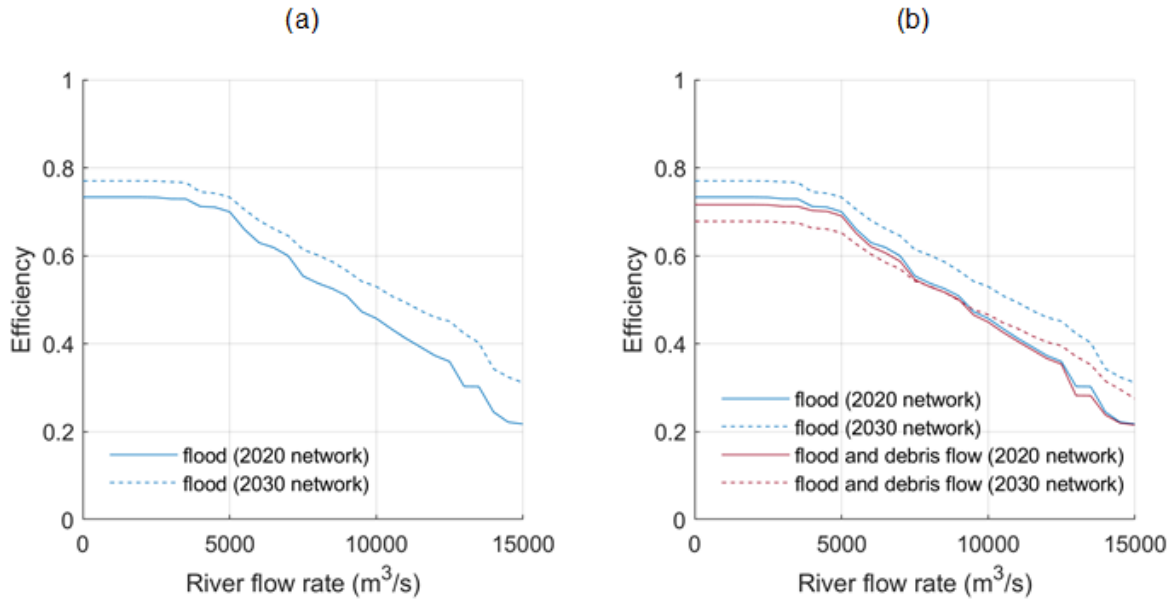

Figure 5.9 (a) The efficiency of the road network under incremental flood magnitudes, and (b) the efficiency of the road network under incremental flood magnitudes both without and with debris flows.

5.5 Discussion

The results show that both betweenness and efficiency provide interesting and potentially valuable ways of quantifying the effects of hazards on infrastructure. Both can also be used to look at the combined effects of hazards on the network. This section discusses some of the limitations and challenges identified in this study, and opportunities for future work.

5.5.1 Data availability

Limited local information was available for this study, both about the infrastructure and about the hazards. The local data available included the layout of the future road network and a time series of annual maximum river flows. The data was supplemented with additional data sources, including digital elevation models (DEMs) from the Shuttle Radar Topography Mission (SRTM), the ESRI World Imagery satellite imagery, and Baidu maps (the Chinese

Google Maps). Specifically, both 30 m and 90 m products from the SRTM DEM were used. The 90 m DEM from Yamazaki et al. (2019) has greater vertical precision, and allows a reasonable run time for the flood model, while the 30 m DEM from NASA Earthdata provides higher horizontal precision and is suitable for modelling the debris flows. The ESRI World Imagery was used to determine the extent of the current road network, and Baidu maps was found to be useful for gathering information at street level on the elevation and characteristics of the roads. Model parameters for the hazards were determined by making reasonable assumptions, informed by previous studies using the models.

Road data was easier to obtain than other types of infrastructure data, which is likely to also be true in other areas (Barrington-Leigh & Millard-Ball, 2017). Figure 5.9 for examples compares four alternative open sources of road data, including the global Roads Open Access DataSet (gROADS) (CIESIN, 2013), the Global Roads Inventory Project (GRIP) (Meijer et al., 2018), and Open Street Map (OSM) (Haklay & Weber, 2008). Many of the current roads are mapped in OSM, and GRIP provides a cleaned up version focused on the main roads. For Jingdezhen, many of the roads are seen to be mapped in both the GRIP and OSM data, but pre-processing and checking of the data would be crucial when using it for analysis. Several pre-processing steps were necessary even when using the local road data provided, to convert the network to a suitable graph. The quality and format of the data, and the amount of pre-processing required, will influence the feasibility of carrying out this type of analysis. Relating city functionality to the performance of the road network would be a valuable area for future research. For example, Bozza et al. (2016) suggested using artificial neural networks to relate indicators of social well-being and the performance of urban networks. This idea would be most useful through relating the performance to the layout of the road network. However progress in this direction is still in

its infancy, and it is still unclear to what extent measurable indicators of social well-being do indeed correlate with the condition of infrastructure systems.

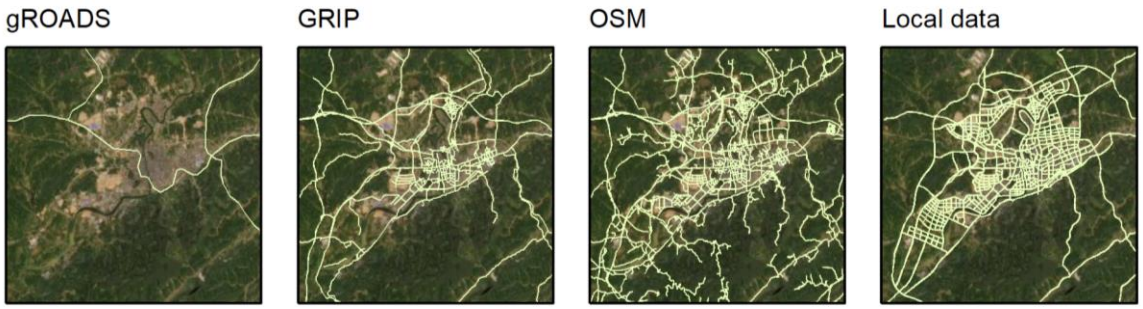

Figure 5.9 Road information for Jingdezhen city from three global datasets and local data, including (a) the global Roads Open Access DataSet (CIESIN, 2013) (b) the Global Roads Inventory Project (Meijer et al., 2018), (c) Open Street Map (Haklay & Weber, 2008) (d) local data.

Data on other critical infrastructure, including drainage, water supply and electricity, was not available in digital format. The drainage network for example is important for determining how surface flooding could disrupt road transport (Pregnolato et al., 2016). Other systems like water supply and electricity are also critical to enable the population to cope during the hazard. Future work could explore the possibility of using emerging datasets that are providing information of these systems globally, for example by using machine learning to learn the features of the systems in areas where data is available, and extend the same patterns to data scarce areas (Arderne et al., 2020). Meanwhile, road data is often the most likely to be available, and the performance of roads is a foundation for the functioning of other urban systems (Reiner & McElvaney, 2017).

The extent of flooding is the biggest uncertainty in this analysis. The flood model focuses on flows in the main channel, without including the inflow from tributaries. However, while approximately 80% of the flow comes from the main channel, 20% is provided by tributaries

(assumed based on the upstream catchment area of each). Therefore, the timing of peaks in the tributaries and main channel could lead to patterns of flooding that are not captured in our model. While local flood maps were not available in digital georeferenced format for analysis, they were provided as images (PDF files), allowing a visual comparison of the flood extents with those of a previous modelling study. The comparison was used when calibrating the model (Figure 5.10).

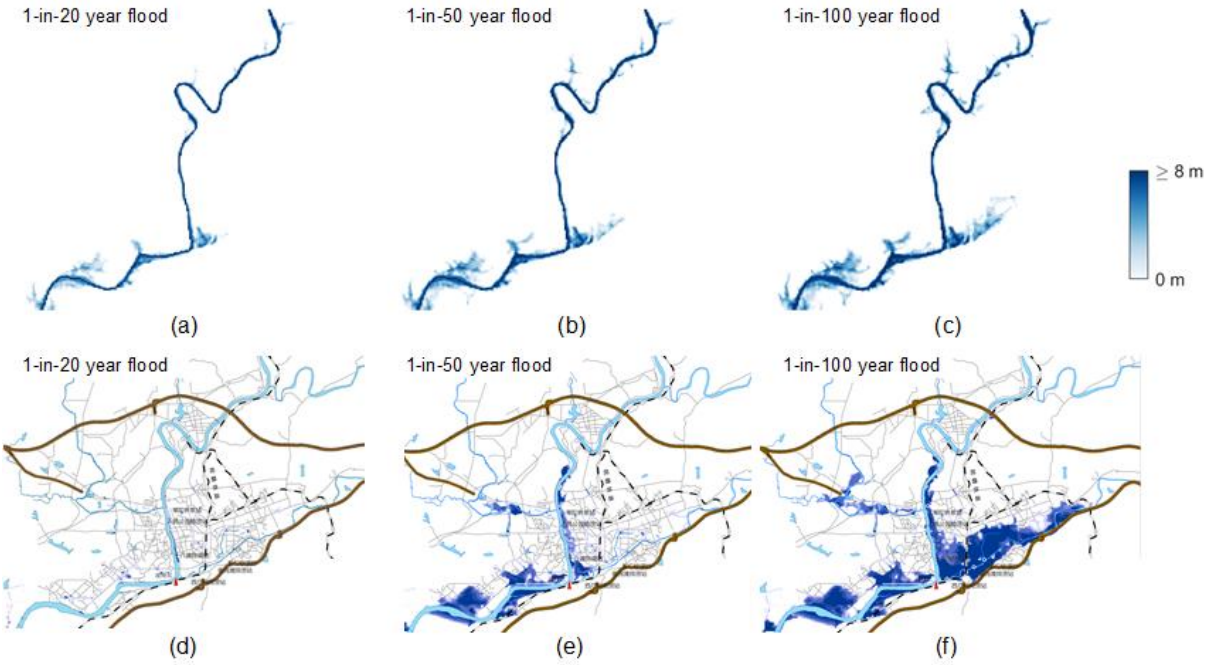

Figure 5.10 (a), (b), and (c) show the modelled flood scenarios. (d), (e), and (f) show the flood extents from a previous modelling study for the same return periods

Figure 5.10 shows a comparison of the three flood scenarios with those from the previous modelling study. Overall, discrepancies are largest around the tributaries, suggesting that these should be included in future analysis to provide a more accurate picture of the flood extents. The flood extents were found to be most sensitive to variations in channel depth, so additional channel depth information should improve accuracy.

5.5.2 Sensitivity of the results to uncertainties in the data

A key uncertainty of the analysis relates to the elevation of roads. The road layout data does not distinguish different types of roads (e.g. bridge, overpass). Therefore, a simple approach where the roads are assumed to be at the same elevation as the terrain results in a complete loss of access between urban areas on opposite sides of the river (Figure 5.11 (a)). In practice, the motorway that crosses the river can be seen to be elevated relative to other roads (Figures 5.11 (e) and (f)), and therefore is likely to remain accessible even when other roads become flooded. On the other hand, bridges are at the same level as the rest of the roads in the city, except for roads directly alongside the river that are much lower than the rest of the city, and pass under the bridge (Figure 5.11 (g) – (i)). Therefore, the scenario modelled in this study assumes that the motorway remains accessible, while bridges are flooded in the same way as other roads. The varying geometry of the channel makes it difficult to determine exactly when the bridges would become inaccessible. Instead, sensitivity of the results is assessed for three different possibilities. Figure 5.11 (d) compares how efficiency decreases with increasing flow rates for the 2030 network, with three different assumptions:

1. The elevation of all roads is equal to the terrain elevation (red line),
2. road elevation is equal to terrain elevation except for the motorway which is automatically removed from the list of flooded roads in all scenarios (blue line), and
3. road elevation is equal to terrain elevation except for the motorway and bridges which are automatically removed from the list of flooded roads in all scenarios (green line).

Figure 5.11 shows that efficiency is (nearly) maximum if bridges are accessible, until the channel overflows, and then it decreases abruptly. For flow rates above 8000 m^3/s, the efficiency is equivalent to that of the network with flooded bridges. This is likely because at this flow rate, the roads connecting to the bridge become flooded, preventing access to the

bridge in the first place. This suggests that even without detailed information about the characteristics or height of the bridge, simply considering that the bridge is not flooded can produce a reasonable representation of accessibility and traffic during a flood event.

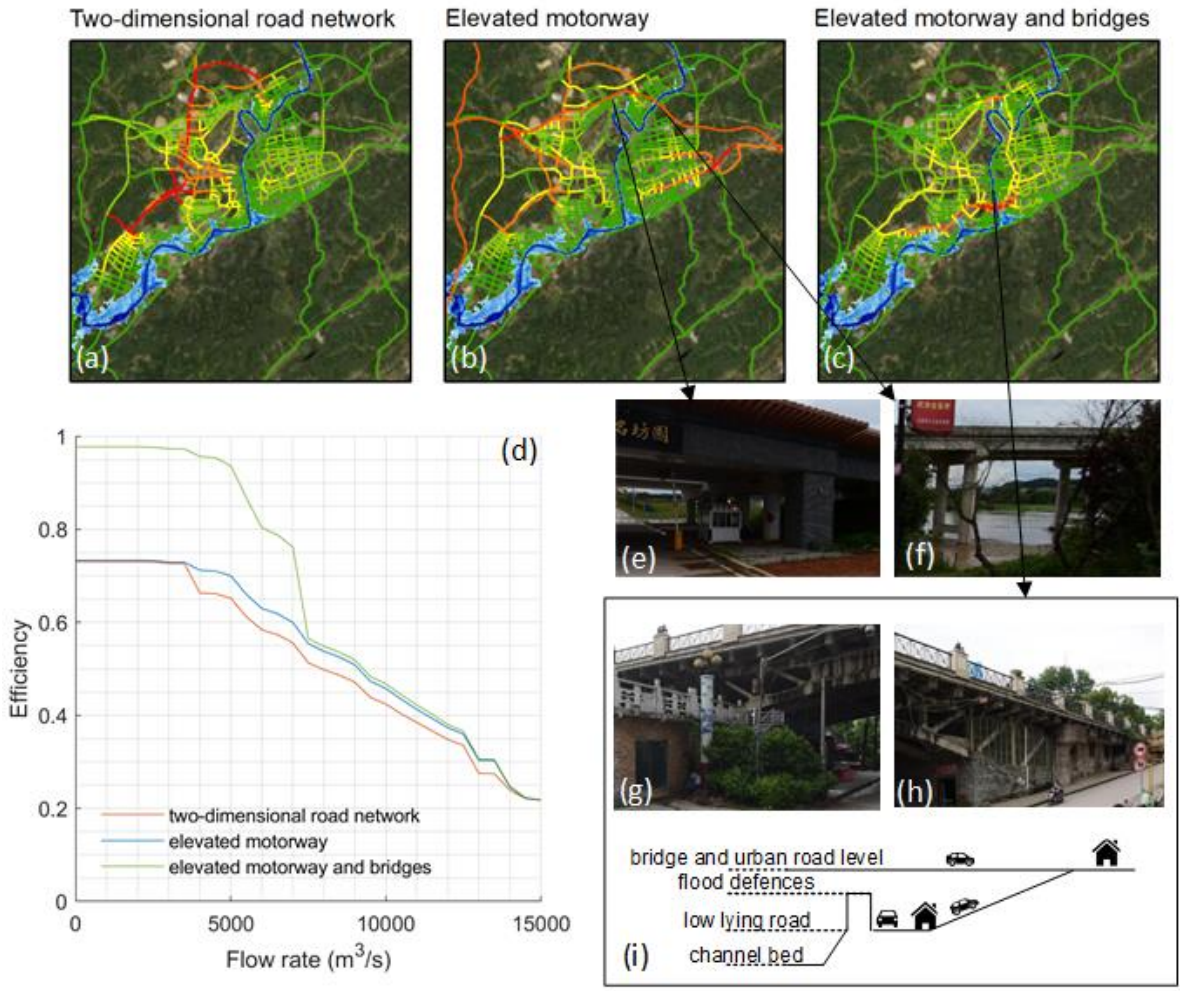

Figure 5.11 The influence of road elevation information on the results. (a) – (c) show the betweenness of the 2030 network in a 20-year flood, using three different assumptions: (a) all roads are at the same elevation as the ground (b) the motorway is raised above the ground, (c) the bridges are raised above the ground. (e) – (i) show pictures of the roads, and (d) compares the efficiency using the three assumptions.

Among the parameters studied, flood extents are found to be most sensitivity to the channel depth (Figures 5.12 and 5.13). Channel depth is calculated based on the flow rate at which the channel starts to overflow. Using this approach, depths of 10.9 m, 13.7 m, and 15.4 m are

obtained for a maximum channel capacity equivalent to the 2-, 5-, or 10- year flood, respectively. The resulting extent of flooding can be seen to vary significantly, from 39.6 km^2 for a 2-year return period capacity, to 17.9 km^2 for a 10-year return period capacity (Figure 5.12 (a) – (c)). In contrast, less variability can be seen with variations in floodplain roughness ((d) – (f)) or channel roughness ((g) – (i)). Interestingly, the maximum flood extent is also not very sensitive to changes in the duration (Figure 5.13 (a) – (c)) and shape (Figure 5.13 (d) – (f)) of the flood hydrograph.

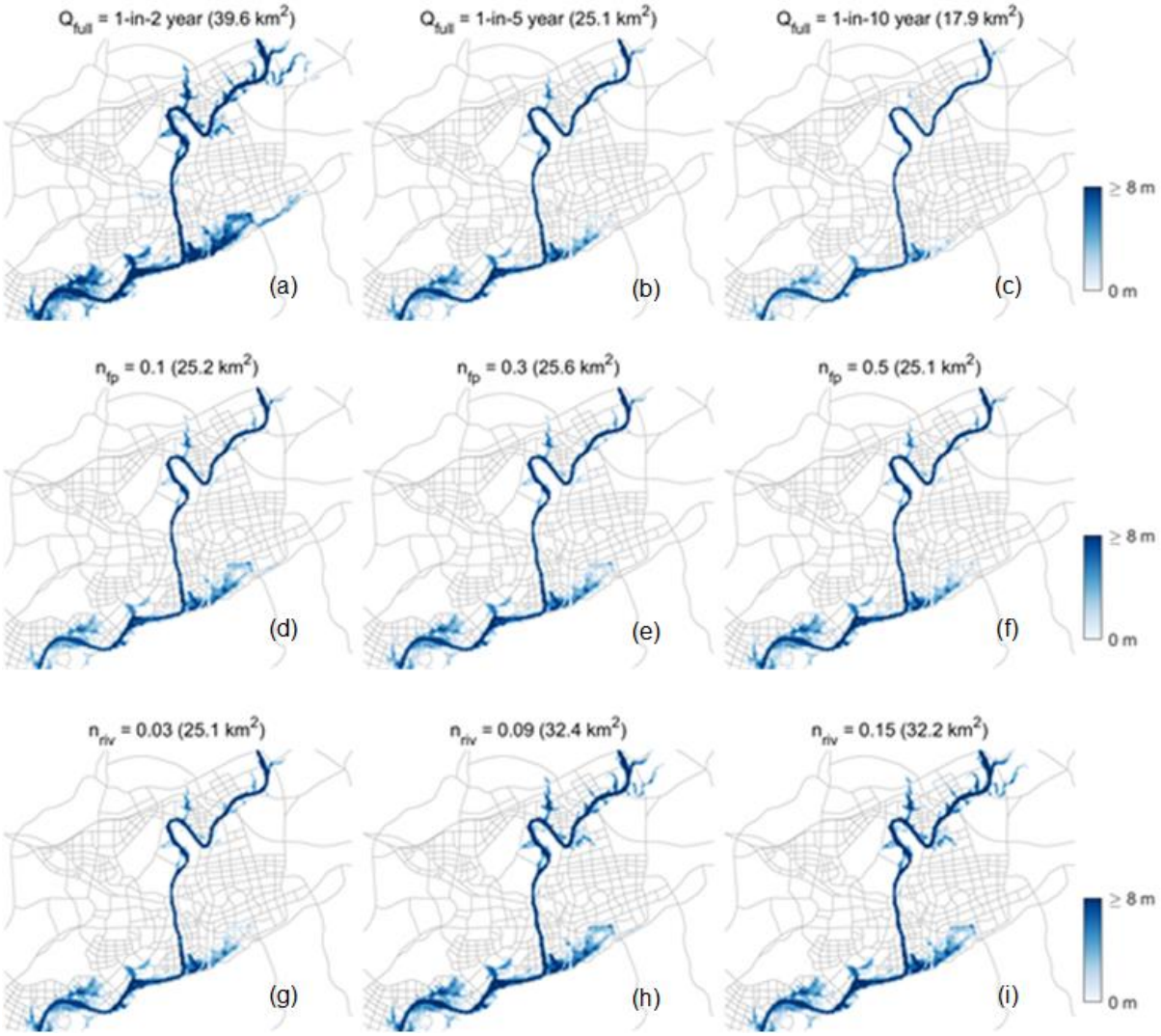

Figure 5.12 Sensitivity of flood extents to the characteristics of the channel. (a) – (c) shows variation in the channel capacity, (d) – (f) shows variation in floodplain roughness, (g) – (i) shows variation in channel roughness.

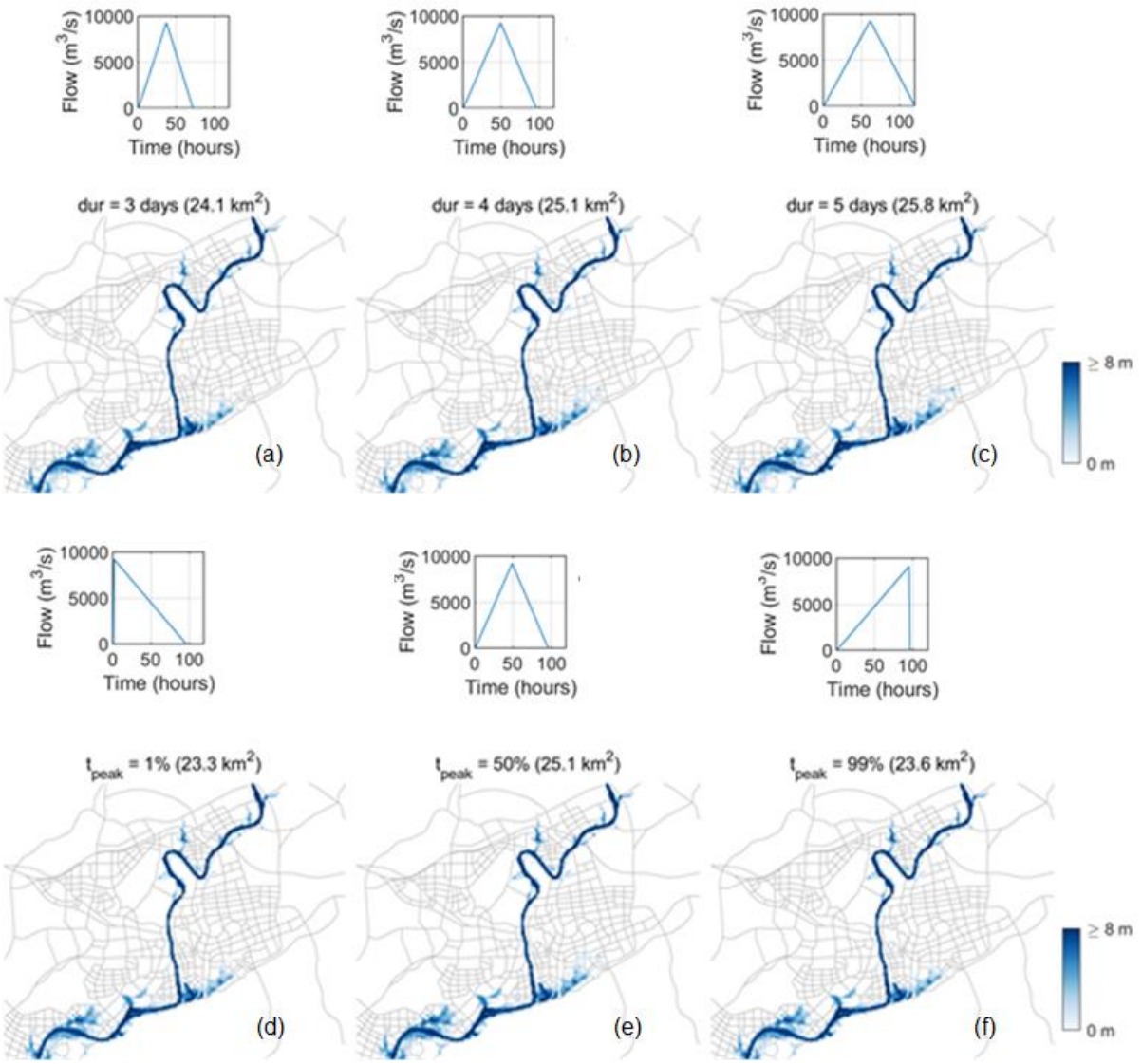

Figure 5.13 sensitivity of flood extents to the inflow hydrograph. (a) – (c) shows variation in flood duration, (d) – (f) shows variation in hydrograph shape.

On the other hand, hazardous areas tend to become smaller when the parameters of the debris flow model are varied. In particular, decreasing the mass-to-drag ratio significantly reduces the affected area. Figure 5.14 shows the difference between the extreme and maximum parameter values used (extreme scenario: M/D = 30, maximum scenario: M/D = 200). The difference influences whether certain roads are indeed susceptible or not. The difference has a strong

effect on the loss of efficiency, suggesting that the roads that are only damaged in the maximum scenario are critical to the efficiency of the network as a whole.

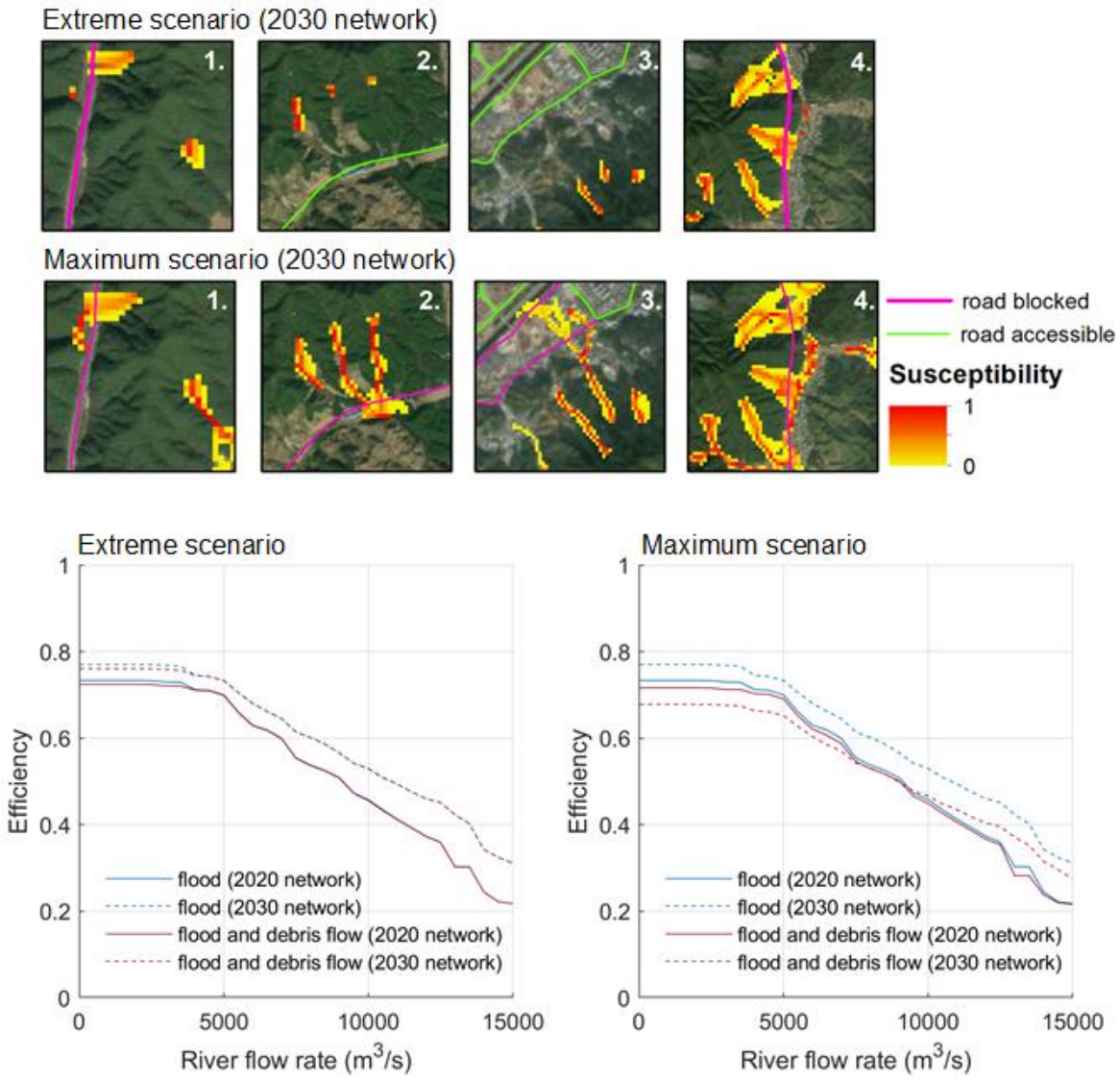

Figure 5.14 Sensitivity of the debris flow to mass-to-drag ratio (extreme scenario: M/D = 30, maximum scenario: M/D = 200), and of the resulting difference in efficiency at the network scale. The location of subfigures 1 – 4 relative to the network can be seen in Figure 5.6.

5.5.3 Towards multi-hazard analysis in practice

Decision makers may find it relevant and desirable to include additional hazards in the analysis, including non-natural hazards (e.g. random accidents or intentional attacks). From a modelling point of view, adding both random failures and intentional attack is relatively straight forward compared to natural hazards, as it can be done simply using information about the system, without requiring knowledge about the natural environment. Random hazards can be modelled by stochastically sampling roads to fail, for example, while intentional attack can be modelled by identifying and targeting the assets that create the highest disruption, such as the busiest or most central road sections.

To make the results useful in a decision making context, it may also be valuable to provide estimates of the probability of occurrence of the hazard scenarios. Debris flows in this analysis are represented by a measure of susceptibility (between 0 and 1). This study assumes a worst case scenario where all roads with a susceptibility of 0.1 or above are effected. However, it is possible that only a subset of those roads may be affected given the same scenario. The debris flows are indirectly related to rainfall intensity, based on a relation between slope angle and upslope catchment area, that has been empirically observed to be critical for the initiation of debris flows in case of a severe rainfall event. Flooding on the other hand is represented deterministically for a given channel characteristics and inflow, as a map of flood depths. By using different models and units to represent the two hazards, the present analysis is mostly suited to understanding how the hazards relate in space, but cannot easily provide information on the probability of the events coinciding. To analyse both the consequences and the probability of the two hazards, it may be necessary to use an integrated hazard model, such as for example OpenLISEM (Bout et al., 2018).

5.6 Conclusions

The study demonstrates an approach for determining the effect of multiple hazards (in this case debris flows and river flooding) on the functionality of a city (Jingdezhen city in China). The study represents city functionality through the performance of the road network. The study aims to explore an important barrier to multi-hazard studies in practice, which are often hindered by a lack of data availability (Ciurean et al., 2018). This study demonstrates a method for analysing the performance of the road network that can be used with low data availability. While the process provides helpful insights into what might happen during a combined hazard event, the results are found to be sensitive to both road elevations and hazard parameters. However, the approach used helped to identify critical information (e.g. the susceptibility to debris flow at specific locations, probability of flooding of road bridges) for further analysis.

This page was intentionally left blank

Chapter 6. Conclusions and recommended future work

6.1 Conclusions

The overall aim of this thesis was to integrate knowledge of hazards and of urban infrastructure systems to contribute towards increasing the resilience of cities to multi-hazard events.

First, a review of the literature provided a summary of the research on infrastructure resilience and multi-hazards (Chapter 2). Then, hazard datasets for five hazards were combined and analysed to provide a global overview of exposure of urban areas to combinations of hazards (Chapter 3). Two case studies were then carried out at the city scale to better understand the consequences of multi-hazard events. The first was a scenario of a consecutive earthquake and storm event affecting a water supply system (Chapter 4), and the second was a coinciding river flood and debris flow affecting an urban road network, carried out for the city of Jingdezhen in China (Chapter 5).

In summary, the work presented includes three main contributions: (1) it provides a global assessment of the hazard exposure of urban infrastructure systems to five different hazards, (2) it contributes evidence showing the effect of consecutive hazards on water supply, and (3) it provides insights into the practical aspects of addressing multi-hazard risks at the city scale.

6.1.1 Global hazard exposure

Lack of awareness of exposure to multiple hazards is a limitation in making cities better prepared against multi-hazard events. Previously, studies had shown the total number of

different hazards to which a city is exposed, but to increase resilience it is important to also distinguish the types of hazards involved.

This study analyses the exposure of urban infrastructure systems to five hazards (earthquakes, cyclone wind, river flooding, coastal flooding, and landslides). The analysis makes use of global hazard datasets. Results show that joint exposure to two or more hazards is common (overall, 11% of cities are exposed to high levels of two or more hazards, and 45% are exposed to low or above levels of two or more hazards), showing the importance of accounting for multiple hazards at the city scale. Hazards seen to both affect the same urban areas include strong wind and river flooding, strong wind and coastal flooding (particularly in Asia and North America), and river and coastal flooding (particularly in Asia and Europe). Interestingly, the study also shows that a quarter of cities are exposed to both (low) earthquake hazard and to (low) cyclone winds. Evaluation of the data shows higher accuracy for hazards that vary gradually over space (i.e. earthquakes and wind), than for hazards that are more localised (i.e. river flooding). The study also discusses possible applications of the combined hazard levels (COHAZLE) dataset developed. The data could be useful to increase communication between professionals (e.g. urban planners, local authorities, engineers, infrastructure service providers) across cities with similar multi-hazard profiles. The study demonstrates a short example of this for the city of Bristol.

6.1.2 Consecutive impacts to water supply

Studies of performance of infrastructure systems under damage has been mostly focused on single hazard events. While there are concerns that the consequences of a combined event can be more than the sum, evidence of this is scarce. There is therefore limited evidence that would justify carrying out this kind of assessments in practice.

This study models a consecutive hazard event, where an earthquake and storm occur within hours or days of each other. To account for uncertainty in the damage caused by each event, as well as uncertainty in the relative timing of occurrence of each event, a Monte Carlo simulation approach is used. Specifically, a procedure is demonstrated for monitoring the change in disruption relative to the two events occurring individually. The approach makes it possible to investigate the causes of increased disruption. The results are analysed to identify characteristics of the system that make it uniquely vulnerable to a consecutive occurrence of the two events. The approach is applied and demonstrated with an example water supply system representative of a typical system supplying water to a small town. The study finds that the relative timing of events had a strong influence on the increase in consequences. The model produces similar response patterns both when the earthquake is followed by the storm, and when the storm is followed by the earthquake. Specifically, results show that shortly after the first hazard, the occurrence of the second event does not increase disruption; in fact, overall disruption is less, as the effect of the second hazard is 'absorbed' into that already present due to the first hazard. However, a time window is identified (in this case between approximately 5 and 25 hours after the first event) when the system is particularly vulnerable to the second event, meaning that its occurrence in that time window can significantly increase the consequences, relative to if it had happened under normal conditions. The same modelling approach used here could also be applied to other systems and hazard combinations, to help identify system vulnerabilities to consecutive events.

6.1.3 Road network assessment in a real city

Many cities, particularly in Asia, and a large number in China, are prone to multiple hazards. However, researching and understanding multi-hazard risks in those cities requires overcoming

barriers in data availability, privacy concerns, and accessibility to information, both regarding hazards and the infrastructure systems that it could affect.

This study models the consequences of a multi-hazard event in the case study city of Jingdezhen in China. Specifically, the performance of the road network to a combined river flooding and debris flows scenario is analysed. Metrics from graph theory are used to represent the performance of the road network. The results suggest that the performance of the future road network (planned for 2030) will be higher than that of the current network, both under normal conditions and during a flood scenario. However, if the flood coincides with debris flow, the performance would instead fall below that of the current network. Therefore, the study identifies a potential area of susceptibility to debris flows. The findings however are sensitive to data uncertainty. Important gaps that will require further understanding include understanding how the river flow affects bridges, understanding the depth of the channel, and understanding the mass-to-drag ratio of debris flow. Through sensitivity analysis, it was possible to identify specific locations where (i.e. which road sections) should be prioritised for detailed studies, as they have the greatest influence on the calculated functionality.

6.2 Recommended future work

6.2.1 Short term: building an evidence base for increased impacts

In the short term, it would be interesting to extend the study from Chapter 4 (i.e. the comparison the single- and multi-hazard impacts on water supply) to other water supply system configurations. Chapter 4 shows results for the water supply in the hypothetical city of C-Town, characterised by a relatively steep topography and strongly reliant on pumping and tank storage for its operations. Applying the same analysis to systems with different characteristics could help understand whether the observed increase also occurs with other system configurations.

For example, in a relatively flat water distribution network powered by pumps, increased impacts might result primarily from patterns of combined damage to pipes and pumps (as opposed to patterns of tank and pump damage that are the cause of the greatest increase in C-Town). Different mechanisms of failure may help to identify other vulnerabilities within the systems.

The analysis could also be extended to other combinations of hazards. For example, flooding could affect the functionality of pumping stations (e.g. Arrighi et al., 2017) similarly to a cyclone or windstorm. Depending on the layout of the system, flooding may also damage storage tanks or pipes (Copeland, 2005). These effects could be represented in the same way as with the earthquake and storm, assigning each component a probability of failure (a delay in recovery times may need to be included to account for the duration of the flood). Landslides are another hazard that could damage water infrastructure, and they could be included in a similar way, using a probability of failure derived from landslide susceptibility or hazard maps. Further work could also extend the model to explicitly account for increased damage to components, and increased recovery times due to the combination of hazards.

Extending the analysis to other systems hazards combinations would be a valuable way of increasing understanding of combined impacts. It would highlight cases in which these combined impacts are significant, and build up the evidence base for justifying assessments of combined impacts in practice. Indeed, further evidence could encourage infrastructure providers in hazard prone cities to carry out assessments on their own systems. By using real component fragilities and hazard-informed patterns of damage, the assessment aims to be representative of real conditions. The approach follows that used for single hazards, making it in theory relatively straight forward to implement.

6.2.2 Long term: towards interdisciplinary, problem-driven research

Understanding combined impacts only represents the first step towards reducing those impacts in practice. One difficulty is that risk-based thinking still dominates many hazard mitigation decisions. Risk-based thinking compares mitigation options based on both the severity and the probability of an event, such that low-probability high-consequence events (e.g. consecutive earthquake and cyclone) may be given relatively low importance. Therefore, alternative ways of valuing solutions may need to be agreed on, and embraced, before mitigation of combined hazard events is seen in practice. An interesting possibility would be to compare alternative mitigation options based on the benefits for single hazard events, as well as on the benefits during combined hazard events (i.e. the 'synergistic' value). Another difficulty is that beyond a certain event magnitude, the engineering solutions available to infrastructure service providers may not be sufficient to maintain service levels within acceptable boundaries. In that case, resilience may have to be provided at the level of the community, for example through evacuation or temporary relocation of the population, emergency response, or partnerships with surrounding cities. The assessment of combined impacts to infrastructure services could help inform broader community-level decisions by providing information such as which areas are likely to experience disruptions, and how severely they could they be affected. Using the information in wider community planning could help to reduce consequences when disruption does occur.

Therefore, making systems more resilient to combined hazards in practice goes beyond the scope of engineering, and requires an interdisciplinary approach. Indeed, to effectively address multi-hazard challenges in practice (e.g. developing new ways of valuing solutions, informing community-based approaches), collaboration with social scientists, local authorities, emergency planners and the wider society will be needed. These collaborations need to find

common ground in other ways than through shared disciplinary knowledge. One alternative is to focus on shared problems. These problems, to be compelling, should be grounded in real contexts. Such a problem-focused approach has been embraced by the NERC funded Tomorrow's Cities research hub, an interdisciplinary research hub working to "bring multi-hazard disaster risk management to the centre of urban policy and practice". (https://www.tomorrowscities.org). The project centres on four cities with distinct multi-hazard challenges: Kathmandu, Istanbul, Nairobi, and Quito.

Cities have a wide variety of hazard conditions (shown in Chapter 3), each of which require targeted approaches (Chapter 5), so selecting appropriate case studies is crucial. Priority should be given to cities where analysis of combined hazards is expected to be most valuable. To identify suitable case studies, three aspects are highlighted for consideration. The first aspect is whether the city faces significant risk from multiple types of hazards. The second aspect is the vulnerability of the population of that city; cities with a larger vulnerable population would benefit more from improved mitigation decisions. The third aspect are prospects for change within the city. Cities undergoing rapid change, receiving large investment, or that are in the process of redeveloping areas or industries, provide an opportunity for new knowledge to be applied and immediately add value at scale, while generating new evidence.

The value of multi-hazard research can be increased through partnerships between cities based on hazard similarity. Using the growing availability of hazard data along with similarity indices, as proposed in Chapter 3, targeted solutions developed in one context could be transferred to other similar areas. Of course, the diversity of societal behaviours, cultures, values, and perceptions of hazards would also determine how suitable solutions are for a given context. Therefore, hazard similarity could be taken forward to include both natural and societal factors that play a role in disaster risk reduction.

In conclusion, (1) based on global data analysis and two modelling case studies, the thesis demonstrates a need, and potential, to better understand the consequences of combined hazards on the functionality of critical urban infrastructure, as a first step towards better preparing infrastructure services in the face of combined hazards; (2) to generate value from combined hazard assessments in practice, partnerships between engineers and other stakeholders will be needed, requiring a shift towards interdisciplinary and problem-oriented research, a timely change that will help make our cities more resilient to the complex and interconnected challenges coming our way.

Appendix

A. Supplements to Chapter 3

A.1 Exposure results

Table A.1 provides an overview of exposure values for the combinations of hazards. Rows represent different combinations. The total exposure values T1 to T4 show all cities exposed to at least 1, 2, 3 and 4 hazards, respectively. Columns show the values for different hazard levels. Approximately half of cities (4,396 cities) are exposed to high levels of at least one hazard.

Table A.1 Number of urban areas exposed to single and combinations of hazards (out of 9,031 cities in the urban areas dataset).

	Hazards					High hazard level		Medium+ hazard level		Low+ hazard level	
	Earthquake	River flood	Coastal flood	Cyclone wind	Landslide	Cities	Population (millions)	Cities	Population (millions)	Cities	Population (millions)
T1	All 1+ hazards					4396	2748	6186	3307	7712	3665
S1	■					192	157	2347	1168	4683	2255
S2		■				2760	2079	2852	2109	2959	2140
S3			■			475	890	857	1180	866	1191
S4				■		2038	1199	2884	1586	4440	2184
S5					■	90	217	205	314	409	437
T2	All 2+ hazards					1023	1141	2363	1865	4089	2546
C1	■	■				57	89	642	554	1496	1202
C2	■		■			15	70	253	418	502	733
C3	■			■		54	64	662	440	2234	1265
C4	■				■	12	63	193	306	402	433
C5		■	■			176	610	277	732	286	748
C6		■		■		682	751	970	956	1535	291
C7		■			■	8	139	25	167	82	228
C8			■	■		228	559	444	730	523	843
C9			■		■	21	159	64	222	105	259
C10				■	■	52	113	117	186	252	344
T3	All 3+ hazards					127	517	511	807	1354	1343
C11	■	■	■			4	54	42	183	142	447
C12	■	■		■		13	45	160	201	783	754
C13	■	■			■	2	52	23	110	80	227
C14	■		■	■		9	45	160	219	320	557
C15	■		■		■	4	54	62	167	103	257
C16	■			■	■	9	44	110	135	248	342
C17		■	■	■		90	421	158	96	180	586
C18		■	■		■	7	139	11	14	19	167
C19		■		■	■	4	79	15	32	43	195
C20			■	■	■	15	98	46	50	84	233
T4	All 4+ hazards					8	99	78	277	188	500
C21	■	■	■	■		3	38	28	171	86	367
C22	■	■	■		■	2	52	11	153	18	166
C23	■	■		■	■	1	36	14	106	42	194
C24	■		■	■	■	3	39	46	148	83	232
C25		■	■	■	■	3	79	7	100	15	155
C26	■	■	■	■	■	1	36	7	100	14	154

Figure A.1 uses matrices to show the number of urban areas per hazard level. Each matrix shows the results for one combination of two hazards. Individual squares in the matrix show the number of cities for each combination of hazard levels. The sum of pixel values in each matrix is equal to the total number of cities in the analysis. The numbers on the x- and y-axis correspond to the hazards levels, with 1 = very low, 2 = low, 3 = medium, 4 = high. The figure shows that almost all combinations of hazard levels occur in at least one urban area.

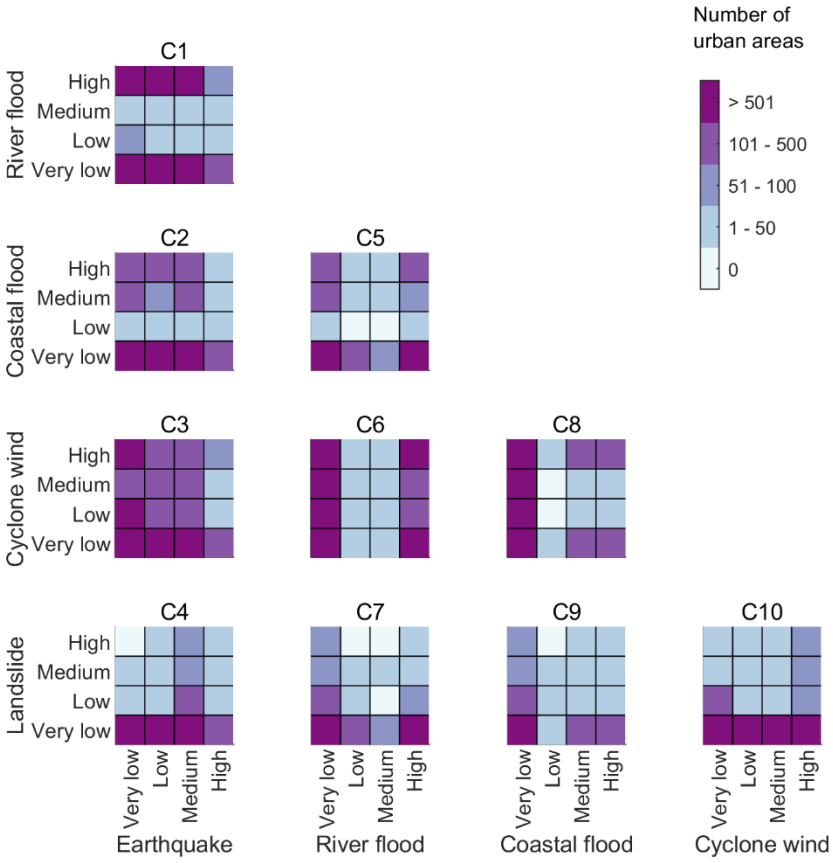

Figure A.1 The number of urban areas exposed to combinations of two hazards.

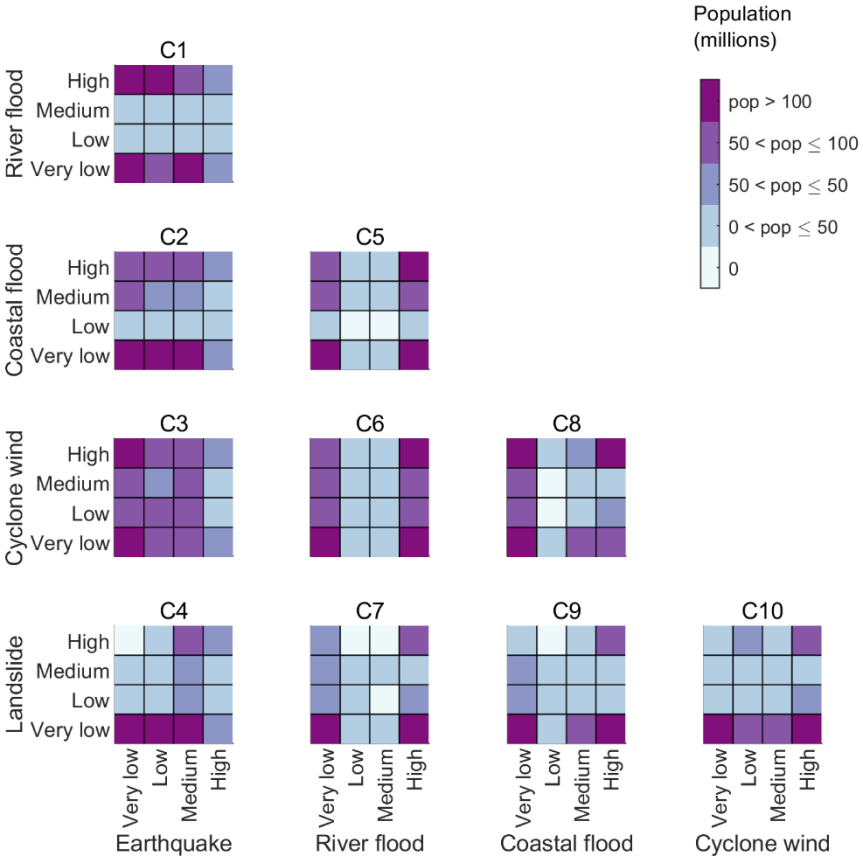

Figure A.2 The population exposed to combinations of two hazards.

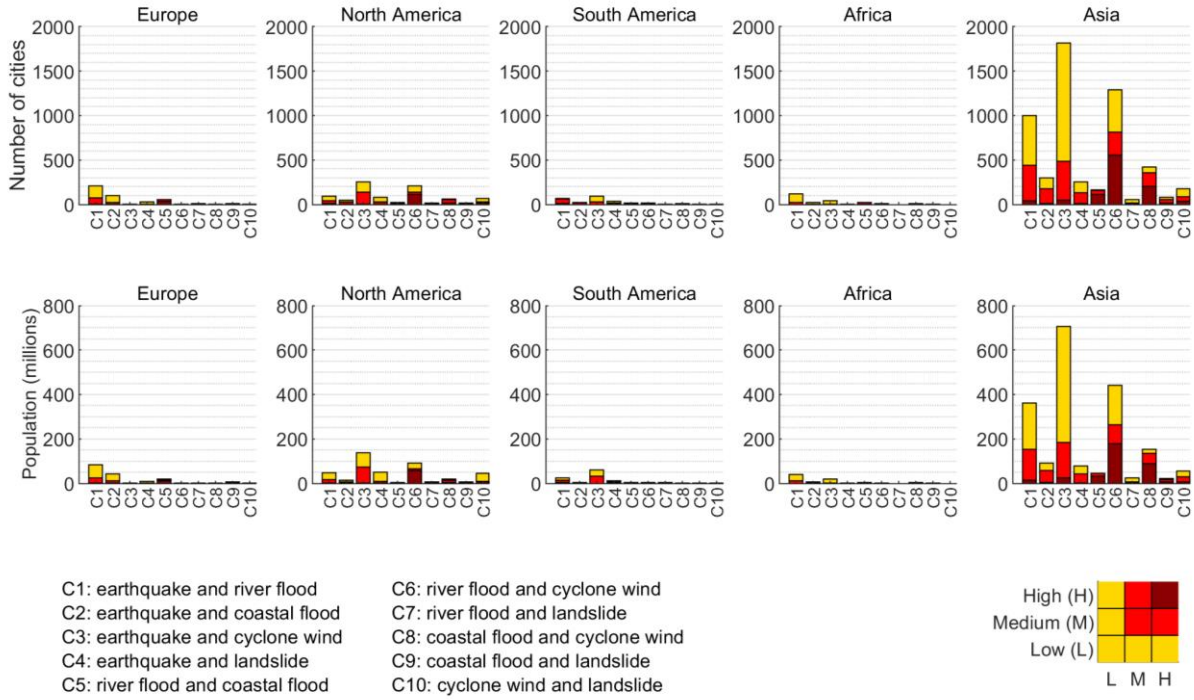

Figure A.3 Exposure to combinations of two hazards (C1 – C10) by continent, with equal ranges on the y-axis. Colours correspond to combinations of hazard levels as shown in the legend (bottom right). The total number of cities and the corresponding population is shown for each continent.

A.2 Additional sensitivity analysis results

Sensitivity analysis is used to determine how the results are affected by the choice of return period and threshold value. Several cases are explored (Table A.2). In each case, changes are made to one or more values to look at the influence on the findings. The analysis focuses on values that are expected to have the largest influence on the results, particularly earthquake, river flooding, and cyclone hazards. The exposure to one, two, and three hazards for each of the cases in Table A.2 can be seen in Figure A.3.

Table A.2 Alternative threshold values used in the sensitivity analysis. Each case corresponds to one or more changes to the threshold values. The table includes the reason for selecting the changes. The values that are different to the baseline in each case are shown in blue.

Hazard	High	Medium	Low
Baseline: No change *Baseline values used for the results in Chapter 3.*			
Earthquake	196 cm/s^2 in 250 years	98 cm/s^s in 475 years	98 cm/s^2 in 2475 years
River flood	0.5 m in 10 years	0.5 m in 50 years	0.5 m in 500 years
Coastal flood	2.0 m in 10 years	0.5 m in 50 years	0.5 m in 100 years
Cyclone	80 km/h in 50 years	80 km/h in 100 years	80 km/h in 1000 years
Landslide	250 per 1 x 10^6 years	125 per 1 x 10^6 years	63 per 1 x 10^6 years
Case 1: Lower earthquake return period *Low earthquake hazard is defined relative to a longer return period than other hazards.*			
Earthquake	196 cm/s^2 in 250 years	98 cm/s^s in 475 years	98 cm/s^2 in **975** years
Case 2: Higher earthquake intensity *The threshold for medium and low earthquake hazard is set to a lower intensity than the high hazard threshold.*			
Earthquake	196 cm/s^2 in 250 years	**196** cm/s^s in 475 years	**196** cm/s^2 in 975 years
Case 3: Lower cyclone wind return period *Low cyclone wind hazard is defined relative to a longer return period than flooding.*			
Cyclone	80 km/h in 50 years	80 km/h in 100 years	80 km/h in **250** years
Case 4: Higher cyclone wind intensity *The cyclone intensity may be low in terms of possible damage relative to the intensities of other hazards.*			
Cyclone	**180** km/h in 50 years	**180** km/h in 100 years	**180** km/h in 1000 years
Case 4: Combined cyclone wind and earthquake lower bounds *Different, but still plausible, thresholds for earthquakes and wind can significantly influence the results*			
Earthquake	196 cm/s^2 in 250 years	**198** cm/s^s in 475 years	**198** cm/s^2 in **975** years
Cyclone	**180** km/h in 50 years	**180** km/h in 100 years	**180** km/h in **250** years

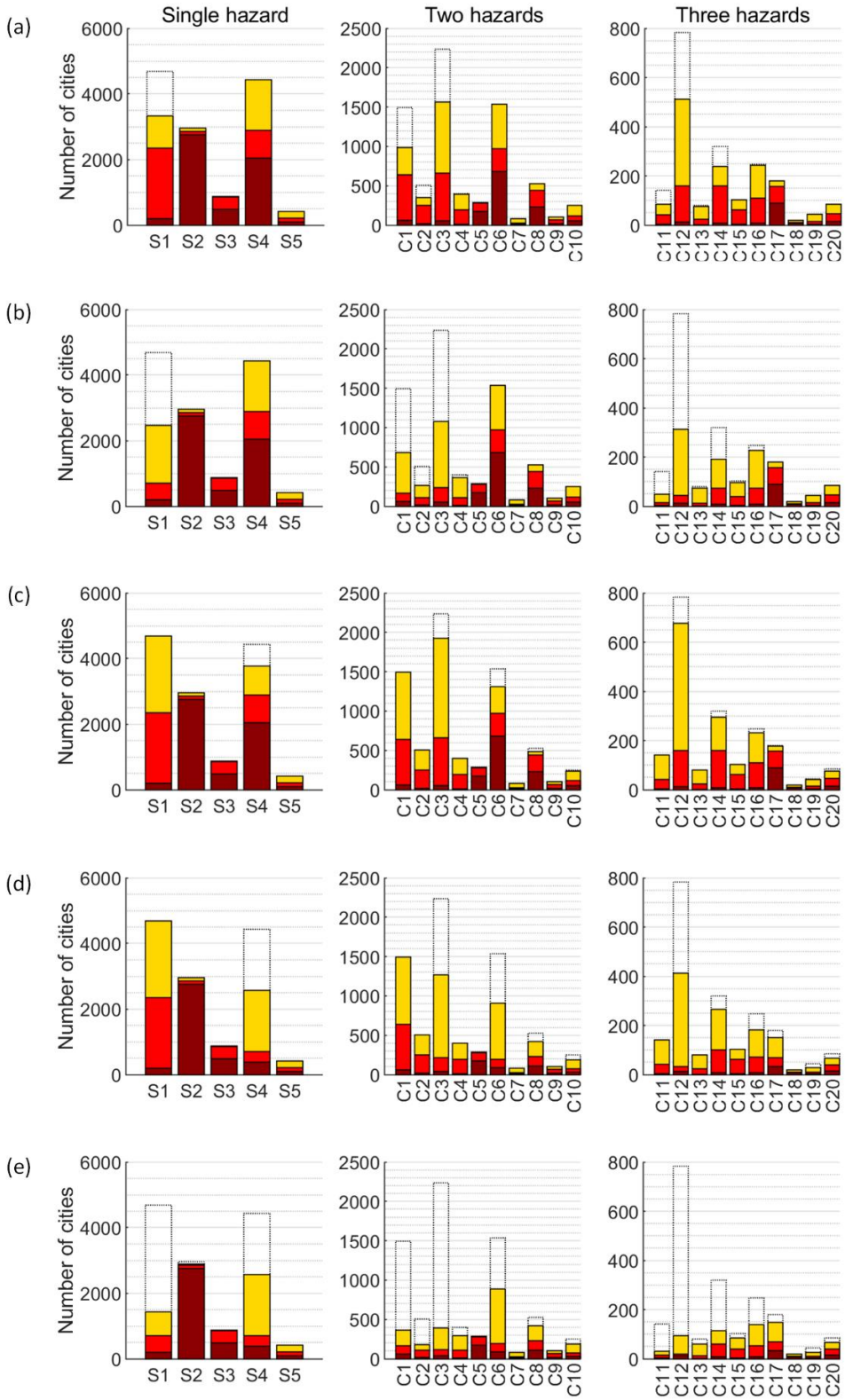

Figure A.4 Additional sensitivity analysis results corresponding to the cases presented in Table A.2.

A.3 Comparison with other global hazard datasets

River flooding

The 100-year return period river flood map from Dottori et al. (2016) is compared with the river flood map used for the UNISDR Global Assessment Report 2015 (Herold & Rudari, 2013). The map is available from https://preview.grid.unep.ch/. Unlike the flood maps in Dottori et al. (2016), Herold and Rudari (2013) include flooding over small catchment areas. The map by Herold and Rudari (2013) is aligned to the urban areas in the same way as the other hazard maps, and maximum flood depths are recorded from each urban area.

Cyclone wind

The cyclone wind data from Cardona et al. (2014) is compared with the cyclone wind map by Tan and Fang (2018). The two use a similar approach to calculate the wind hazard, but Tan and Fang (2018) provide the results at much higher resolution (30 arc-second or approximately 1 km resolution). The data from Tan and Fang (2018) is processed in the same way as the other datasets and maximum wind speeds are recorded for each urban area.

Results

Figure A.4 compares river flood and wind speed values with those obtained from alternative global hazard datasets. The figure shows a higher correlation for the wind datasets than for the river flood datasets.

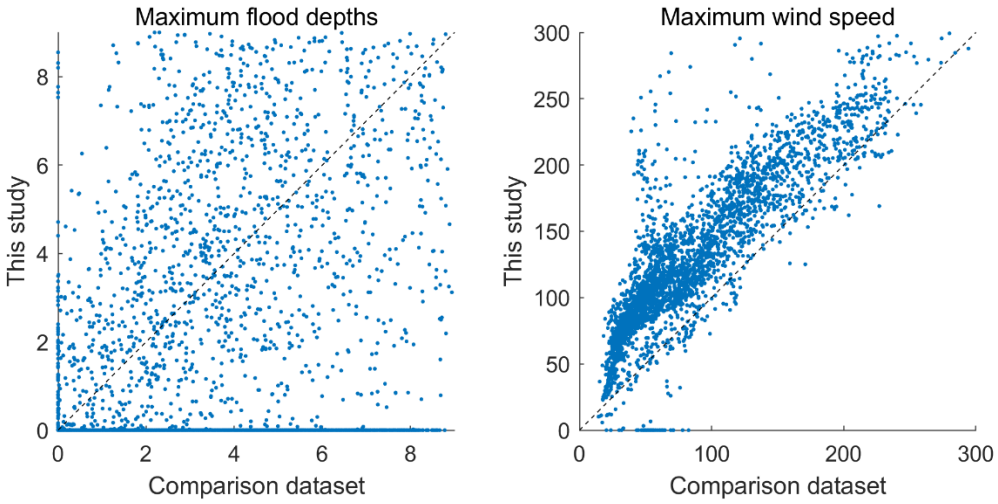

Figure A.5 The left panel compares the maximum flood depths per urban area in Dottori et al. (2016) and Herold and Rudari (2013). The right panel compares the maximum wind speeds per urban area in Cardona et al. (2014) and in Tan and Fang (2018).

This page was intentionally left blank

Bibliography

Adachi, T., & Ellingwood, B. R. (2008). Serviceability of earthquake-damaged water systems: Effects of electrical power availability and power backup systems on system vulnerability. *Reliability Engineering & System Safety*, *93*(1), 78–88.

Alexander, D. E. (2013). Resilience and disaster risk reduction: an etymological journey. *Natural Hazards & Earth System Sciences*, *13*(11).

Arderne, C., Zorn, C., Nicolas, C., & Koks, E. E. (2020). Predictive mapping of the global power system using open data. *Scientific Data*, *7*(1), 1–12.

Arosio, M., Martina, M.L.V., & Figueriedo, R. (2020). The whole is greater than the sum of its parts: a holistic graph-based assessment approach for natural hazard risk of complex systems. *Natural Hazards and Earth System Sciences*, *20*(2), 521-547.

Arrighi, C., Tarani, F., Vicario, E., & Castelli, F. (2017). Flood Impacts on a Water Distribution Network. *Natural Hazards and Earth System Sciences*, *17*(12), 1–22.

Ashford, S. A., Jakrapiyanun, W., & Lukkunaprasit, P. (2000). Amplification of earthquake ground motions in Bangkok. In *Proceedings of the 12th World Conference on Earthquake Engineering, Auckland, New Zealand*. Paper no. 1466.

Aven, T. (2015). Implications of black swans to the foundations and practice of risk assessment and management. *Reliability Engineering & System Safety, 134*, 83–91.

Ayyub, B. M. (2014). *Risk analysis in engineering and economics*. Crc Press.

Bagheri, A., Darijani, M., Asgary, A., & Morid, S. (2010). Crisis in Urban Water Systems during the Reconstruction Period: A System Dynamics Analysis of Alternative Policies after the 2003 Earthquake in Bam-Iran. *Water Resources Management*, *24*(11), 2567–2596.

Balk, D. L., Deichmann, U., Yetman, G., Pozzi, F., Hay, S. I., & Nelson, A. (2006). Determining global population distribution: methods, applications and data. *Advances in Parasitology*, *62*, 119–156.

Barrington-Leigh, C., & Millard-Ball, A. (2017). The world's user-generated road map is more than 80% complete. *PloS One*, *12*(8), e0180698.

Bates, P. D., Horritt, M. S., & Fewtrell, T. J. (2010). A simple inertial formulation of the shallow water equations for efficient two-dimensional flood inundation modelling. *Journal of Hydrology*, *387*(1–2), 33–45.

Bates, P., Trigg, M., Neal, J., & Dabrowa, A. (2013). LISFLOOD-FP User's manual. School of Geographical Sciences, University of Bristol.

Berkowitz, M., & Kramer, A. M. (2018). Helping cities drive transformation: the 100 Resilient Cities Initiative. Interviews with Michael Berkowitz, president of 100 Resilient Cities, and Dr. Arnoldo Matus Kramer, Mexico City's Chief Resilience Officer. *Field Actions Science Reports. The Journal of Field Actions, (Special Issue 18)*, 52–57.

Bernier, C., & Padgett, J. E. (2019). Fragility and risk assessment of aboveground storage tanks subjected to concurrent surge, wave, and wind loads. *Reliability Engineering & System Safety*, *191*, 106571.

Birkmann, J., Welle, T., Solecki, W., Lwasa, S., & Garschagen, M. (2016). Boost resilience of small and mid-sized cities. *Nature*, *537*(7622), 605–608.

Bout, B., Lombardo, L., Van Westen, C. J., & Jetten, V. G. (2018). Integration of two-phase solid fluid equations in a catchment model for flashfloods, debris flows and shallow slope failures. *Environmental Modelling & Software, 105*, 1-16.

Bozza, A., Asprone, D., Parisi, F., & Manfredi, G. (2017). Alternative resilience indices for city ecosystems subjected to natural hazards. *Computer-Aided Civil and Infrastructure Engineering*, *32*(7), 527–545.

Bozza, A., Asprone, D., & Fabbrocino, F. (2017). Urban resilience: A civil engineering perspective. *Sustainability*, *9*(1), 103.

Bozzolan, E., Holcombe, E., Pianosi, F., & Wagener, T. (2020). Including informal housing in slope stability analysis – an application to a data-scarce location in the humid tropics. *Natural Hazards and Earth System Sciences, 20*(11), 3161-3177.

Bristol City Council. (2016). Bristol resilience strategy. Bristol.

Bross, L., Krause, S., Wannewitz, M., Stock, E., Sandholz, S., & Wienand, I. (2019). Insecure Security: Emergency Water Supply and Minimum Standards in Countries with a High Supply Reliability. *Water*, *11*(4), 732.

Bruneau, M., Chang, S. E., Eguchi, R. T., Lee, G. C., O'Rourke, T. D., Reinhorn, A. M., … Von Winterfeldt, D. (2003). A framework to quantitatively assess and enhance the seismic resilience of communities. *Earthquake Spectra*, *19*(4), 733–752.

Buldyrev, S. V, Parshani, R., Paul, G., Stanley, H. E., & Havlin, S. (2010). Catastrophic cascade of failures in interdependent networks. *Nature*, *464*(7291), 1025–1028.

Butler, D., Farmani, R., Fu, G., Ward, S., Diao, K., & Astaraie-Imani, M. (2014). A new approach to urban water management: Safe and sure. In *16th Water Distribution System Analysis Conference, WDSA, Procedia Engineering*. 347–354.

Campbell, K. W., & Bozorgnia, Y. (2008). NGA ground motion model for the geometric mean horizontal component of PGA, PGV, PGD and 5% damped linear elastic response spectra for periods ranging from 0.01 to 10 s. *Earthquake Spectra*, *24*(1), 139–171.

Cardona, O. D., Ordaz, M. G., Mora, M. G., Salgado-Gálvez, M. A., Bernal, G. A., Zuloaga-Romero, D., … González, D. (2014). Global risk assessment: A fully probabilistic

seismic and tropical cyclone wind risk assessment. *International Journal of Disaster Risk Reduction, 10*(B), 461–476.

Carpenter, S., Walker, B., Anderies, J. M., & Abel, N. (2001). From Metaphor to Measurement: Resilience of What to What? *Ecosystems*, *4*(8), 765–781.

Cavalieri, F., Franchin, P., & Giovinazzi, S. (2016). Earthquake-altered flooding hazard induced by damage to storm water systems. *Sustainable and Resilient Infrastructure*, *1*(1–2), 14–31.

Cavallaro, M., Asprone, D., Latora, V., Manfredi, G., & Nicosia, V. (2014). Assessment of urban ecosystem resilience through hybrid social--physical complex networks. *Computer-Aided Civil and Infrastructure Engineering*, *29*(8), 608–625.

Hyder Consulting (2013). Central Area Flood Risk Assessment – Summary Report.

Chang, S. E., Yip, J. Z. K., de Jong, S. L. van Z., Chaster, R., & Lowcock, A. (2015). Using vulnerability indicators to develop resilience networks: a similarity approach. *Natural Hazards*, *78*(3), 1827–1841.

Chang, S. E., McDaniels, T. L., Mikawoz, J., & Peterson, K. (2007). Infrastructure failure interdependencies in extreme events: power outage consequences in the 1998 Ice Storm. *Natural Hazards*, *41*(2), 337–358.

Chang, S. E., & Shinozuka, M. (2004). Measuring improvements in the disaster resilience of communities. *Earthquake Spectra*, *20*(3), 739–755.

Chang, S. E., Svekla, W. D., & Shinozuka, M. (2002). Linking infrastructure and urban economy: Simulation of water-disruption impacts in earthquakes. *Environment and Planning B: Planning and Design*, *29*(2), 281–301.

CIESIN (2013). Global Roads Open Access Data Set, Version 1 (gROADSv1). *NASA Socioeconomic Data and Applications Center (SEDAC).*

Cimellaro, G. P., Christovasilis, I. P., Reinhorn, A. M., De Stefano, A., & Kirova, T. (2010). L'Aquila earthquake of April 6th, 2009 in Italy: rebuilding a resilient city to multiple hazard. *MCEER Technical Rep*. MCEER-10, 10.

Cimellaro, G. P., Solari, D., & Bruneau, M. (2014). Physical infrastructure interdependency and regional resilience index after the 2011 Tohoku Earthquake in Japan. *Earthquake Engineering & Structural Dynamics*, *43*(12), 1763–1784.

Ciurean, R., Gill, J., Reeves, H. J., O'Grady, S., & Aldridge, T. (2018). Review of multi-hazards research and risk assessments.

Copeland, C. (2005). Hurricane-Damaged Drinking Water and Wastewater Facilities: Impacts, Needs, and Response. *The Library of Congress*.

Couasnon, A., Eilander, D., Muis, S., Veldkamp, T. I. E., Haigh, I. D., Wahl, T., … Ward, P. J. (2020). Measuring compound flood potential from river discharge and storm surge

extremes at the global scale. *Natural Hazards and Earth System Sciences*, *20*(2), 489–504.

CRED (Centre for Research on the Epidemiology of Disasters). (2020). EM-DAT: The Emergency Events Database - Universite catholique de Louvain (UCL) - www.emdat.be, Brussels, Belgium.

Crowl, D. A., & Louvar, J. F. (2001). *Chemical process safety: fundamentals with applications. Pearson Education.*

Cubrinovski, M., Hughes, M., Bradley, B. A., Noonan, J., Hopkins, R., McNeill, S., & English, G. (2014). Performance of horizontal infrastructure in Christchurch city through the 2010-2011 Canterbury earthquake sequence.

Cutter, S. L., Burton, C. G., & Emrich, C. T. (2010). Disaster resilience indicators for benchmarking baseline conditions. *Journal of Homeland Security and Emergency Management*, *7*(1).

Davidson, R. A. (2015). Integrating disciplinary contributions to achieve community resilience to natural disasters. *Civil Engineering and Environmental Systems*, *32*, 55–67.

Davis, C. A. (2014). Water system service categories, post-earthquake interaction, and restoration strategies. *Earthquake Spectra*, *30*(4), 1487–1509.

Dawson, R. J., Peppe, R., & Wang, M. (2011). An agent-based model for risk-based flood incident management. *Natural Hazards*, *59*(1), 167–189.

De Bruijn, K. M. (2005). Resilience and flood risk management. A systems approach applied to lowland rivers. DUP Science, Delft University Press.

De Bruijn, K. M. (2004). Resilience and flood risk management. *Water Policy*, *6*(1), 53–66.

De Neufville, R., & Scholtes, S. (2011). *Flexibility in engineering design*. MIT Press.

De Ruiter, M. C., Couasnon, A., van den Homberg, M. J. C., Daniell, J. E., Gill, J. C., & Ward, P. J. (2019). Why we can no longer ignore consecutive disasters. *Earth's Future*. *8*(3), e2019EF001425.

Di Baldassarre, G., Viglione, A., Carr, G., Kuil, L., Salinas, J. L., & Blöschl, G. (2013). Socio-hydrology: Conceptualising human-flood interactions. *Hydrology and Earth System Sciences*, *17*(8), 3295–3303.

Di Baldassarre, Giuliano, & Montanari, A. (2009). Uncertainty in river discharge observations: a quantitative analysis. *Hydrology & Earth System Sciences*, *13*(6). 913-921.

Di Mauro, C., Bouchon, S., Logtmeijer, C., Pride, R. D., Hartung, T., & Nordvik, J. P. (2010). A structured approach to identifying European critical infrastructures. *International Journal of Critical Infrastructures*, *6*(3), 277–292.

Diao, K., Sweetapple, C., Farmani, R., Fu, G., Ward, S., & Butler, D. (2016). Global resilience analysis of water distribution systems. *Water Research*, *106*, 383–393.

Didier, M., Broccardo, M., Esposito, S., & Stojadinovic, B. (2018). A compositional demand/supply framework to quantify the resilience of civil infrastructure systems (Re-CoDeS). *Sustainable and Resilient Infrastructure*, *3*(2), 86–102.

Dilley, M., Chen, R. S., Deichmann, U., Lerner-Lam, A. L., & Arnold, M. (2005). *Natural disaster hotspots: a global risk analysis*. The World Bank.

Djalante, R., Holley, C., & Thomalla, F. (2011). Adaptive governance and managing resilience to natural hazards. *International Journal of Disaster Risk Science*, *2*(4), 1–14.

Dong, S., Wang, H., Mostafizi, A., & Song, X. (2020). A network-of-networks percolation analysis of cascading failures in spatially co-located road-sewer infrastructure networks. *Physica A: Statistical Mechanics and Its Applications*, *538*, 122971.

Dottori, F., Di Baldassarre, G., & Todini, E. (2013). Detailed data is welcome, but with a pinch of salt: Accuracy, precision, and uncertainty in flood inundation modeling. *Water Resources Research*, *49*(9), 6079–6085.

Dottori, F., Salamon, P., Bianchi, A., Alfieri, L., Hirpa, F. A., & Feyen, L. (2016). Development and evaluation of a framework for global flood hazard mapping. *Advances in Water Resources*, *94*, 87–102.

Douglas, J. (2014). Ground motion prediction equations 1964--2014. *PEER Report 2011*, *102*.

Dueñas-Osorio, L., Craig, J. I., & Goodno, B. J. (2007). Seismic response of critical interdependent networks. *Earthquake Engineering & Structural Dynamics*, *36*(2), 285–306.

Dueñas-Osorio, L., & Kwasinski, A. (2012). Quantification of lifeline system interdependencies after the 27 February 2010 Mw 8.8 offshore Maule, Chile, earthquake. *Earthquake Spectra*, *28*(1_suppl1), 581–603.

Dunn, G., Brown, R. R., Bos, J. J., & Bakker, K. (2017). Standing on the shoulders of giants: Understanding changes in urban water practice through the lens of complexity science. *Urban Water Journal*, *14*(7), 758–767.

Dunn, S. (2014). An investigation to improve community resilience using network graph analysis of infrastructure systems. Newcastle University.

Dunn, S., Fu, G., Wilkinson, S., & Dawson, R. (2013). Network theory for infrastructure systems modelling. *Engineering Sustainability*, *166*(5), 281–292.

Dunn, S., Wilkinson, S., Alderson, D., Fowler, H., & Galasso, C. (2018). Fragility Curves for Assessing the Resilience of Electricity Networks Constructed from an Extensive Fault Database. *Natural Hazards Review*, *19*(1), 1–10.

Edgington, D. W. (2016). Reflections on the Hanshin Earthquake of 1995 and the Reconstruction of Kobe, Japan. *Rebuilding Asia Following Natural Disasters*, 108–140.

Eidinger, J. M. (2012). Performance of water systems during the Maule Mw 8.8 earthquake of 27 February 2010. *Earthquake Spectra*, *28*(1_suppl1), 605–620.

Elmqvist, T., Andersson, E., Frantzeskaki, N., McPhearson, T., Olsson, P., Gaffney, O., … Folke, C. (2019). Sustainability and resilience for transformation in the urban century. *Nature Sustainability*, *2*(4), 267–273.

Elmqvist, T., Folke, C., Nyström, M., Peterson, G., Bengtsson, J., Walker, B., & Norberg, J. (2003). Response diversity, ecosystem change, and resilience. *Frontiers in Ecology and the Environment*, *1*(9), 488–494.

Fang, Y., & Sansavini, G. (2017). Emergence of antifragility by optimum postdisruption restoration planning of infrastructure networks. *Journal of Infrastructure Systems*, *23*(4), 1–13.

FEMA (Federal Emergency Management Agency) (2003). Multi-hazard loss estimation methodology: Earthquake model. Department of Homeland Security, FEMA, Washington, DC.

Field, C. B., Barros, V., Stocker, T. F., & Dahe, Q. (2012). *Managing the risks of extreme events and disasters to advance climate change adaptation: special report of the intergovernmental panel on climate change.* Cambridge University Press.

Flax, L., Armstrong, A., & Yee, L. (2016). Measuring Urban Resilience As You Build It-Insights from 100 Resilient Cities. *IRGC Resource Guide on Resilience. Lausanne: EPFL International Risk Governance Center*.

Florczyk, A. J., Corbane, C., Ehrlich, D., Freire, S., Kemper, T., Maffenini, L., … others. (2019). GHSL data package 2019. European Commission Joint Research Center, 29788.

Folke, C. (2006). Resilience: The emergence of a perspective for social-ecological systems analyses. *Global Environmental Change*, *16*(3), 253–267.

Fraser, S., Simpson, A., Núñez, A., Deparday, V., Balog, S., Jongman, B., … others. (2016). ThinkHazard! Delivering natural hazard information for decision making. In *2016 3rd International Conference on Information and Communication Technologies for Disaster Management (ICT-DM)*. (pp. 1-6).

Fu, G., Wilkinson, S., & Dawson, R. J. (2016). A spatial network model for civil infrastructure system development. *Computer-Aided Civil and Infrastructure Engineering*, *31*(9), 661-680.

Gallina, V., Torresan, S., Critto, A., Sperotto, A., Glade, T., & Marcomini, A. (2016). A review of multi-risk methodologies for natural hazards: Consequences and challenges for a climate change impact assessment. *Journal of Environmental Management*, *168*, 123–132.

Galvan, G., & Agarwal, J. (2020). Assessing the vulnerability of infrastructure networks based on distribution measures. *Reliability Engineering & System Safety*, *196*, 106743.

Gardoni, P., & LaFave, J. M. (2016). Multi-hazard approaches to civil infrastructure engineering: Mitigating risks and promoting resilience. In *Multi-hazard approaches to civil infrastructure engineering* (pp. 3–12). Springer.

Gehl, P., & D'Ayala, D. (2018). System loss assessment of bridge networks accounting for multi-hazard interactions. *Structure and Infrastructure Engineering*, *14*(10), 1355–1371.

Gill, J. C., & Malamud, B. D. (2014). Reviewing and visualizing the interactions of natural hazards. *Reviews of Geophysics*, *52*(4), 680–722.

Gill, J. C., & Malamud, B. D. (2017). Anthropogenic processes, natural hazards, and interactions in a multi-hazard framework. *Earth-Science Reviews*, *166*, 246–269.

Giuliani, G., & Peduzzi, P. (2011). The PREVIEW Global Risk Data Platform: a geoportal to serve and share global data on risk to natural hazards. *Natural Hazards and Earth System Science*, *11*(1), 53–66.

Godfrey, N., & Savage, R. (2012). *Future proofing cities: Risks and opportunities for inclusive urban growth in developing countries*. Atkins.

Godschalk, D. R. (2003). Urban Hazard Mitigation: Creating Resilient Cities. *Natural Hazards Review*, *4*(3), 136–143.

Golz, S., Schinke, R., & Naumann, T. (2015). Assessing the effects of flood resilience technologies on building scale. *Urban Water Journal*, *12*(1), 30–43.

Goodall, D. W. (1966). A new similarity index based on probability. *Biometrics*, *22*(4), 882–907.

Gordon, J. E. (1978). Structures: Or Why Things Don't Fall Down. London: Pitman Publishing Ltd.

Gower, J. C. (1971). A general coefficient of similarity and some of its properties. *Biometrics*, *27*(4), 857–871.

Gu, D. (2019). Exposure and vulnerability to natural disasters for world's cities.

Guerreiro, S. B., Glenis, V., Dawson, R. J., & Kilsby, C. (2017). Pluvial flooding in European cities: A continental approach to urban flood modelling. *Water*, *9*(4), 296.

Guidotti, R., Chmielewski, H., Unnikrishnan, V., Gardoni, P., McAllister, T., & van de Lindt, J. (2016). Modeling the resilience of critical infrastructure: The role of network dependencies. *Sustainable and Resilient Infrastructure*, *1*(3–4), 153–168.

Guidotti, R., Gardoni, P., & Rosenheim, N. (2019). Integration of physical infrastructure and social systems in communities' reliability and resilience analysis. *Reliability Engineering & System Safety*, *185*, 476–492.

Haasnoot, M., Kwakkel, J. H., Walker, W. E., & ter Maat, J. (2013). Dynamic adaptive policy pathways: A method for crafting robust decisions for a deeply uncertain world. *Global Environmental Change*, *23*(2), 485–498.

Haklay, M., & Weber, P. (2008). Openstreetmap: User-generated street maps. *IEEE Pervasive Computing*, *7*(4), 12–18.

Haraguchi, M., & Kim, S. (2016). Critical infrastructure interdependence in New York City during Hurricane Sandy. *International Journal of Disaster Resilience in the Built Environment. 7*(2), 133-143.

Hart, D. E., Byun, D. S., Giovinazzi, S., Hughes, M. W., Gomez, C. (2015). Relative sea level changes on a seismically active urban coast: Observations from laboratory Christchurch. In *Australasian Coasts & Ports Conference 2015: 22nd Australasian Coastal and Ocean Engineering Conference and the 15th Australasian Port and Harbour Conference*, 384-390.

Hashimoto, T. (1982). Reliability, resiliency, and vulnerability criteria for water resource system performance evaluation. *Water Resources Research*, *18*(1), 14–20.

Hawker, L., Bates, P., Neal, J., & Rougier, J. (2018). Perspectives on digital elevation model (DEM) simulation for flood modeling in the absence of a high-accuracy open access global DEM. *Frontiers in Earth Science*, *6*, 233.

Herold, C., & Rudari, R. (2013). Improvement of the Global Flood Model for the GAR 2013 and 2015. *United Nations Office for Disaster Risk Reduction (UNISDR): Geneva, Switzerland.*

Hickford, A. J., Blainey, S. P., Hortelano, A. O., & Pant, R. (2018). Resilience engineering: theory and practice in interdependent infrastructure systems. *Environment Systems and Decisions*, *38*(3), 278–291.

Hohai University (2015). Consulting Services for: Development of Master Plan for Jingdezhen City Integrated Flood Risk Management.

Holling, C. S. (1973). Resilience and stability of ecological systems. *Annual Review of Ecology and Systematics*, *4*(1), 1–23.

Horton, P., Jaboyedoff, M., Rudaz, B., & Zimmermann, M. (2013). Flow-R, a model for susceptibility mapping of debris flows and other gravitational hazards at a regional scale. *Natural Hazards and Earth System Sciences*, *13*(4), 869–885.

Horton, P., Jaboyedoff, M., Zimmermann, M., Mazotti, B., & Longchamp, C. (2011). Flow-R, a model for debris flow susceptibility mapping at a regional scale-some case studies. *Italian Journal of Engineering Geology*, *2*, 875–884.

Hu, F., Yeung, C. H., Yang, S., Wang, W., & Zeng, A. (2016). Recovery of infrastructure networks after localised attacks. *Scientific Reports*, 6, 1–10.

Hudson, S., Cormie, D., Tufton, E., & Inglis, S. (2012). Engineering resilient infrastructure. *Proceedings of the Institution of Civil Engineers: Civil Engineering*, *165*(6), 5–12.

Isoyama, R., Ishida, E., Yune, K., & Shirozu, T. (2000). Seismic damage estimation procedure for water supply pipelines. *Water Supply*, *18*(3), 63–68.

Jebson, S. (2007). Fact sheet number 6: The Beaufort scale.

Jongman, B., Ward, P. J., & Aerts, J. C. J. H. (2012). Global exposure to river and coastal flooding: Long term trends and changes. *Global Environmental Change*, *22*(4), 823–835.

Kameshwar, S., & Padgett, J. E. (2014). Multi-hazard risk assessment of highway bridges subjected to earthquake and hurricane hazards. *Engineering Structures*, *78*, 154–166.

Kammouh, O., Cimellaro, G. P., & Mahin, S. A. (2018). Downtime estimation and analysis of lifelines after an earthquake. *Engineering Structures*, *173*, 393–403.

Kappes, M. S., Keiler, M., von Elverfeldt, K., & Glade, T. (2012). Challenges of analyzing multi-hazard risk: a review. *Natural Hazards*, *64*(2), 1925–1958.

Kappes, M. S., Papathoma-Koehle, M., & Keiler, M. (2012). Assessing physical vulnerability for multi-hazards using an indicator-based methodology. *Applied Geography*, *32*(2), 577–590.

Karamouz, M., Razmi, A., Nazif, S., & Zahmatkesh, Z. (2017). Integration of inland and coastal storms for flood hazard assessment using a distributed hydrologic model. *Environmental Earth Sciences*, *76*(11), 395.

Kaufman, S., Qing, C., Levenson, N., & Hanson, M. (2012). Transportation During and After Hurricane Sandy. *Rudin Center for Transportation, NYU Wagner Graduate School of Public Service.*

Kitagawa, Y., & Hiraishi, H. (2004). Overview of the 1995 Hyogo-Ken Nanbu Earthquake and Proposals for Earthquake Mitigation Measures. *Journal of Japan Association for Earthquake Engineering*, *4*(3), 1–29.

Kitagawa, M. (2004). Technology of the akashi kaikyo bridge. *Structural Control and Health Monitoring*, *11*(2), 75-90.

Klinger, C., & Owen Landeg, V. M. (2014). Power outages, extreme events and health: a systematic review of the literature from 2011-2012. *PLoS Currents*, *6*.

Klise, K. A., Bynum, M., Moriarty, D., & Murray, R. (2017). A software framework for assessing the resilience of drinking water systems to disasters with an example earthquake case study. *Environmental Modelling and Software*, *95*, 420–431.

Koks, E., Rozenberg, J., Zorn, C., Tariverdi, M., Vousdoukas, M., Fraser, S. A., … Hallegatte, S. (2019). A global multi-hazard risk analysis of road and railway infrastructure assets. *Nature Communications*, *10*(1), 1–11.

Koks, E., Pant, R., Thacker, S., & Hall, J. W. (2019). Understanding business disruption and economic losses due to electricity failures and flooding. *International Journal of Disaster Risk Science*, *10*(4), 421–438.

Kong, J., Simonovic, S. P., & Zhang, C. (2019). Sequential hazards resilience of interdependent infrastructure system: A case study of Greater Toronto Area energy infrastructure system. *Risk Analysis*, *39*(5), 1141–1168.

Kwadijk, J. C. J., Haasnoot, M., Mulder, J. P. M., Hoogvliet, M. M. C., Jeuken, A. B. M., Van der Krogt, R. A. A., … de Wit, M. J. M. (2010). Using adaptation tipping points to prepare for climate change and sea level rise: A case study in the Netherlands. *Wiley Interdisciplinary Reviews: Climate Change*, *1*(5), 729-740.

Lekkas, E., Andreadakis, E., Alexoudi, V., Kapourani, E., & Kostaki, I. (2011). The Mw= 9.0 Tohoku Japan earthquake (March 11, 2011) tsunami impact on structures and infrastructure. In *Environmental Geosciences and Engineering Survey for Territory Protection and Population Safety (EngeoPro) International conference, Moscow* (pp. 97–103).

Leonard, M., Westra, S., Phatak, A., Lambert, M., van den Hurk, B., McInnes, K., … Stafford-Smith, M. (2014). A compound event framework for understanding extreme impacts. *Wiley Interdisciplinary Reviews: Climate Change*, *5*(1), 113–128.

Lhomme, S., Serre, D., Diab, Y., & Laganier, R. (2013). Analyzing resilience of urban networks: a preliminary step towards more flood resilient cities. *Natural Hazards and Earth System Sciences*, *13*(2), 221.

Li, Y., Ahuja, A., & Padgett, J. E. (2012). Review of methods to assess, design for, and mitigate multiple hazards. *Journal of Performance of Constructed Facilities*, *26*(1), 104–117.

MacAskill, K., & Guthrie, P. (2014). Multiple interpretations of resilience in disaster risk management. *Procedia Economics and Finance*, *18*(Suppl. C), 667–674.

Makropoulos, C., Nikolopoulos, D., Palmen, L., Kools, S., Segrave, A., Vries, D., … Medema, G. (2018). A resilience assessment method for urban water systems. *Urban Water Journal*, *15*(4), 316–328.

Manyena, S. B. (2006). The concept of resilience revisited. *Disasters*, *30*(4), 434–450.

Marchi, A., Salomons, E., Ostfeld, A., Kapelan, Z., Simpson, A. R., Zecchin, A. C., … Asadzadeh, M. (2014). Battle of the Water Networks II. *Journal of Water Resources Planning and Management*, *140*(7), 1–14.

Markolf, S. A., Chester, M. V, Eisenberg, D. A., & Iwaniec, D. M. (2018). Interdependent Infrastructure as Linked Social, Ecological, and Technological Systems (SETSs) to Address Lock-in and Enhance Resilience. *Earth's Future*, *6*(12), 1638–1659.

Martin-Breen, P., & Anderies, J. M. (2011). Resilience: *A Literature Review. The Bellagio Initiative The Future of Philanthropy and Development in the Pursuit of Human Wellbeing.*

Matthews, Tom, Wilby, R. L., & Murphy, C. (2019). An emerging tropical cyclone--deadly heat compound hazard. *Nature Climate Change*, *9*(8), 602–606.

Mattsson, L.-G., & Jenelius, E. (2015). Vulnerability and resilience of transport systems--A discussion of recent research. *Transportation Research Part A: Policy and Practice*, *81*, 16–34.

McCullough, M. C., Kareem, A., Donahue, A. S., & Westerink, J. J. (2013). Structural damage under multiple hazards in coastal environments. *Journal of Disaster Research*, *8*(6), 1042–1051.

McDaniels, T., Chang, S., Peterson, K., Mikawoz, J., & Reed, D. (2007). Empirical framework for characterizing infrastructure failure interdependencies. *Journal of Infrastructure Systems*, *13*(3), 175–184.

Meerow, S., Newell, J. P., & Stults, M. (2016). Defining urban resilience: A review. *Landscape and Urban Planning*, *147*, 38–49.

Meijer, J. R., Huijbregts, M. A. J., Schotten, K. C. G. J., & Schipper, A. M. (2018). Global patterns of current and future road infrastructure. *Environmental Research Letters*, *13*(6), 64006.

Miles, S. B., & Chang, S. E. (2011). ResilUS: A community based disaster resilience model. *Cartography and Geographic Information Science*, *38*(1), 36–51.

Moreno-Monroy, A. I., Schiavina, M., & Veneri, P. (2020). Metropolitan areas in the world. Delineation and population trends. *Journal of Urban Economics*, 103242.

Morley, M. S., & Tricarico, C. (2008). Pressure-driven demand extension for EPANET (EPANETpdd).

Mostafavi, A., Ganapati, N. E., Nazarnia, H., Pradhananga, N., & Khanal, R. (2018). Adaptive capacity under chronic stressors: Assessment of water infrastructure resilience in 2015 Nepalese earthquake using a system approach. *Natural Hazards Review*, *19*(1), 5017006.

Mugume, S. N., Gomez, D. E., Fu, G., Farmani, R., & Butler, D. (2015). A global analysis approach for investigating structural resilience in urban drainage systems. *Water Research*, *81*, 15–26.

Muis, S., Verlaan, M., Winsemius, H. C., Aerts, J. C. J. H., & Ward, P. J. (2016). A global reanalysis of storm surges and extreme sea levels. *Nature Communications*, *7*, 11969.

Munasinghe, M. (2007). The importance of social capital: Comparing the impacts of the 2004 Asian Tsunami on Sri Lanka, and Hurricane Katrina 2005 on New Orleans. *Ecological Economics*, *64*(1), 9-11.

MunichRE. (2018). Topics Geo. Natural catastrophes 2017. Analyses, Assessments, Positions.

Muranho, J., Ferreira, A., Sousa, J., Gomes, A., & Sá Marques, A. (2012). WaterNetGen: an EPANET extension for automatic water distribution network models generation and pipe sizing. *Water Science and Technology: Water Supply*, *12*(1), 117–123.

Murdock, H. J., De Bruijn, K. M., & Gersonius, B. (2018). Assessment of critical infrastructure resilience to flooding using a response curve approach. *Sustainability*, *10*(10), 3470.

Nachtergaele, F., van Velthuizen, H., Verelst, L., Batjes, N. H., Dijkshoorn, K., van Engelen, V. W. P., … Montanarela, L. (2010). The harmonized world soil database. In *Proceedings of the 19th World Congress of Soil Science, Soil Solutions for a Changing World, Brisbane, Australia, 1-6 August 2010* (pp. 34–37).

Nadim, F., Kjekstad, O., Peduzzi, P., Herold, C., & Jaedicke, C. (2006). Global landslide and avalanche hotspots. *Landslides*, *3*(2), 159–173.

National Research Council (2012). Disaster resilience: A national imperative. *The National Academies Press*. Washington, DC.

Neal, J., Schumann, G., & Bates, P. (2012). A subgrid channel model for simulating river hydraulics and floodplain inundation over large and data sparse areas. *Water Resources Research*, 48(11).

Ning, X., Liu, Y., Chen, J., Dong, X., Li, W., & Liang, B. (2013). Sustainability of urban drainage management: A perspective on infrastructure resilience and thresholds. *Frontiers of Environmental Science and Engineering*, *7*(5), 658–668.

Nojima, N. (2012). Restoration processes of utility lifelines in the great east Japan earthquake disaster, 2011. In *15th World Conference on Earthquake Engineering (15WCEE)* (pp. 24–28).

Cabinet Office. (2011). Keeping the country running: Natural hazards and infrastructure. *Improving the UK's Ability to Absorb, Respond to and Recover from Emergencies*.

Ostfeld, A., Salomons, E., Ormsbee, L., Uber, J. G., Bros, C. M., Kalungi, P., … McKillop, R. (2012). Battle of the water calibration networks. *Journal of Water Resources Planning and Management*, *138*(5), 523–532.

Ouyang, M. (2014). Review on modeling and simulation of interdependent critical infrastructure systems. *Reliability Engineering and System Safety*, *121*, 43–60.

Pant, R., Thacker, S., Hall, J. W., Alderson, D., & Barr, S. (2018). Critical infrastructure impact assessment due to flood exposure. *Journal of Flood Risk Management*, *11*(1), 22–33.

Pathirana, A. (2010). EPANET2 desktop application for pressure driven demand modeling. In *Water Distribution Systems Analysis 2010* (pp. 65–74).

Patterson, C. L., Impellitteri, C. A., Fox, K. R., Haught, R. C., Meckes, M. C., & Blannon, J. C. (2007). Emergency response for public water supplies after Hurricane Katrina. In

World Environmental and Water Resources Congress 2007: Restoring Our Natural Habitat (pp. 1–9).

Pawlak, P. (2016). *Risk and resilience in foreign policy*. EPRS.

Pearson, J., Punzo, G., Mayfield, M., Brighty, G., Parsons, A., Collins, P., … Tagg, A. (2018). Flood resilience: consolidating knowledge between and within critical infrastructure sectors. *Environment Systems and Decisions*, *38*(3), 318–329.

Perla, R., Cheng, T. T., & McClung, D. M. (1980). A two-parameter model of snow-avalanche motion. *Journal of Glaciology*, *26*(94), 197–207.

Perrow, C. (2011). *Normal accidents: Living with high risk technologies*. Princeton university press.

Pesaresi, M., Ehrlich, D., Kemper, T., Siragusa, A., Florczyk, A. J., Freire, S., & Corbane, C. (2017). Atlas of the human planet 2017. *Global Exposure to Natural Hazards*.

Pescaroli, G., & Alexander, D. (2016). Critical infrastructure, panarchies and the vulnerability paths of cascading disasters. *Natural Hazards*, *82*(1), 175–192.

Pescaroli, G., & Alexander, D. (2018). Understanding compound, interconnected, interacting, and cascading risks: a holistic framework. *Risk Analysis*, *38*(11), 2245–2257.

Petley, D. N., Dunning, S. A., Rosser, N. J., & Hungr, O. (2005). The analysis of global landslide risk through the creation of a database of worldwide landslide fatalities. *Landslide Risk Management. Balkema, Amsterdam*, 367–374.

Pitidis, V., Tapete, D., Coaffee, J., Kapetas, L., & de Albuquerque, J. (2018). Understanding the implementation challenges of urban resilience policies: investigating the influence of urban geological risk in Thessaloniki, Greece. *Sustainability*, *10*(10), 3573.

Pitt, M. (2008). *The Pitt Review: Learning lessons from the 2007 floods*. Pitt Review.

Podani, J. (1999). Extending Gower's general coefficient of similarity to ordinal characters. *Taxon*, 48(2), 331–340.

Pokharel, T., & Goldsworthy, H. M. (2017). Lessons learned from the Nepal earthquake 2015. *Australian Journal of Structural Engineering*, *18*(1), 11-23.

Pregnolato, M., Ford, A., Robson, C., Glenis, V., Barr, S., & Dawson, R. (2016). Assessing urban strategies for reducing the impacts of extreme weather on infrastructure networks. *Royal Society Open Science*, *3*(5), 160023.

SwissRe. (2013). Mind the risk: a global ranking of cities under threat from natural disasters. Swiss Re.

Reiner, M., & McElvaney, L. (2017). Foundational infrastructure framework for city resilience. *Sustainable and Resilient Infrastructure*, *2*(1), 1–7.

Rinaldi, S. M., Peerenboom, J. P., & Kelly, T. K. (2001). Identifying, understanding, and analyzing critical infrastructure interdependencies. *IEEE Control Systems Magazine*, *21*(6), 11–25.

Rogers, C. D. F., Bouch, C. J., Williams, S., Barber, A. R. G., Baker, C. J., Bryson, J. R., … Jefferson, I. (2012). Resistance and resilience-paradigms for critical local infrastructure. In *Proceedings of the Institution of Civil Engineers-Municipal Engineer 165*(2), 73–83.

Rogers, P. D., & Grigg, N. S. (2008). Failure assessment model to prioritize pipe replacement in water utility asset management. In *Water Distribution Systems Analysis Symposium 2006* (pp. 1–17).

Rose, A. (2004). Defining and measuring economic resilience to disasters. *Disaster Prevention and Management: An International Journal*, *13*(4), 307–314.

Rossman, L. A. (2000). EPANET 2: user manual.

Sage, D., Sircar, I., Dainty, A., Fussey, P., & Goodier, C. (2015). Understanding and enhancing future infrastructure resiliency: a socio-ecological approach. *Disasters*, *39*(3), 407–426.

Scussolini, P., Aerts, J. C. J. H., Jongman, B., Bouwer, L. M., Winsemius, H. C., de Moel, H., & Ward, P. J. (2016). FLOPROS: an evolving global database of flood protection standards. *Natural Hazards & Earth System Sciences*, *16*(5), 1049-1061.

Selva, J. (2013). Long-term multi-risk assessment: Statistical treatment of interaction among risks. *Natural Hazards*, *67*(2), 701–722.

Serre, D. (2018). DS3 model testing: assessing critical infrastructure network flood resilience at the neighbourhood scale. In *Urban Disaster Resilience and Security* (pp. 207–220). Springer.

Shaw, E. M., Beven, K. J., Chappell, N. A., & Lamb, R. (2010). *Hydrology in practice*. CRC press.

Shen, S., Cheng, C., Song, C., Yang, J., Yang, S., Su, K., … Chen, X. (2018). Spatial distribution patterns of global natural disasters based on biclustering. *Natural Hazards*, *92*(3), 1809–1820.

Shiraki, N., Shinozuka, M., Moore, J. E., Chang, S. E., Kameda, H., & Tanaka, S. (2007). System risk curves: probabilistic performance scenarios for highway networks subject to earthquake damage. *Journal of Infrastructure Systems*, *13*(1), 43–54.

Simpson, A., Murnane, R., Saito, K., Phillips, E., Reid, R., & Himmelfarb, A. (2014). Understanding risk in an evolving world: Emerging best practices in natural disaster risk assessment. *Global Facility for Disaster Reduction and Recovery, The World Bank, UN International Strategy for Disaster Reduction, Washington, DC.*

Sitzenfrei, R., Mair, M., Möderl, M., & Rauch, W. (2011). Cascade vulnerability for risk analysis of water infrastructure. *Water Science and Technology*, *64*(9), 1885–1891.

Smith, K. (2013). *Environmental Hazards: Assessing Risk and Reducing Disaster* (6th ed.). Routledge.

Spaans, M., & Waterhout, B. (2017). Building up resilience in cities worldwide-Rotterdam as participant in the 100 Resilient Cities Programme. *Cities*, *61*, 109–116.

Stanley, T., & Kirschbaum, D. B. (2017). A heuristic approach to global landslide susceptibility mapping. *Natural Hazards*, *87*(1), 145–164.

Sterbenz, J. P. G., Hutchison, D., Çetinkaya, E. K., Jabbar, A., Rohrer, J. P., Schöller, M., & Smith, P. (2010). Resilience and survivability in communication networks: Strategies, principles, and survey of disciplines. *Computer Networks*, *54*(8), 1245–1265.

Tabucchi, T., Davidson, R., & Brink, S. (2010). Simulation of post-earthquake water supply system restoration. *Civil Engineering and Environmental Systems*, *27*(4), 263–279.

Taleb, N. N. (2012). *Antifragile: Things that gain from disorder* (Vol. 3). Random House Incorporated.

Tan, C., & Fang, W. (2018). Mapping the wind hazard of global tropical cyclones with parametric wind field models by considering the effects of local factors. *International Journal of Disaster Risk Science*, *9*(1), 86–99.

Tellman, B., Bausch, J. C., Eakin, H., Anderies, J. M., Mazari-Hiriart, M., Manuel-Navarrete, D., & Redman, C. L. (2018). Adaptive pathways and coupled infrastructure: Seven centuries of adaptation to water risk and the production of vulnerability in Mexico city. *Ecology and Society*, *23*(1), 1.

Terzi, S., Torresan, S., Schneiderbauer, S., Critto, A., Zebisch, M., & Marcomini, A. (2019). Multi-risk assessment in mountain regions: A review of modelling approaches for climate change adaptation. *Journal of Environmental Management*, *232*, 759–771.

Tilloy, A., Malamud, B. D., Winter, H., & Joly-Laugel, A. (2019). A review of quantification methodologies for multi-hazard interrelationships. *Earth-Science Reviews*, *196*, 102881.

Timmerman, P. (1981). Vulnerability resilience and collapse of society. *A Review of Models and Possible Climatic Applications. Toronto, Canada. Institute for Environmental Studies, University of Toronto.*

Todini, E. (2000). Looped water distribution networks design using a resilience index based heuristic approach. *Urban Water*, *2*(2), 115–122.

Trifunovic, N. (2006). *Introduction to Urban Water Distribution: Unesco-IHE Lecture Note Series*. CRC Press.

Tugade, M. M., & Fredrickson, B. L. (2004). Resilient individuals use positive emotions to bounce back from negative emotional experiences. *Journal of Personality and Social Psychology*, *86*(2), 320.

European Union. (2016). Shared vision, common action: A stronger Europe. A global strategy for the European Union's foreign and security policy. European Union Brussels.

UNDRR (United Nations office for Disaster Risk Reduction) (2019). Global Assessment Report on Disaster Risk Reduction. Geneva, Switzerland.

UNISDR (United Nations International Strategy for Disaster Reduction) (2015a). *Sendai Framework for Disaster Risk Reduction 2015–2030. A/CONF.224/CRP.1.*

UNISDR (United Nations International Strategy for Disaster Reduction) (2015b). *Global Assessment Report on Disaster Risk Reduction 2015: Making Development Sustainable: the Future of Disaster Risk Management*. UN.

UNISDR (United Nations International Strategy for Disaster Reduction) (2005). *Hyogo framework for action 2005-2015: building the resilience of nations and communities to disasters.* A/CONF.206/6.

Vale, L. J., & Campanella, T. J. (2005). *The resilient city: How modern cities recover from disaster*. Oxford University Press.

Van Zyl, J. J. (2001). The Shuttle Radar Topography Mission (SRTM): a breakthrough in remote sensing of topography. *Acta Astronautica*, *48*(5–12), 559–565.

Vogus, T. J., & Sutcliffe, K. M. (2007). Organizational resilience: towards a theory and research agenda. In *2007 IEEE International Conference on Systems, Man and Cybernetics* (pp. 3418–3422).

Wagner, J. M., Shamir, U., & Marks, D. H. (1988). Water distribution reliability: simulation methods. *Journal of Water Resources Planning and Management*, *114*(3), 276–294.

Wahl, T., Jain, S., Bender, J., Meyers, S. D., & Luther, M. E. (2015). Increasing risk of compound flooding from storm surge and rainfall for major US cities. *Nature Climate Change*, *5*, 1093-1097.

Wang, W., Yang, S., Stanley, H. E., & Gao, J. (2019). Local floods induce large-scale abrupt failures of road networks. *Nature Communications*, *10*(1), 1–11.

Wang, Z., Wang, H., Huang, J., Kang, J., & Han, D. (2018). Analysis of the public flood risk perception in a flood-prone city: The case of Jingdezhen city in China. *Water*, *10*(11), 1577.

Ward, P. J., Blauhut, V., Bloemendaal, N., Daniell, J. E., Ruiter, M. C. de, Duncan, M. J., … Winsemius, H. C. (2020). Natural hazard risk assessments at the global scale. *Natural Hazards and Earth System Sciences*, *20*(4), 1069–1096.

Wisetjindawat, W., Kermanshah, A., Derrible, S., & Fujita, M. (2017). Stochastic modeling of road system performance during multihazard events: Flash floods and earthquakes. *Journal of Infrastructure Systems*, *23*(4), 1–13.

Wood, H. O., & Neumann, F. (1931). Modified Mercalli intensity scale of 1931. *Bulletin of the Seismological Society of America*, *21*(4), 277–283.

Worden, C. B., Gerstenberger, M. C., Rhoades, D. A., & Wald, D. J. (2012). Probabilistic relationships between ground-motion parameters and modified mercalli intensity in California. *Bulletin of the Seismological Society of America*, *102*(1), 204–221.

Yamazaki, D., Ikeshima, D., Sosa, J., Bates, P. D., Allen, G. H., & Pavelsky, T. M. (2019). MERIT Hydro: a high-resolution global hydrography map based on latest topography dataset. *Water Resources Research*, *55*(6), 5053–5073.

Zaghi, A. E., Padgett, J. E., Bruneau, M., Barbato, M., Li, Y., Mitrani-Reiser, J., & McBride, A. (2016). Establishing common nomenclature, characterizing the problem, and identifying future opportunities in multihazard design. *Journal of Structural Engineering*, *142*(12), H2516001.

Zhang, X., Xie, H., Zhou, C., & Zeng, B. (2020). Jingdezhen: The millennium porcelain capital. *Cities*, *98*, 102569.

Zhao, B., & Taucer, F. (2010). Performance of infrastructure during the May 12, 2008 Wenchuan earthquake in China. *Journal of Earthquake Engineering*, *14*(4), 578–600.

Zong, Y., & Chen, X. (2000). The 1998 flood on the Yangtze, China. *Natural Hazards*, *22*(2), 165–184.

Zscheischler, J., Westra, S., Van Den Hurk, B. J. J. M., Seneviratne, S. I., Ward, P. J., Pitman, A., … Zhang, X. (2018). Future climate risk from compound events. *Nature Climate Change*, *8*(6), 469–477.